NOAA Technical Report NESDIS 61

TROPICAL CYCLOGENESIS IN THE WESTERN NORTH PACIFIC

Raymond M. Zehr
RAMM Branch
Colorado State University
Fort Collins, CO

Washington, D.C.
July 1992

U.S. DEPARTMENT OF COMMERCE
Barbara H. Franklin, Secretary

National Oceanic and Atmospheric Administration
John A. Knauss, Under Secretary

National Environmental Satellite, Data, and Information Service
Thomas N. Pyke, Jr. , Assistant Administrator

ABSTRACT

Tropical cyclogenesis in the western North Pacific is typically characterized by an early convective maximum which precedes the initial appearance of a tropical depression. The convection is quantified from cloud areas specified by cold infrared temperature thresholds with 3-hourly GMS satellite data. It is hypothesized that this convective maximum represents an important process associated with tropical cyclogenesis and is a response to large-scale (synoptic-scale) forcing. A conceptual model is described in which the early convective maximum is viewed as a necessary but not sufficient condition for tropical cyclone formation. An important change in the wind field takes place in response to the convective maximum. A weak mesoscale vortex is initiated which is located within the larger broad-scale cyclonic circulation of a pre-existing tropical disturbance. However, the first substantial decrease in central sea-level pressure and resultant increase in surface wind speed occur at a later stage of tropical cyclogenesis. This early convective maximum and associated mesoscale vortex formation precede first designation as a tropical storm by an average period of about 3 days.

The 850 mb and 200 mb objective analyses of conventional data are used to classify different synoptic-scale patterns associated with the formation of fifty individual tropical storms and typhoons during 1983-1984. Animated satellite imagery and aircraft reconnaissance data provide observations of deep convection and low-level winds for more detailed analysis.

Twenty-two non-developing tropical disturbances which persisted for at least two days in the climatologically favorable genesis region are also investigated. Quantitative IR techniques and objective analyses of relative vorticity, divergence, and vertical wind shear allow comparisons among individual non-developing and developing disturbances. Small vertical wind shear, sufficient low-level convergence, and sufficient low-level relative vorticity are shown to be necessary conditions for tropical cyclogenesis. One or more of the three conditions can usually be identified as being deficient with individual cases of non-developing disturbances.

TABLE OF CONTENTS

1 INTRODUCTION 1
1.1 Terminology and Definitions . . . 2
1.1.1 Genesis Versus Intensification . . . 2
1.2 Current Knowledge and Previous Research . . . 2
1.2.1 Climatology . . . 4
1.2.2 Early Studies . . . 4
1.2.3 Observational Studies . . . 6
1.2.4 Satellite Studies . . . 7
1.2.5 Numerical Model Experiments . . . 7
1.2.6 Theoretical Studies . . . 8
1.3 Research Approach Used with the Present Study . . . 8

2 DATA SOURCES 10
2.1 Satellite Data . . . 10
2.2 Aircraft Reconnaissance Data . . . 14
2.3 Conventional Data . . . 17

3 GMS IR SATELLITE DATA ANALYSIS 19
3.1 Characteristics of Deep Convective Clouds Associated with Tropical Cyclones . 19
3.2 Convective Maximum Associated with Tropical Cyclogenesis . . . 19
3.2.1 Occurrence and Definition of the Early Convective Maximum . . . 19
3.2.2 Time of Early Convective Maximum . . . 24
3.2.3 Amplitude of Early Convective Maximum . . . 26
3.2.4 Satellite Image Characteristics . . . 28
3.2.5 A Secondary Convective Maximum Associated with Tropical Cyclogenesis . . 28
3.2.6 Concentration of Convection Near the Center . . . 28
3.3 Deep Convective Clouds Associated with Non-developing Tropical Disturbances 37
3.4 Summary . . . 38

4 TWO STAGES OF TROPICAL CYCLOGENESIS 41
4.1 Quantitative IR Satellite Analysis . . . 41
4.2 Qualitative Description . . . 43
4.3 Wind Surges . . . 43

5 SYNOPTIC-SCALE ANALYSIS OF WESTERN NORTH PACIFIC TROPICAL CYCLOGENESIS 45
5.1 Season and Geographical Location . . . 45
5.2 Low-level Patterns . . . 45
5.2.1 Summary . . . 55

5.3 Wind Surges . . . 56
5.3.1 Aircraft Reconnaissance . . . 56
5.3.2 Conventional Analysis . . . 57
5.3.3 Satellite Images . . . 57
5.3.4 Direction of the Surge . . . 61
5.3.5 Summary . . . 65
5.4 Upper-level Wind Direction and Speed . . . 65
5.5 Subtropical Ridge . . . 66
5.6 Tropical Upper Tropospheric Trough . . . 68
5.7 Summary . . . 68

6 QUANTITATIVE COMPARISON OF PRE–TROPICAL STORM AND NON–DEVELOPING DISTURBANCES 70
6.1 Synoptic–Scale Conditions Associated with Non-Developing Disturbances . . . 70
6.1.1 Low-Level . . . 70
6.1.2 Upper-Level . . . 70
6.2 Method of Quantitative Analysis . . . 72
6.2.1 Interpolation to Best Track . . . 72
6.2.2 Combined Mean Values . . . 74
6.3 850 mb Relative Vorticity . . . 75
6.3.1 Comparison of Individual Cases . . . 76
6.3.2 Summary . . . 76
6.4 850 mb Convergence . . . 77
6.4.1 Comparison of Individual Cases . . . 79
6.4.2 Summary . . . 79
6.5 200–850 mb Vertical Wind Shear . . . 83
6.5.1 Individual Case Analysis . . . 84
6.5.2 Direction of Vertical Wind Shear . . . 84
6.5.3 Summary . . . 84
6.6 200 mb Divergence . . . 84
6.7 200 mb Relative Vorticity . . . 88
6.8 Summary . . . 88
6.9 Objective Techniques and Forecast Aids for Tropical Cyclogenesis . . . 96
6.9.1 Combining Areas Defined by Threshold Values . . . 96
6.9.2 Genesis Parameter, GP . . . 98
6.10 Evaluation of the Objective Techniques . . . 103
6.10.1 The Threshold Method . . . 103
6.10.2 Genesis Parameter (GP) Method . . . 108
6.10.3 Summary . . . 111

7 DETAILED CASE STUDIES 114
7.1 Low-level Wind Pattern Changes During Tropical Cyclogenesis . . . 114
7.1.1 Pre-Stage 1 . . . 114
7.1.2 Stage 1 . . . 114
7.1.3 Stage 2 . . . 116
7.2 Visible Satellite Images of Low-level Circulation Centers . . . 116
7.2.1 Doyle . . . 116
7.2.2 Additional Examples of Stage 1 Genesis in Satellite Images . . . 116

7.3 Westerly Surge Initiating a Convective Maximum 124
7.3.1 Forrest, Stage 1 124
7.3.2 Forrest, Stage 2 130
7.3.3 Quantitative Combined Satellite-Aircraft Analysis 133
7.3.4 Summary 133

8 DISCUSSION **141**
8.1 Detailed Conceptual Model 141
8.1.1 Summary 145
8.2 Initial Mesoscale Vortex Formation 146
8.2.1 Summary 147
8.3 Initial MSLP Decrease 147
8.3.1 Summary 148
8.4 Role of Sea Surface Temperature, Thermodynamics, and Deep Convective Clouds 148
8.5 Role of Low–Level Convergence and Surges 150
8.6 Role of Synoptic–Scale Low–Level Vorticity 150
8.7 Role of Vertical Wind Shear 151
8.8 Upper-level Flow Patterns 152

9 CONCLUDING REMARKS **154**

ACKNOWLEDGEMENTS **155**

REFERENCES **156**

A Best Track Plots of the Non-Developing Disturbances **164**

B Center Locations of the Non-Developing Disturbances used in the Chapter 6 Analysis at 12-hour Intervals **172**

C Center Locations of the Pre-Tropical Storm Disturbances used in the Chapter 6 Analysis at 12-hour Intervals **176**

LIST OF SYMBOLS AND ACRONYMS

AMEX : Australian Monsoon Experiment

BMRC : (Australian) Bureau of Meteorology Research Centre

Cb : Cumulonimbus clouds

CISK : Conditional Instability of the Second Kind

–DIV :Convergence

DIV : Divergence

DMSP : Defense Meteorological Satellite Program

ECMWF : European Center for Medium-Range Weather Forecasts

f : Coriolis parameter

GMS : Geostationary Meteorological Satellite Program

GMT : Greenwich Mean Time

GP : Genesis parameter

ISCCP : International Satellite Cloud Climatology Program

IR : Infrared

ITCZ : Intertropical Convergence Zone

JMA : Japan Meteorological Agency

JTWC : Joint Typhoon Warning Center

LLCC : Low-level circulation center

mb : Millibar

MCC : Mesoscale Convective Complex

MCV : Mesoscale Convectively generated Vortex

MSLP : Minimum sea level pressure

ND : Non-developing

NOAA : National Oceanic and Atmospheric Administration

PS : Pre-tropical Storm

R : Radius

SLP : Sea-Level Pressure

SST : Sea-Surface Temperature

STR : Sub-Tropical Ridge

STY : Supertyphoon

T_B : Equivalent Blackbody Temperature (infrared brightness temperature)

TC : Tropical Cyclone

TD : Tropical Depression

TS : Tropical Storm

TY : Typhoon

TUTT : Tropical Upper Tropospheric Trough

u : East-West wind component

v : North-South wind component

V_{max} : Maximum sustained surface wind speed (1 minute average)

V_T : Tangential wind

VOR : Relative Vorticity

w : Vertical velocity (in height coordinates)

ω : Vertical velocity (in pressure coordinates)

ζ : Relative vorticity

Chapter 1

INTRODUCTION

One of the greatest remaining challenges in meteorology is to adequately understand and explain the process of tropical cyclogenesis. Our knowledge of the dynamics and structure of mature tropical cyclones has grown, aided by extensive observational analysis and numerical models. However, our understanding of the initiation or genesis of tropical cyclones remains incomplete and speculative. The key to understanding tropical cyclogenesis is to explain the transformation of a pre-existing tropical disturbance into a tropical cyclone. The pre-existing disturbances are characterized by broad low-level and mid-level cyclonic circulations, often appearing as easterly waves along the inter-tropical convergence zone. The associated minimum sea level pressure (MSLP) is typically only 1-2 mb lower than the surrounding environment. Some of those tropical disturbances remain non-developing disturbances throughout their lifetimes, while others evolve into tropical cyclones. Pre-tropical storm disturbances have characteristics very similar to non-developing disturbances. However, as a tropical cyclone forms, two important structural changes take place, in the following order: 1) A weak tropical cyclone scale (mesoscale) vortex is initiated within the disturbance; 2) The MSLP with that vortex begins to decrease, falling below the MSLP associated with non-developing disturbances.

Once sufficient lowering of the tropical cyclone vortex central pressure has occurred, intensification will take place under favorable environmental conditions. The inward pressure gradient by itself will not only maintain the tropical cyclone, but intensify it, provided there is sufficient evaporation of warm ocean water, deep convective clouds, and low vertical wind shear. But what causes the tropical cyclone scale vortex to form in the first place? Furthermore, under what conditions will the central pressure of the vortex fall sufficiently so that intensification will begin to occur. In more practical terms, how can one predict when and where a tropical depression will form and will it become a tropical storm (defined by maximum sustained surface winds of at least 17.5 ms^{-1})? The purpose of this investigation is to try to answer such questions and present the supporting observational evidence.

Some of the necessary conditions for tropical cyclogenesis have been known for many years. For example, tropical cyclones form only over oceans with sea-surface temperatures of at least 26.5°C (Palmén, 1948). Also, it has long been recognized that tropical cyclones form from pre-existing disturbances having deep convective clouds (Riehl, 1954). One of the goals of the present investigation is to provide a quantitative evaluation of all the necessary conditions for tropical cyclogenesis. The approach taken to achieve that goal is to analyze the observational data including satellite imagery, for a large sample of individual cases of both pre-tropical storm and non-developing disturbances.

Available data sources and how they are used are described in Chapter 2. Quantitative satellite analyses of the formative stages of tropical cyclones are given in Chapter 3. This includes the period from initial cloud cluster formation up to designation as a tropical storm. Chapter 4 describes a conceptual framework which includes two distinct stages of tropical cyclogenesis based on the satellite analyses of Chapter 3 and previous observational studies. The lower and upper tropospheric flow features associated with the formation of all western North Pacific tropical storms during 1983-1984 are summarized in Chapter 5. Pre-tropical storm environmental conditions are compared with those of persistent non-developing tropical disturbances as determined by 2.5° latitude resolution objective meteorological analyses in Chapter 6. Chapter 7 includes specific examples from detailed case studies to illustrate particular important points. Finally, the overall findings

are summarized and discussed in relation to other recent tropical cyclogenesis research papers.

1.1 Terminology and Definitions

Confusion sometimes arises when research studies use inconsistent or nonstandard terminology. The present study uses terminology as described here.

The conventional, specific definitions are used for typhoon, hurricane, tropical storm, and tropical depression (Huschke, 1959). "Tropical cyclone" is a generic term which includes all of the above designations. Tropical "cyclogenesis" and tropical cyclone "formation" or "genesis" refer to the weather systems and their ongoing atmospheric processes during the time periods before initial designation as a tropical storm. Tropical cyclone "intensification" refers to those time periods after tropical storm designation. Tropical cyclone "development" is more general, referring to both formation and intensification, and its use is avoided.

The terms, "tropical disturbance" and "cloud cluster" both refer to a tropical weather system which has not yet, or never does, become a tropical cyclone. "Pre-tropical storm" and "non-developing" are used to differentiate those tropical disturbances which eventually become tropical storms from those that do not. The commonly used terms "tropical wave" and "easterly wave" are synonymous with tropical disturbance.

1.1.1 Genesis Versus Intensification

For the purposes of the present study, tropical depressions are considered to still be undergoing cyclogenesis, while tropical storms (named storms) have completed the genesis process, and are undergoing intensification. It is important to make this distinction, as depicted in Fig. 1.1, because the atmospheric processes which control and influence genesis are likely different than those involved with intensification (Gray, 1989).

The dynamics of intensifying tropical cyclones are predominated by the atmosphere's response to the pressure field. The effects of friction and deep convective clouds provide the necessary convergence, while the warm ocean surface and evaporation provide the energy source which results in the maintenance and intensification of the pressure field. The tropical cyclone can then be viewed as a self-sustaining weather system and may persist and intensify without any aid of external forcing. The only required necessary conditions are a sufficiently warm ocean surface and environmental wind shear effects which are small enough so the circulation is sustained through the depth of the troposphere. Such dynamical considerations are just beginning to influence the pre-tropical storm disturbance during its final stages as a tropical depression. Prior to that time, and through most of the tropical cyclogenesis periods the important dynamical mechanisms are different.

Certain atmospheric processes, external to the disturbance itself, are hypothesized to be required for tropical cyclogenesis (Gray, 1988). These will be studied in great detail in the present investigation. Such external processes are likely not required for intensification, although they may be influential. Processes internal to the disturbance itself predominate with intensification. Those processes are not dealt with in the present study.

The exact time when genesis processes give way to intensification processes is not well known. It is sometime around the time a tropical cyclone first becomes a "named storm", which coincides with the minimal tropical storm designation. This study uses that point in time to mark the end of genesis and the beginning of intensification. It is not only a convenient method, but it also provides consistency among individual cases.

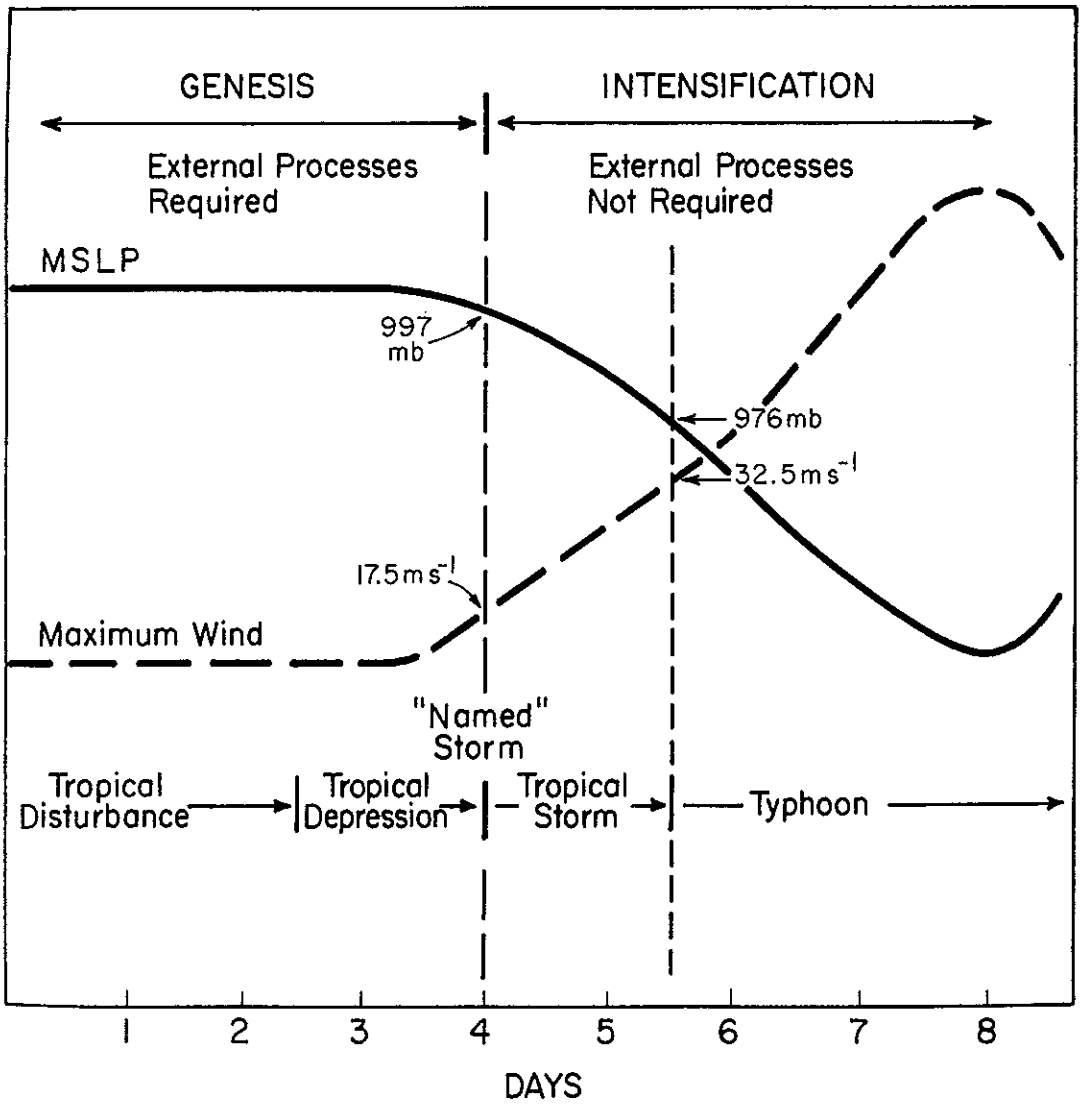

Figure 1.1: Depiction of typical genesis and intensification periods and their associated MSLP and maximum surface wind speed.

1.2 Current Knowledge and Previous Research

1.2.1 Climatology

Some insight into the conditions under which tropical cyclones form, is gained by simply looking at when and where they form and the seasonal climatology of those regions. Gray (1979) has subdivided global genesis regions into seven different areas, or basins (Fig. 1.2). He also showed that those areas can be delineated by a combination of seasonal parameters derived from climatological data. The six climatological factors which favor tropical cyclogenesis are:

1. high sea surface temperature,
2. high mid-tropospheric relative humidity,
3. large surface to 500 mb lapse rates of equivalent potential temperature,
4. small tropospheric vertical wind shear,
5. high low-level relative vorticity, and
6. sufficiently high Coriolis parameter.

The first three factors are grouped together to derive a thermodynamic parameter, while the final three are combined into a dynamic parameter. This information is important in defining some of the necessary conditions for tropical cyclone formation. However, the six variables are seasonal means and their numerical values are likely not applicable for determining whether or not genesis will occur for individual cases. For example, sea-surface temperature and Coriolis parameter may show very little day-to-day variation in association with a particular tropical disturbance. They are usually favorable for tropical cyclogenesis, even when evaluated with many non-developing disturbances. Yet, they can be used on a day-to-day basis to eliminate large areas from consideration as possible tropical cyclogenesis locations. Other parameters, such as vertical wind shear, might be expected to show large day-to-day variations within the areas in which tropical cyclones originate. Earlier studies (Gray, 1968; Fett, 1968) have also identified the higher low-level vorticity often associated with the equatorial trough (intertropical convergence zone-ITCZ), and low vertical wind shear as favorable conditions for tropical cyclone formation. The monsoon trough, characterized by westerly component winds on its equatorial side, is a prominent feature of most tropical cyclone formation basins (Gray, 1968; Ramage, 1974; McBride and Keenan, 1982).

The present study deals with the western North Pacific tropical cyclone basin, which is the most active of the seven regions defined by Gray (1979). The tropical area between 180° longitude and the South China Sea accounts for the formation of about 33% of the global total of tropical cyclones (Fig. 1.2).

1.2.2 Early Studies

Much of the early pioneering work on tropical cyclogenesis is reviewed by Riehl (1954). Dunn (1940) demonstrates that tropical weather systems can be tracked westward in the Atlantic-Caribbean region using isallobaric analysis. The first studies of typhoon formation in the western North Pacific are summarized by Deppermann (1947). Palmén (1948) relates tropical cyclone formation to the distribution of warm sea-surface temperatures. Dunn (1951) documents global tropical cyclone regions, seasons, and frequencies of occurrence.

Riehl (1948, 1954) recognizes the existence of easterly waves as pre-existing disturbances from which hurricanes develop. He documents the structure of easterly waves and

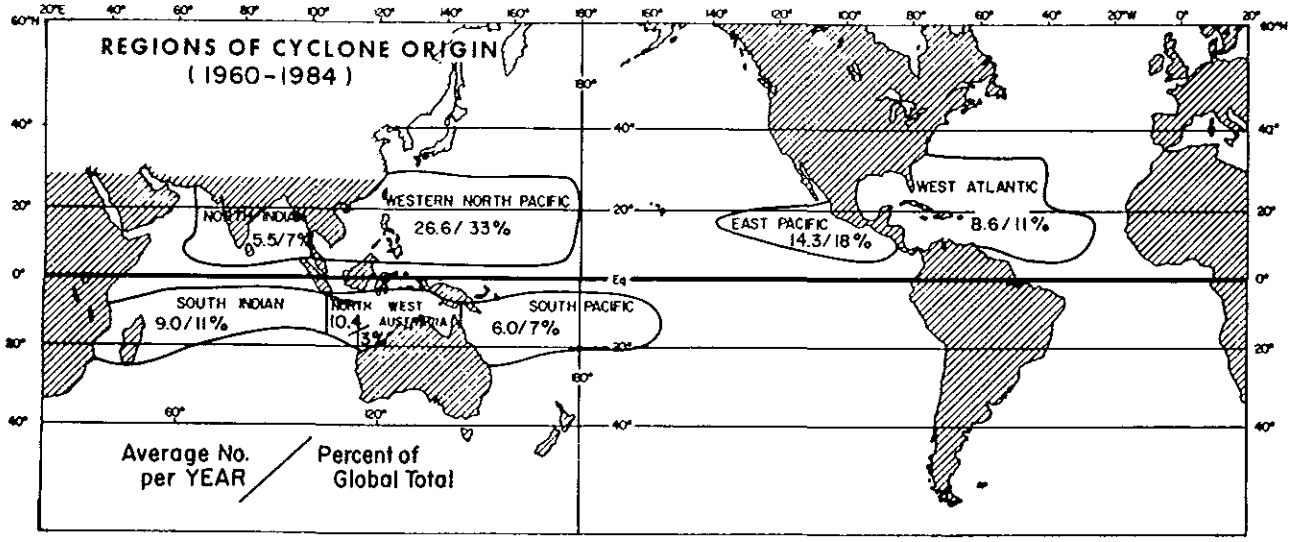

Figure 1.2: Average number of tropical cyclones per year for 1960–1984 in each of the seven tropical cyclone formation regions as defined by Gray (1979).

views tropical cyclone formation to be a result of an easterly wave encountering favorable upper-level conditions. Yanai (1961a, 1968) presents detailed case studies of tropical cyclone formation for both the western North Pacific and the Atlantic regions. Some of the important structural characteristics of the early stages of tropical cyclones are depicted. Yanai (1961b) and Hubert (1955) emphasize the transformation of a cold-core to a warm-core system in the lower troposphere during tropical cyclogenesis.

The energy source for tropical cyclones is attributed to the release of latent heat in deep cumulonimbus convection (Palmén and Riehl, 1957; Riehl and Malkus, 1961). The primary mechanism which provides sufficient moist static energy for sustained deep convection, is evaporation from the ocean surface. Thus, tropical cyclones require a very warm ocean surface and deep cumulonimbus clouds in order to overcome dissipative forces and intensify. A pre-existing disturbance having deep cumulonimbus clouds, located over a warm ocean, has long been recognized as a precursor to tropical cyclogenesis.

Some of the early studies proposed theories for tropical cyclone formation which are likely invalid, at least for the majority of tropical cyclones. In fact, no unified theory is likely adequate to explain tropical cyclogenesis (Gray, 1989). Additionally, some of those theories may be more applicable to tropical cyclone intensification rather than genesis.

Sawyer (1947) and Alaka (1962) contend that an upper tropospheric dynamic instability leads to tropical cyclogenesis. This theory depends on the existence of strongly anticyclonic flow such that the absolute vorticity becomes negative. This mechanism would then trigger tropical cyclogenesis due to the associated highly divergent flow, situated above the low-level convergence associated with a tropical disturbance. There is little or no evidence to support this argument as a valid description of tropical cyclogenesis.

Yanai (1961b) proposed baroclinic inertial instability as an explanation for tropical cyclogenesis. This view requires baroclinic forcing to release instability which enhances deep convection, leading to a tropospheric warming which initiates tropical cyclone formation. However, since baroclinic forcing is typically observed to be very weak in the genesis regions, this is likely an inadequate explanation of tropical cyclogenesis.

Charney and Eliassen (1964) introduce the concept of CISK (Conditional Instability of the Second Kind). CISK refers to the growth of weak cyclonic disturbances resulting from low-level frictional convergence (Ekman pumping) which supplies ample water vapor necessary for the disturbance to sustain deep convective clouds. The feedback effects of those clouds induce vortex growth and intensification which further enhance convergence.

This frictional convergence predominates the mass inflow of mature tropical cyclones and undoubtedly plays an important role in the maintenance and intensification of the tropical cyclone circulation. The CISK mechanism and its role in tropical cyclone formation has received much attention over the years, particularly as a basis for numerous numerical modeling experiments (Ooyama, 1969, 1982). The concept of CISK and its role in tropical cyclogenesis are discussed in Chapter 8.

1.2.3 Observational Studies

There are two basic types of observational research: case studies and composite studies. A case study generally applies all available data to a particular weather event or weather system. It often includes special data sets or operational data with exceptionally good spatial coverage. Composite studies (Frank, 1977a,b; McBride, 1981a,b; Weatherford and Gray, 1988a,b) employ a particular data type (e.g. radiosonde or aircraft observations) and average large quantities of data on a grid with respect to the known location of numerous weather systems. Comparisons can then be made by stratifying the data according to a variety of weather system characteristics. Knowledge of the structure of developing tropical cyclones and their important physical mechanisms have been gained from both of these approaches.

Colon and Nightingale (1963) analyze 200 mb patterns associated with Atlantic hurricane development and find anticyclonic southerly flow to be the most common feature. Sadler (1976, 1978) shows that the Tropical Upper Tropospheric Trough (TUTT) is often present with western North Pacific tropical cyclogenesis. The TUTT is generally located to the north or northwest of a developing tropical cyclone. Sadler's reasoning is that the TUTT enhances upper tropospheric outflow which leads to tropical cyclone development. Those papers, like earlier studies (Sawyer, 1947; Riehl, 1948), view the large-scale upper tropospheric flow patterns to be important factors in tropical cyclogenesis.

Many additional observational studies have investigated the upper-level environmental wind patterns which accompany tropical cyclogenesis (Fett, 1966; Dvorak, 1977, 1984; Love, 1982; McBride and Keenan, 1982; Holland, 1984; Lee, 1989a, 1989b; Foster and Lyons, 1988). They include the presence and location of the mid-latitude trough, the TUTT, and the upper-level anticyclone. From these studies, it is difficult to arrive at a consensus on the role of upper-level environmental flow features in tropical cyclogenesis.

McBride and Zehr (1981) show large differences in the low-level (900 mb) relative vorticity between composites of pre-tropical storm disturbances and non-developing cloud clusters. The developing cases have approximately twice as much mean relative vorticity out to 6° latitude radius from the circulation center. Their study also shows more negative relative vorticity at 200 mb associated with the developing cases. Another characteristic feature of pre-tropical storm disturbances is that they tend to be located very close to the zero line of vertical shear of the zonal wind (u-component difference between 900 and 200 mb) (Gray, 1968; McBride and Zehr, 1981).

Small vertical wind shear through a deep tropospheric layer appears to be a necessary condition for tropical cyclogenesis. Large vertical wind shear environments will ventilate the upper tropospheric warm core and prevent surface pressure falls near the active lower portion of the disturbance. The process of ventilation and the importance of small vertical wind shear are topics covered by Gray (1968), Lopez (1968), Zehr (1976), and more recently, Lunney (1988). It is important to note, however, that composite studies of non-developing cloud clusters also show the associated vertical wind shear to be relatively small (Williams and Gray, 1973; Ruprecht and Gray, 1976; McBride and Zehr, 1981).

Lee (1986, 1989a,b) expanded on the composite data set comparisons of McBride and Zehr (1981) and performed tangential momentum budget studies. He showed that sizable inward eddy vorticity fluxes are required to explain the observed tangential wind increases during tropical cyclogenesis.

Various case studies suggest that low-level external forcing in the form of wind speed maxima penetrating the circulation of a pre-existing disturbance may initiate tropical cyclogenesis (Love, 1985; Molinari and Skubis, 1985; Lee, 1986; Lunney, 1988; Zehr, 1989).

Such features are referred to as surges. Evidence of surges is also found in radiosonde data composites (Lee, 1989a,b) and aircraft data composites (Middlebrooke, 1988). Surges and their role in tropical cyclogenesis are discussed in Chapters 4 and 5.

The Australian Monsoon Experiment (AMEX) provided special data sets for two case studies of tropical cyclogenesis in the northern Australia region during 1987 (Davidson *et al.*, 1990; Davidson and Kumar, 1990). Their results show the detailed characteristics of the structural evolution of the pre-existing disturbance into a tropical cyclone for two very similar cases located within the monsoon trough.

Mesoscale convective complexes (Maddox, 1980), which occur over the central U.S. Plains States during summer, frequently produce mesoscale vortices which persist for days (Johnston, 1981; Menard and Fritsch, 1989; Bartels and Maddox, 1991). These mesoscale convectively generated vortices (MCVs) appear qualitatively to be very similar to those observed with pre-tropical storm disturbances. In fact, such land-based MCVs have occasionally been observed to develop into tropical cyclones (Velasco and Fritsch, 1987). The observational studies (Smull and Houze, 1987; Leary and Rappaport, 1987; Cotton *et al.*, 1989; Johnson *et al.*, 1989; and Johnson and Bartels, 1991) and numerical simulations (Zhang and Fritsch, 1988; Tripoli and Cotton, 1989) of mesoscale convective complexes may be pertinent to tropical cyclogenesis studies.

1.2.4 Satellite Studies

Early applications of satellite imagery (Fritz, 1962; Frank, 1963; Fett, 1966) not only provided useful insight on understanding tropical cyclogenesis, but also revealed that some tropical cyclones, particularly in the eastern Pacific, had likely gone undetected before the advent of satellites (Oliver and Anderson, 1969). The capability of quickly assessing atmospheric motions at both the lower and upper levels of tropical weather systems using animated satellite imagery is discussed by Oliver and Anderson (1969). They also demonstrate the utility of cloud motion vectors which are derived from a time series of geostationary satellite images. The use of infrared radiation data to measure and monitor deep convective clouds and meso-scale convective systems has evolved from the early applications (Bandeen *et al.*, 1964; Allison *et al.*, 1966) to current techniques using digital satellite data (Zehr, 1987; Zehr, 1988).

Arnold (1977) analyzed DMSP satellite images and showed a tendency for deep convection to become more concentrated near a circulation center during tropical cyclone formation. Erickson (1977) concluded that there are no apparent differences in the overall amount and intensity of convective cloudiness between non-developing cloud clusters and pre-tropical storm disturbances.

A technique to estimate tropical cyclone intensity based solely on satellite imagery is widely used operationally. This technique, developed by Dvorak (1984), also includes the very early pre-tropical storm stages. Cyclonically curved, deep cumulonimbus bands and a persistent, identifiable cloud system center, typically appear 36 hr prior to initial tropical storm stage.

1.2.5 Numerical Model Experiments

Beginning with the work of Kuo (1965) and Ooyama (1969), there have been many papers involving research numerical models of tropical cyclones. Anthes (1982) includes a thorough review of tropical cyclone modeling. The numerical simulations often include the early stages of tropical cyclones and therefore are pertinent to tropical cyclogenesis studies.

However, the interpretation of the modeling research must also be subject to the distinction between cyclogenesis and intensification. Many numerical model simulations begin with initial conditions which are unrealistic with regard to cyclogenesis processes, but may be applicable to intensification.

Undoubtedly, recent improvement in numerical models and available data for initialization, show great promise in their applicability to tropical cyclogenesis. However, no

numerical models have yet adequately simulated the important detailed structural changes which take place during genesis (Gray, 1988, 1989). The inadequacies of the numerical modeling studies of tropical cyclogenesis are discussed further in Chapter 8.

1.2.6 Theoretical Studies

Shapiro (1977) views tropical cyclogenesis as the transformation of an easterly wave, which is characterized by linear dynamics, to a disturbance in which non-linear effects become more dominant. The non-linear effects, which may be provided by large-scale forcing, initiate tropical cyclogenesis.

The Rossby radius of deformation (Rossby, 1938) is typically large in tropical regions due primarily to the low absolute vorticity. Since tropical cloud clusters have associated length scales less than the radius of deformation, convective heating is rapidly dispersed by gravity waves and results in only very small local atmospheric warming (Frank, 1983; Schubert *et al.*, 1980). For the same reason, tropical weather systems are often characterized by mass fields which adjust to changes in the wind field (Silva Dias and Schubert, 1979; Schubert *et al.*, 1980). Schubert and Hack (1982) show that the convective heating efficiency is closely related to the atmosphere's inertial stability. This concept is discussed further in Chapter 8.

Rotunno and Emanuel (1987) and Emanuel (1989) conclude that a threshold amplitude exists, which will result in tropical cyclogenesis once it is attained. This amplitude is given by the azimuthal wind velocity and minimum central pressure of a cyclonic circulation. They do not address the initial vortex formation.

Challa and Pfeffer (1990) attribute the transformation of cloud clusters and tropical depressions into hurricanes to large-scale eddy processes. This view which involves external upper-level forcing is comparable to that of Holland and Merrill (1984) and Molinari and Vollaro (1989) which describe environmental influences on tropical cyclone intensity change rather than genesis.

It is clear that a consistent theoretical approach to the problem of tropical cyclogenesis has not yet evolved. Recent studies seem to be moving toward the viewpoint that external environmental influences (Gray, 1988) rather than internal tropical disturbance dynamics or instability (e.g. CISK) must be invoked. Hopefully, the present study will shed some light on the current theoretical ideas.

1.3 Research Approach Used with the Present Study

Two unique aspects of this study distinguish it from previous observational studies of tropical cyclogenesis. (1) A compositing approach is not used and 2) satellite data are used extensively.

Compositing techniques were devised to overcome the problem of sparse observations. This is still a problem. However, satellite cloud drift winds and aircraft observations are now routinely incorporated with radiosonde observations to obtain grid-point objective analyses. Such analyses are applicable to a quantitative evaluation of individual weather systems and their surrounding environment at synoptic analysis times.

Many previous observational studies have been based on radiosonde composites which have one significant drawback. The detailed individual case characteristics are often lost in the averaging process of the composite analysis. Therefore, such studies do not reveal the variety of conditions under which tropical cyclone formation occurs. Individual case studies have shown that western North Pacific tropical cyclones form within a variety of large scale environmental flow patterns (Lee, 1986).

On the other hand, a drawback of the individual case study is that an exhaustive study is a major task and is very time consuming. Furthermore, how an individual case compares with the variety of numerous other cases is often not well known. To overcome these drawbacks, some aspects of the conditions associated with all cases of tropical cyclogenesis over a few years must be studied. This approach may then produce a reliable synoptic climatology of tropical cyclogenesis. Lee (1986) proceeded in this manner to investigate

individual cases of western North Pacific tropical cyclone formation during the 1979 FGGE (First GARP Global Experiment) year. The present study can be viewed as a follow up study to Lee's research.

A major improvement over Lee's study is provided by the availability of digital Geostationary Meteorological Satellite (GMS) data and the quantitative information extracted from extensive processing of those data. Information extracted from satellite images are absolutely critical to the present study. Image data are used both qualitatively and quantitatively. Details are given in Chapter 2. In addition, the investigative reconnaissance flight data (Middlebrooke, 1988 and Lunney, 1988) are also incorporated into the present study.

To complete a thorough study of western North Pacific tropical cyclogenesis during 1983-1984 and also overcome the drawbacks of voluminous data sets and the time required for individual case studies, is a difficult undertaking. Therefore, some aspects but not all the details of each individual case during the entire two-year period are analyzed. This includes the pre-tropical storm disturbances with 50 named storms (22 tropical storms, 22 typhoons, and 6 supertyphoons), and 22 persistent non-developing tropical disturbances. Based on data availability and individual case characteristics, a small subset of cases have been chosen for more detailed case studies (Chapter 7).

Chapter 2

DATA SOURCES

The sparse distribution of weather observing stations has always been a problem for forecasting and analysis in the tropics. This has been alleviated somewhat in recent years with the increasing availability of satellite images, products, and techniques. Objective analyses of tropical regions have improved due in part to inclusion of satellite cloud drift winds. Digital satellite data and improved data processing techniques are also now available. This study exploits that improved capability to investigate tropical cyclogenesis.

To properly analyze individual cases, it is important that all available observational data be used. The data needs to be combined in an optimal manner to arrive at a depiction of the atmosphere which best describes the phenomenon of interest. For this study, three basic data sets have been used. They are satellite, aircraft, and objectively analyzed conventional data. The conventional data include surface observations, radiosonde thermodynamic and wind observations, satellite cloud drift wind observations, and aircraft wind observations.

2.1 Satellite Data

The primary satellite data source is three-hourly, 10-km resolution infrared and visible digital data from the GMS (Geostationary Meteorological Satellite). The GMS series of satellites has been operated by the Japan Meteorological Agency (JMA) since July, 1977. GMS-1 and GMS-3 data are used in this study. GMS is positioned in geostationary orbit above the Equator at 140°E longitude.

The digital GMS data were obtained from the ISCCP (International Satellite Cloud Climatology Project) archive, with 10 km resolution full disk image files for both visible and infrared, at three-hour intervals (Schiffer and Rossow, 1983; Rossow *et al.*, 1988). Each 10 km by 10 km data point (pixel) has an integer value between 0 and 255, which is calibrated to radiance. For each infrared (IR) image a calibration file is appended which converts the integer values to brightness temperature (equivalent blackbody temperature, T_B). The T_B interval associated with each integer value of digital IR data, ranges from about 0.5°C for the warmer temperatures to about 2.0°C for the colder temperatures. Thus, the IR images can be contoured, color enhanced, or shaded to a resolution of about 2.0°C at typical tropical cyclone cloud top temperatures.

The IR image data is sensed at the 11.2 micrometer wavelength at which the clear atmosphere is nearly transparent except for a small water vapor absorption and emittance. Therefore, T_B is largely a measure of the radiative temperature of the clouds or the earth's surface. However, with clouds having emissivity significantly less than 1.0, such as thin cirrus, the T_B is a measure of a combination of infrared emittance from both the thin cirrus and the surface or clouds below. In the tropics, large, very cold IR cloud areas are produced by ongoing deep cumulonimbus convection and mesoscale convective systems.

One of the advantages of digital IR satellite data as opposed to hard-copy satellite images, is that quantitative information can be extracted from the data in an objective and consistent manner. A data processing method was designed such that large volumes of IR data could quickly be processed and analyzed, but yet at the same time give the user considerable options to choose from a variety of derived quantities and cloud areas specified by T_B.

It is important that the IR data be analyzed with respect to the circulation center of the tropical cyclone or disturbance. The post-analysis positions of tropical cyclone

center locations were obtained from the Joint Typhoon Warning Center (JTWC). This is referred to as Best Track data. Along track interpolation was used to obtain center positions corresponding to satellite image times.

For this study in which the very early genesis periods are of primary interest, it was sometimes necessary to append additional positions to the Best Track data file. The JTWC Best Track data often included positions of the tropical disturbance several days before it was classified as a tropical depression. In a few cases when those positions were not available, the early positions were obtained by simply extrapolating the Best Track data backward in time. It was required that the Best Track data used for the IR data analysis extend at least two full days backward in time from first classification as a tropical depression. For a few select cases, satellite images were used to make small revisions to the Best Track data or to add positions to include not only the two days prior to tropical depression classification but also the initial formation of the pre-existing tropical disturbance. The satellite images were also used to obtain Best Track data for the non-developing tropical disturbance cases since no other Best Track data were available. Center positions were qualitatively determined from satellite image data according to apparent circulation centers or the approximate center of the associated deep convective cloud areas weighted by area.

After suitable Best Track data were obtained, the IR data were processed by the following method. First, the navigation information appended to each image file from the ISSCP archive, was used to locate the Best Track center location. 512 by 512 pixels were then sectorized, centered on the Best Track position. Images of this size were saved for additional image processing and display, including animation and hard copy enhanced images. Figure 2.1 shows matching visible and IR images. The IR images are enhanced as shown in Fig. 2.1c, with black thresholds corresponding to both $-65°$C and $-80°C$. This enhancement is used for all IR images throughout the paper. To save quantitative information from each image for quick access and analysis, a grid was used with 11 radial areas (e.g. 0-2° latitude, 2-4 ° latitude radius, etc.) and four quadrants (Fig. 2.2) which defined 55 different areas according to direction and distance from the Best Track center. The number of IR pixels for every digital value (T_B) were tabulated and saved for each grid area. Those "histogram" files were then used as input for various plotting routines.

The most useful of those routines is a time series plot where the user specifies one of the pre-defined grid areas, and a T_B temperature threshold. The plotting routine then accesses the "histogram" files for every Best Track position for a particular tropical cyclone, counts the number of pixels colder than the threshold for each image and plots a time series (Fig. 2.3). Since the area of each pixel is known, the plot shown is a time series of cloud areas relative to the center of the tropical cyclone. In Fig. 2.3, this is expressed as the percent area of the 2° latitude radius circle with T_B less than 75°C. Furthermore, it is well known that clouds with very cold T_B (near tropopause) are directly related to ongoing deep convection. The IR satellite data provide a quantitative assessment of the deep convective clouds and mesoscale convective systems. The amount, intensity and distribution of the deep convection is very important in assessing the dynamics of an evolving tropical cyclone. This IR data analysis technique has been used for other tropical cyclone studies and is suitable for investigating a wide variety of research topics in addition to tropical cyclogenesis (Zehr, 1987,1988; Shoemaker, 1989; Mundell, 1990; and Lubich and Zehr, 1989).

The primary interest of the present study is analysis of the time series plots for the periods preceding tropical storm stage and for non-developing tropical disturbances throughout their lifetime. Grid areas used, are primarily 0-2, 0-4, and 0-6° latitude radius circles. Generally, areas colder than T_B thresholds of $-60°$C to $-75°$C are used to evaluate the deep convective activity for a particular tropical disturbance or tropical depression.

Other satellite image products are used for various aspects of this study to augment the digital IR analysis. Animated satellite images (loops), which are simply a time series of satellite images viewed in rapid sequence on a TV monitor are a valuable satellite research tool. Two types of loops are used. A geography fixed reference frame shows actual cloud motions as viewed from the satellite. A "storm relative" loop uses satellite images which

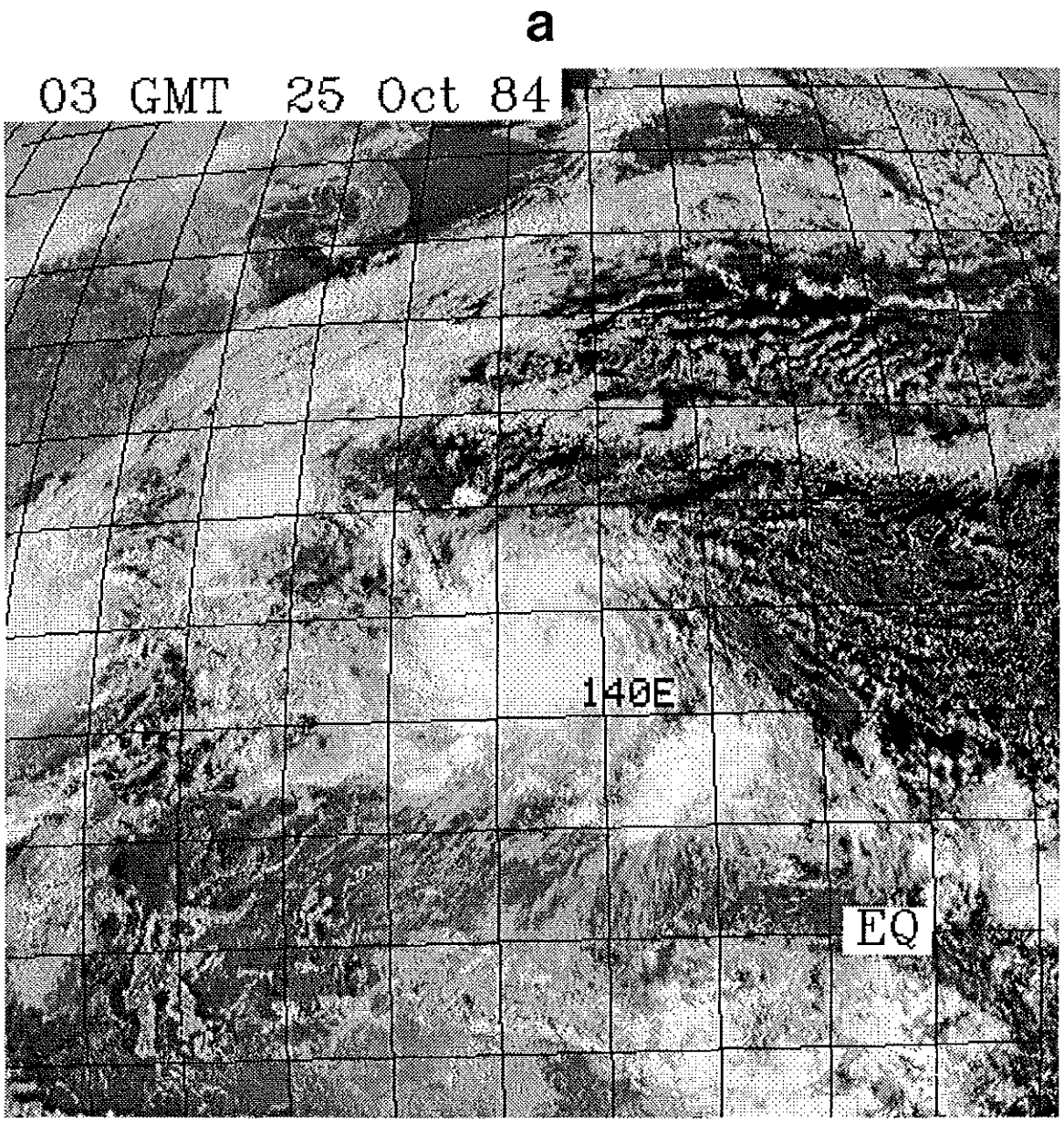

Figure 2.1: 512 x 512 10 km resolution matching sectors of GMS data. a) visible. b) infrared (IR). The IR data is enhanced as indicated, c) with $-65°C$ and $-80°$C thresholds. This same enhancement is used on all IR images throughout this paper.

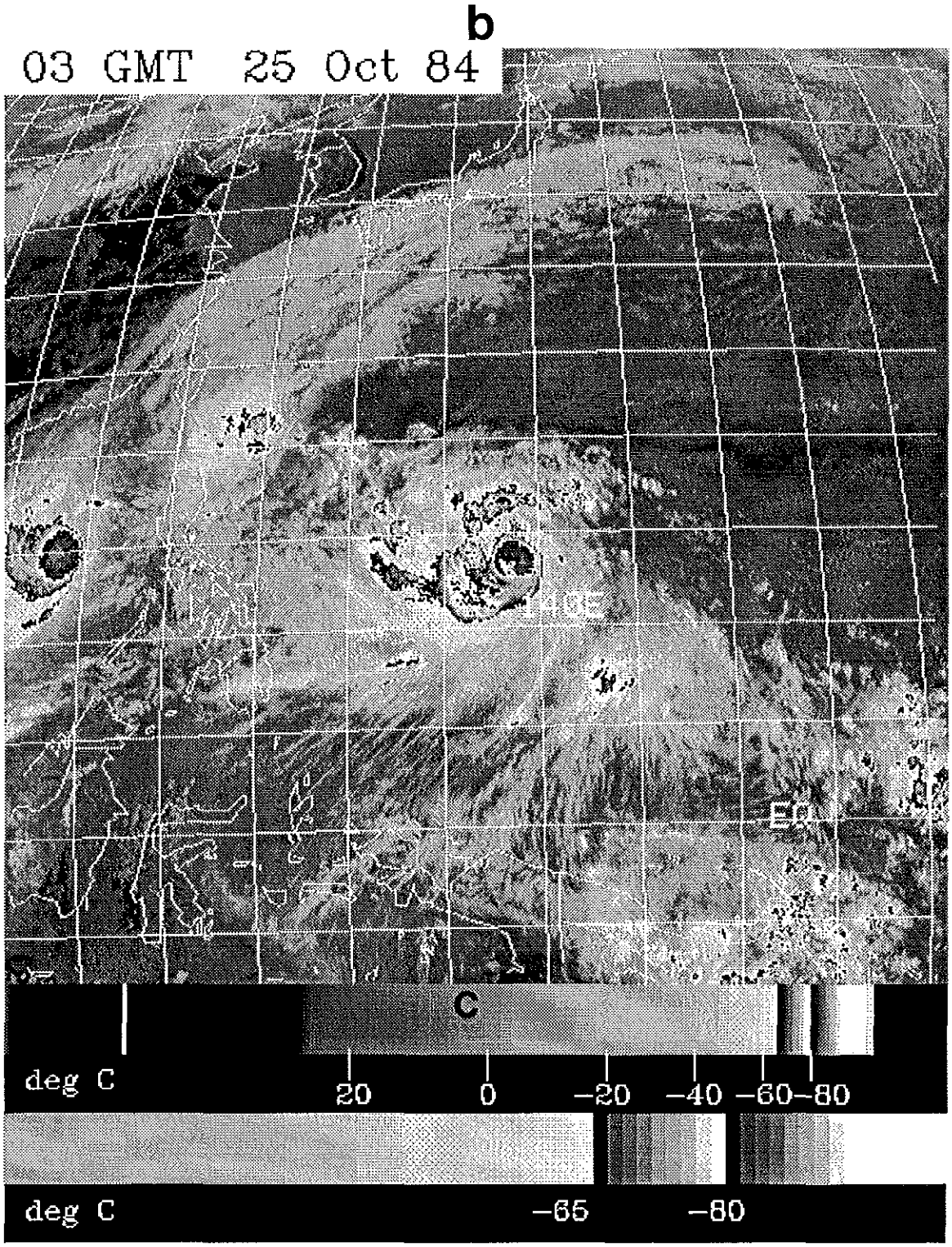

Figure 2.1: Continued.

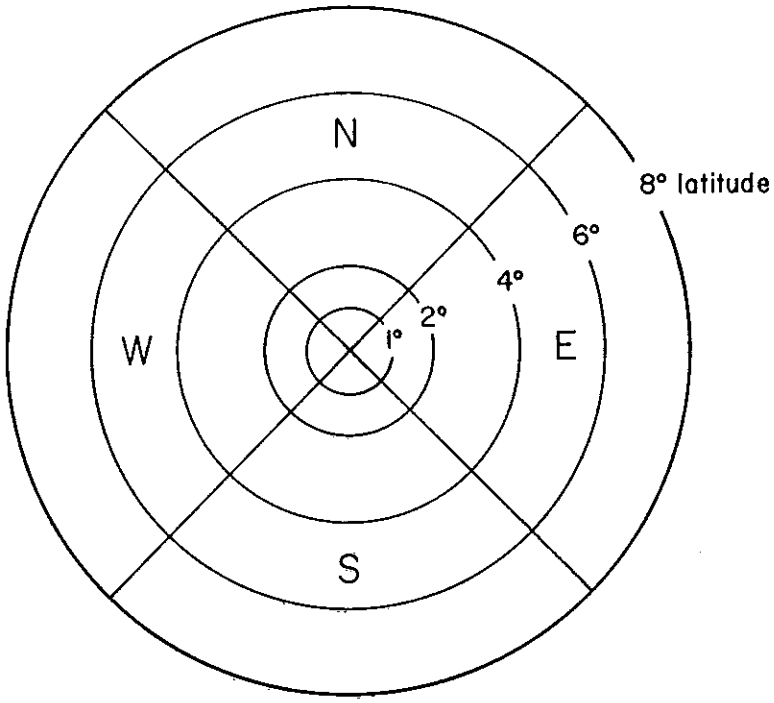

Figure 2.2; Grid used in IR data processing.

are centered on the Best Track center positions. This shows cloud motions relative to the tropical cyclone or disturbance center. The satellite loops are typically a sequence of 15 images representing a time period of about two days and are viewed with a pause on the final image. The satellite loops are essential in interpreting some of the important findings of this study.

Various image processing routines are available to generate high quality, color enhanced images from the digital GMS data. Both hard-copy color capability and color monitors are readily available. In addition, navigation information and graphic overlay capability allow aircraft observations and an objective analysis to be viewed with the satellite images (Fig. 2.4).

In addition, 3-hourly, full-disk, black-and white GMS images are available on microfilm. A few high resolution visible images from the DMSP and NOAA polar-orbiting satellites are also available. Those images were used in a recent study of tropical cyclone formation by Lunney (1988).

2.2 Aircraft Reconnaissance Data

Observations from the U.S. Air Force reconnaissance missions during 1977 through 1984 have been compiled at Colorado State University by Dr. William M. Gray and staff. The data have been used for previous studies of typhoon wind profile variability (Weatherford, 1985, 1989; Weatherford and Gray, 1988a, 1988b) and tropical cyclone formation (Lunney, 1988 and Middlebrooke, 1988). The observations were taken aboard WC-130 aircraft at 15-minute intervals. They include measurements of sea surface temperature, flight level temperature and dew point, flight level wind direction and speed, and sea-level pressure extrapolated from a flight-level D-value (Henderson, 1978). Two types of flight missions are flown: investigative missions (invests) and fix missions. The invests are flown at low-level (457.2 m = 1500 ft) constant elevation into tropical weather systems which are not well-developed tropical storms. The purpose is to determine whether are not a

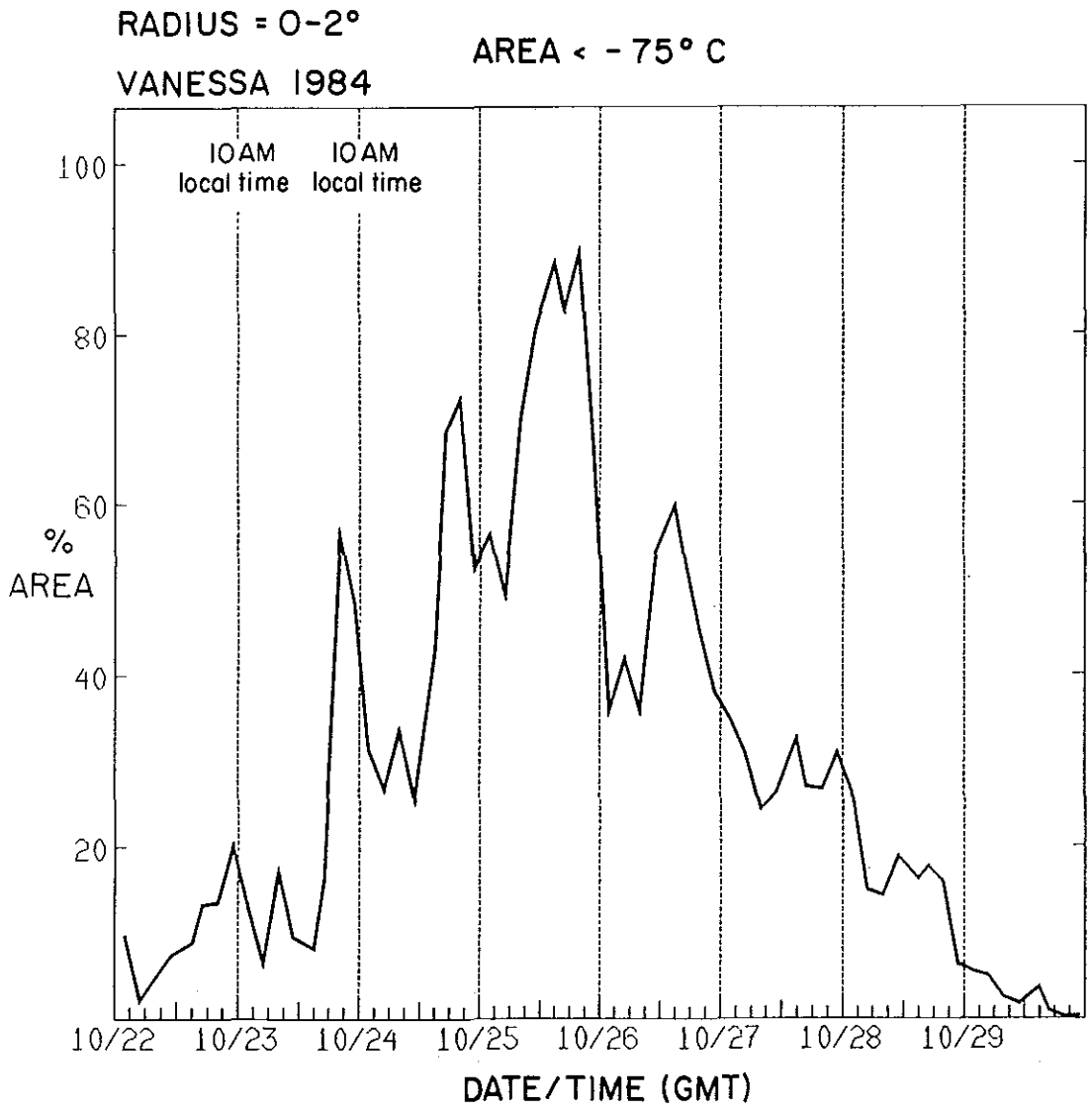

Figure 2.3: Percent area with T_B less than –75° for Typhoon Vanessa in the area of 0–2° latitude radius.

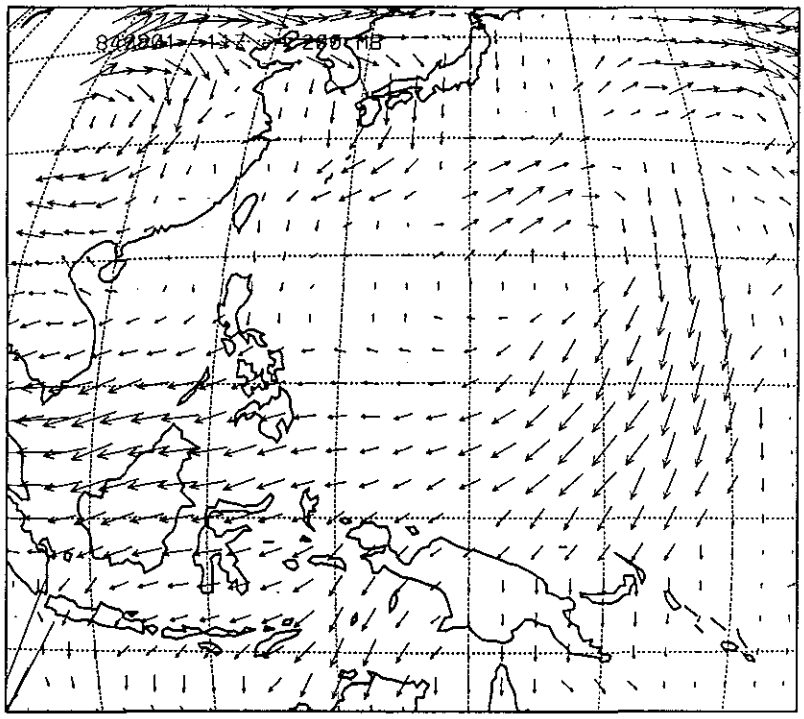

Figure 2.4: 200 mb wind vectors from a 2.5° latitude resolution objective analysis plotted in GMS satellite projection. Length of arrow is proportional to wind speed.

tropical cyclone-scale cyclonic circulation center exists in a suspect area. Thus a specific flight pattern may not be followed. In contrast, fix missions fly a specific flight pattern at 700 mb constant pressure surface to pinpoint the location of a tropical cyclone already known to exist.

The flight data used for this study are from the invest flights during 1983 and 1984, which include 162 flights into the early stages of 45 tropical disturbances which eventually attained at least tropical storm intensity (17.5 ms^{-1}). Of those, 28 later developed into typhoons. In addition, there were 16 flights into 12 tropical disturbances which did not develop into tropical cyclones and 12 flights into 3 disturbances which were eventually designated as tropical depressions but did not become tropical storms.

Examples of wind and pressure observations from an invest flight are plotted in Fig. 2.5. Each flight typically includes 6-8 hr of observations at 15-min interval within the tropical disturbance area. During this time, a low-level circulation center may typically move 170-230 km, assuming a propagation speed of 8 ms^{-1}. Since wind speeds are relatively weak, subtracting the propagation vector from the observed wind vectors may result in a quite different wind pattern (Fig. 2.5b). Therefore, it is important that observations be analyzed in a "storm relative" framework, in which the winds are computed and plotted relative to a moving tropical disturbance center, given by the Best Track positions.

It is also desirable for analysis purposes to compute certain quantities such as divergence and relative vorticity. If the observations are well distributed around a tropical disturbance, a representative value of vorticity or divergence can be obtained from a single invest flight. For the purposes of this study, the components of relative vorticity and radial wind from each wind observation are averaged. The computations are with respect to circular areas centered on the disturbance, in the storm motion relative coordinates, and give estimates of mean relative vorticity and divergence within the specified circular areas. One of the more useful observations from the invest flights is the minimum sea-level pressure (MSLP). The MSLP, generally located near the low-level circulation center, gives a good estimate of the degree of tropical cyclone development and is related to the maximum surface winds of a disturbance.

2.3 Conventional Data

Radiosonde observations, cloud drift wind vectors, aircraft data, and surface observations including ships, are analyzed twice daily (00 and 12 GMT). An objective interpolation scheme quantifies standard meteorological variables to a 2.5° latitude resolution grid at standard pressure levels. The analyses include routinely available operational data and do not include any special observing networks or programs. The cloud drift wind vectors are particularly important for tropical analysis. The Japan Meteorological Agency (JMA) produces twice daily (00 and 12 GMT) cloud drift wind vectors, which are incorporated into the objective analysis and are also published in a widely distributed monthly report (JMA, 1983, 1984).

Objective analyses of this type from two sources are used in this study. Daily wind vector and isotach analyses at 850 mb and 200 mb are available from the European Centre for Medium-range Weather Forecasts (ECMWF, 1983, 1984). In addition, a data set was obtained on magnetic tape from the Australia Bureau of Meteorology Research Centre (BMRC), for 1984, which includes twice daily, 2.5° latitude resolution objective analyses of wind data on standard pressure levels, and surface (sea-level) pressure. Details of the analysis technique for the BMRC data are found in Davidson and McAvaney (1981). Derived products and contoured data fields such as divergence, relative vorticity, sea-level pressure, streamlines-isotachs are particularly useful for case studies. Also, the BMRC data set is used for the quantitative comparison of non-developing and pre-tropical storm disturbances presented in Chapter 6.

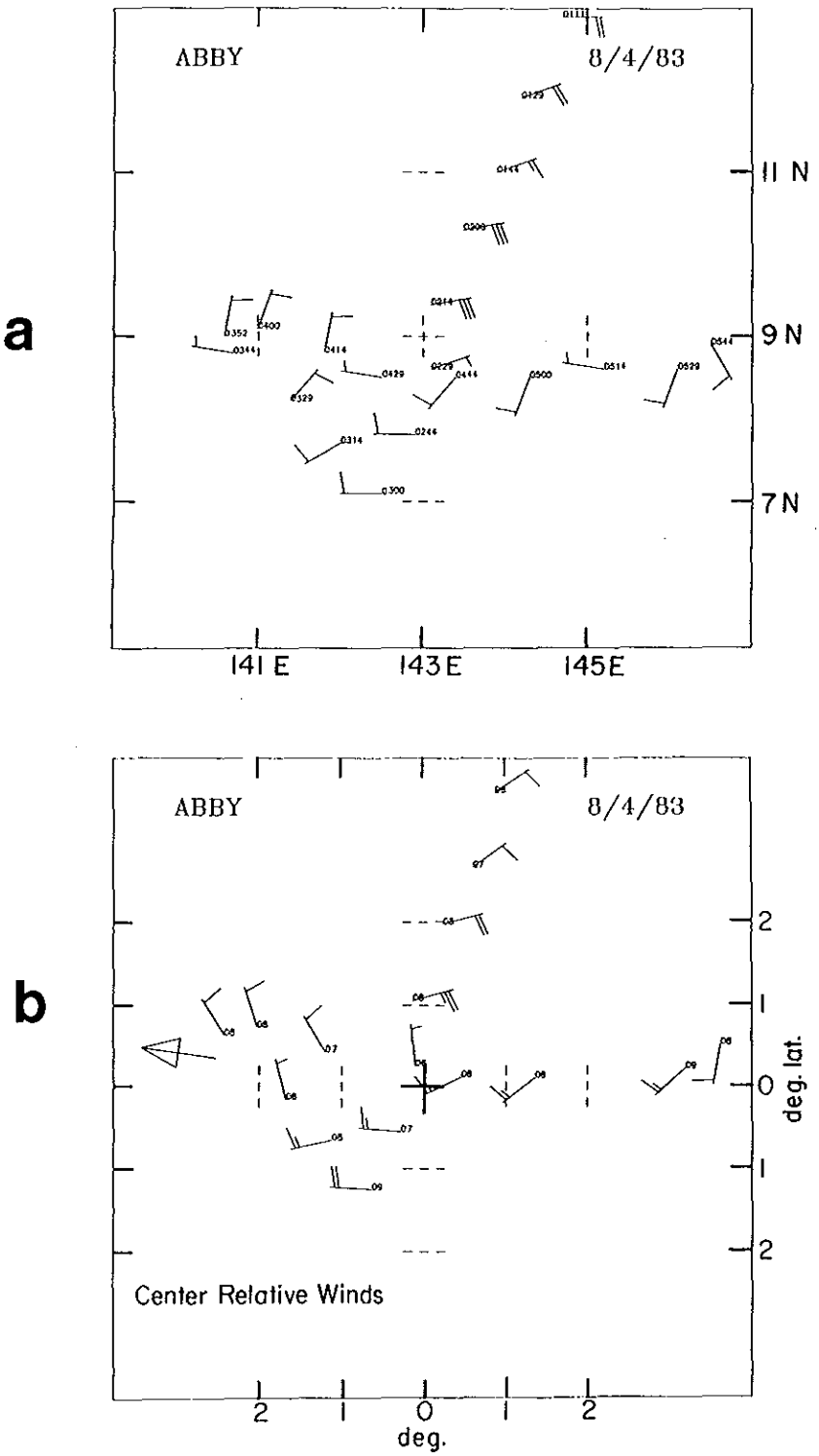

Figure 2.5: a) Wind observations from an investigative flight. Time (GMT) of each observation is plotted. (One full barb = 5 ms^{-1}). b) Same observations as in (a), plotted relative to center location, with center movement vector (direction shown by the arrow) subtracted from each observation.

Chapter 3

GMS IR SATELLITE DATA ANALYSIS

3.1 Characteristics of Deep Convective Clouds Associated with Tropical Cyclones

Time series of cloud areas with IR temperature (T_B) colder than –65°C associated with each of the 1983-1984 western North Pacific tropical cyclones have been analyzed for all available GMS satellite data. The plotted data is interpreted such that the size of the cold IR cloud area is proportional to the magnitude of the ongoing deep cumulonimbus convection. Figure 3.1a is a plot of this type, for Typhoon Vanessa during its entire life cycle including the pre-tropical storm disturbance. Figure 3.1b is the corresponding plot of aircraft observations of MSLP. Vanessa was an unusually large and intense tropical cyclone, attaining supertyphoon intensity (MSLP < 925 mb) for 36 hr. Typhoon Agnes (Fig. 3.2) was more typical with smaller cold IR cloud areas and a maximum wind of 60 ms^{-1}.

This type of analysis for the entire 1983-1984 data set reveals characteristics common to the majority of cases. Three of the more notable characteristics are as follows:

1. There is a very large diurnal variation with a maximum around 0600 local time (Zehr, 1987).

2. The overall trend of deep convection (24 hr running mean) attains a maximum near the time of maximum intensity increase (most rapid deepening) (Zehr, 1988).

3. There is a convective maximum associated with the pre-tropical storm disturbance before it is even classified as a tropical depression.

Of primary interest to the present study is the third characteristic, that of a very early convective maximum during the formative stages (Figs. 3.1a, 3.2a). Several additional examples of this early convective maximum are shown in Fig. 3.3. Note that there is a period of at least 24 hr following the early convective maximum during which the convection is significantly reduced. The occurrence of the early convective maximum is typically not strongly effected by the T_B threshold or area specified for the time series plot.

3.2 Convective Maximum Associated with Tropical Cyclogenesis

3.2.1 Occurrence and Definition of the Early Convective Maximum

The early convective maximum is defined objectively by the 2° latitude radius area (R = 0–2°) with IR temperature (T_B) colder than –65°C. The early convective maximum occurs at the time of maximum R = 0–2°, T_B < –65°C, area provided that it 1) precedes first designation as a tropical depression, and 2) a 24 hr period including this maximum has a greater average R = 0–2°, T_B < –65°C, area than the 24 hr period following it. Using this specific definition, 58% of the cases have an early convective maximum. For an additional five cases, the early convective maxima are determined by using a different area and IR temperature threshold. For six cases, the early convective maxima are subjectively determined using the microfilm images. The use of the microfilm data is occasionally

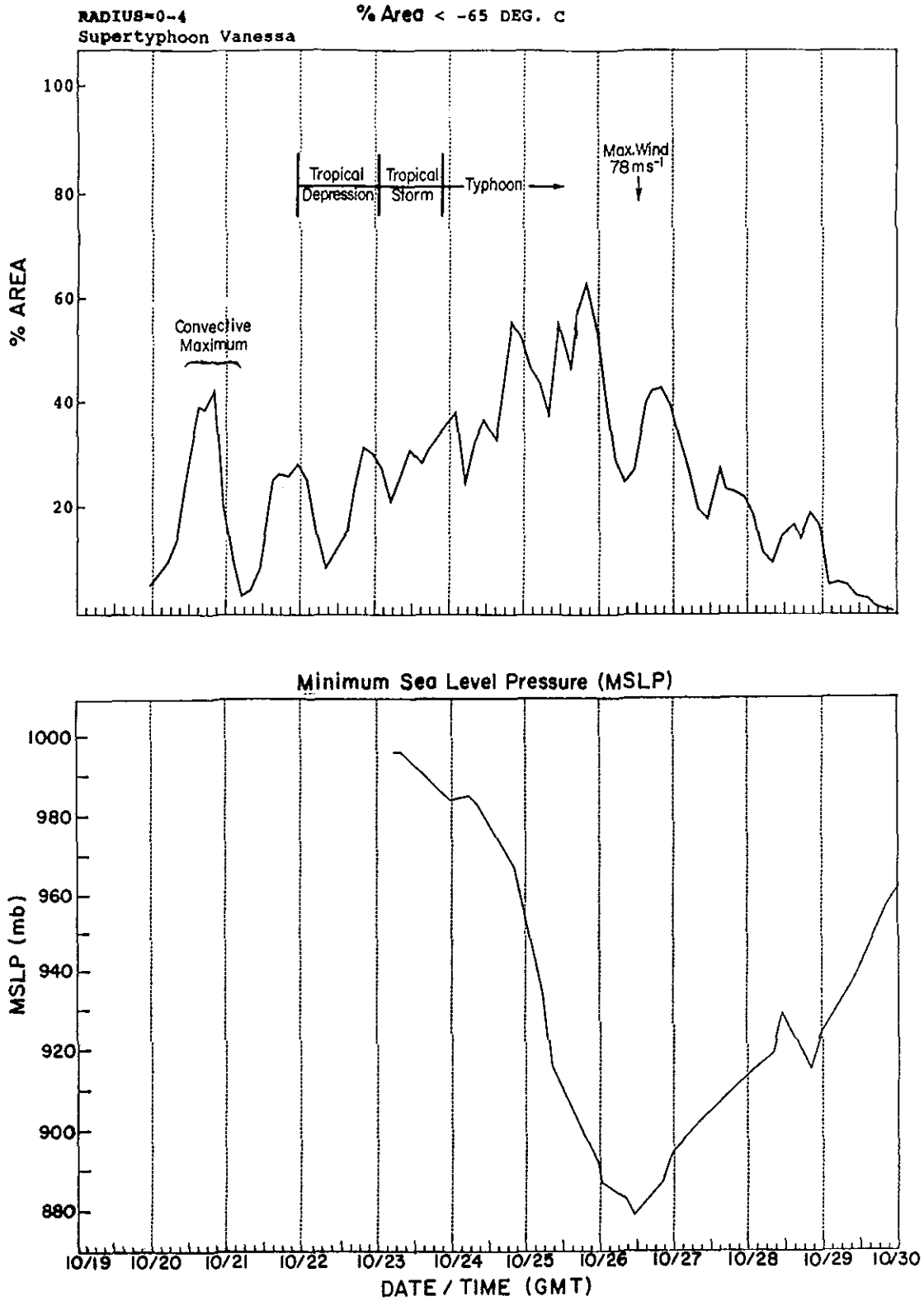

Figure 3.1: Typhoon Vanessa, 1984. a) Time series of percent area at R = 0–4° with $T_B < -65$°C. The time and magnitude of the maximum sustained surface wind speed are indicated. b) Corresponding MSLP (mb) from aircraft observations. Date/Time is in GMT with month/day labels. Vertical lines are about 10 AM local time.

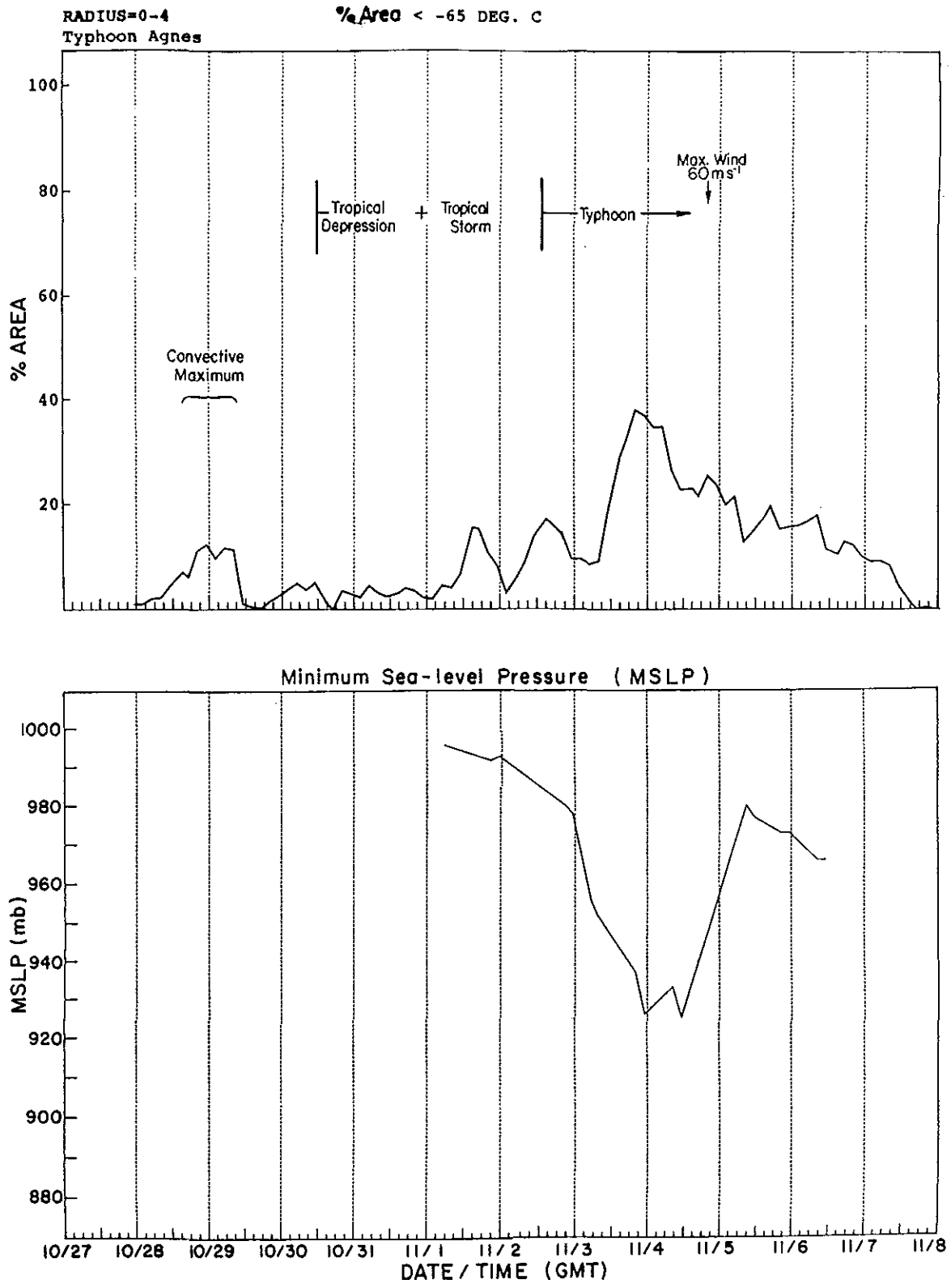

Figure 3.2: Same as Fig. 3.1, except for Typhoon Agnes, 1984.

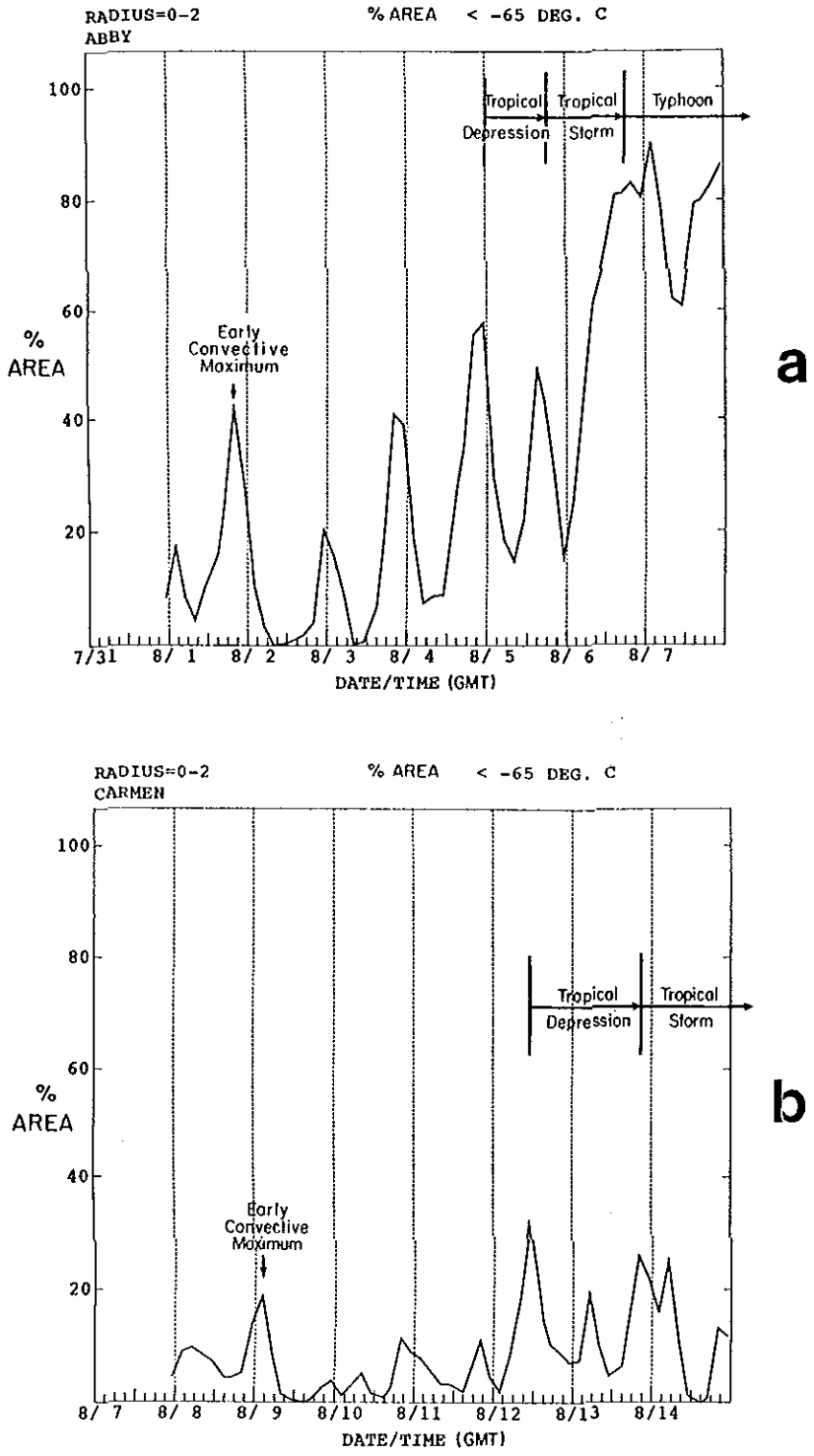

Figure 3.3: Examples of an early convective maximum in time series plots of percent area, R = 0–2° with T_B < –65°C. a) Abby, 1983. b) Carmen, 1983. c) Ogden, 1984. d) Doyle, 1984.

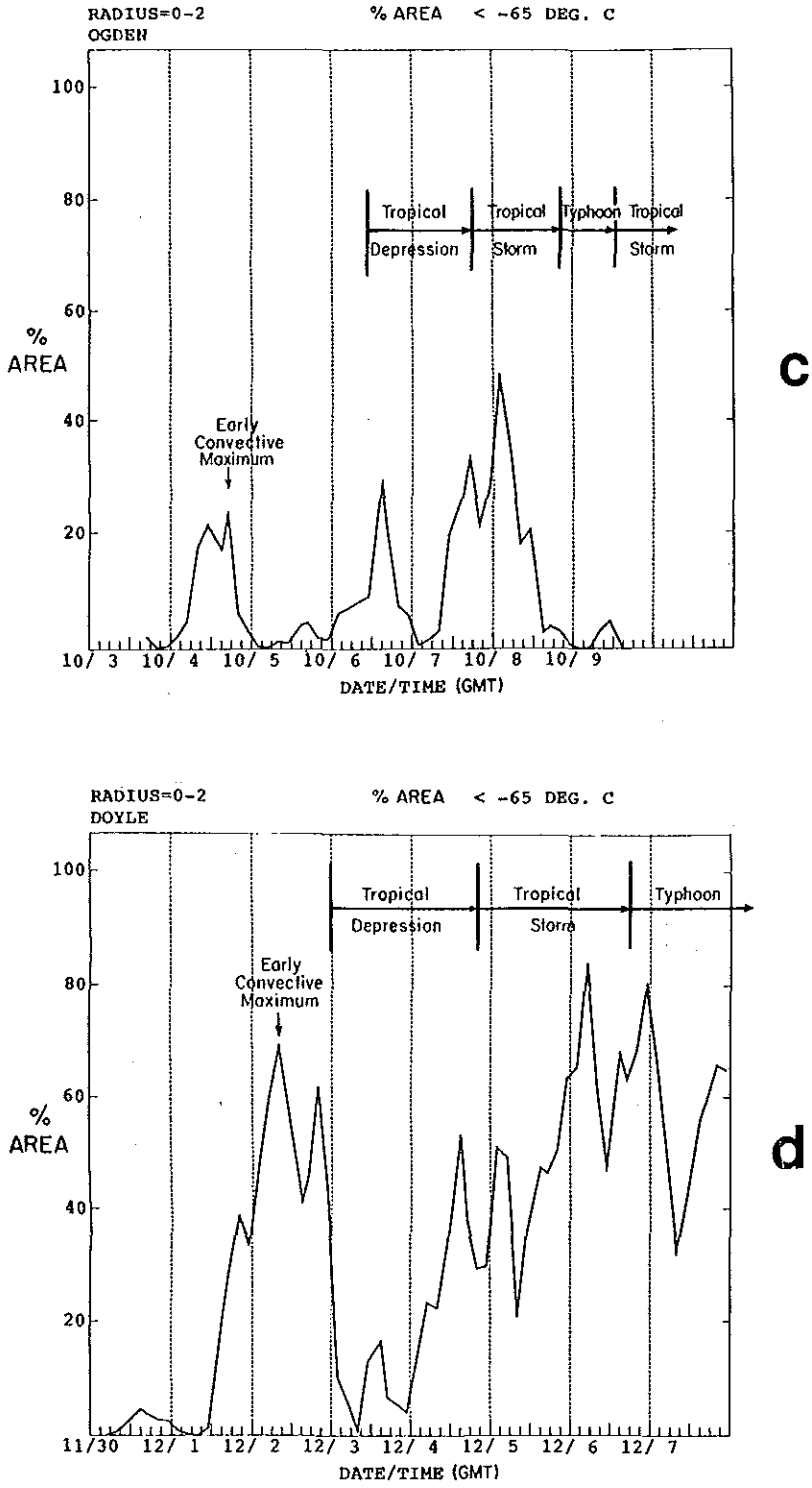

Figure 3.3: Continued.

needed due to missing digital data or inadequate Best Track data. The overall results of the analysis of early convective maximum occurrence are summarized in Table 3.1. Whether or not an early convective maximum is identified, and the method used, are denoted for each case under the column, labeled "Occurrence". A large majority of the tropical cyclones (80%) have an early convective maximum, while ten cases do not have this feature.

The time series plot of cold IR area for one of the 20% of cases which did not have an early convective maximum is shown in Fig. 3.4. Note that even though there is significant convection prior to the tropical depression stage, it is followed by even greater convection in the next 24 hr. Therefore, it does not satisfy the conditions of an early convective maximum. This case might then be analyzed as having a short tropical cyclogenesis period. Lee (1986) designated some of his individual cases as "fast genesis". This appears to be a genesis case of that type.

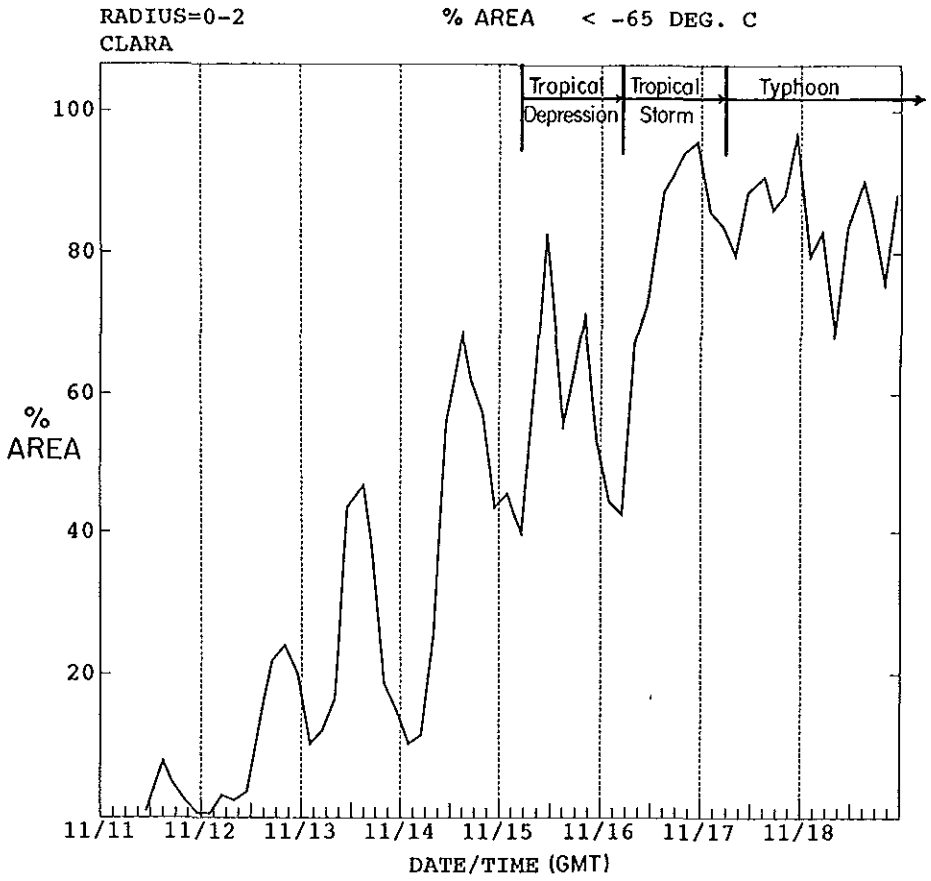

Figure 3.4: Time series of percent area R = 0–2° with T_B < –65°. Typhoon Clara, 1984. An early convective maximum is not observed.

3.2.2 Time of Early Convective Maximum

Typically, the convective maximum precedes first designation as a tropical storm by about three days. However, this time interval is highly variable. The average time interval between the early convective maximum and first tropical depression (TD) designation is 50.2 hr (2.1 days). This convective maximum precedes first designation as a tropical storm (TS) by an average of 76.2 hr (3.2 days). These time intervals are listed in Table 3.1. The

Table 3.1: Characteristics of the early convective maximum.

TC NAME	GENESIS PERIOD	OCCURRENCE OBSERVED with method A	B	C	NOT Observed	TIME (da:hr) Preceding TD	TS	AMPLITUDE % of R = 0–2° area with T_B < −65°C	−75°C
	1983								
TS Sarah	18–25 Jun			X		4:15	6:09	–	–
TY Tip	5–10 Jul			X		3:21	4:18	–	–
TY Vera	8–12 Jul			X		0:09	3:15	–	–
STY Wayne	18–22 Jul			X		2:03	3:12	–	–
STY Abby	1–5 Aug	X				3:03	3:21	42	10
TS Ben	11–12 Aug		X			0:09	0:15	–	–
TS Carmen	9–13 Aug	X				3:09	4:18	19	6
TS Dom	17–19 Aug	X				0:09	1:09	49	26
TY Ellen	26 Aug–2 Sep	X				1:15	2:06	44	20
STY Forrest	18–20 Sep	X				1:15	1:21	89	64
TS Georgia	28 Sep				X	–	–	–	–
TS Herbert	3–7 Oct	X				3:09	3:21	68	26
TY Ida	5–7 Oct			X		2:15	2:18	–	–
TY Joe	6–11 Oct	X				2:18	4:18	36	22
TS Kim	12–16 Oct	X				3:06	4:06	10	2
TY Lex	19–22 Oct	X				3:00	3:06	39	14
STY Marge	28–31 Oct	X				2:06	3:06	37	13
TS Norris	7–8 Nov				X	–	–	–	–
TY Orchid	14–17 Nov				X	–	–	–	–
TY Percy	17–19 Nov				X	–	–	–	–
TS Ruth	19–27 Nov	X				1:12	8:09	43	34
TS Sperry	30 Nov–3 Dec			X		3:00	3:06	–	–
TS Thelma	12–15 Dec	X				1:18	3:00	65	39
	1984								
TS Vernon	6–9 Jun	X				1:03	2:09	28	6
TS Wynne	19–19 Jun				X	–	–	–	–
TY Alex	30 Jun–1 Jul				X	–	–	–	–
TS Betty	2–7 Jul	X				1:21	4:15	27	6
TY Cary	5–7 Jul	X				0:21	1:15	26	4
TY Dinah	21–24 Jul	X				2:03	2:21	19	4
TY Ed	25 Jul				X	–	–	–	–
TS Freda	4–5 Aug	X				1:06	1:18	55	39
TS Gerald	14–15 Aug	X				1:12	1:18	20	10
TY Holly	12–15 Aug	X				2:18	2:18	19	8
TY Ike	25–27 Aug	X				1:00	1:06	44	27
TS June	25–27 Aug	X				2:00	2:12	27	13
TY Kelly	11–13 Sep		X			1:03	1:21	–	–
TS Lynn	23–24 Sep				X	–	–	–	–
TS Maury	25–27 Sep				X	–	–	–	–
TS Nina	25–28 Sep		X			1:18	2:06	17	10
TY Ogden	4–7 Oct	X				1:18	3:00	23	10
TY Phyllis	8–11 Oct	X				1:03	2:03	57	46
TS Roy	8–11 Oct	X				1:21	2:09	33	13
TS Susan	10–12 Oct	X				1:00	1:21	29	8
TY Thad	17–19 Oct		X			0:18	1:09	–	–
STY Vanessa	20–23 Oct	X				1:12	2:12	76	52
TY Warren	18–23 Oct	X				4:12	5:00	52	37
TY Agnes	28 Oct–1 Nov	X				1:12	3:03	22	10
STY Bill	2–8 Nov		X			5:03	5:21	–	–
TY Clara	13–15 Nov				X	–	–	–	–
TY Doyle	2–4 Dec	X				0:03	2:09	70	43
AVERAGE						2:02 (50.18 hr)	3:04 (76.20 hr)	39.5	20.7
TOTAL		29	5	6	10				
PERCENT		58%	10%	12%	20%				
			40 80%						

Method A: Digital data: R=0–2°, T_B < −65°C
Method B: Digital data, with a different R and T_B
Method C: Microfilm Images

tropical cyclogenesis period begins near the time of convective maximum and ends with tropical storm designation and is referred to as the "genesis period". The distribution of the genesis period time intervals is shown in Fig. 3.5. The genesis period varies greatly among individual cases, ranging from less than a day to more than eight days. If one considers the 20% of cases with no early convective maximum (Fig. 3.4) as having shorter genesis periods, this changes the distribution slightly in Fig. 3.5 and decreases the average time intervals in Table 3.1. If the genesis periods for those ten cases are designated by the time from first tropical depression to first tropical storm, the overall average genesis period is 69.8 hr (2.9 days).

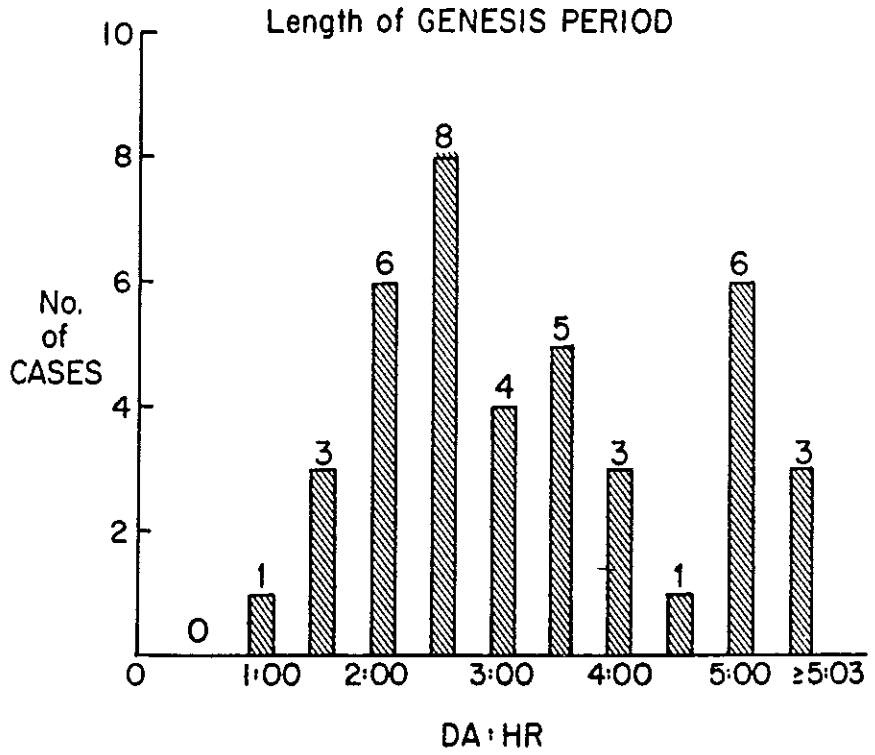

Figure 3.5: Histogram in 12 hr increments of the time interval between the early convective maximum and first designation as a tropical storm. The DA:HR label refers to the preceding 12 hr interval. (2:00 = 1:12–2:00).

3.2.3 Amplitude of Early Convective Maximum

The amplitudes of the early convective maximum are also highly variable as shown in Figs. 3.1, 3.2, and 3.3. The amplitude is strongly dependent on the T_B threshold. The amplitudes for two IR temperature thresholds, –65°C and –75°C, are also listed in Table 3.1. The amplitudes are expressed in percent coverage of the R = 0–2° area, ranging from 2 to 52% for $T_B < -75$°C, and 10 to 89% for $T_B < -65$°C. The average amplitudes are 20.7% and 39.5% for –75°C and –65°C thresholds, respectively.

To evaluate the magnitude of the early convective maximum, those amplitudes are compared to the average maximum areas during tropical depression, tropical storm, and typhoon stages in Table 3.2. The amplitudes for the later stages are only slightly greater than the average amplitude of the early convective maximum. Using the Table 3.2 averages and additional information on the average duration of each stage, a typical time series of cold IR cloud areas is depicted in Fig. 3.6.

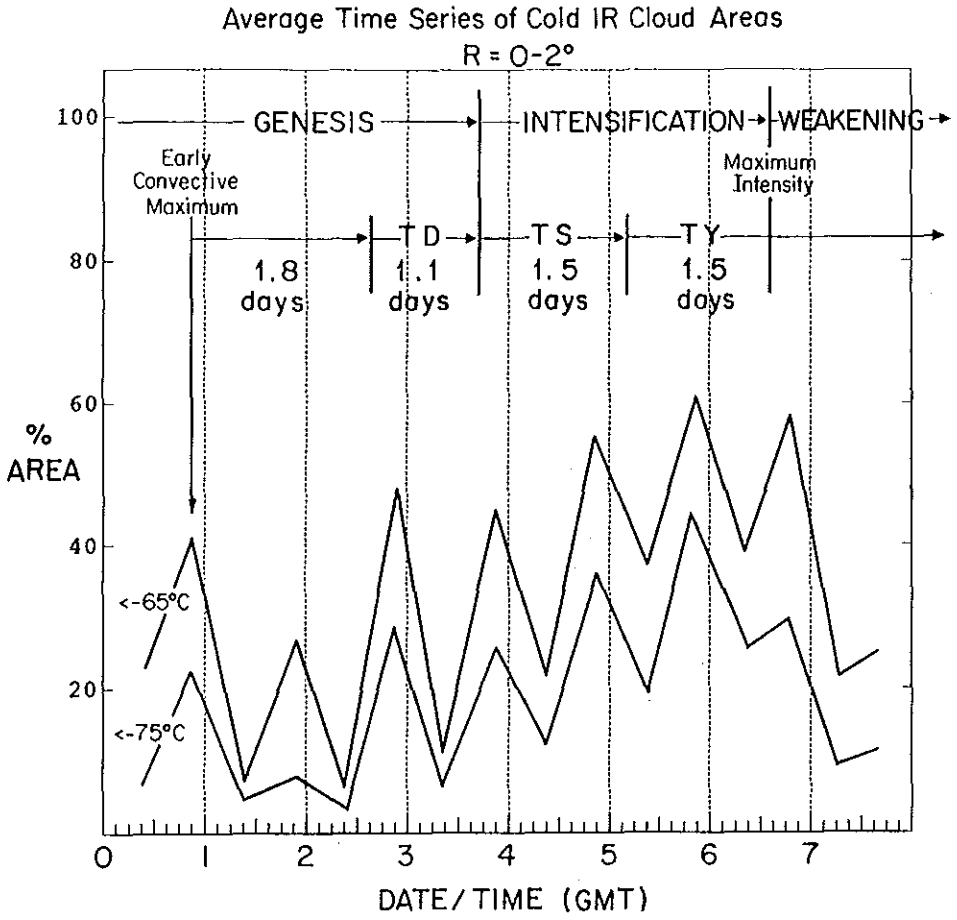

Figure 3.6: Typical time series of cold IR areas during the genesis period.

Table 3.2: Average amplitudes of the convective maxima.

Type	% area R = 0–2° T_B < –65°C	% area R = 0–2° T_B < –75°C
Early	40	21
Tropical Depression	47	27
Tropical Storm	53	35
Typhoon	60	37

3.2.4 Satellite Image Characteristics

A qualitative description of what one sees in the IR and visible satellite loops is very important. Although there is high variability among individual cases, several prevalent common characteristics can be identified.

Before the early convective maximum occurs, there is little or no curvature in the deep convective cloud bands, or there are no bands at all. There may be evidence of a broad-scale cyclonic circulation in the middle or low levels, but there are usually no signs of a tropical cyclone scale circulation center.

After the convective maximum: 1) well-defined, persistent, cyclonic curvature in the deep cumulonimbus clouds first appears. 2) a distinct circulation center often appears for the first time. 3) the overall deep convection significantly decreases for at least 24 hr. Visible and infrared satellite images showing pre-tropical storm disturbances which exhibit the above characteristics are shown in Fig. 3.7. The IR images show the typical appearance of the pre-tropical storm disturbance before (Fig. 3.7a), during (Fig. 3.7b), and after (Fig. 3.7c) the early convective maximum. This example is from pre-tropical storm Ruth and depicts a very prominent early convective maximum. Some cloud pattern features have a more distinct appearance in visible images. A series of visible images (Figs. 3.7d,e,f) show a distinct early convective maximum with the pre-tropical storm Doyle disturbance.

3.2.5 A Secondary Convective Maximum Associated with Tropical Cyclogenesis

A secondary convective maximum is often observed just prior to or during the tropical depression stage, although it is not as frequent an occurrence as the early convective maximum. A distinct secondary convective maximum is noted in the R = 0–2°, T_B < –65°C, time series in Fig. 3.8. This characteristic is also present in Figs. 3.3a and 3.3b. In fact, with Joe (Fig. 3.8) and Carmen (Fig. 3.3b), this secondary maximum is the overall maximum for the entire lifetime of the tropical cyclone. Any maximum of the R = 0–2°, T_B < –65°C area is termed a secondary convective maximum if it is followed by a 24 hr period with smaller average cold IR area and occurs prior to tropical storm stage. Using this criteria, 52% of the cases have a secondary convective maximum.

3.2.6 Concentration of Convection Near the Center

Some of the pre-tropical storm disturbances have a distinct tendency for the cold IR areas to become concentrated near the center, particularly during the tropical depression stage. This characteristic is illustrated in Fig. 3.9 by time series plots of T_B < –75°C areas for R = 1–2° and R = 0–1°, as well as the ratio of those two areas. The ratio plot (Fig. 3.9c) is computed using a 24 hr running mean of the data. During tropical depression stage, the R = 0–1° cold IR area increases, while at the same time it decreases in the R = 1–2° area. This is denoted in Fig. 3.9 as the concentration period.

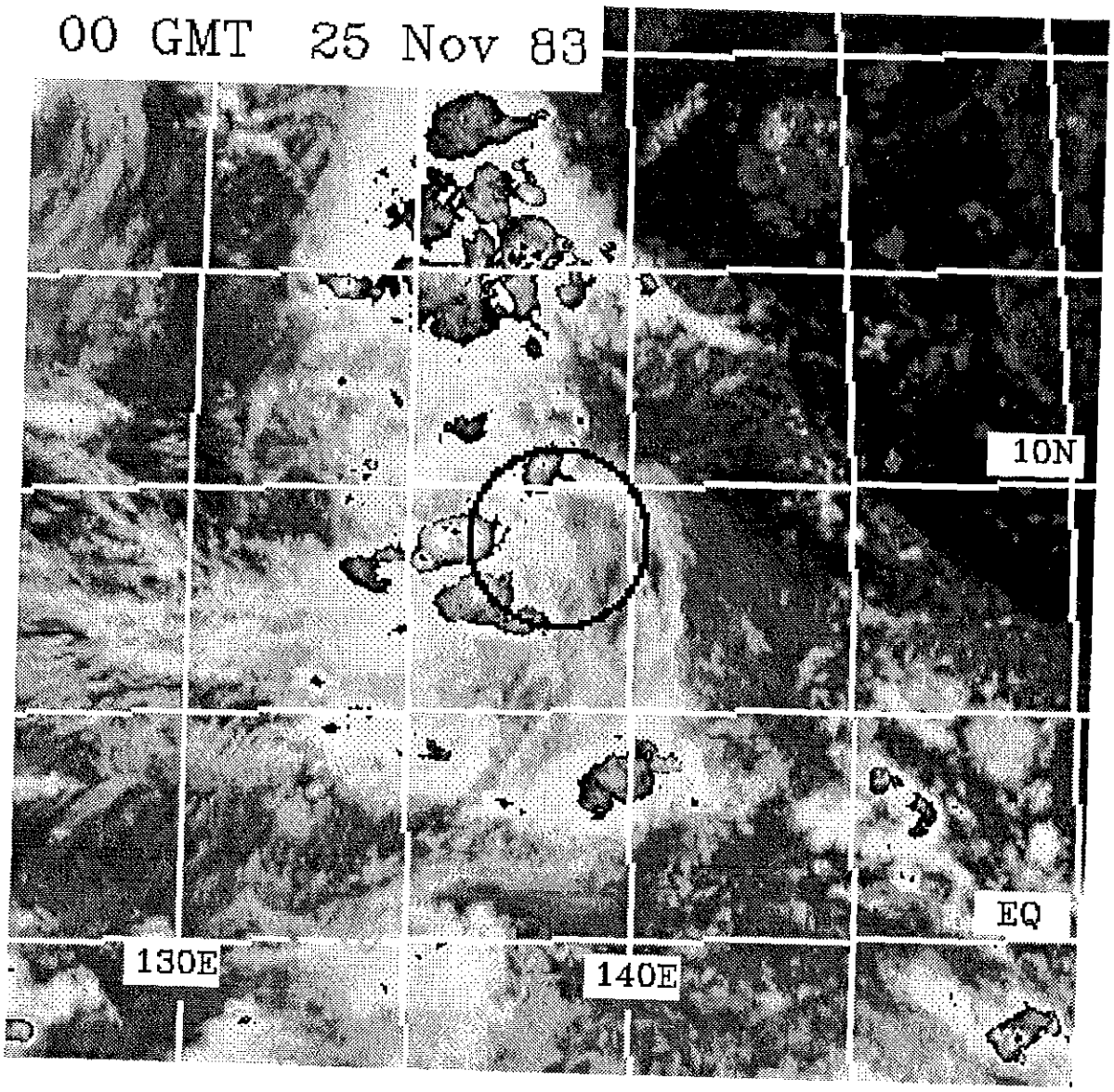

Figure 3.7: Satellite images before, during and after the early convective maximum. Enhanced IR images, Ruth, 1983. a) Before, 00 GMT 25 Nov. b) During, 12 GMT 25 Nov. c) After, 12 GMT 27 Nov. Visible images, Doyle, 1984. d) Before, 03 GMT 1 Dec. e) During, 03 GMT 2 Dec. f) After, 03 GMT 3 Dec.

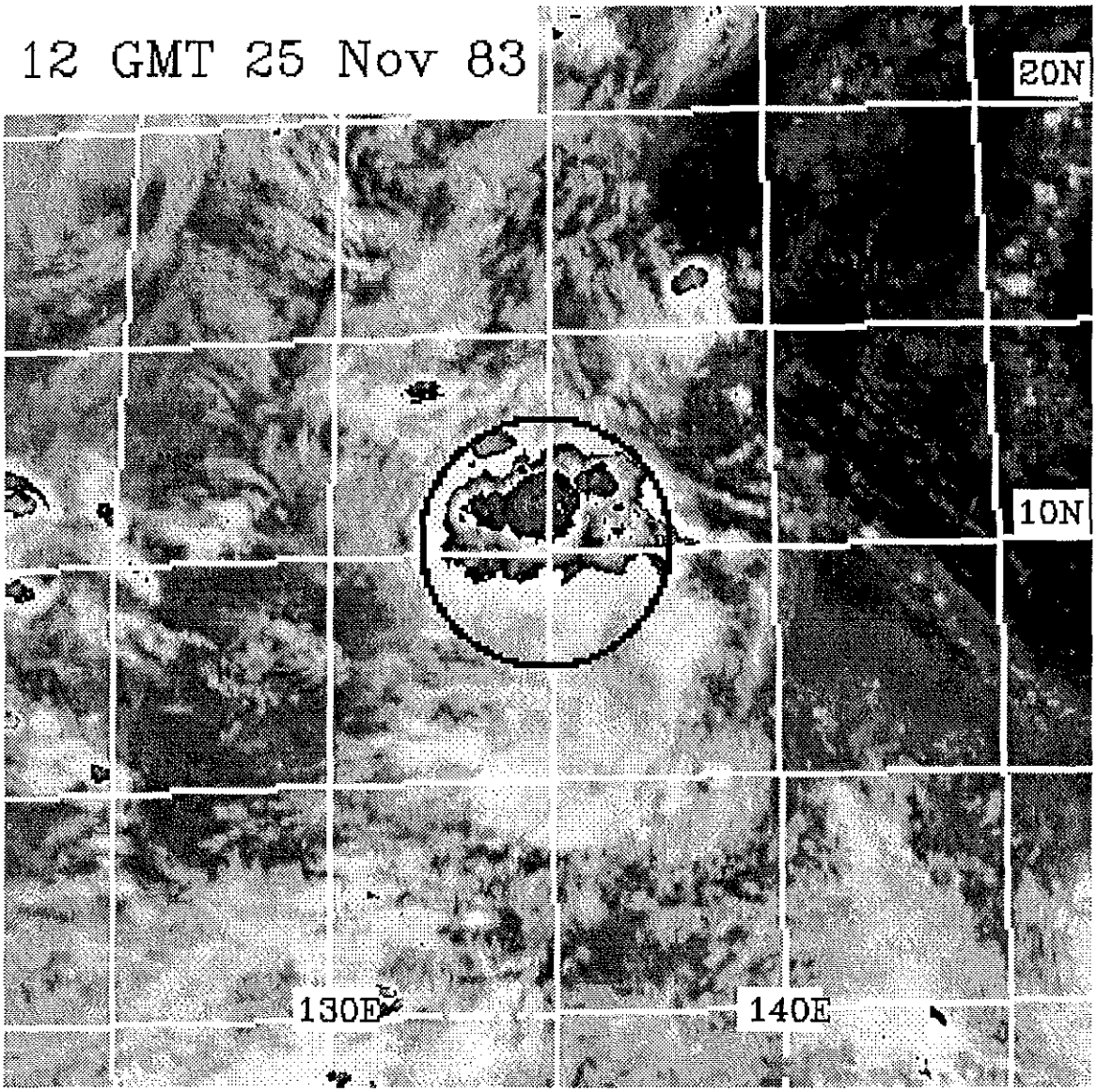

Figure 3.7: b.

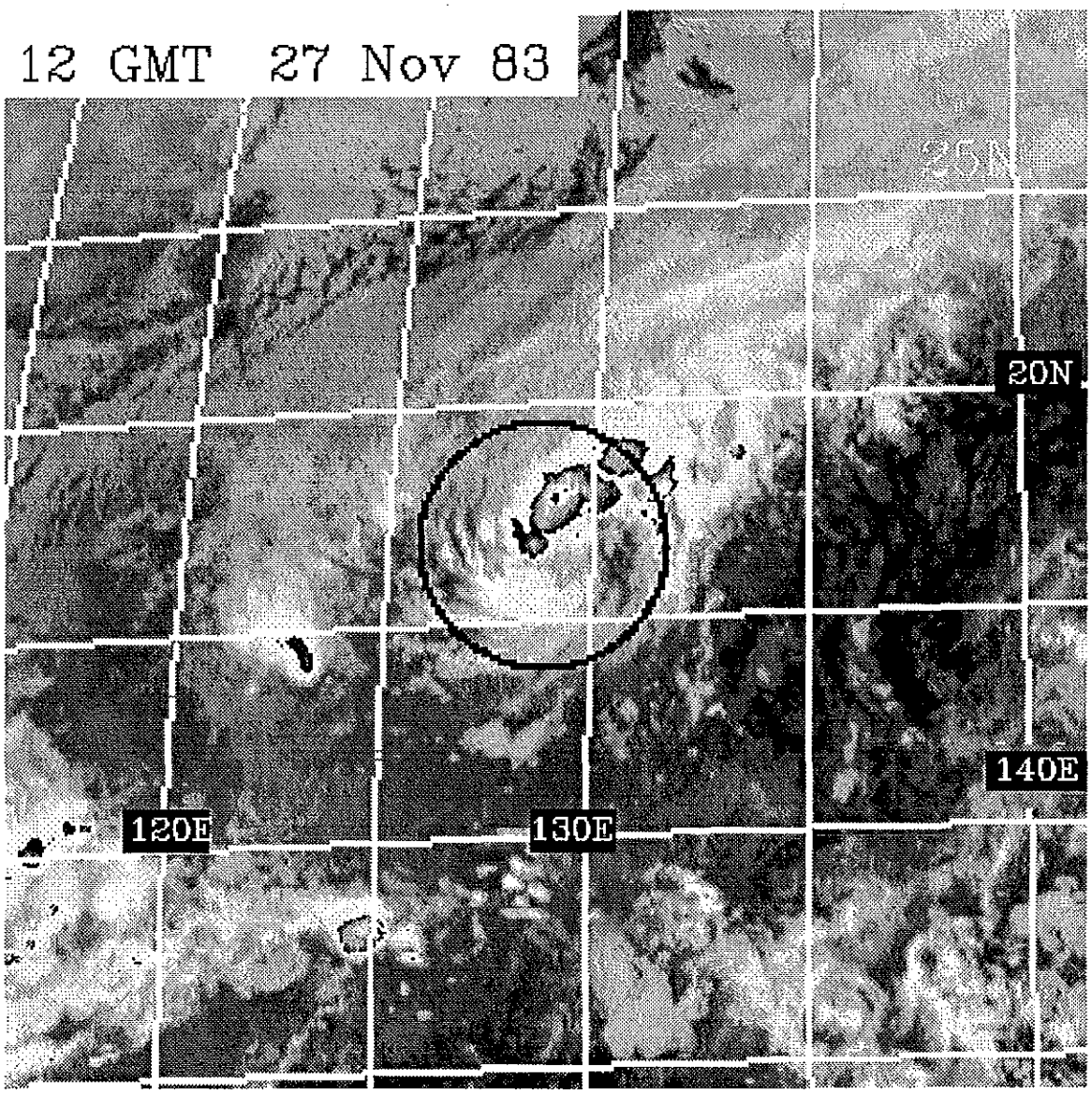

Figure 3.7: c.

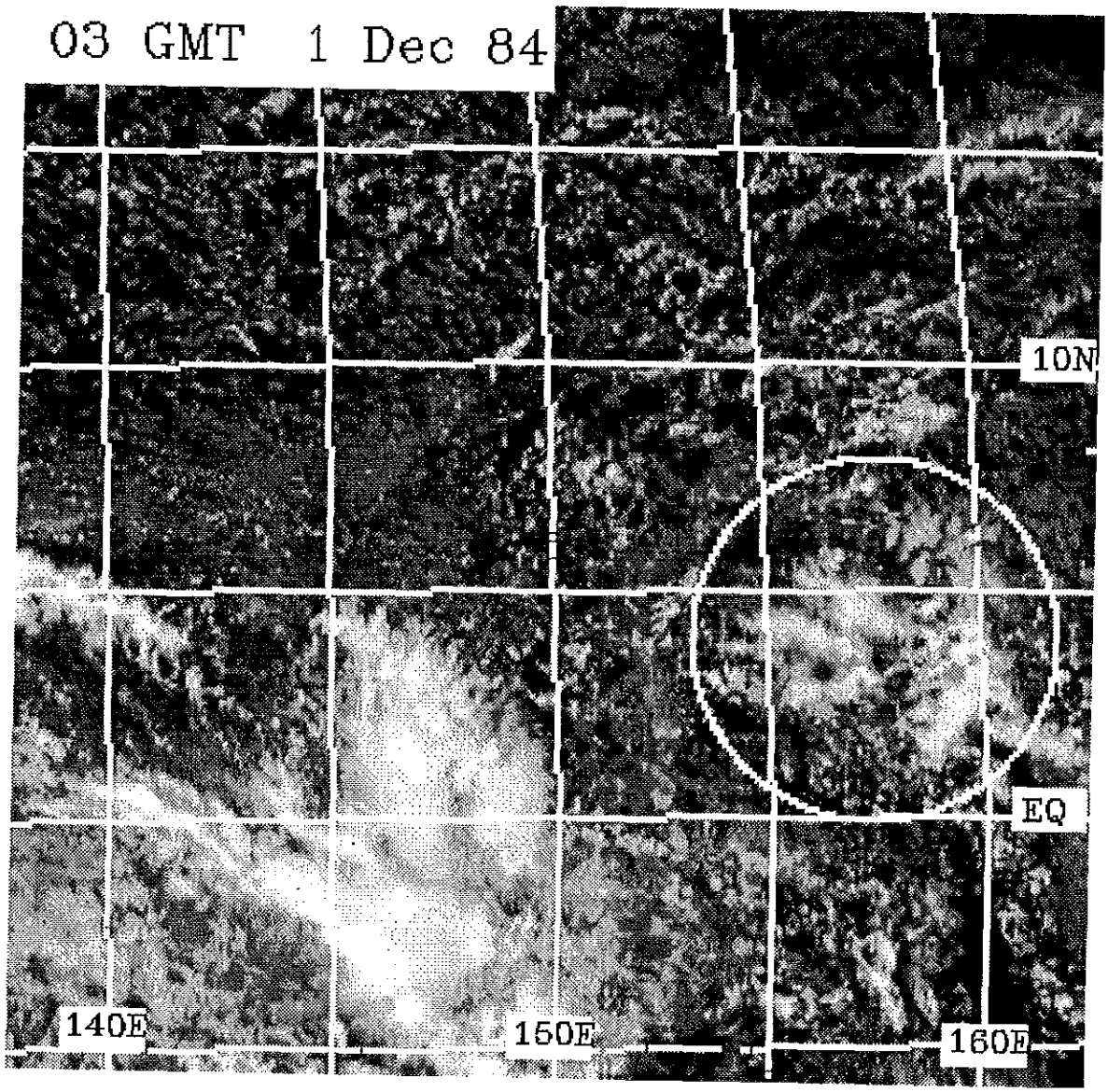

Figure 3.7: d.

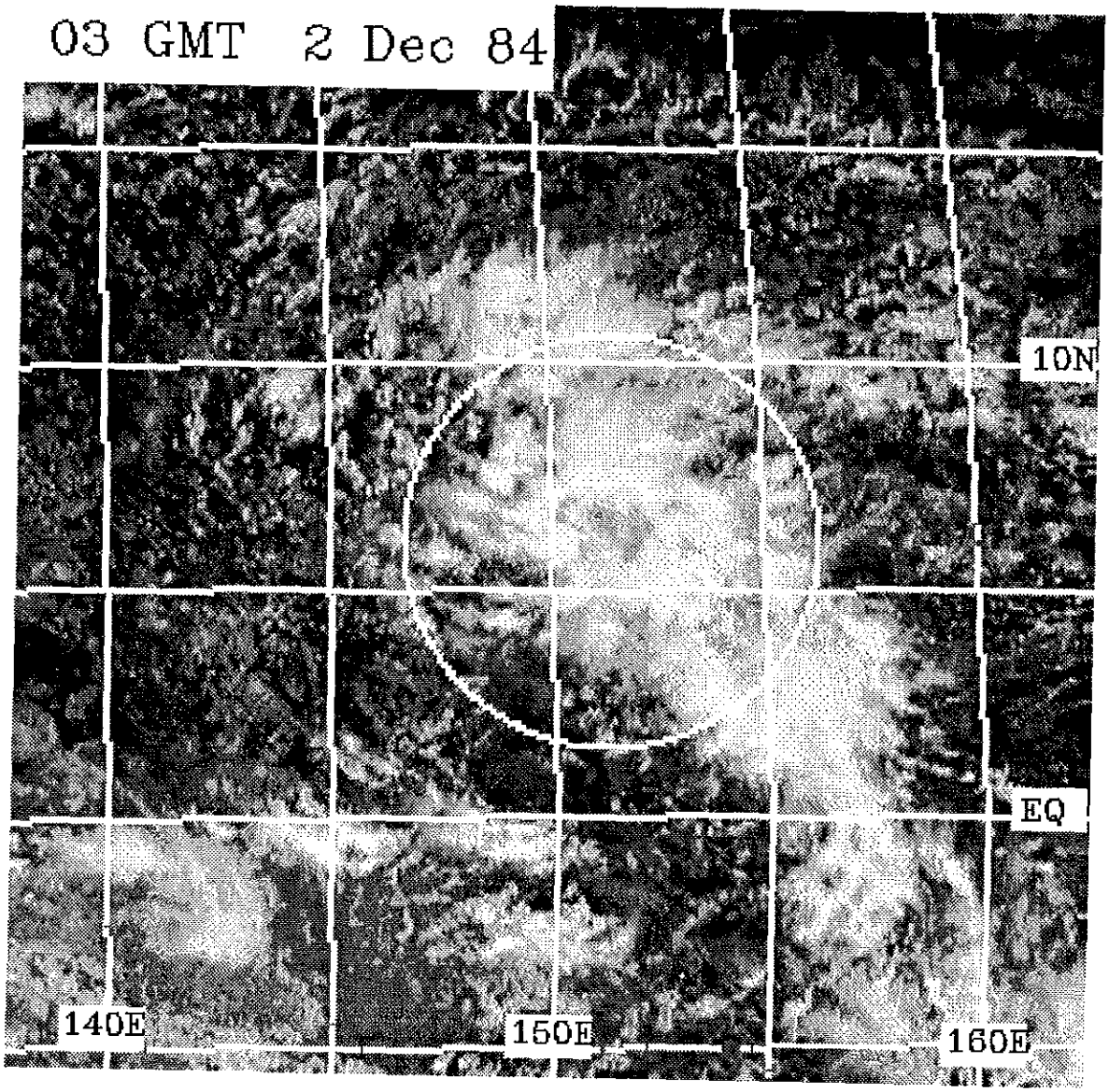

Figure 3.7: e.

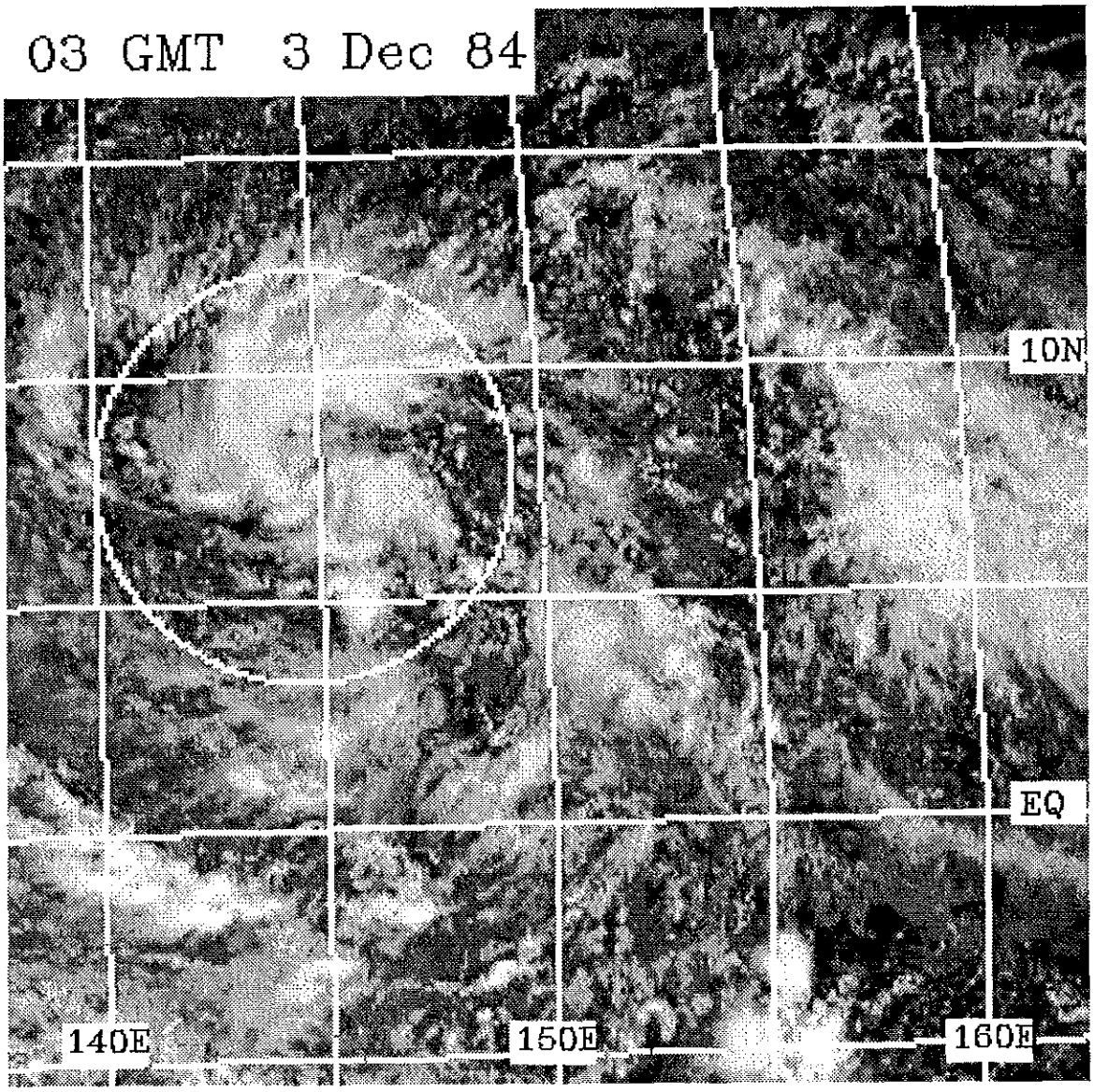

Figure 3.7: f.

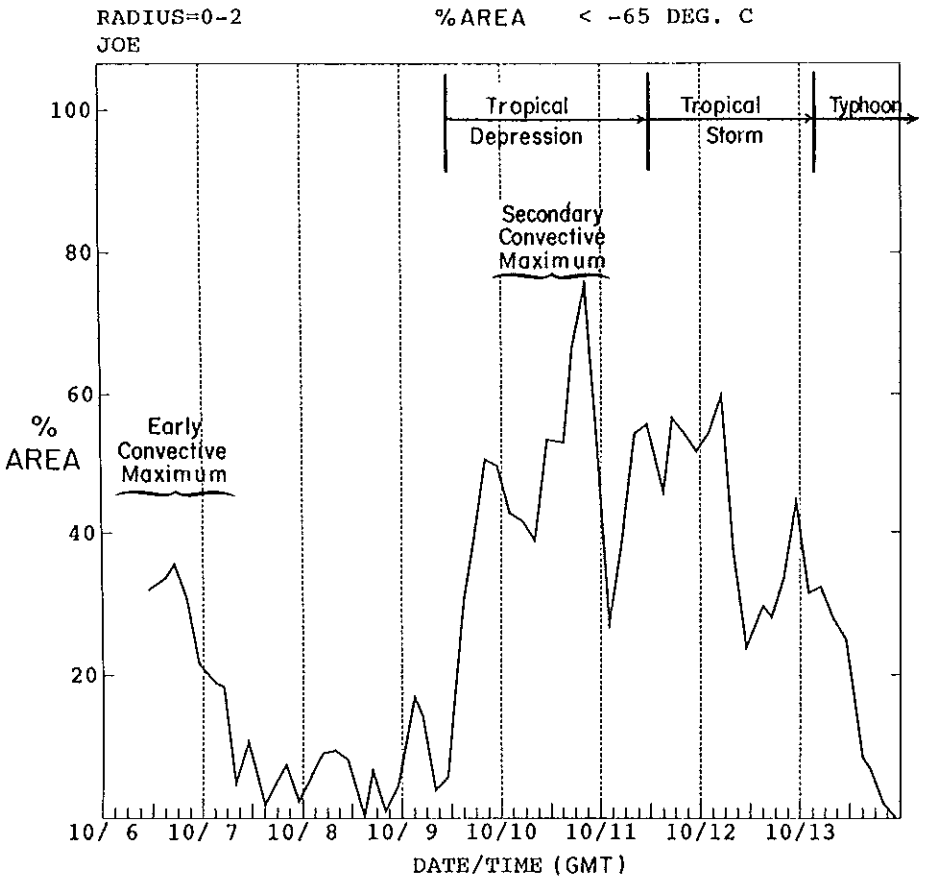

Figure 3.8: Example of a large secondary convective maximum with the pre-tropical storm disturbance of Typhoon Joe. Percent area R = 0–2°, T_B < -65°C.

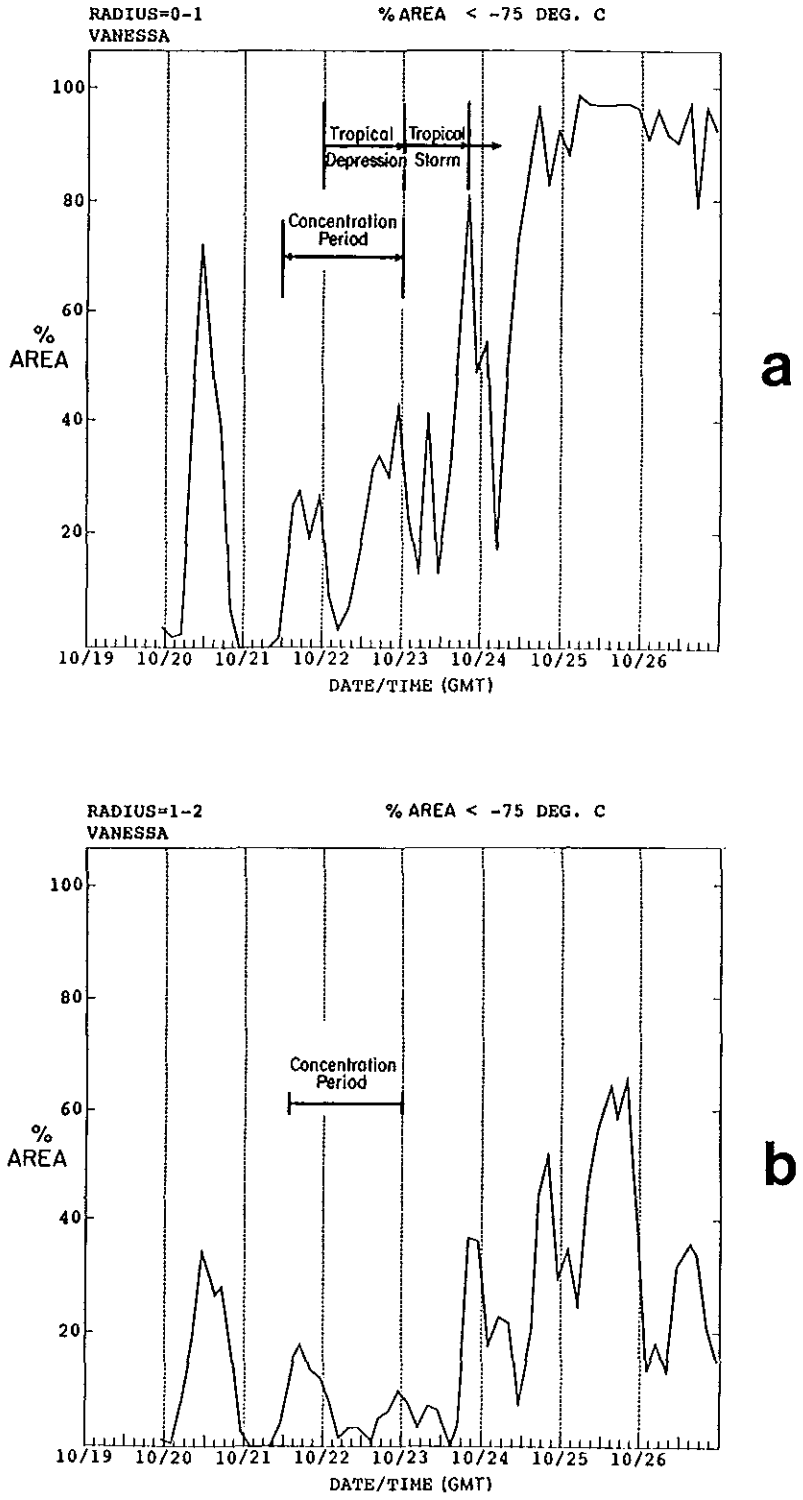

Figure 3.9: Time series plots of percent area with $T_B < -75°$, showing concentration of cold IR areas for Vanessa, 1984. a) R = 0–1°. b) R = 1–2°. c) Ratio of R = 0–1° to R = 1–2°, using a 24 hr running mean.

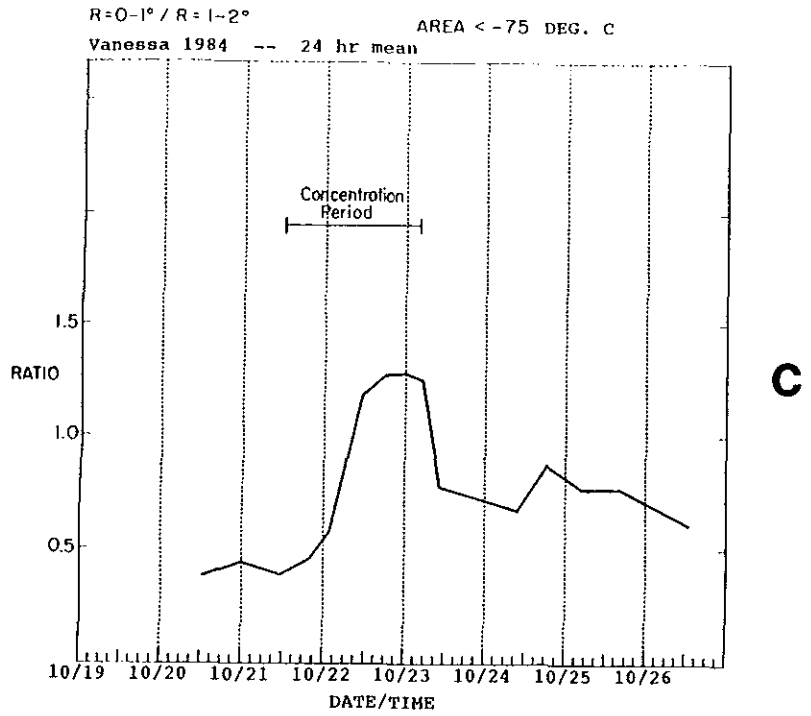

Figure 3.9: c.

3.3 Deep Convective Clouds Associated with Non-developing Tropical Disturbances

Non-developing tropical disturbances which can be tracked in the satellite imagery typically do not persist very long. To obtain a non-developing data set for comparison purposes, the microfilm images were used to track all non-developing cloud clusters during the July 1 through December 31 period in the area equatorward of 30°N, between the Philippines and 180° longitude. Only those that persisted for two days or more were selected for study. Their "Best Track" center positions are plotted in Appendix A. Only seven such disturbances existed during 1983. However, during 1984 there were fifteen persistent non-developing disturbances. Those numbers are reasonable in comparison with Lee's (1986) study of 11 years of western North Pacific non-genesis cloud clusters. Of 660 total cases, only 12.7% (10–11 per year) could be identified for three consecutive 24 hr periods using daily pictures.

How does the early convective maximum described in section 3.2 compare to the typical convection associated with non-developing tropical disturbances? Time series of cold IR cloud areas for two persistent, non-developing cases are plotted in Fig. 3.10. The example in Fig. 3.10a is quite active, showing three maxima of 40% or more, R = 0–2°, $T_B < -65$°C, areal coverage. In contrast, the cold IR areas with the disturbance in Fig. 3.10b are considerably smaller.

Examination of plots for all of the non-developing cases leads to several conclusions.

1. Many of the non-developing cases have at least one convective maximum comparable in magnitude and duration to those typical of the pre-tropical storm cases. The average amplitude of the maximum R = 0–2°, $T_B < -65$°C area during the entire lifetime of each non-developing disturbance is 44%, compared with 40% for the early convective maximum. The average amplitude of the $T_B < -75$°C maximum is 19% for the non-developers, compared to 21% for the early convective maximum.

2. A few of the non-developing cases have very small cold IR areas during their entire lifetime.

3. Overall there are no large differences in the magnitude and extent of deep convection, between non-developing and pre-tropical storm disturbances.

4. However, there are distinct differences when non-developing disturbances are compared with the observed deep convective cloud patterns and low-level cloud lines during the developing stages just prior to first designation as a tropical storm. The pre-tropical storm disturbances typically have persistent cyclonically curved deep convective cloud bands. A distinct low-level circulation center is often indicated by low-level cloud motions and alignment. Those characteristics are described in 3.2.4 and also follow closely the guidelines detailed by Dvorak (1984), for the tropical depression stage. Such features typically are not observed or do not persist with non-developing disturbances.

The objective satellite analyses of the non-developing cases raises the possibility that a convective maximum typical of those observed with pre-tropical storm disturbances, may also occur with non-developing cases. Therefore, although the early convective maximum is likely an important feature of the genesis process, it is not by itself uniquely associated with genesis.

3.4 Summary

Since the early convective maximum is such a prevalent feature of the tropical cyclone formation period, it is used as a reference point for the analyses in the following chapters. This feature is used to mark the beginning of the tropical cyclogenesis period. More importantly, the qualitative satellite analysis suggests that a mesoscale vortex first appears, embedded within the larger scale disturbance, immediately following the early convective maximum. This weak vortex, then evolves into a tropical storm. Aircraft observations to support this analysis are presented in Chapter 7.

Deep convection in the form of cloud clusters and tropical disturbances, do not occur randomly or persist in a particular area. They form and persist only where they are forced by synoptic-scale low-level convergence. The satellite analysis presented here suggests that such forcing is required during tropical cyclogenesis to produce an early convective maximum. That forcing is likely larger than what is required to maintain a tropical disturbance as a persistent cloud cluster. However, its influence on the pre-tropical storm disturbance may only need to persist for a few hours in order to be effective in initiating a mesoscale vortex. Furthermore, there is evidence of a secondary convective maximum associated with the tropical depression stage. This is accompanied by the initial significant decrease in MSLP. Thus the satellite observations along with aircraft measurements of MSLP provide the basis for a two-stage conceptual model of tropical cyclogenesis which is presented in the next chapter. The model proposes that the tropical cyclogenesis period consists of two distinct events which occur on relatively short time scales (24 hr or less) and are separated by a highly variable time period. This is in contrast to a viewpoint in which tropical cyclogenesis occurs as a gradual transition over a particular time period.

The amount, intensity, and patterns of the convection during the cyclogenesis period is highly variable. Nevertheless, several typical cloud features and their sequence of occurrence have been identified. These are depicted by the schematics and the cloud features described in Fig. 3.11a. Figure 3.11b uses similar schematics to show four possible scenarios for tropical disturbances which do not become tropical cyclones.

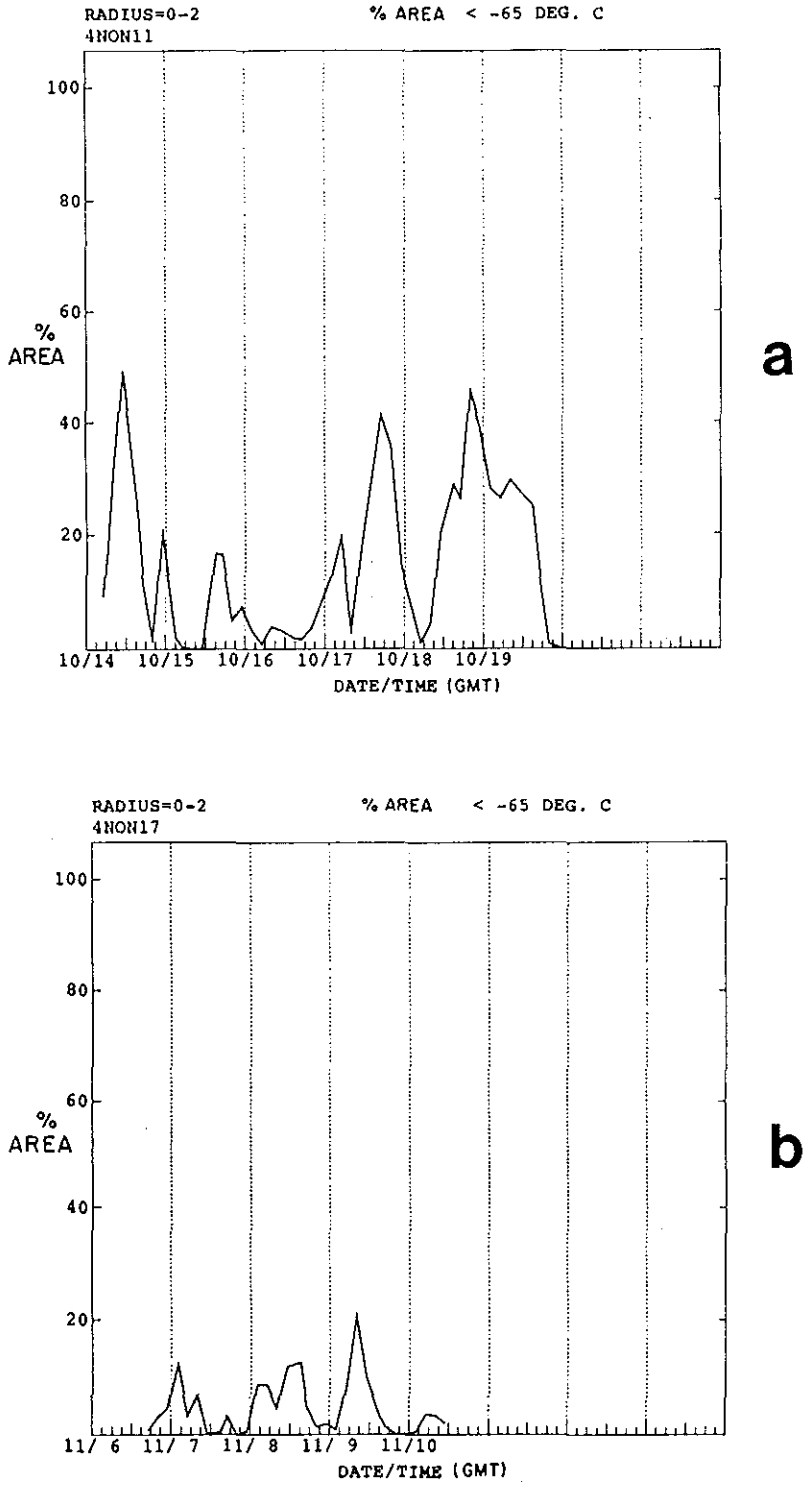

Figure 3.10: Time series of percent area, R = 0–2° with T_B < –65°C, for two 1984 persistent non-developing disturbances, named a) 4NON11 and b) 4NON17.

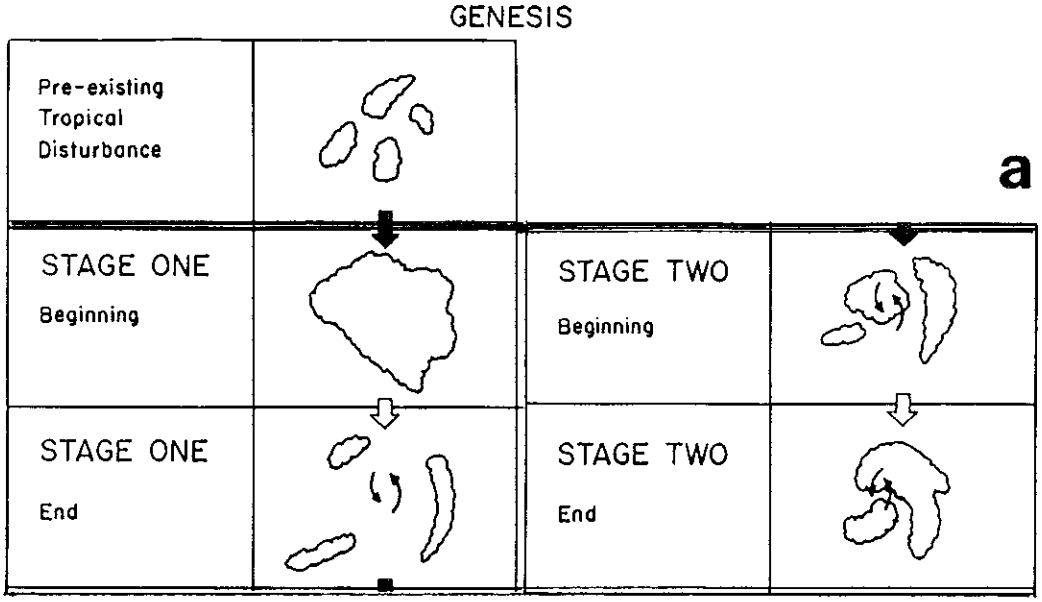

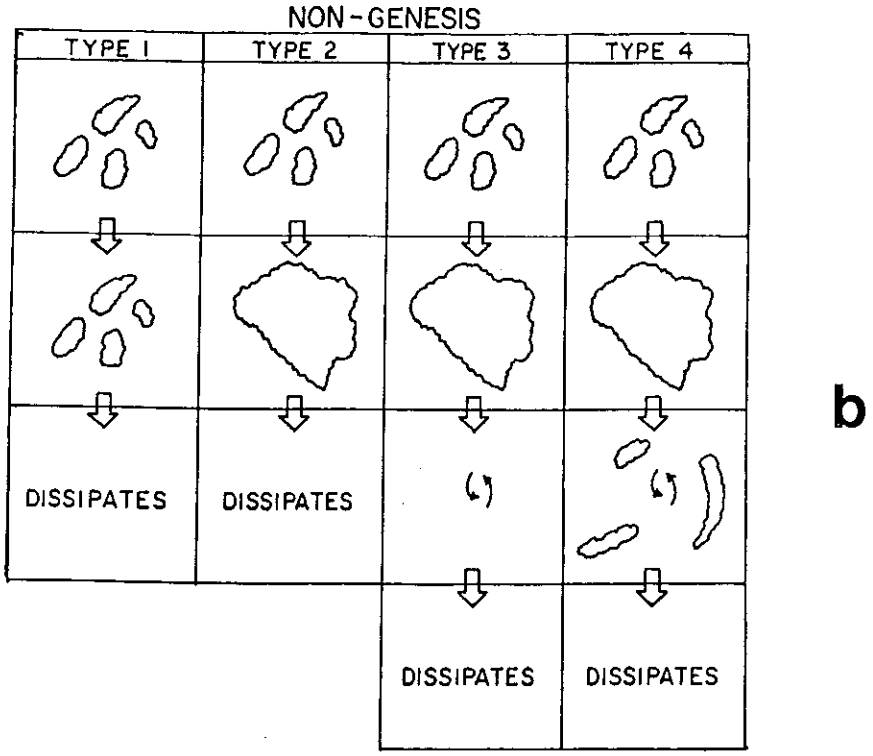

Figure 3.11: Idealized schematics of the satellite observed cloud patterns associated with (a) tropical cyclogenesis, and (b) non-genesis showing four types of non-developing tropical disturbances.

Chapter 4

TWO STAGES OF TROPICAL CYCLOGENESIS

Observational studies suggest that tropical cyclogenesis is a process which takes place over the course of several days. Therefore, this entire period must be studied carefully. Since the early convective maximum is likely an important feature of tropical cyclogenesis, it must be included in observational investigations. However, since it typically occurs so early and is highly variable, with respect to the time when a definitive tropical cyclone is first recognized to exist, it has likely been omitted or not recognized in many previous studies of tropical cyclogenesis.

To overcome this problem and to aid in the discussion of the overall process of tropical cyclogenesis, it is desirable to define two distinct stages. This results in a conceptual model of tropical cyclogenesis which includes two distinct events that can be observed by satellite data alone (Fig. 3.10). However, additional observations of wind and pressure provided largely by aircraft reconnaissance, provide important details and more clearly define the two stages. Case studies and findings from previous studies (Lee, 1986, 1989a,b; Lunney, 1988; Middlebrooke, 1988) along with the quantitative IR satellite information from Chapter 3 provide the basis for the model. It is presented here to provide a framework for discussion of the results presented in the following chapters. The conceptual model is based entirely on observations and a more detailed description is given in Chapter 8. Discussion of theoretical approaches to support such a model and implications for numerical modeling studies are also included in Chapter 8.

4.1 Quantitative IR Satellite Analysis

Figures 4.1 and 4.2 show how the two stages relate to the quantitative IR satellite data illustrated by the areas colder than $-70°C$ for two individual cases. The beginning of Stage 1 is marked by the onset of the enhanced convection associated with the early convective maximum. Stage 1 also includes the period following the convective maximum where the overall convection is considerably reduced. It is typically during this period that a distinct low-level circulation center can first be identified, and persistent cyclonically curved convective cloud lines are observed.

The end of Stage 1 and the onset of Stage 2 is marked by the onset of increasing deep convective activity associated with a low-level circulation center. It is usually during Stage 2 that the disturbance is first designated as a tropical depression (Fig. 4.2). However, this may occur much earlier, as in Fig. 4.1. It is therefore desirable to use the objective satellite measure of cold IR areas to define the onset of Stage 2. The end of Stage 2 is marked by first designation as a tropical storm. At this time the tropical cyclogenesis process is considered to be complete, and further evolution to a mature typhoon or hurricane is attributed to the intensification process.

The first designation as a tropical storm (named storm) is more consistently analyzed than the first tropical depression designation. It requires a distinct tropical cyclone scale circulation center and a 17.5 ms^{-1} maximum sustained surface wind speed. This is chosen to represent the end of the genesis period, both for consistency and convenience, as discussed in section 1.1.1. The time when the mechanisms important to cyclogenesis no longer predominate, and intensification mechanisms take over, marks the end of the genesis period.

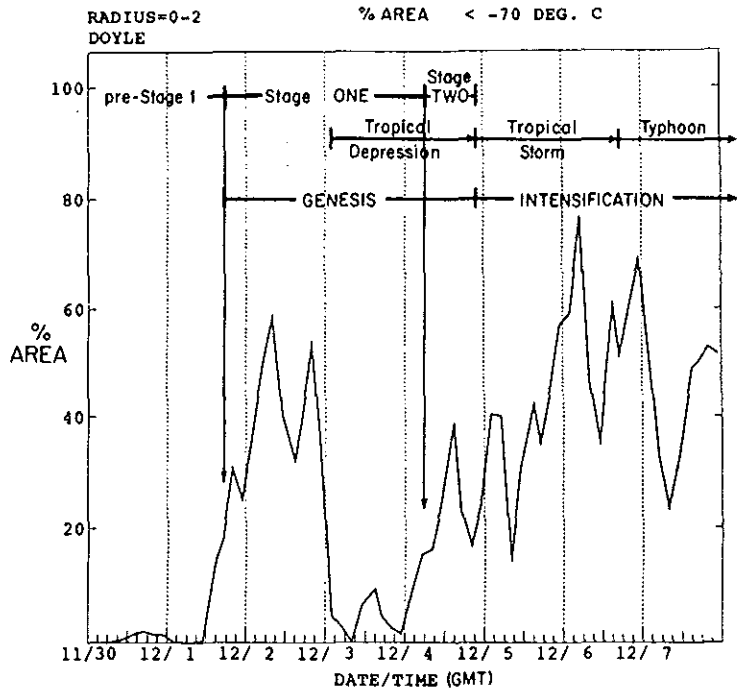

Figure 4.1: Stage 1 and Stage 2 periods depicted on a time series of R = 0–2° area, T_B < –70°C. Typhoon Doyle, 1984.

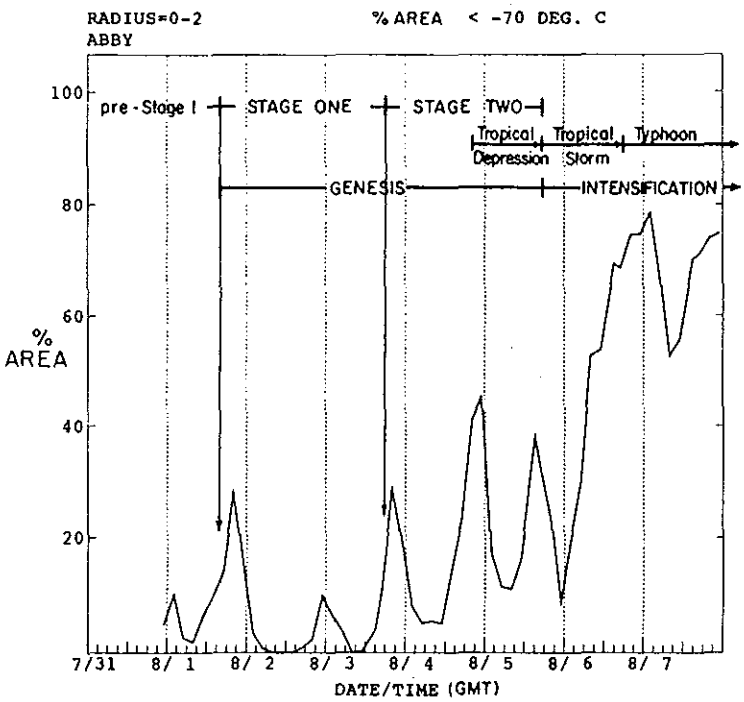

Figure 4.2: Stage 1 and Stage 2 periods depicted on a time series of R = 0–2° area, T_B < –70°C. Typhoon Abby, 1983.

4.2 Qualitative Description

Additional characteristics of the two-stage conceptual model of tropical cyclogenesis are illustrated in Fig. 4.3. As discussed previously, the time periods associated with the genesis period are highly variable. The time scale in Fig. 4.3 represents average time rates of change. The plot of deep convective clouds (Cb) is an idealized depiction of cold IR areas (Figs. 4.1 and 4.2) with diurnal variations removed. Similarly, the associated trends of minimum sea-level pressure (MSLP) and maximum surface wind speeds (V_{max}) do not include diurnal and short term small variations which may likely take place. Stage 1 is characterized by V_{max} and MSLP which are not much different from those associated with the pre-Stage 1 disturbance or with a non-developing tropical disturbance. During Stage 2, the MSLP begins to decrease faster, lowering to an average value of 997 mb at the end of Stage 2. This coincides with V_{max} increasing to 17.5 ms^{-1} (35 kt), according to the average pressure-wind relationship for the western North Pacific (Atkinson and Holliday, 1977). This represents a minimum sea-level pressure about 10 mb lower than the average of 1007 mb associated with non-developing tropical disturbances. Nearly all of this pressure drop occurs during Stage 2. These idealized changes in MSLP and V_{max} during tropical cyclogenesis are also supported by previous studies (Middlebrooke, 1988).

The time evolution of deep convective clouds (Cb) in the conceptual model includes two convective maxima. The Stage 1 convective maximum is referred to as the early convective maximum in Chapter 3. It marks the beginning of the genesis process. Stage 1 also includes an inactive period in which Cb activity is considerably less than that associated with either the Stage 1 convective maximum or with Stage 2. Stage 2 is characterized by increasing Cb clouds which may occur as a secondary convective maximum as discussed in section 3.2.5, and seen in Fig. 4.2. Stage 2 Cb activity may also occur as part of a general increasing trend which continues into the intensification period as shown in Fig. 4.1.

The main differentiating feature of Stage 2's convection is that it is organized in a pattern curved about a cyclonic circulation center (Fig. 3.11). It also becomes more concentrated around that center with time, as discussed in section 3.2.6. These observations are closely related to the widely used current intensity numbers or T-numbers of the Dvorak technique (Dvorak, 1984) of tropical cyclone intensity analysis (Fig. 4.3). Specific cloud pattern characteristics must be observed before an initial Dvorak classification of T1.0 is assigned to a particular disturbance. This is typically followed one or two days later by the first designation as a tropical storm (T2.5). Stage 1 in Fig. 4.3 corresponds with Dvorak's T1.0–1.5 and Stage 2 with T2.0–2.5. However, as noted by Dvorak (1984), the cloud patterns during the early stages are highly variable and objective assignments of the extent to which cyclogenesis has occurred, are very difficult and sometimes unreliable.

Additional important features of this conceptual model with regard to low-level vorticity and convergence are presented in Chapter 8.

4.3 Wind Surges

Figure 4.3 also denotes the occurrence of a surge associated with the onset of increasing deep convection. A surge is defined here as a low-level wind speed maximum typically appearing in the 850 mb analysis. An area of low-level mass convergence is associated with a surge. When the surge interacts with a tropical disturbance or depression, it will enhance the low-level convergence which results in more deep convection. Therefore, the conceptual model in Fig. 4.3 includes a surge interaction immediately preceding enhanced deep convection. Identification of surges and observations supporting the inclusion of surges in the model are discussed in Chapters 5 and 7.

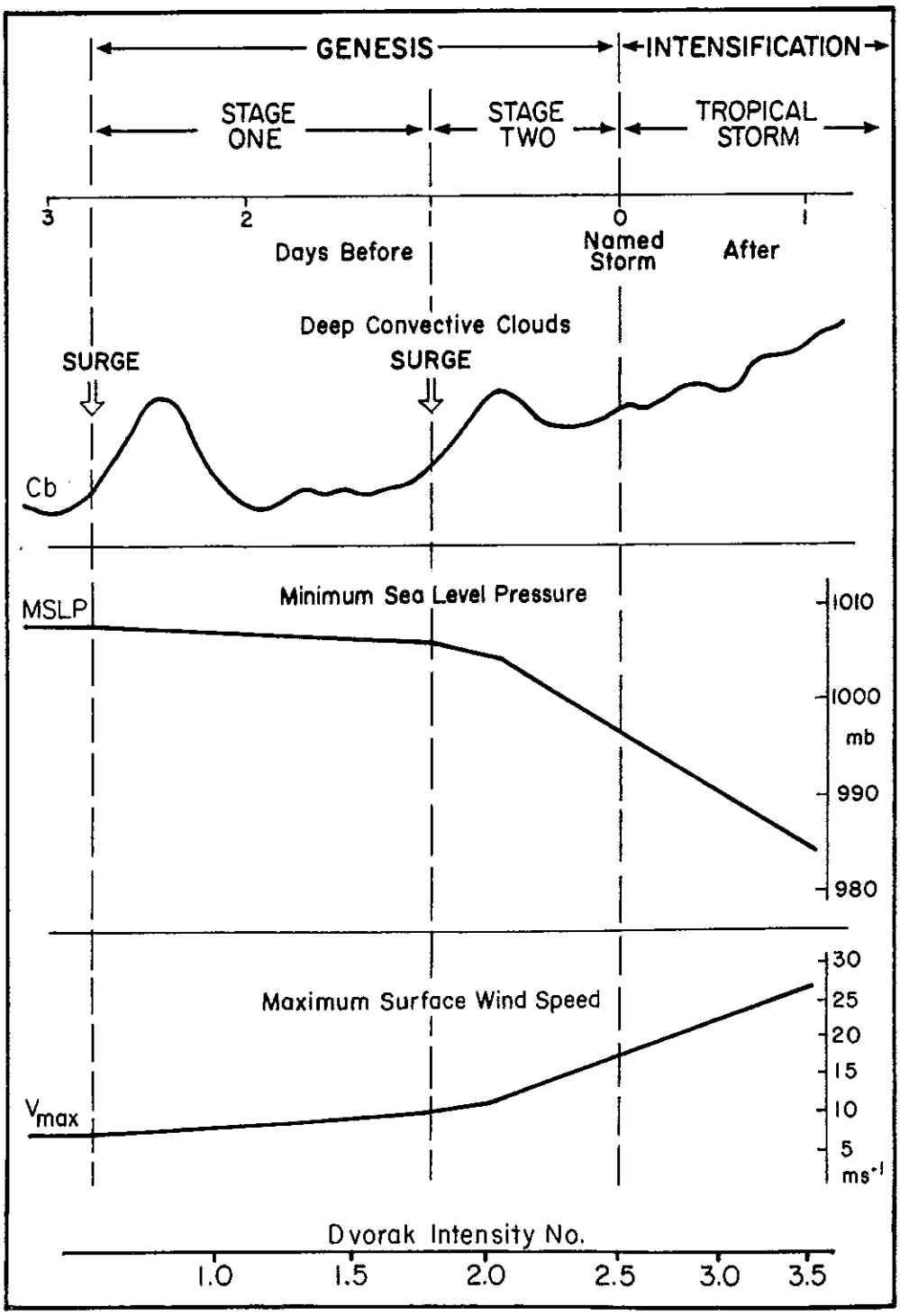

Figure 4.3: A conceptual model of the important changes of Cb, MSLP, and V_{max} during tropical cyclogenesis and estimates of the associated numerical values. The associated Dvorak intensity T-numbers are also shown.

Chapter 5

SYNOPTIC-SCALE ANALYSIS OF WESTERN NORTH PACIFIC TROPICAL CYCLOGENESIS

The location and time of the Stage 1 convective maximum and the first designation as a tropical storm (end of Stage 2) are compiled for all 50 tropical storms during 1983-1984. This marks the date and time (to the nearest 3 hr) and center location (to the nearest degree latitude and longitude) of the disturbance near the beginning of Stage 1 and at the end of Stage 2. The synoptic-scale analysis is done for both locations and times, with each individual case.

The wind analyses at 850 mb and 200 mb from 2.5° latitude resolution objective analyses are used to compile information on the synoptic-scale flow characteristics. Table 5.1 includes the results from the 850 mb analyses. Table 5.2 is for the 200 mb analyses and is discussed later in sections 5.3–5.5.

For those ten cases which do not have an identifiable Stage 1 maximum, the maximum R = 0–2°, T_B < –65°C, area prior to or at the time of first tropical depression designation is used to define Stage 1. That maximum usually occurs at the time of first tropical depression designation, and the associated time and location are entered for Stage 1 in Tables 5.1 and 5.2. Therefore, the genesis period generally coincides to the tropical depression period for the cases which do not have a distinct Stage 1 convective maximum.

Note that two of the cases (Ellen and Ruth) have two entries in Tables 5.1 and 5.2. They were unusual cases that underwent genesis more than once. Tropical Storm Ellen formed, then weakened, and its classification was downgraded to a tropical disturbance before it re-developed again. Therefore, two separate entries are used in the analysis. Tropical Storm Ruth was tracked as a tropical disturbance or depression for thirteen days before it finally became a tropical storm. It may have had several Stage 1 convective maxima, of which two are entered in Tables 5.1 and 5.2.

5.1 Season and Geographical Location

The tropical cyclone season in the western North Pacific has a primary 6-month period of July through December which includes most storms. However, occasional tropical cyclones have been observed during all months (Gray, 1981). All typhoons and tropical storms in 1983–1984, occurred during June through December.

The Stage 1 and Stage 2 locations from Table 5.1 are plotted in Fig. 5.1. The primary genesis region is between 5°N and 20°N latitude, and 125°E and 160°E. This area accounts for 69% of all Stage 1 locations. The South China Sea region includes 13% of Stage 1 points and 27% for Stage 2. Small percentages of cases are observed north of 20°N, south of 5°N, and east of 160°E. Table 5.3 and Fig. 5.1b summarize the regional distribution of the genesis beginning (Stage 1) and end points (Stage 2). Their average locations are also plotted in Fig. 5.1. The average location of Stage 2 points is to the west-northwest of the average Stage 1 location. This represents the mean motion during the tropical cyclogenesis period.

5.2 Low-level Patterns

Four primary 850 mb synoptic-scale flow patterns are identified in association with the 50 tropical cyclogenesis cases (Fig. 5.2). In addition, two unusual patterns have been

Table 5.1: 850 mb genesis characteristics.

STAGE ONE -- Early Convective Maximum						STAGE TWO -- First "named storm"				
TC NAME 1983	MO/DA Hr (GMT)	LAT/LON	850 mb PATTERN	SURGE DIR	SURGE DATA	MO/DA Hr (GMT)	LAT/LON	850 mb PATTERN	SURGE DIR	SURGE DATA
Sarah	6/18 21	6N 137E	Easterly			6/25 06	15N 110E	Monsoon-Stg		
Tip	7/5 21	7N 139E	Monsoon-Wk			7/10 15	14N 119E	Monsoon-Wk		
Vera	7/8 21	9N 147E	Monsoon-E			7/12 12	12N 130E	Monsoon-Wk	WSW	A
Wayne	7/18 21	8N 151E	Monsoon-E	WNW	C	7/22 09	15N 134E	Monsoon-E	W, WNW	A, S
Abby	8/1 21	7N 146E	Monsoon-E	SE	C	8/5 18	10N 139E	Monsoon-Wk	E,WSW,W	A, A, S
Ben	8/11 15	22N 144E	Monsoon-Stg			8/12 06	25N 146E	Monsoon-Stg		
Carmen	8/9 03	14N 115E	Monsoon-Stg			8/13 21	20N 121E	Monsoon-Stg		
Dom	8/17 15	15N 139E	Weak			8/19 00	16N 134E	Monsoon-Wk	N, SW	A, C
Ellen (2)	8/30 18	11N 160E	Easterly	WSW	A	9/2 00	9N 143E	Easterly	NW	A
Ellen (1)	8/26 18	9N 175W	Easterly			8/29 00	13N 171E	Easterly		
Forrest	9/18 21	6N 153E	Monsoon-Wk	WSW	A, S, C	9/20 18	11N 143E	Monsoon-Stg	W	A
Georgia	9/28 00	17N 118E	Monsoon-Stg			9/28 18	19N 116E	Monsoon-Stg		
Herbert	10/3 03	6N 129E	Monsoon-E			10/7 00	11N 114E	Monsoon-Wk		
Ida	10/5 03		Easterly			10/7 21	19N 139E	Easterly	SSE	C
Joe	10/6 18	5N 140E	Monsoon-Wk			10/11 12	17N 119E	Monsoon-Stg	WNW	A
Kim	10/12 06	10N 138E	Monsoon-Wk			10/16 12	10N 111E	Monsoon-Wk		
Lex	10/19 00	14N 132E	Easterly			10/22 06	16N 116E	Monsoon-Wk	W	A
Marge	10/28 00	5N 160E	Monsoon-E			10/31 06	10N 146E	Monsoon-Stg	WSW	A, C
Norris	11/7 18	16N 157E	Easterly			11/8 12	18N 153E	Easterly		
Orchid	11/14 15	13N 148E	Easterly			11/17 18	12N 132E	Monsoon-Stg	SW, SW	A, C
Percy	11/17 06	10N 111E	Monsoon-Stg			11/19 00	9N 113E	Monsoon-Stg	ENE	C
Ruth (2)	11/25 12	10N 135E	Monsoon-Wk	W	C	11/27 21	17N 129E	Monsoon-Wk		
Ruth (1)	11/19 12	4N 148E	Monsoon-Stg	N, W	A, C					
Sperry	11/30 18	10N 141E	Monsoon-E	SW	C	12/3 00	16N 132E	Monsoon-Wk	N, N	A, C
Thelma	12/12 18	5N 156E	Easterly	E	C	12/15 18	12N 136E	Monsoon-Stg	W	A

STAGE ONE						STAGE TWO				
TC NAME 1984	MO/DA Hr (GMT)	LAT/LON	850 mb PATTERN	SURGE DIR	SURGE DATA	MO/DA Hr (GMT)	LAT/LON	850 mb PATTERN	SURGE DIR	SURGE DATA
Vernon	6/6 21	12N 117E	Monsoon-Wk			6/9 06	14N 112E	Monsoon-Wk	W	C
Wynne	6/17 21	20N 139E	Weak			6/19 18	21N 132E	Monsoon-Wk	WSW	C
Alex	6/30 18	16N 125E	Monsoon-E			7/1 12	16N 124E	Monsoon-E	WNW	A
Betty	7/2 21	8N 134E	Easterly	NE	C	7/7 12	18N 117E	Monsoon-E	N, W	A
Cary	7/5 21	17N 150E	TUTT-LLCC			7/7 12	19N 146E	Weak	WSW, N	A
Dinah	7/21 15	21N 162E	Mid-latitude	ESE	C	7/24 12	21N 156E	Mid-latitude		
Ed	7/25 00	28N 135E	Mid-latitude			7/25 18	26N 136E	Mid-latitude		
Freda	8/4 00	18N 137E	Monsoon-E	WSW	C	8/5 18	19N 126E	Monsoon-Stg	W, NW	A
Gerald	8/14 00	17N 116E	Monsoon-Stg			8/15 18	20N 119E	Monsoon-Stg		
Holly	8/12 12	16N 139E	Monsoon-Stg	SW	C	8/15 06	20N 135E	Monsoon-Stg	WSW	C
Ike	8/25 18	7N 146E	Monsoon-E	W	C	8/27 00	11N 145E	Monsoon-E	WSW	C
June	8/25 00	17N 138E	Monsoon-Stg			8/27 12	17N 127E	Monsoon-Stg	W	A
Kelly	9/11 21	21N 175E	Mid-latitude			9/13 18	21N 172E	Mid-latitude		
Lynn	9/23 18	19N 117E	Monsoon-E			9/24 18	18N 114E	Monsoon-Stg		
Maury	9/25 03	19N 148E	Mid-latitude			9/27 18	24N 152E	Monsoon-Stg	SW	C
Nina	9/25 18	17N 139E	Monsoon-Stg			9/28 00	24N 141E	Monsoon-Stg	E	C
Ogden	10/4 18	12N 151E	Monsoon-E	S	C	10/7 18	22N 153E	Monsoon-Wk	SW, SSW	A, C; S
Phyllis	10/8 21	17N 150E	Monsoon-Stg			10/11 00	20N 153E	Monsoon-Stg	SSW	C
Roy	10/8 21	8N 136E	Monsoon-Stg	W	C	10/11 06	13N 143E	Monsoon-Stg		
Susan	10/10 03	11N 114E	Monsoon-Stg			10/12 00	12N 112E	Monsoon-Stg		
Thad	10/17 21	7N 151E	Monsoon-Stg	W	C, S	10/19 06	13N 148E	Monsoon-Stg		
Vanessa	10/20 12	4N 163E	Monsoon-E	W	S	10/23 00	9N 154E	Monsoon-E	W, W	C, S
Warren	10/18 18	12N 128E	Monsoon-Wk	E, ESE	C, S	10/23 18	12N 116E	Monsoon-Stg		
Agnes	10/28 21	2N 148E	Easterly	E, E	C, S	11/1 00	5N 144E	Easterly	ENE	C
Bill	11/2 21	22N 177E	TUTT-LLCC			11/8 18	14N 153E	Weak	WSW	C, S
Clara	11/13 12	6N 156E	Monsoon-E	S	S	11/15 06	8N 150E	Monsoon-Wk	NW	A, C, S
Doyle	12/2 09	6N 150E	Monsoon-E	WSW, S	S, C	12/4 18	8N 138E	Monsoon-Wk		

A = aircraft
C = conventional
S = satellite

DIR = Direction
SPD = Speed

Table 5.2: 200 mb genesis characteristics.

STAGE ONE -- Early Convective Maximum							STAGE TWO -- First "named storm"					
TC NAME 1983	MO/DA Hr (GMT)	LAT/LON	DIR	SPD	Unidirectional Y or N	TUTT Y or N	MO/DA Hr (GMT)	LAT/LON	DIR	SPD	Unidirectional Y or N	TUTT Y or N
Sarah	6/18 21	6N 137E					6/25 06	15N 110E	ENE	Wk	Y	N
Tip	7/5 21	7N 139E					7/10 15	14N 119E	E	Stg	Y	N
Vera	7/8 21	9N 147E	E	Wk	N	Y	7/12 12	12N 130E	NE	Wk	Y	N
Wayne	7/18 21	8N 151E	E	Wk	N	N	7/22 09	15N 134E	NE	Mod	N	Y
Abby	8/1 21	7N 146E	E	Wk	N	N	8/5 18	10N 139E		Wk	N	Y
Ben	8/11 15	22N 144E	W	Stg	N	Y	8/12 06	25N 146E	WNW	Mod	N	N
Carmen	8/9 03	14N 115E		Wk	N	Y	8/13 21	20N 121E	E	Wk	N	Y
Dom	8/17 15	15N 139E	ENE	Mod	Y	N	8/19 00	16N 134E	E	Mod	N	N
Ellen (2)	8/30 18	11N 160E	E	Stg	N	N	9/2 00	9N 143E	ENE	Mod	N	N
Ellen (1)	8/26 18	9N 175W		Wk		Y	8/29 00	13N 171E	E	Mod	N	Y
Forrest	9/18 21	6N 153E	ENE	Wk	N	Y	9/20 18	11N 143E	E	Wk	N	Y
Georgia	9/28 00	17N 118E					9/28 18	19N 116E	E	Wk	N	N
Herbert	10/3 03	6N 129E					10/7 00	11N 114E	E	Wk	N	N
Ida	10/5 03						10/7 21	19N 139E	E	Wk	N	N
Joe	10/6 18	5N 140E	SE	Wk	N	Y	10/11 12	17N 119E	E	Wk	N	N
Kim	10/12 06	10N 138E	E	Mod	Y	N	10/16 12	10N 111E	E	Mod	Y	N
Lex	10/19 00	14N 132E	S	Wk	N	N	10/22 06	16N 116E	S	Wk	N	N
Marge	10/28 00	5N 160E	NE	Mod	N	N	10/31 06	10N 146E	-	Wk	N	Y
Norris	11/7 18	16N 157E					11/8 12	18N 153E	E	Wk	N	N
Orchid	11/14 15	13N 148E	S	Wk	Y	N	11/17 18	12N 132E	SE	Mod	N	N
Percy	11/17 06	10N 111E					11/19 00	9N 113E	E	Mod	N	N
Ruth (2)	11/25 12	10N 135E	ESE	Stg	Y	N	11/27 21	17N 129E	E	Wk	N	N
Ruth (1)	11/19 12	4N 148E	SE	Mod	Y	N						
Sperry	11/30 18	10N 141E	E	Mod	N	N	12/3 00	16N 132E	E	Mod	N	N
Thelma	12/12 18	5N 156E	E	Wk	Y	N	12/15 18	12N 136E	E	Wk	N	N

STAGE ONE							STAGE TWO					
TC NAME 1984	MO/DA Hr (GMT)	LAT/LON	DIR	SPEED	Unidirectional Y or N	TUTT Y or N	MO/DA Hr (GMT)	LAT/LON	DIR	SPD	Unidirectional Y or N	TUTT Y or N
Vernon	6/6 21	12N 117E	WNW	Wk	N	Y	6/9 06	14N 112E	ENE	Wk	Y	Y
Wynne	6/17 21	20N 139E	N	Mod	N	Y	6/19 18	21N 132E	E	Wk	N	N
Alex	6/30 18	16N 125E					7/1 12	16N 124E	NE	Mod	N	Y
Betty	7/2 21	8N 134E	SE	Wk	N	N	7/7 12	18N 117E	ESE	Mod	N	N
Cary	7/5 21	17N 150E		Wk	N	Y	7/7 12	19N 146E	SSW	Wk	N	Y
Dinah	7/21 15	21N 162E	W	Wk	N	Y	7/24 12	21N 156E	NE	Wk	N	Y
Ed	7/25 00	28N 135E					7/25 18	26N 136E		Wk	N	Y
Freda	8/4 00	18N 137E	E	Wk	Y	Y	8/5 18	19N 126E	E	Wk	N	Y
Gerald	8/14 00	17N 116E		Wk	N	N	8/15 18	20N 119E	E	Wk	N	N
Holly	8/12 12	16N 139E	E	Wk	N	Y	8/15 06	20N 135E	ENE	Wk	N	N
Ike	8/25 18	7N 146E	SE	Wk	N	N	8/27 00	11N 145E	N	Wk	N	N
June	8/25 00	17N 138E	E	Mod	Y	N	8/27 12	17N 127E	E	Wk	Y	N
Kelly	9/11 21	21N 175E		Wk	N	Y	9/13 18	21N 172E		Wk	N	Y
Lynn	9/23 18	19N 117E					9/24 18	18N 114E	SE	Wk	N	N
Maury	9/25 03	19N 148E					9/27 18	24N 152E		Wk	N	N
Nina	9/25 18	17N 139E	W	Wk	N	Y	9/28 00	24N 141E	SW	Wk	N	Y
Ogden	10/4 18	12N 151E	SW	Wk	N	Y	10/7 18	22N 153E	SSW	Wk	N	Y
Phyllis	10/8 21	17N 150E	SE	Wk	N	N	10/11 00	20N 153E	SSW	Wk	N	Y
Roy	10/8 21	8N 136E	S	Wk	N	N	10/11 06	13N 143E	ESE	Mod	N	N
Susan	10/10 03	11N 114E	E	Wk	Y	N	10/12 00	12N 112E	E	Wk	Y	N
Thad	10/17 21	7N 151E	NE	Wk	N	Y	10/19 06	13N 148E	SE	Wk	N	Y
Vanessa	10/20 12	4N 163E	ENE	Mod	Y	Y	10/23 00	9N 154E	E	Mod	Y	N
Warren	10/18 18	12N 128E	E	Stg	Y	N	10/23 18	12N 116E	ESE	Mod	Y	N
Agnes	10/28 21	2N 148E	S	Wk	Y	N	11/1 00	5N 144E	SE	Wk	Y	N
Bill	11/2 21	22N 177E	N	Wk	N	Y	11/8 18	14N 153E	SE	Wk	N	Y
Clara	11/13 12	5N 156E	E	Mod	N	N	11/15 06	8N 150E	E	Wk	N	Y
Doyle	12/2 09	6N 150E	E	Stg	Y	N	12/4 18	8N 138E	SE	Mod	Y	N

DIR = Direction
SPD = Speed

Wk = <6 m/s
Mod = 6-12 m/s
Stg = >12 m/s

TUTT = Tropical Upper Tropospheric Trough

Y = Yes
N = No

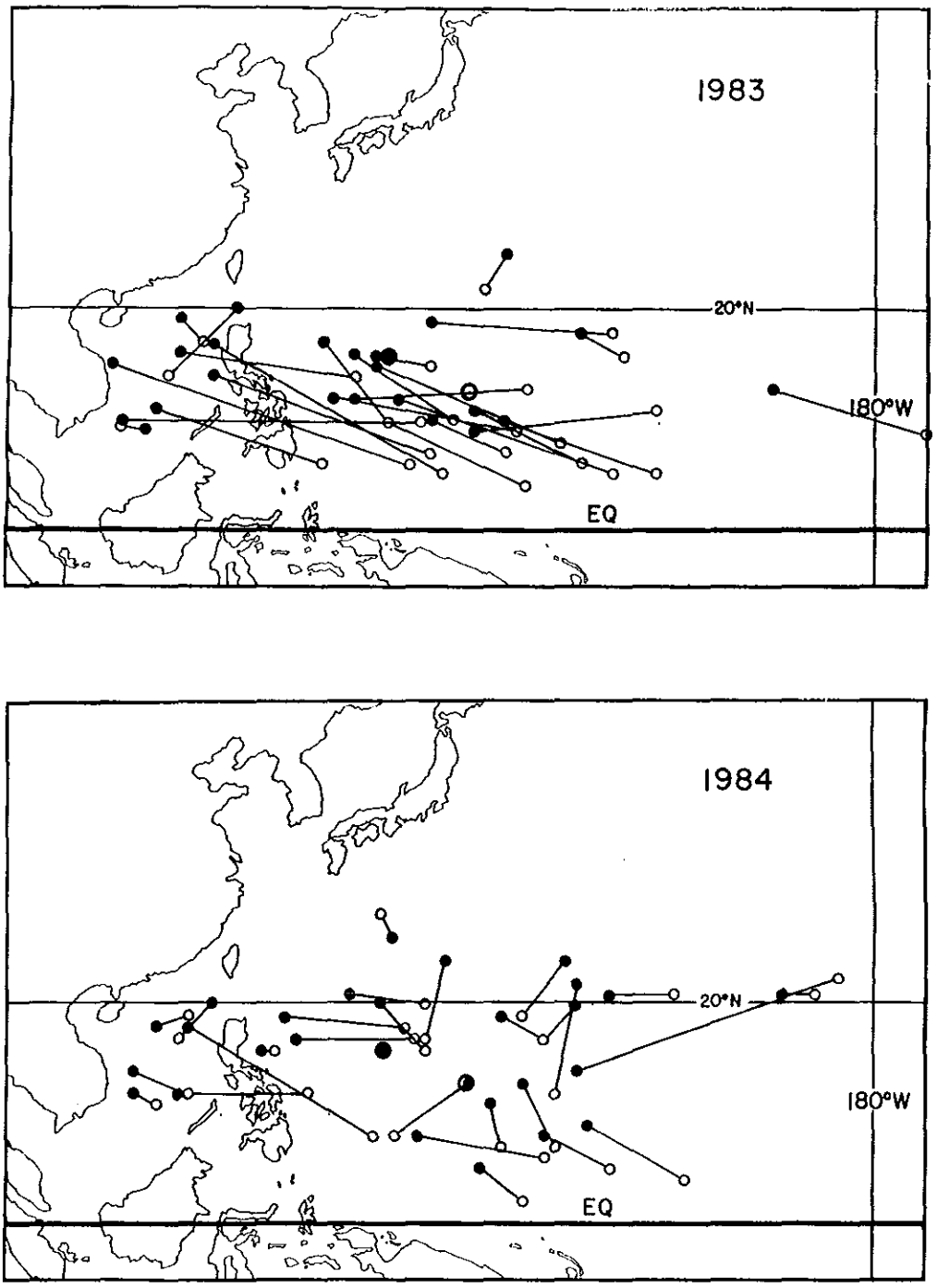

Figure 5.1: a) Stage 1 locations (open circles) and Stage 2 locations (black dots) for each individual case entry from Table 5.1. The large circles are the 1983–1984 average locations. b) Primary and surrounding genesis regions and the corresponding Stage 1 percentages from Table 5.3.

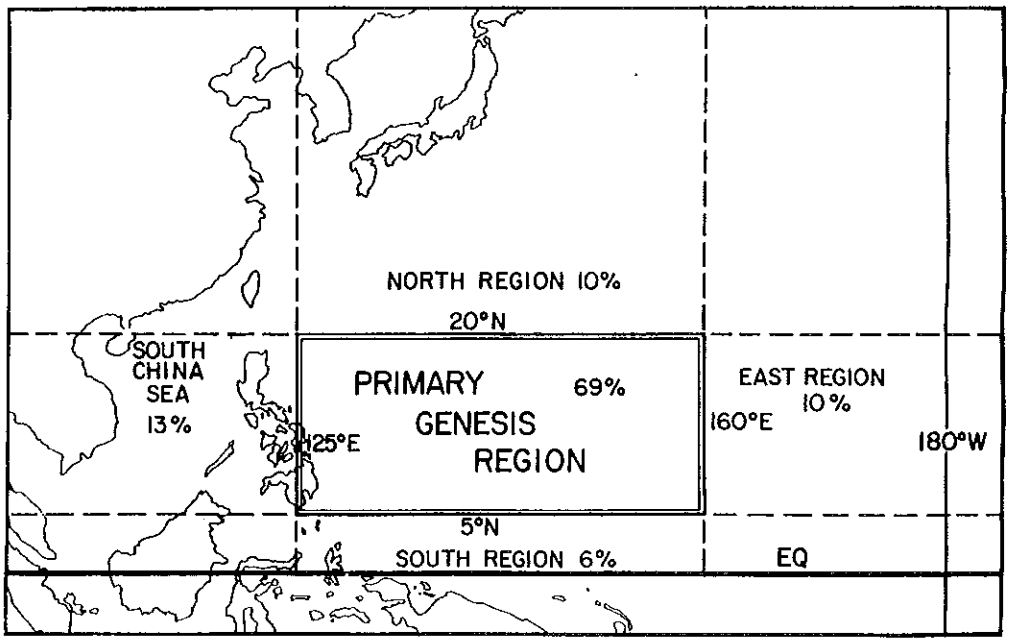

Figure 5.1: b: Primary and surrounding genesis regions and the corresponding Stage 1 percentages from Table 5.3.

Table 5.3: Geographical distribution of tropical cyclogenesis.

Region	Latitude–Longitude	% of Stage 1	% of Stage 2
Primary	5–20°N, 125–160°E	69	55
South China Sea	West of 125°E	13	27
North	North of 20°N	10	16
South	South of 5°N	6	0
East	East of 160°E	10	4

noted. All Stage 1 and Stage 2 cases have been classified, if possible, into one of the six patterns and listed in Table 5.1. A very few cases, were associated with very weak or indeterminate flow patterns.

The monsoon trough with easterly component winds on the poleward side and westerly component winds equatorward is a semi-permanent flow feature. Three of the patterns are associated with the monsoon trough. The patterns are defined by the objective analyses of 850 mb wind speeds and directions in the area out to 5° latitude radius from the center locations, as follows:

1. Easterly—easterly component winds in all four quadrants
2. Monsoon-E—easterly component winds in all quadrants except the southwest quadrant which has westerly component winds
3. Monsoon-Wk—within the monsoon trough with westerly component wind speeds 10 ms^{-1} (20 kt) or less
4. Monsoon-Stg—within the monsoon trough with westerly component wind speeds greater than 10 ms^{-1}
5. TUTT-LLCC—the low-level circulation center (LLCC) is the downward extension of an upper-level cold low, often referred to as a TUTT (Tropical Upper Tropospheric Trough) cell
6. Mid-latitude—within the horizontal shear region associated with what was once a mid-latitude cold front
7. Weak (Indeterminate)—very weak winds, or winds that cannot be classified into any of the other six patterns

Table 5.4 lists the number of cases classified into each of the pattern types for Stage 1 and Stage 2. Figure 5.2 illustrates each of the four primary 850 mb patterns with idealized streamline-isotach depictions, while Figs. 5.3 through 5.6 are Stage 1 examples of each type from the BMRC 2.5° latitude resolution objective analysis.

Table 5.4: Number and percentage of cases with each 850 mb pattern type.

Pattern	Stage 1		Stage 2	
	No.	%	No.	%
Easterly	10	19	5	10
Monsoon–E	14	27	5	10
Monsoon–Wk	7	13	14	27
Monsoon–Stg	13	25	22	43
Mid-latitude	4	8	3	6
TUTT–LLCC	2	4	0	0
Indeterminate	2	4	2	4
Monsoon	34	65	41	80
Other	18	35	10	20

The Easterly pattern is a cyclonically sheared region of the trade winds. Tropical disturbances with this pattern often resemble the classical easterly wave as described by Riehl (1954). Nineteen percent of Stage 1 cases and 10% of Stage 2 are classified with

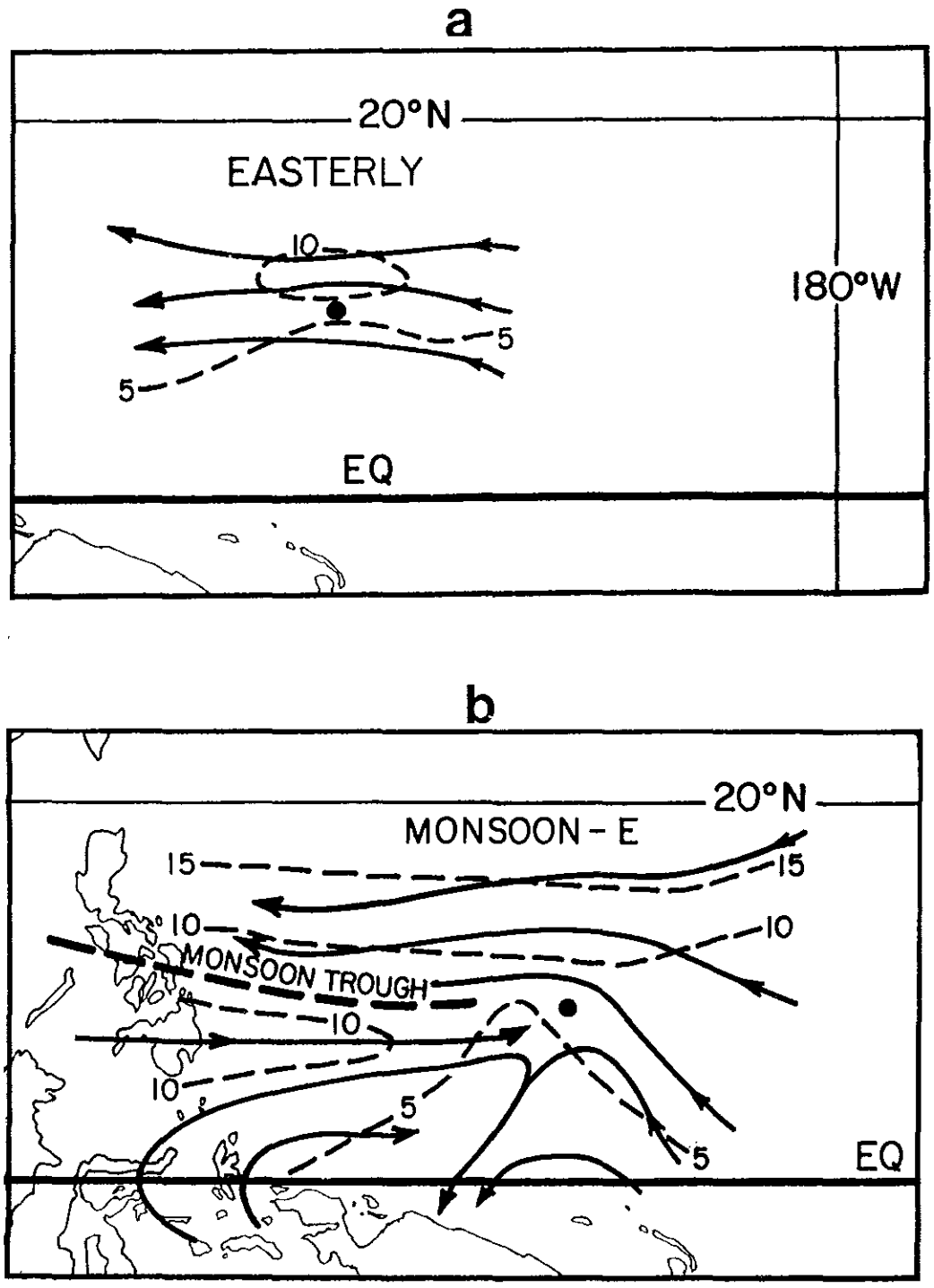

Figure 5.2: Idealized streamline–isotach patterns portraying the four primary 850 mb synoptic scale patterns associated with tropical cyclogenesis. The large dot marks the circulation center of the pre-tropical storm disturbance. The dashed lines are isotachs are in ms^{-1}. (a) Easterly, (b) Monsoon-E, (c) Monsoon-Wk, and (d) Monsoon-Stg.

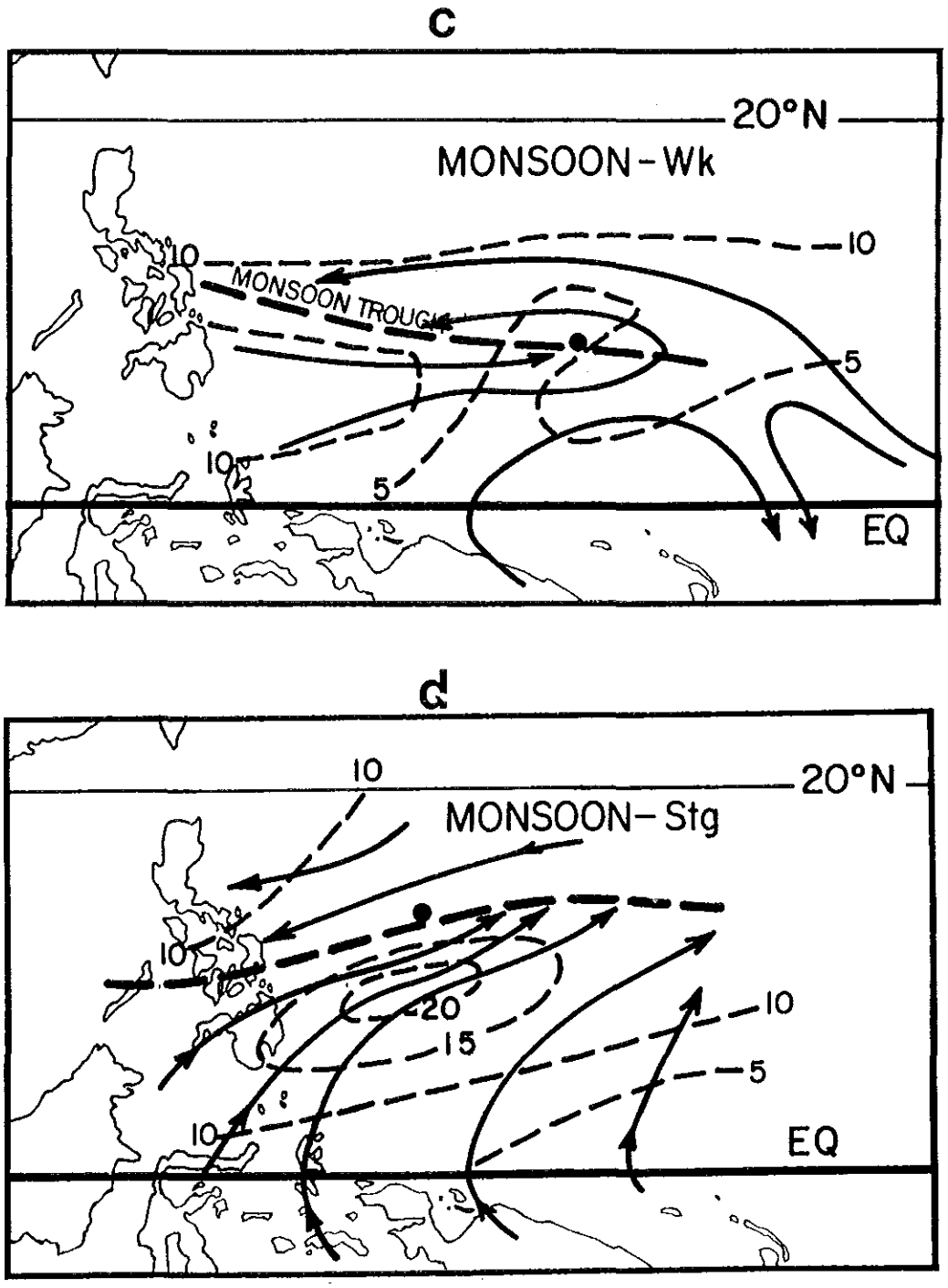

Figure 5.2: Continued.

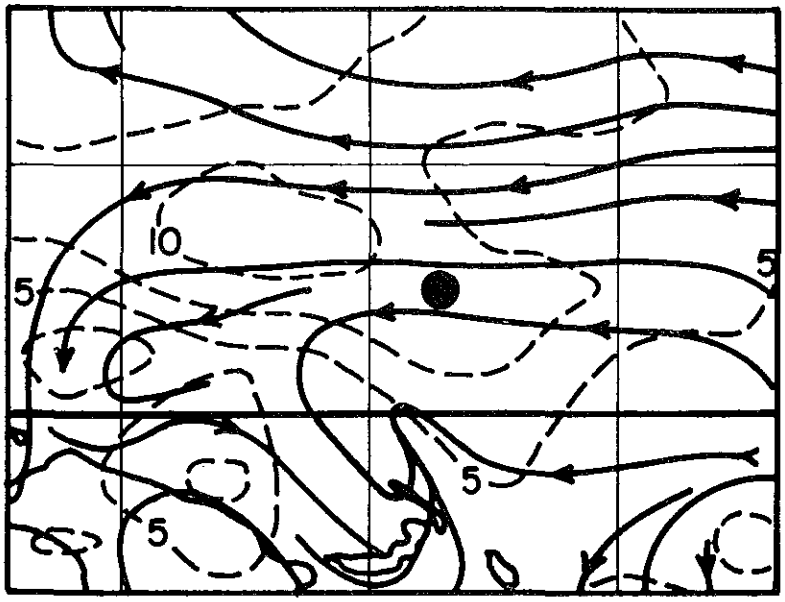

Figure 5.3: Easterly pattern in 850 mb objective streamline–isotach (ms^{-1}) analysis. The large dot is the center location of the pre–tropical storm Agnes disturbance. 12 GMT 28 October 1984.

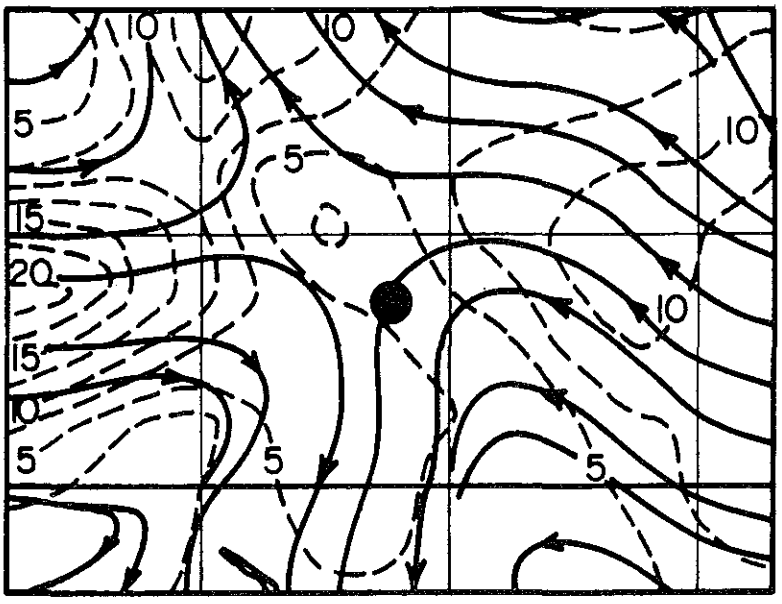

Figure 5.4: Monsoon–E pattern in 850 mb objective streamline–isotach (ms^{-1}) analysis. The large dot is the center location of the pre–tropical storm Vanessa disturbance. 00 GMT 21 October 1984.

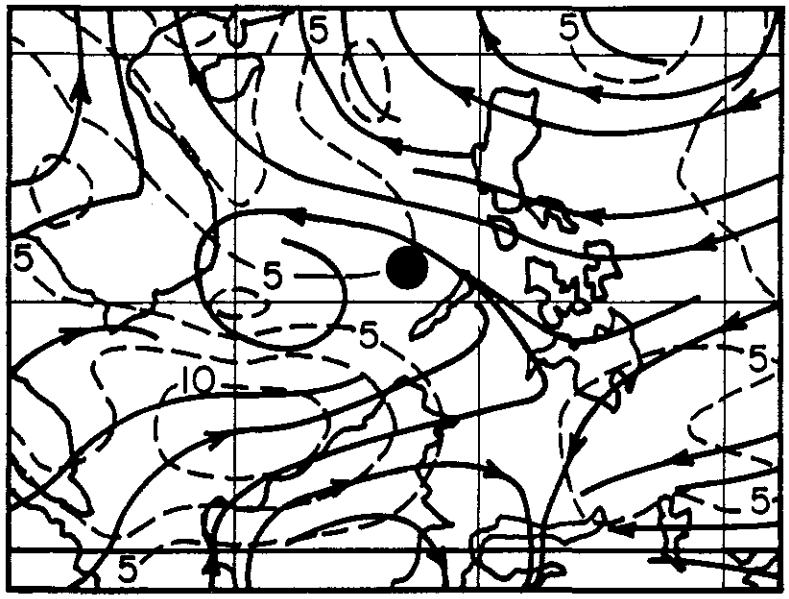

Figure 5.5: Monsoon–Wk pattern in 850 mb objective streamline–isotach (ms^{-1}) analysis. The large dot is the center location of the pre–tropical storm Vernon. 12 GMT 6 June 1984.

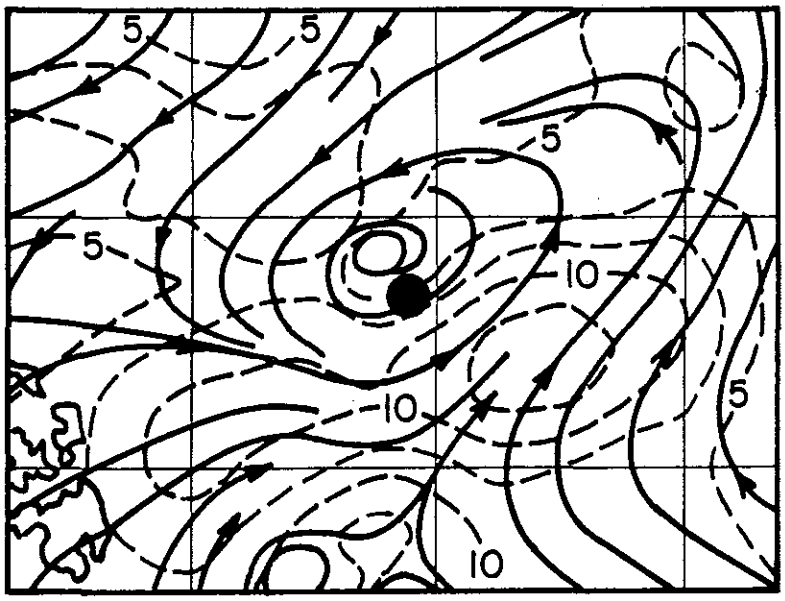

Figure 5.6: Monsoon–Stg pattern in 850 mb objective streamline–isotach (ms^{-1}) analysis. The large dot is the center location of the pre–tropical storm Nina. 00 GMT 26 September 1984.

this pattern. An example is shown in Fig. 5.3. It should be noted that as the tropical cyclone develops, westerly component winds will appear quite early, south of the center, particularly at Stage 2. The 2.5° resolution analysis will not always resolve those winds. However, the pattern is used to describe the pre-tropical storm environment. It is also noted that winds associated with an easterly wave will often take the appearance of a closed circulation if they are analyzed relative to an westward moving wave axis. The Easterly pattern represents tropical cyclogenesis which is not associated with the monsoon trough. This pattern has been described in previous studies (Gray, 1968), and it is likely the predominant pattern in the Atlantic-Caribbean tropical cyclogenesis region where the monsoon trough is seldom observed.

The Monsoon-E pattern is used to describe the situations in which a westward moving disturbance first encounters the westerly winds associated with the eastern end of the monsoon trough, as shown in Figs. 5.2 and 5.4. This is the preferred pattern with which the Stage 1 convective maximum is observed for the cases not located in the South China Sea. Twenty-seven percent of Stage 1 cases were associated with this pattern but only 10% of Stage 2 cases. This is an expected result with westward moving disturbances which are more likely to become embedded within the monsoon trough as they move west.

The Monsoon-E pattern has not been specifically identified as a genesis type in previous studies. However, Heta (1990) describes conditions similar to the Monsoon-E pattern as a favored western North Pacific pattern for development.

The Monsoon-Wk pattern is shown in Figs. 5.2 and 5.5, where the center is located within the monsoon trough, but the winds associated with the trough are relatively weak. The monsoon trough is often observed to extend quite far to the east particularly at low latitudes, but the associated westerly or southwesterly winds are often very weak. The Monsoon-Wk pattern accounts for 13% of Stage 1 and 27% of Stage 2 genesis cases.

In the western North Pacific, particularly in the South China Sea, a very strong and deep monsoon trough is commonly observed. This pattern is termed Monsoon-Stg and an example is shown in Fig. 5.6. Winds in excess of 15 ms^{-1} (30 kt) are often observed with this pattern on both sides of the monsoon trough. Twenty-five percent of Stage 1 cases and 43% of Stage 2 are attributed to the Monsoon-Stg pattern. Disturbances, referred to as monsoon depressions, are often associated with this pattern. Some of these systems evolve into tropical cyclones while others do not.

The TUTT-LLCC pattern is an unusual occurrence in the western North Pacific with only two cases identified out of 50. The low-level circulation center (LLCC) which eventually becomes the tropical cyclone is originally a downward extension of an upper-level cold core cyclonic circulation (TUTT cell). However, by the time tropical storm intensity is attained, the LLCC has either decoupled from the upper cold low or the upper low has filled. This type pattern may be more prevalent in other tropical cyclogenesis regions. Hurricane Claudette formed with this type pattern in the Atlantic in 1985 (Case, 1986).

The Mid-latitude pattern is also somewhat of a rare event in the western North Pacific, accounting for four Stage 1 patterns and three Stage 2 patterns. All of the occurrences were in 1984 and were mostly outside the primary genesis region. When a cold front which originates in mid-latitudes, moves into the tropics, it typically slows down and persists for many days as a stationary front or a low-level cyclonic shear zone. This provides the positive relative vorticity required for tropical cyclogenesis. Once again, this pattern is more likely to be associated with tropical cyclogenesis in the Atlantic-Caribbean area, particularly in the Gulf of Mexico. Hurricane Alicia was one of several tropical storms that formed in the Gulf of Mexico with this type pattern in 1983 (Case and Gerrish, 1984).

5.2.1 Summary

The low-level flow patterns in which western North Pacific tropical cyclones form, are usually associated with the monsoon trough. As shown in Table 5.3, this applies to 65% of the Stage 1 patterns and 80% of the Stage 2 patterns. The monsoon trough is also a semi-permanent feature in the eastern North Pacific, the North Indian, and the North

Australia tropical cyclone regions. Tropical cyclone formation in the other regions (South Indian, South Pacific, and Atlantic-Caribbean) may be associated more with the other patterns (Easterly, Mid-latitude, and TUTT-LLCC).

5.3 Wind Surges

A thorough study of surges as described in section 4.3 has not been attempted for the present study. This is because the available data sources are insufficient for an adequate study. However, when surges were identified with either Stage 1 or Stage 2, they were entered in Table 5.1. It is important to note that entries in Table 5.1 which have no surge information does not imply that a surge is not present. Surges have been detected by all three data types—aircraft, conventional, and satellite. The data type and wind direction associated with each surge has been compiled in Table 5.1. Table 5.5 lists the number of surges detected by each data source for both Stage 1 and Stage 2. Note that very few aircraft detected surges are analyzed for Stage 1, simply because very few reconnaissance flights were flown during Stage 1. Also, there are very few instances in which a surge was detected by all three data types.

Table 5.5: Number of surges identified using the three data sources.

	Stage 1	Stage 2
Aircraft Reconnaissance	3	20
Conventional Analysis	18	18
Satellite Images	7	6
Total	28	44

5.3.1 Aircraft Reconnaissance

Aircraft reconnaissance observations of wind velocity at 457 m (1500 ft flight level) sometimes provide the most direct evidence of surges. However, the purpose of the flights was to locate circulation centers (vortex fixes), not to identify surges. The flight data is not available on a regular basis since flights were scheduled according to operational forecast needs. Figure 5.7 shows the distribution of the times of the flights with respect to the Stage 1 convective maximum. Most of the aircraft data are applicable to the later part of Stage 1, following the convective maximum, or to Stage 2.

All available flight data was analyzed to identify surges. Three were found during Stage 1 and twenty for Stage 2 as denoted in Table 5.5. The time of the flights which indicated surges do not necessarily coincide with the times listed in Table 5.1 but rather with any portion of Stage 1 or 2 as depicted in Figs. 4.1 and 4.2.

Figure 5.8 is a plot of wind observations with a Stage 1 surge for Forrest which is characterized by west-southwest winds just south of a weak monsoon trough. Figure 5.8b shows the same observations relative to the tropical disturbance center location which was moving to the west at about 8 ms^{-1}. This storm relative depiction results in larger wind speeds to the south of the center and a more distinct surge. Figure 5.9 shows another westerly surge which occurred two days later with Stage 2 of Forrest, at which time Forrest was a tropical depression. The surges associated with pre-tropical storm Forrest are discussed further in Chapter 7.

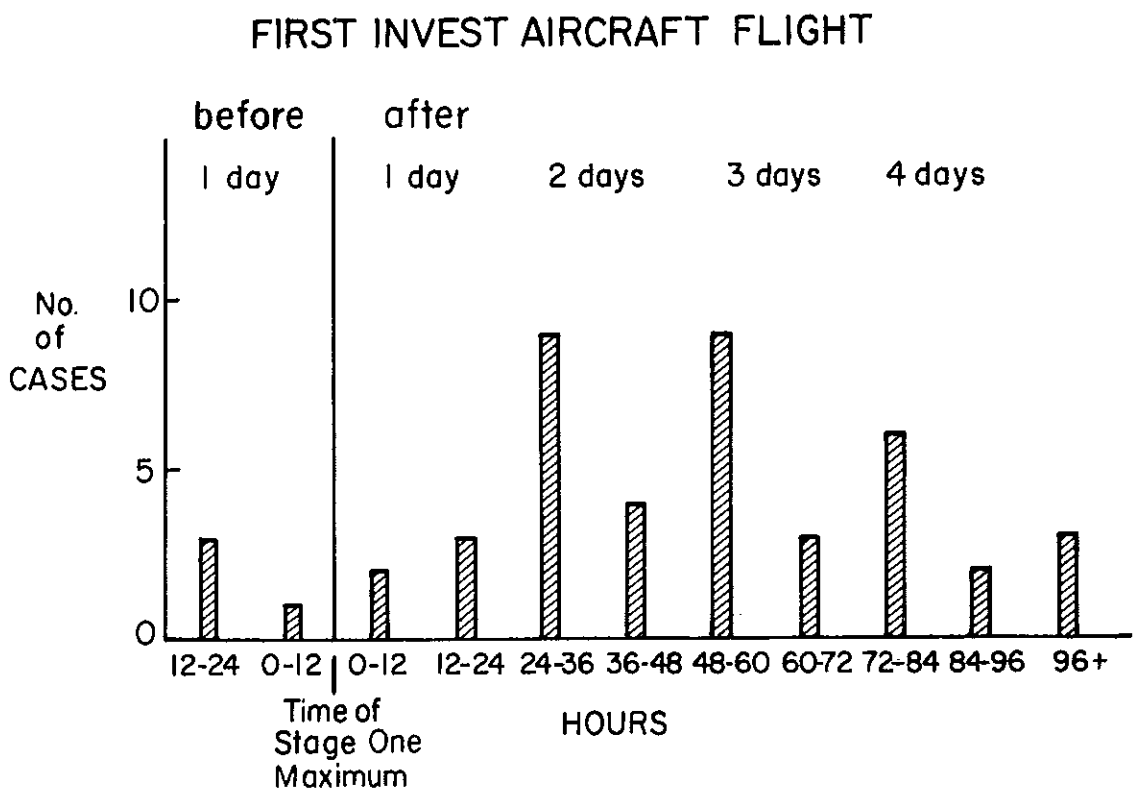

Figure 5.7: Frequency distribution of the time of the first investigative reconnaissance flight for each of the 1983–1984 cases, with respect to the time of the Stage 1 convective maximum.

5.3.2 Conventional Analysis

The objective analyses include radiosonde observations and satellite cloud drift wind vectors. The radiosonde stations have a relatively sparse distribution. The cloud drift wind vectors are quite variable both in terms of number of observations and their distribution. Those considerations along with the 2.5° resolution of the analysis are limitations on the detection of surges. Many surges likely go undetected or are not well depicted in the conventional data. Nevertheless, 18 surges were identified with Stage 1 cases and 18 for Stage 2 (Table 5.5) with the conventional data. Figure 5.10 shows an easterly surge and Fig. 5.11 shows a westerly surge as depicted in the 850 mb streamline-isotach analyses. The objective analyses are available for all cases in Table 5.1, and the identification of surges has been attempted for all cases. However, the quality of products are highly variable and the analyses are not available in storm relative framework. Many cases involved a surge analysis that was not definitive. Therefore, the present study cannot be considered a thorough study of surges with conventional objective analysis data.

5.3.3 Satellite Images

Since a surge is a wind feature, the way it can best be detected with satellite data is through cloud motions. However, surges may also appear in satellite data due to the associated deep convective clouds. Cloud motions of very small, low-level cumulus clouds may specify the location and direction of the wind speed maximum. This observation of a surge can generally be seen best with high resolution visible images in time series with 30-minute or less image intervals. Infrared images may not adequately resolve the small, low-level clouds. Surges revealed in this way cannot be identified in the present study due to the 10 km resolution and 3 hr time interval of the satellite data. However, in the western North Pacific, surges often have some deep convective clouds associated

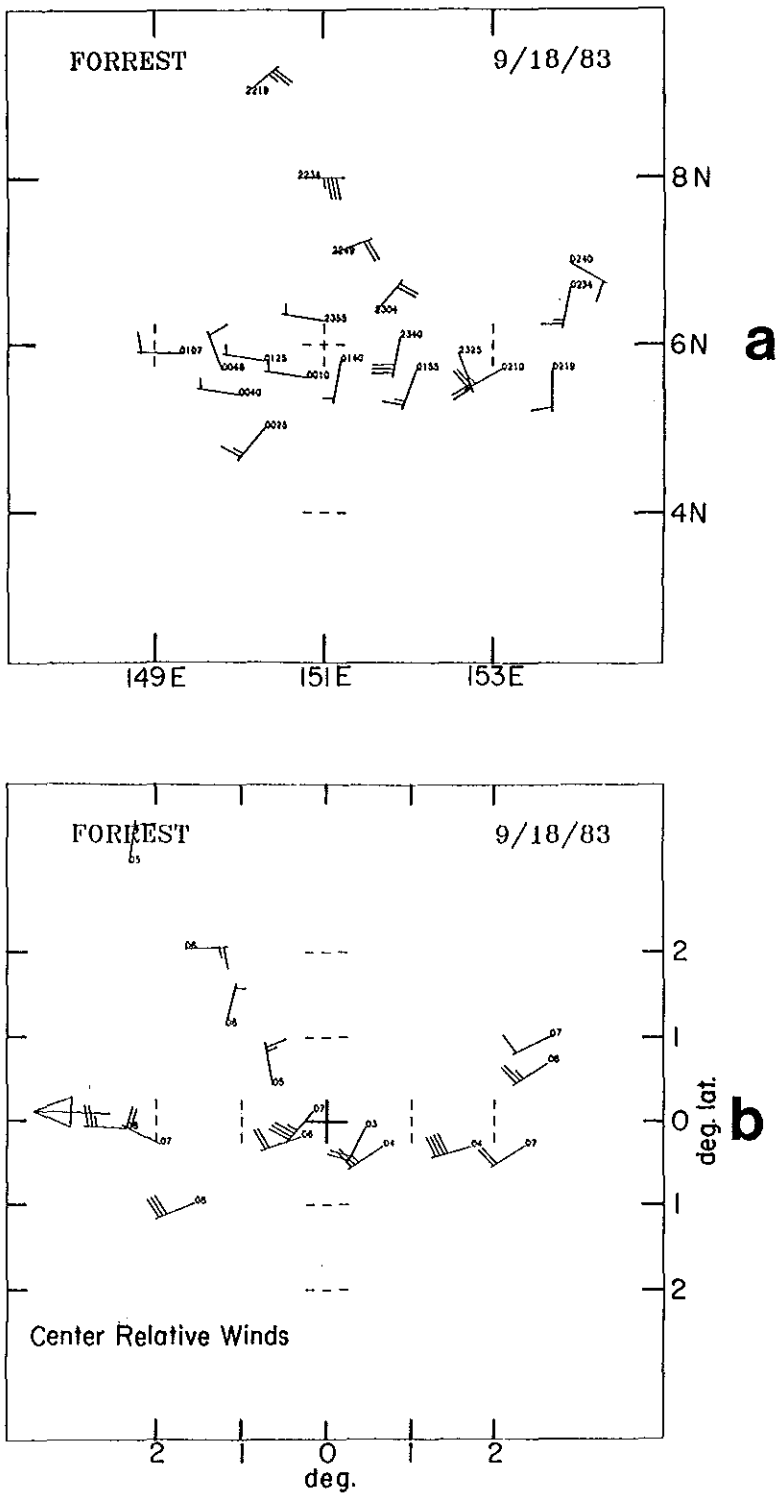

Figure 5.8: a) Wind observations during Stage 1 of Typhoon Forrest cyclogenesis. The track of the disturbance center during the flight is plotted. b) Observations in the motion relative coordinate system.

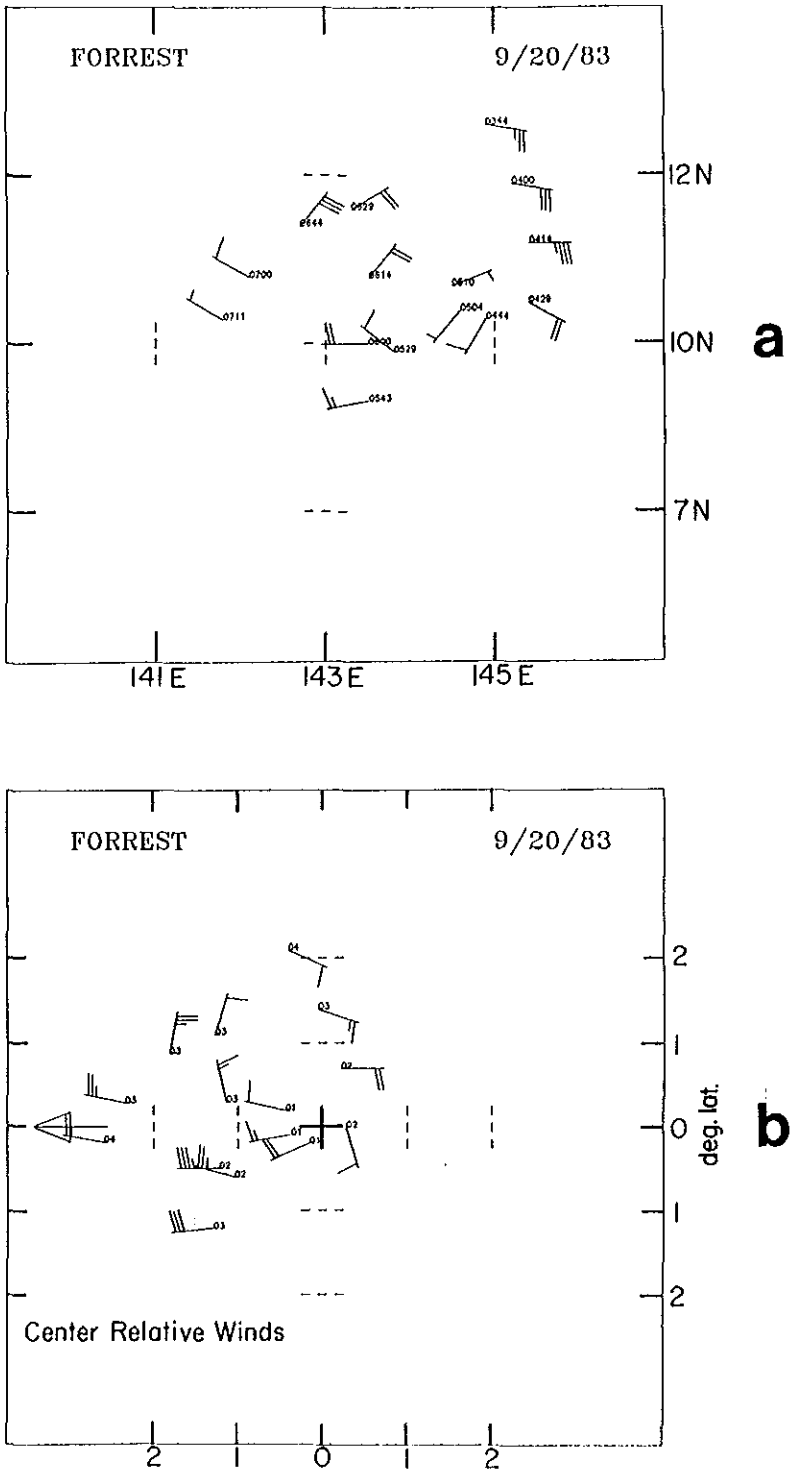

Figure 5.9: Same as Fig. 5.8, except two days later during Stage 2 of Typhoon Forrest cyclogenesis.

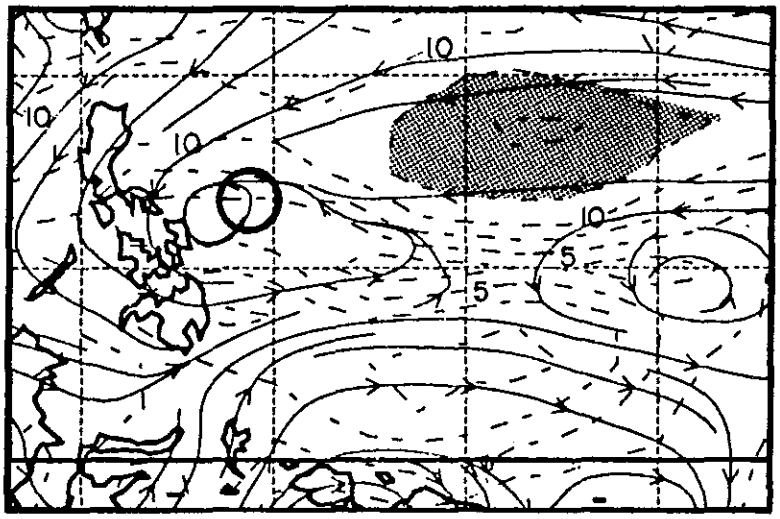

Figure 5.10: Easterly surge with the pre-tropical storm Warren disturbance (circle). 850 mb streamline-isotachs (m s^{-1}). 12 GMT 18 October, 1984. Wind speeds greater than 12.5 m s^{-1} associated with the surge are shaded.

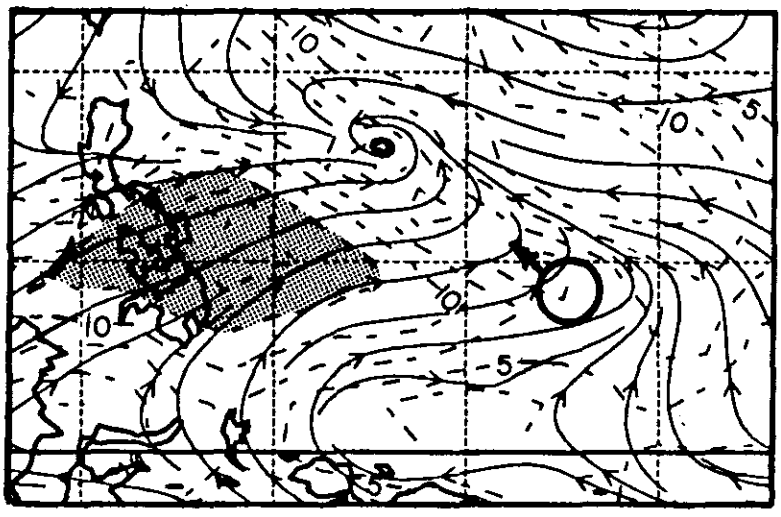

Figure 5.11: Westerly surge with the pre-tropical storm Ike disturbance (circle). 850 mb streamline-isotachs (m s^{-1}). 00 GMT 26 August, 1984. Wind speeds greater than 12.5 m s^{-1} associated with the surge are shaded.

with them. Therefore, three-hourly enhanced IR images will often show cloud features that have continuity and are associated with the low-level convergence field of the surge. Careful analyses of animated IR imagery viewed both in the earth fixed and the center relative framework may reveal the presence of surges. A surge interacting with a pre-existing disturbance will often appear as merging convective systems or cloud clusters. The cloud amount associated with the surge is generally smaller than that associated with the disturbance.

Since analysis of surges with satellite data requires considerable computer resources and time, and because of satellite data limitations, a thorough study of surges for the present study was not attempted. Nevertheless, seven Stage 1 surges and six Stage 2 surges and their direction (Table 5.1) were identified. The series of IR images in Fig. 5.12 show one such example of a westerly surge. A small area of deep convection is located to the west-southwest of the pre–Stage 1 tropical disturbance which developed into Typhoon Vanessa. This convection is tracking to the east and is associated with a surge (Figs. 5.12a,b). The pre-existing tropical disturbance is propagating to the west. During the period shown in Fig. 5.12, the two convective systems merge, resulting in the Stage 1 convective maximum (Fig. 5.12c). This qualitative analysis of the satellite imagery requires time continuity in order to see cloud motions and identify the surge interacting with the tropical disturbance. Animated satellite imagery is needed to perform such analyses. Additional examples of surges in the satellite imagery appear in section 7.3.

It is important to note that satellite imagery is the only routinely available data source to observe surges. High quality cloud drift wind data, and techniques for satellite image identification of surges is required. Studies to evaluate the application of satellite imagery to surge analysis are needed. Also, a better understanding of their origin, dynamics, and interactions with pre-existing tropical disturbances, requires additional research studies.

5.3.4 Direction of the Surge

The present study has identified 72 surges using the three independent data sources as shown in Table 5.5. The frequency distribution of surge direction is of particular interest. Each surge was assigned a direction given by one of 16 compass directions (i.e. N,NNE,NE,ENE...) according to the wind direction of the wind speed maximum. This generally corresponds with the direction from which the surge approaches the disturbance center. This direction is also associated with the direction of propagation of the surge.

The frequency distribution for surge direction is given in Fig. 5.13. Surges have been observed to occur with nearly all directions. However, the majority of surges have a westerly component and WNW through WSW is the most common direction accounting for more than half of the cases. This is due to the influence of the monsoon trough. Surges often occur in the westerly component monsoon flow but are also observed in the easterly trade winds and may approach the disturbance from nearly any direction. Surges which cross the equator and move northward to interact with a tropical disturbance have also been observed.

As depicted in Figs. 5.8 and 5.9, the wind velocity associated with a surge, may be different when computed in a coordinate system relative to the disturbance center and its propagation speed. The surge is properly analyzed when the propagation vector of the tropical disturbance is subtracted from the observed wind vectors.

Figure 5.14 illustrates an idealized low-level wind field typical of the western North Pacific region. When a tropical disturbance moves to the west, it approaches the eastern end of the monsoon trough. The winds south of trough axis are generally from the west or southwest, while the tropical disturbance is embedded in predominantly easterly component winds. When the disturbance first encounters the westerly component winds it experiences a surge from the west due to the combination of its westward propagation and the monsoon westerlies. Therefore, with this scenario, the surge may be characterized by relatively weak winds and may be a quasi-stationary feature. A synoptic analysis may not necessarily identify this feature as a wind speed maxima, but it nevertheless becomes

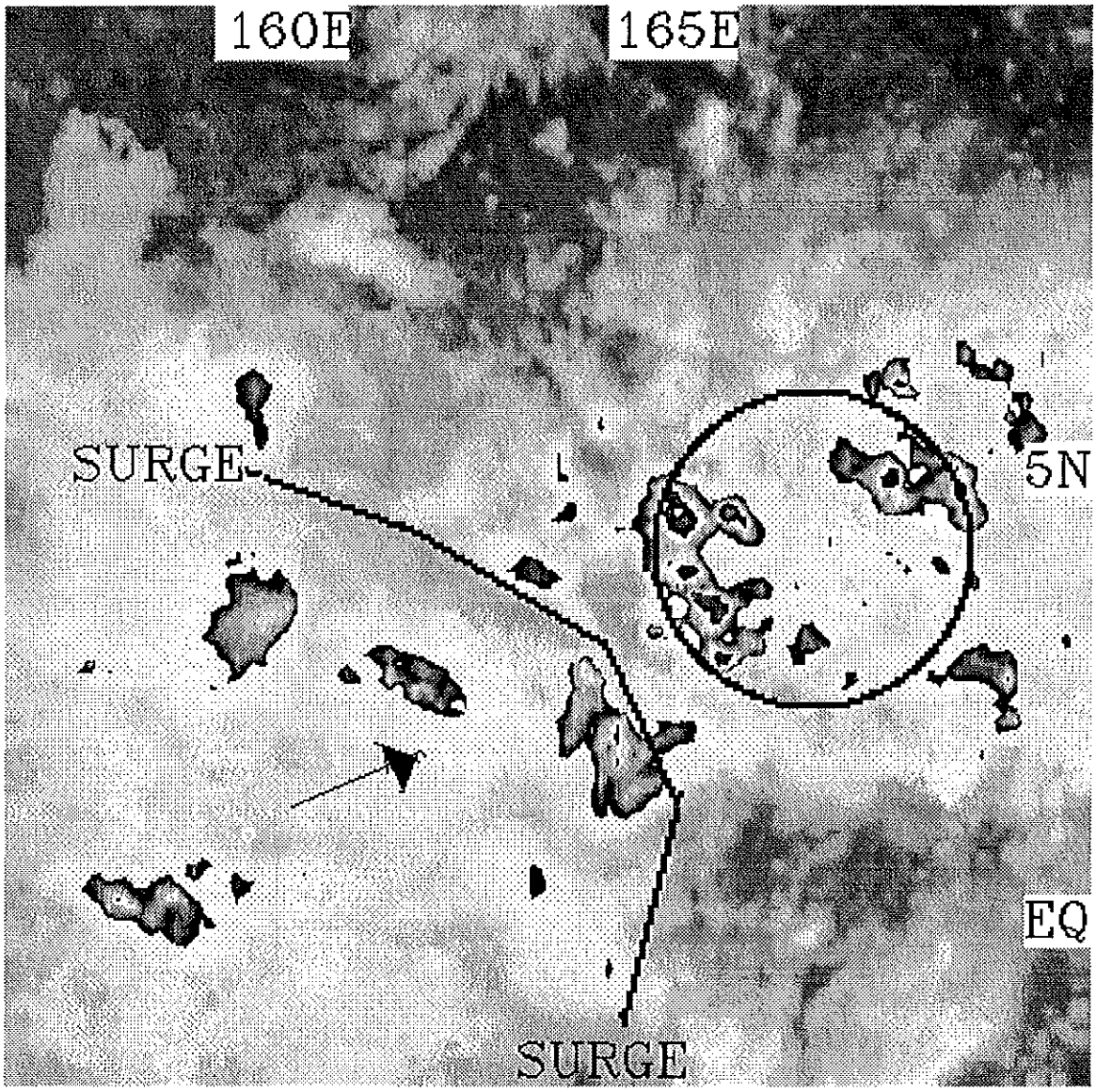

Figure 5.12: Series of IR images, 3 hr apart, during surge interaction period of Pre-Tropical Storm Vanessa. a) 06 GMT. b) 09 GMT. c) 12 GMT. 20 October, 1984.

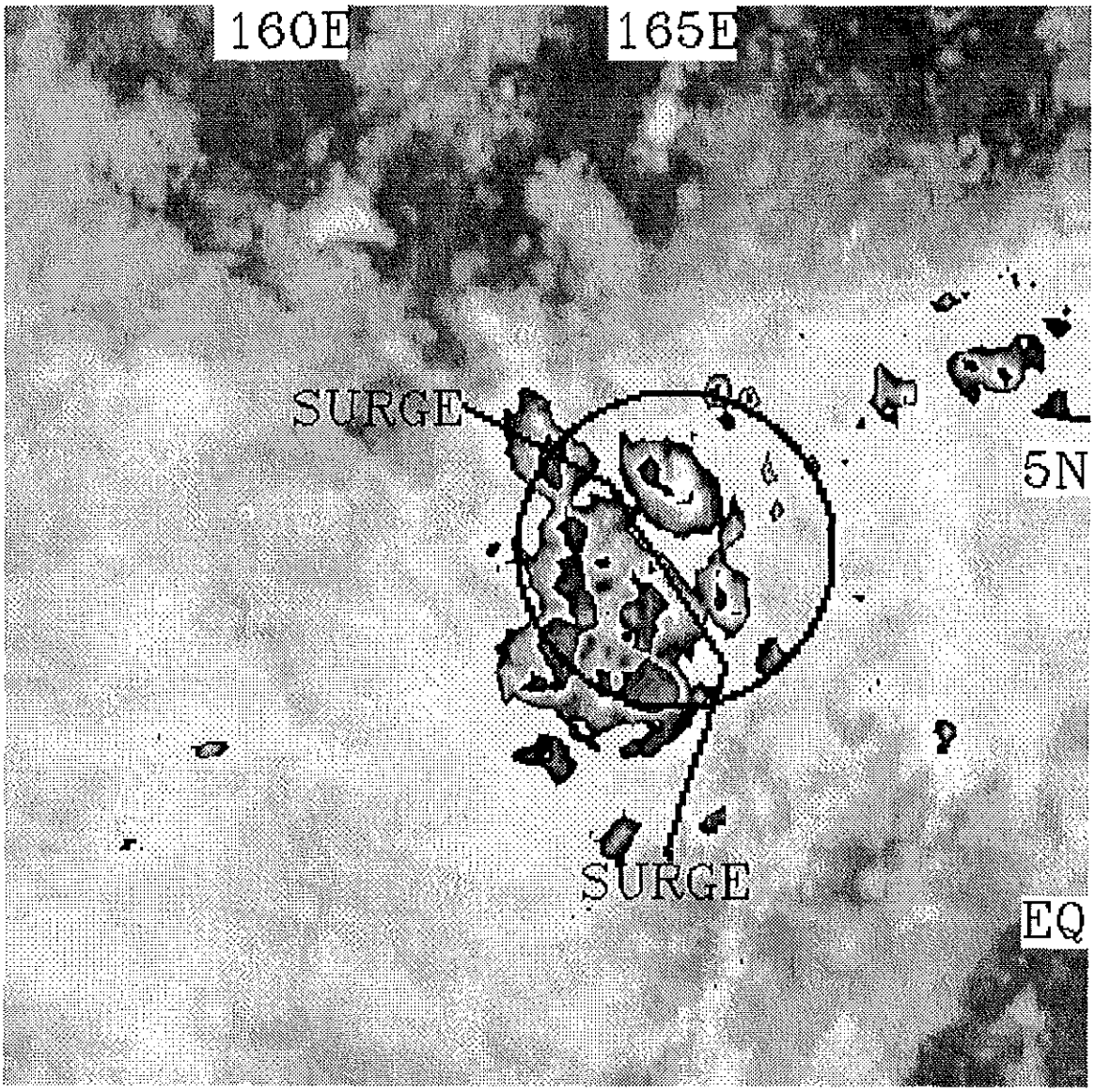

Figure 5.12: b. Continued

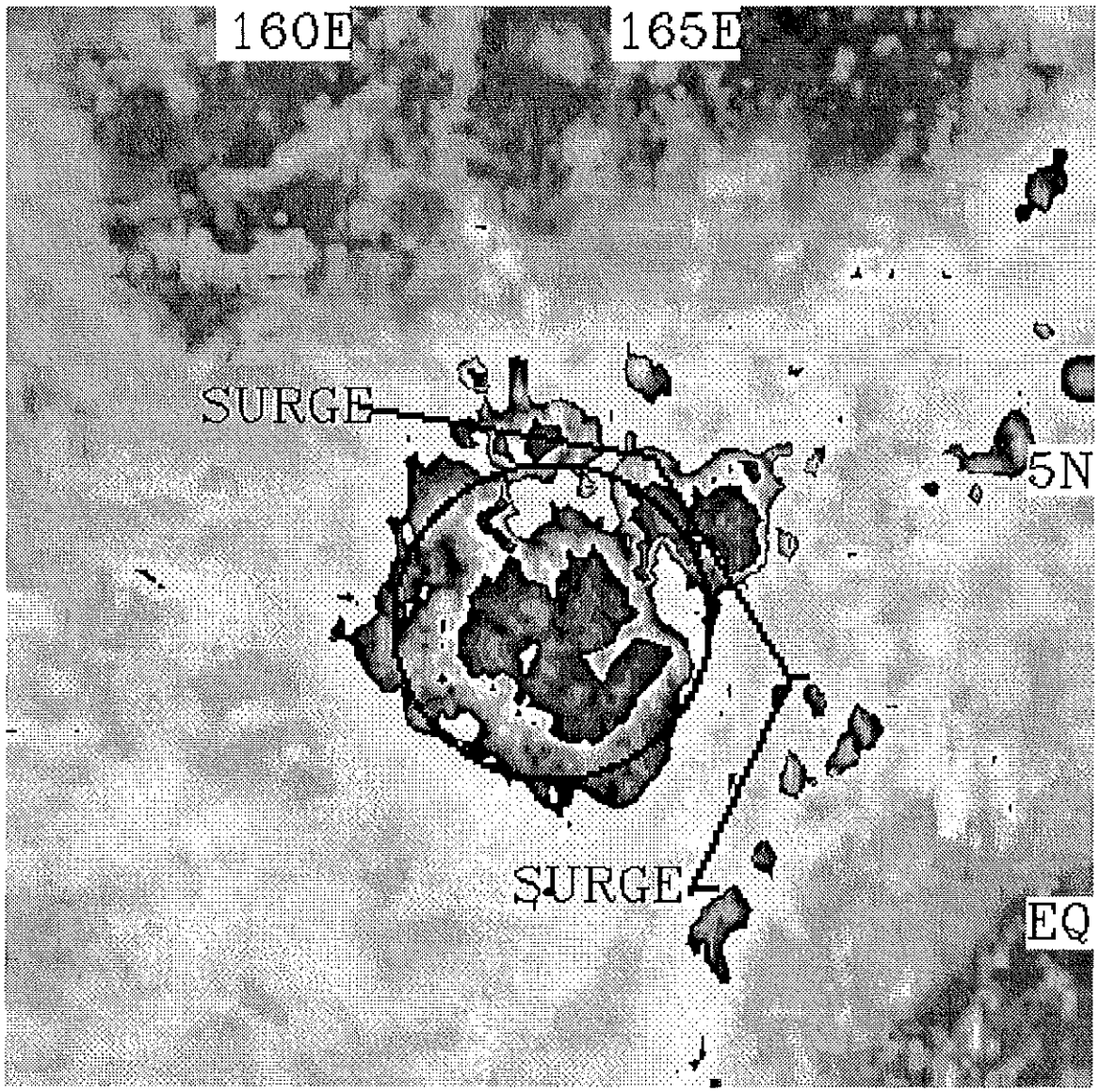

Figure 5.12: c. Continued

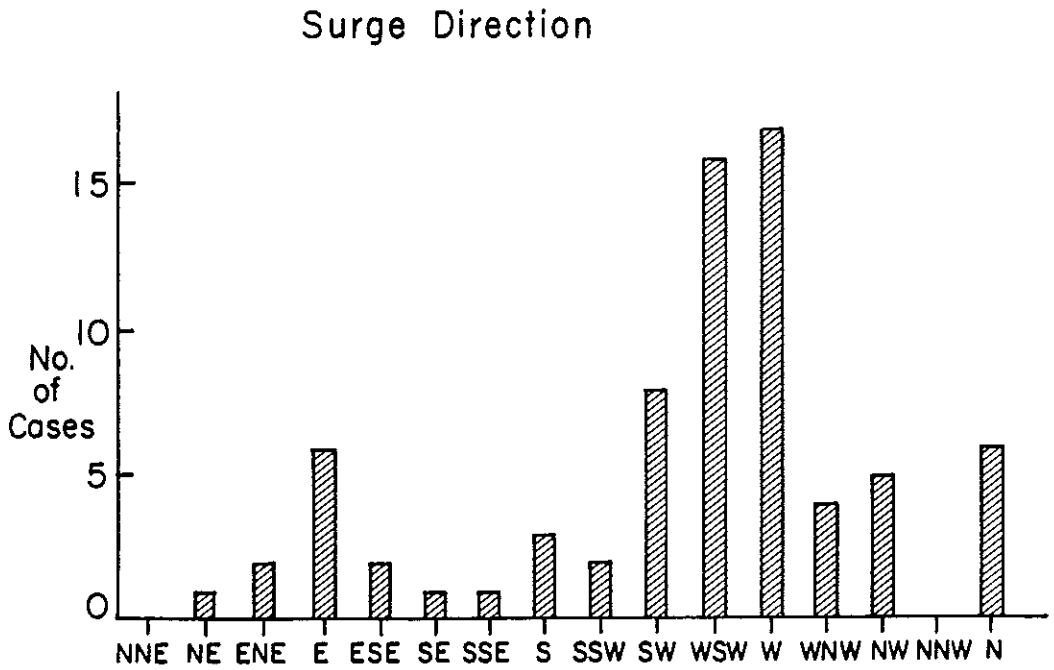

Figure 5.13: Frequency distribution of surge direction.

a surge to a westward propagating disturbance. The present study suggests that the furthest eastward extent of monsoon trough westerly component winds is a preferred location for Stage 1 of tropical cyclogenesis. These winds may be relatively weak and yet act as a surge and a synoptic-scale convergence mechanism to initiate the convective maximum necessary for tropical cyclogenesis.

5.3.5 Summary

Are surges necessary for tropical cyclogenesis? Can they be used to forecast tropical cyclone formation? The only definite conclusions to be drawn from the data presented here are that surges during the cyclogenesis period can be identified in all data sources and often have a westerly component direction. The role of surges in tropical cyclogenesis and how they fit into the conceptual model are discussed further in Chapter 8.

5.4 Upper-level Wind Direction and Speed

Table 5.2 (see p. 48) lists the average 200 mb wind direction in the area out to 3° latitude radius of the center for each case. Directions are assigned according to the 16 compass directions with a frequency distribution as shown in Fig. 5.15. There is a distinct preference for easterly winds, however cases are observed with 200 mb winds from nearly all directions. Sixty-two percent of Stage 1 cases and 76% with Stage 2 have 200 mb wind directions from SE-E-NE. This agrees with composite studies of McBride and Zehr (1981), Lunney (1988) and Lee (1989a) which show upper-level easterly winds for 0–3° radius at 200 mb.

The average 200 mb wind speeds are listed in Table 5.2 as weak (Wk, < 6 ms^{-1}), moderate (Mod, $6 - 12ms^{-1}$), or strong (Stg, > 12 ms^{-1}). Sixty-six percent of Stage 1 cases have weak 200 mb winds and only 12% are strong. For Stage 2, 71% have weak winds and only 2% have strong winds. This is an expected result due to the low vertical wind shear requirement for tropical cyclogenesis as revealed by previous studies (Gray, 1968; McBride and Zehr, 1981). With the very few cases that have strong winds at 200

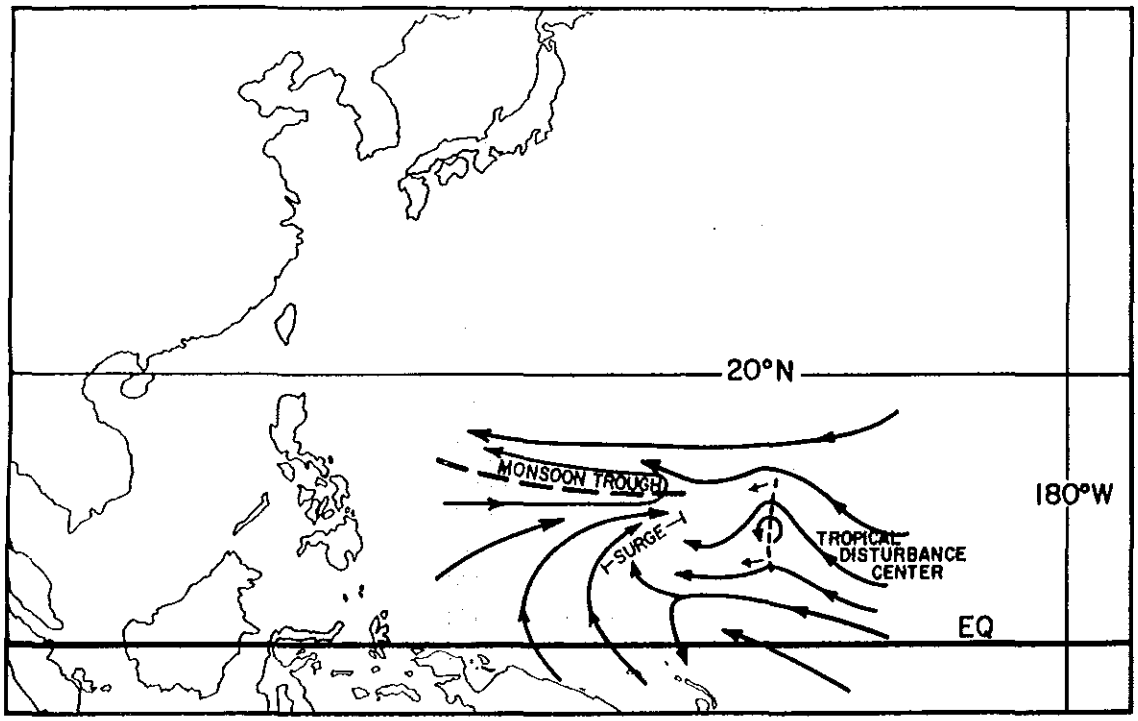

Figure 5.14: Idealized streamline depiction of a westward moving tropical disturbance about to experience a westerly surge by encountering the eastern end of the monsoon trough.

mb, those high wind speeds likely do not persist through the cyclogenesis period. Also, those disturbances which are moving rapidly in the same direction as the 200 mb winds, may still have relatively small vertical shear, provided that the low-level winds have a similar velocity.

McBride and Zehr's (1981) 200 mb wind composites for pre-typhoon disturbances show an anticyclone located about 4° latitude to the east-northeast of the center. The 200 mb composite for non-developing disturbances, on the other hand, shows unidirectional winds from the east-northeast. Dvorak (1984) contends that unidirectional flow is unfavorable for tropical cyclogenesis. Table 5.2 includes a "Y (yes)" or "N (no)" entry indicating whether the 200 mb winds are unidirectional. This is determined according to wind directions out to 5° latitude from the center. If those winds vary by less than 20° in either direction, the case is classified as unidirectional.

Thirty-two percent of the Stage 1 cases and 20% of the Stage 2 cases have unidirectional winds. Therefore, although unidirectional 200 mb flow is usually not associated with tropical cyclogenesis, it does sometimes occur under those conditions.

5.5 Subtropical Ridge

The 200 mb subtropical ridge (STR) is typically located poleward of developing tropical cyclones (Riehl, 1954). The distance and direction of the STR from the disturbance center has been compiled from the 200 mb objective analyses. Table 5.6 shows the number of cases classified into several categories according to the location of the STR. The majority of cases have the STR located within 2–20° latitude to the north. The STR is located very near (within 2° latitude of center) the pre-tropical storm disturbance for 17% of the Stage 1 cases and 20% of the Stage 2 cases. However, it is important to note that tropical cyclogenesis does occasionally occur with the STR located elsewhere.

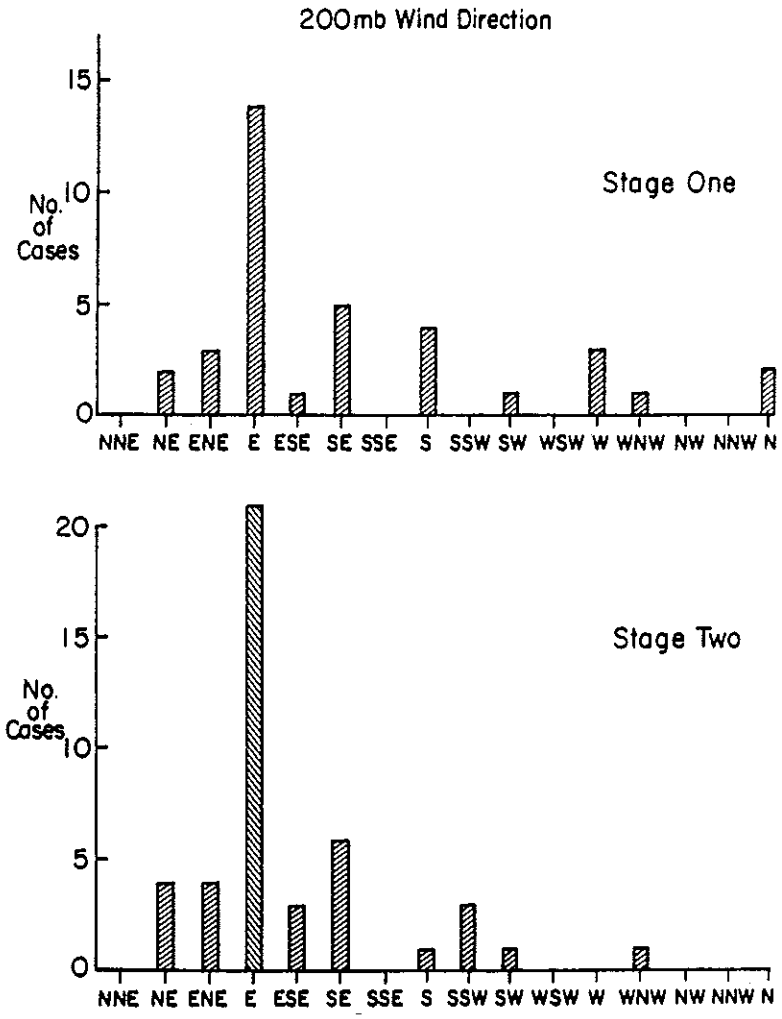

Figure 5.15: Frequency distribution of 200 mb wind direction associated with tropical cyclogenesis.

Table 5.6: Location of Subtropical Ridge (STR) with respect to the genesis location.

STR Location		Percent of Cases	
Direction	Distance	Stage 1	Stage 2
	Within 2° lat.	17	20
North Quadrant	2–10° lat.	36	43
North Quadrant	10–20° lat.	20	23
West Quadrant	2–20° lat.	5	2
East Quadrant	2–20° lat.	10	8
South Quadrant	2–20° lat.	7	4
	> 20° lat. or non-existent	5	0

5.6 Tropical Upper Tropospheric Trough

The Tropical Upper Tropospheric Trough (TUTT) is a semi-permanent feature in the 200 mb analysis during much of the western North Pacific typhoon season (Atkinson, 1971). In a monthly mean 200 mb analysis, the TUTT extends ENE-WSW, located equatorward of the STR. It is typically shallow and usually does not extend downward to 500 mb. It is often comprised of distinct closed cyclonic cold-core lows often referred to as TUTT cells as shown in Fig. 5.16. According to Sadler (1976, 1978) the TUTT may initiate tropical cyclogenesis. Dvorak (1984) attributes tropical cyclogenesis to upper-level mid-latitude troughs.

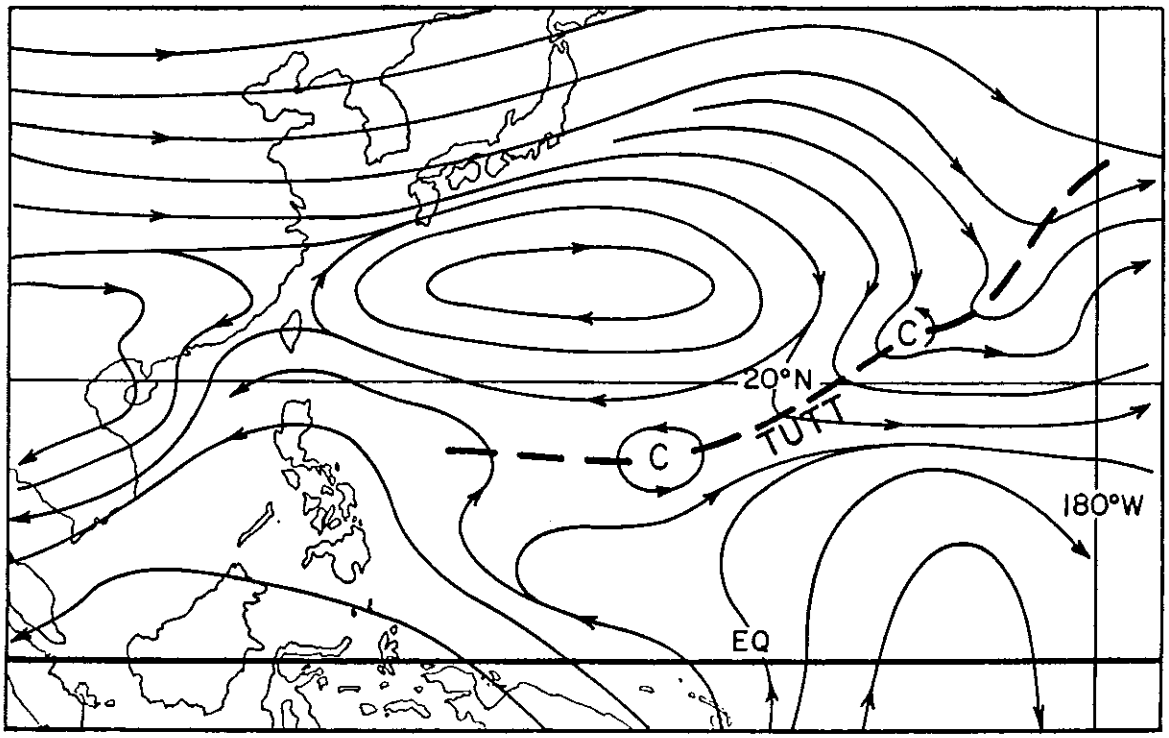

Figure 5.16: 200 mb streamline analysis of a TUTT at 12 GMT, 3 October, 1984.

Table 5.2 includes an entry indicating whether or not the TUTT axis or a TUTT cell center is located within 20° latitude of the disturbance center. Using this criteria, 61% of Stage 1 cases and 54% of Stage 2 cases are associated with the TUTT. When a 10° latitude distance is used, only 41% at Stage 1 and 35% at Stage 2 are associated with the TUTT (Table 5.7). As discussed in section 5.2, two cases are identified for which the low-level cyclonic circulation appears to be a downward extension of an upper low at Stage 1. This is a rare occurrence in the western North Pacific. The disturbance center is located within the cyclonic circulation region of a TUTT cell, in only 10% of the Stage 1 cases and none of the Stage 2 cases.

An analysis of TUTT location is presented for non-developing disturbances in Chapter 6. The influence of the TUTT on tropical cyclogenesis is discussed further in Chapter 8.

5.7 Summary

The purpose of this chapter is to illustrate not only the typical synoptic-scale flow patterns associated with tropical cyclogenesis, but also the entire range of patterns which

Table 5.7: Location of the TUTT relative to the pre-tropical storm disturbance center.

	Trough Axis or Low Center within:	
	20° latitude	10° latitude
Stage 1	61%	41%
Stage 2	54%	35%

are observed. However, to adequately assess the role of synoptic-scale forcing on genesis, one must make comparisons with non-developing disturbances. It is also desirable that quantitative differences between non-developing and developing cases be evaluated. Results of this type are presented in Chapter 6.

Chapter 6

QUANTITATIVE COMPARISON OF PRE–TROPICAL STORM AND NON–DEVELOPING DISTURBANCES

Pre-tropical storm disturbances and non-developing disturbances have many similarities. This is particularly true of disturbances before they become tropical depressions. The amount and intensity of deep convective clouds and associated rainfall are very similar, and thus their appearance in satellite images are similar. The mean vertical motion fields and minimum sea-level pressures are nearly the same. In fact, as discussed in Chapter 4, a pre-tropical storm disturbance prior to the onset of the Stage 1 convective maximum, may be considered a non-developing disturbance.

To better understand the tropical cyclogenesis process, non–developing tropical disturbances are compared with pre–tropical storm disturbances. First, a qualitative synoptic-scale analysis of the non-developing disturbances is presented. Then, a quantitative analysis using the two-stage conceptual model introduced in Chapter 4, is applied to both pre-tropical storm and non-developing cases to look for differences.

6.1 Synoptic–Scale Conditions Associated with Non-Developing Disturbances

6.1.1 Low-Level

The 850 mb wind patterns associated with non-developing disturbances are analyzed using the same method as in section 5.2. The objective analysis time nearest the time of the convective maximum is used to classify the 850 mb pattern type for each non–developing disturbance. If the analysis cannot be classified as one of the six patterns defined in section 5.2, it is termed "Other". The results are given in Table 6.1, and show that only 32% of the cases are associated with the monsoon trough, as opposed to 65% of the pre-tropical storm Stage 1 cases. This suggests that the higher vorticity and convergence associated with the monsoon trough may, in some cases, provide the environmental forcing for tropical cyclogenesis. Most of the non-developing disturbances are embedded in easterly flow at 850 mb.

As discussed in Chapter 3, the non-developing disturbances are limited to those that persist for at least two days and are located in the primary genesis region ($5 - 20°N$, $125°E - 160°E$). Disturbances in other genesis regions may have different 850 mb patterns.

6.1.2 Upper-Level

As mentioned in section 5.6, previous studies (Sadler, 1976) have suggested that the TUTT (Tropical Upper Tropospheric Trough) may be an important mechanism for tropical cyclogenesis. With the pre–tropical storm disturbances, 61% of Stage 1 cases and 54% of Stage 2 cases have center positions located within 20° latitude of a TUTT axis or TUTT cell center. When the same analysis is done with respect to the non-developing disturbances, at the time nearest their convective maximum, 68% are associated with the TUTT. When the distance criteria is reduced to 10° latitude, the percentages are decreased somewhat for both the non-developing and the pre-tropical storm disturbances. The results are summarized in Table 6.2.

There are only very small differences between the number of non-developing disturbances and pre-tropical storm disturbances associated with the TUTT. This suggests that

Table 6.1: 850 mb patterns associated with non–developing disturbances (22 total).

Pattern	No. of Cases	Percentage
Easterly	13	59
Monsoon–E	1	5
Monsoon–Wk	6	27
Monsoon–Stg	0	0
Mid–latitude	0	0
TUTT–LLCC	0	0
Other	2	9

Table 6.2: Pre–tropical storm and non–developing disturbance locations with respect to the TUTT axis.

	Within 10° latitude		Within 20° latitude	
	No.	%	No.	%
Pre–tropical storm Stage 1	17/41	41	25/41	61
Pre–tropical storm Stage 2	18/51	35	28/51	55
Non–developing	9/22	41	15/22	68

the TUTT is not an important mechanism for distinguishing disturbances with regard to genesis. Less than half of both type systems have center locations within 10° latitude of a TUTT. The influences of synoptic-scale upper-level wind patterns are addressed quantitatively in sections 6.6–6.7 and discussed further in Chapter 8.

6.2 Method of Quantitative Analysis

The BMRC 2.5° latitude resolution objective analyses for 1984 are used to quantify the important but subtle differences between pre-tropical storm (PS) disturbances and non-developing (ND) disturbances. Based on the findings of the present study and previous studies, five candidates of analyzed variables have been chosen which may individually or in combination differentiate between PS and ND cases. They are:

1. 850 mb relative vorticity,
2. 850 mb convergence,
3. 200 mb relative vorticity,
4. 200 mb divergence, and
5. 200–850 mb vertical wind shear vector.

Since the grid resolution of the objective analysis is 2.5° ($\sim$ 280 km), only synoptic-scale features are resolved. Relative vorticity and divergence computations are performed using standard finite difference methods on the 2.5° grid. The relative vorticity and divergence at each grid point is determined by the u and v wind components at the adjacent four grid points (see Fig. 6.1). Each grid point value of relative vorticity and divergence represents an average value for a 2.5° radius area or a 5° latitude grid box.

6.2.1 Interpolation to Best Track

The latitude and longitude of the disturbance center locations at the 00 GMT and 12 GMT analysis times are used to extract quantities from the objective analyses. Some revisions have been made to the Best Track information as given in the Annual Tropical Cyclone Report (JTWC, 1984) for the PS cases, based on a re-analysis of the satellite images. Disturbance centers are located at obvious circulation centers, or at the area-weighted center of the deep convective clouds. The same methods are used to obtain the Best Track data for the ND cases. The 12 hr center locations of all ND cases and PS cases used here are listed in Appendix B and C, respectively.

To extract any quantity from the grid point data to a Best Track center location a simple interpolation method is used. The quantities at the four nearest grid points are linearly weighted according to their distance from the Best Track center location, as illustrated in Fig. 6.2.

A sample of 23 PS cases and 15 ND cases are available for the quantitative comparison which follows. This is comprised of 111 ND time periods and 167 PS time periods. The names, dates and times of the ND and PS disturbances are included in Appendices B and C. Individual ND disturbances have been named according to the convention, yNONn, where y indicates the year (3 = 1983, 4 = 1984) and n is the number of the disturbance. For example, 4NON11 is the 11th ND disturbance in 1984. PS disturbances are named according to the storm name used operationally following genesis. The PS designation, however, refers to all periods prior to becoming a named storm (NS). Storms are named when tropical storm intensity ($17.5 ms^{-1}$) is first attained. PS cases were stratified as follows:

1. Time periods prior to 12 hr before the Stage 1 convective maximum (Cb_{max}) are designated as pre-Stage 1 (PS Pre–Max).

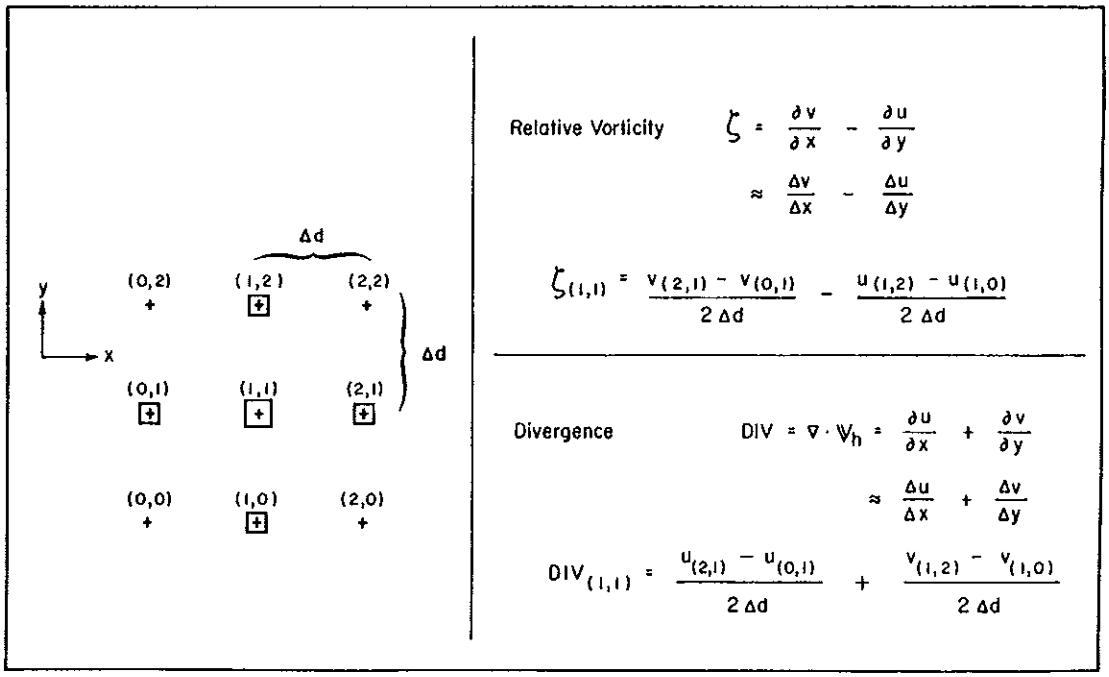

Figure 6.1: Finite difference computations of relative vorticity and divergence.

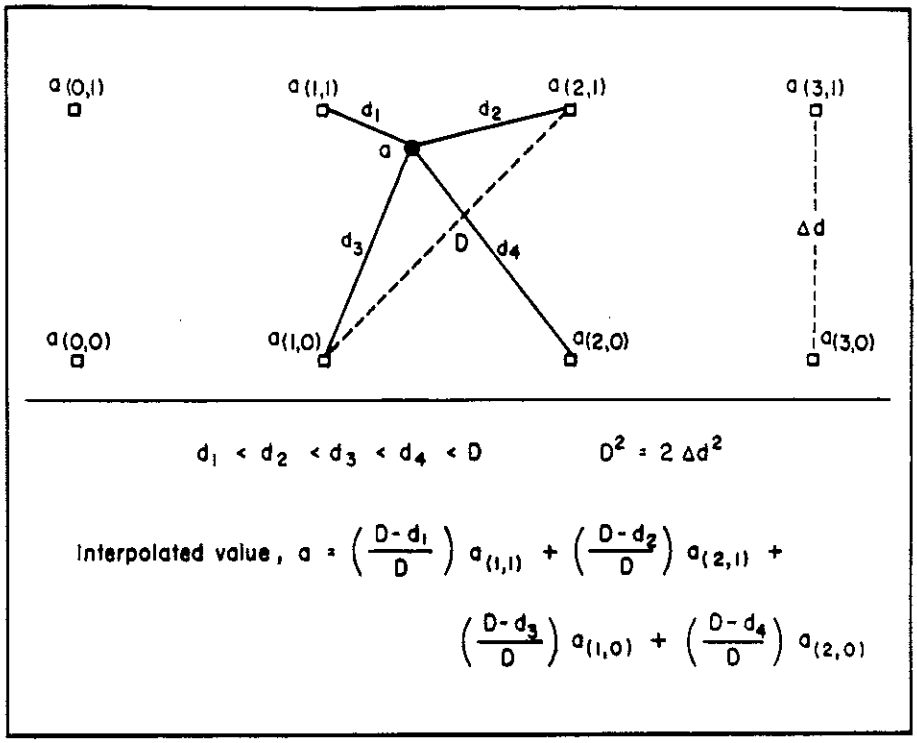

Figure 6.2: Interpolation of grid point quantities to Best Track center position.

2. Time periods within 24 hr preceding the first tropical storm intensity (NS) are designated Stage 2 (PS2).

3. All other intermediate time periods in between are designated as Stage 1 (PS1).

The ND time periods were stratified according to whether they occurred before (Pre-Max) or after (Post-Max) the time of the largest R = 0–2°, T_B < –65°C area (Cb_{max}), for each case.

The PS cases were also stratified according to their Stage 1, 850 mb pattern types (Table 5.1). The Easterly (E), Monsoon–E (M-E), and Monsoon–Wk (M-Wk) patterns were grouped together and labeled "PS-Typical". The Monsoon–Stg pattern was termed "PS-M-Stg" intending to include those disturbances with a strong outer circulation, sometimes referred to as monsoon depressions. The Weak (Wk), Mid–latitude (Mid-lat), and TUTT–LLCC patterns are grouped together and termed 'PS-Other", intending to include the disturbances which are atypical occurrences. The breakdown of time periods with each of the data stratifications for both ND and PS cases are given in Table 6.3.

Table 6.3: Data Stratifications.

Data Set	No. of Time periods (N)	Description
ND	111	All Non-developing
ND Pre–Max	31	Before Cb_{max}
ND Post–Max	80	After Cb_{max}
PS	167	All Pre-tropical storm
PS Pre–Max	44	Before (Stage 1 Cb_{max} - 12 hr)
PS1	77	(Stage 1 Cb_{max} - 12 hr) up to (NS–24hr)
PS2	46	(NS–24hr) up to NS
PS–Typical	81	850 mb Patterns: E, M-E, M-Wk
PS–M–Stg	43	850 mb Patterns: M-Stg
PS–Other	43	850 mb Patterns: Wk, Mid-lat, TUTT

6.2.2 Combined Mean Values

To aid in the quantitative evaluation of ND and PS data, a combined mean value is defined here. This value is used to best differentiate the population of ND quantities from the PS values. Since the latter Stage 2 periods are likely influenced by the structural changes of the end result of the genesis process, they are excluded from the combined mean value. The goal is to differentiate PS from ND disturbances at the earliest possible time in the genesis period.

The combined mean value is the average of the PS Pre-Max and PS1 means, which is then averaged with the ND mean value. It is denoted $\bar{X}_{COMB}$ and is used extensively in the figures, tables, and analysis throughout Chapter 6 as a reference for differentiating PS and ND disturbances.

$$\bar{X}_{COMB} = (\bar{X}_{PRE-MAX} + \bar{X}_{PS1} + \bar{X}_{ND} + \bar{X}_{ND})/4$$

6.3 850 mb Relative Vorticity

Table 6.4 lists the means and standard deviations of the 850 mb relative vorticity (850 VOR) quantities interpolated from the 2.5° objective analyses to the Best Track positions. The PS cases have been subdivided into Pre-Max, PS1, and PS2 data sets and the ND into Pre-Max and Post–Max. The average 850 VOR increases from 0.88 for Pre-Max, to 1.91 for PS1, and to 2.44 for PS2 (850 VOR units are x $10^{-5}s^{-1}$). This is compared with 0.71 for ND cases. The PS Pre-Max cases have 850 VOR which are slightly larger than the ND cases. However, the PS1 and PS2 mean 850 VOR are more than twice as large as the ND mean value.

Table 6.4: 850 VOR ($10^{-5}s^{-1}$) mean ($\bar{X}$) and standard deviation (s) for each data stratification, and the combined mean value, COMB.

Data Set	$\bar{X}$	s	N
PS	1.78	1.26	167
ND	0.71	0.73	111
COMB	1.05		
PS Pre-Max	0.88	0.81	44
PS1	1.91	1.04	77
PS2	2.44	1.44	46
PS–Typical	1.86	1.05	81
PS–M–Stg	2.48	1.49	43
PS–Other	0.95	0.82	43
ND Pre-Max	0.42	0.51	31
ND Post-Max	0.82	0.77	80

It should be emphasized that the 850 VOR values are computed from the 2.5° latitude resolution objective analysis. This resolution is not sufficient to resolve the maximum vorticity associated with the mesoscale vortex. The 850 VOR is more a measure of the synoptic-scale characteristics of the disturbance in which a smaller scale circulation center may or may not exist. It is also to some extent a measure of the synoptic-scale environment surrounding the disturbance.

The results give some insight into the apparent effect of a convective maximum on the synoptic-scale disturbance vorticity. As mentioned in Chapter 3, many of the ND cases have a convective maximum comparable in amplitude to the PS1 cases. The ND Pre-Max to Post-Max mean 850 VOR increase is from 0.42 to 0.82. In comparison, the mean 850 VOR is 0.88 for PS Pre-Max, and increases to 1.91 for PS1. This implies that a convective maximum, even with ND disturbances, may produce a vorticity increase by a factor of two. This increase occurs over a relatively large area on the scale of the disturbance itself.

The influence of the environmental vorticity differences may be seen by comparing the Pre-Max mean 850 VOR of 0.42 for ND to 0.88 for PS. This is also about a two-to-one difference. It is also present following the convective maximum with ND Post-Max mean 850 VOR of 0.82 compared with 1.91 for PS1.

The stratifications according to 850 mb pattern reveal that those disturbances embedded in a strong monsoon trough (PS-M-Stg) have markedly greater 850 VOR. It is interesting to note the small mean 850 VOR in the "PS–Other" data set. The mean 850

VOR for the "PS–Typical" stratification (1.86) is very close to the overall PS mean of 1.78.

The 850 VOR analysis shown here suggests that non-developing disturbances are differentiated from pre-tropical cyclone disturbances by their deficiency of low-level vorticity. This agrees quite well with previous radiosonde composite studies (McBride and Zehr, 1981; Lee, 1989). McBride and Zehr (1981) showed approximately twice as much low-level relative vorticity association with pre-tropical storm disturbances compared with non-developing systems and Lee (1989) reported comparable results.

6.3.1 Comparison of Individual Cases

Figure 6.3 is a time series plot of the 850 VOR associated with a non-developing disturbance (designated 4NON1) and with the genesis periods of the pre-Typhoon Ike disturbance. Large differences in 850 VOR are shown between the two cases. Very high 850 VOR (up to 3.7 x $10^{-5}s^{-1}$) is observed with the PS case (Ike), while the 850 VOR for the ND case remains below the combined mean value ($\bar{X}_{COMB}$) throughout its lifetime. Figure 6.4 is another plot of 850 VOR showing the PS disturbance which developed into Typhoon Doyle and the ND case designated 4NON13. Both disturbances have relatively high 850 VOR quantities. The comparison illustrates that some non-developing disturbances do occur with relatively high low-level relative vorticity and yet do not become tropical storms.

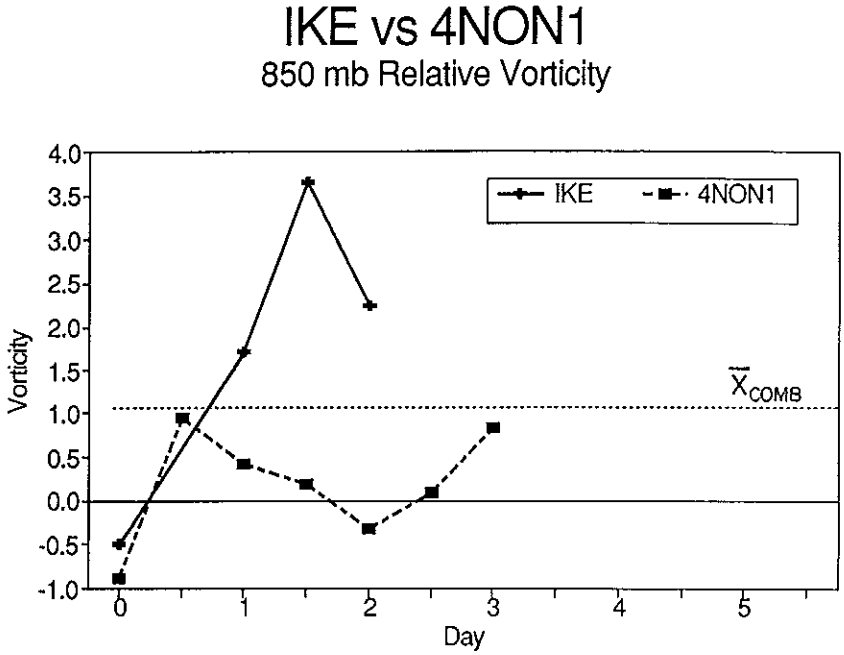

Figure 6.3: Time series of 850 VOR ($10^{-5}s^{-1}$) for pre-tropical storm disturbance Ike and non-developing disturbance, 4NON1. The dotted line is the combined mean, $\bar{X}_{COMB}$.

6.3.2 Summary

The quantitative results indicate that low-level vorticity likely has an important influence on tropical cyclogenesis. However, it apparently is not the only important difference between ND and PS disturbances, since as shown in Fig. 6.4, it may not always show

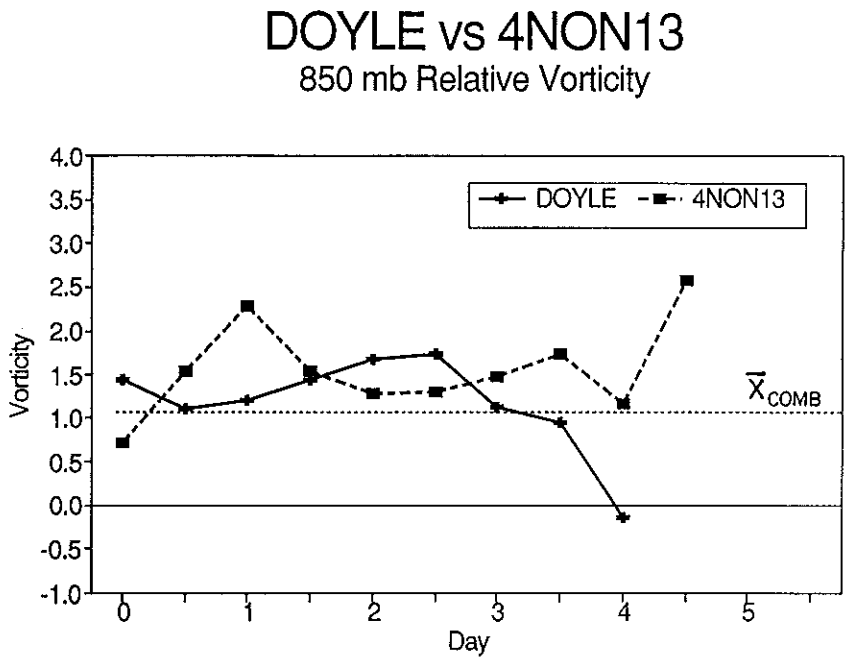

Figure 6.4: Time series of 850 VOR ($10^{-5}s^{-1}$) for pre-tropical storm disturbance Doyle and non-developing disturbance, 4NON13.

large differences. The 850 VOR mean and standard deviations from Table 6.4 are plotted in Fig. 6.5a. The $\bar{X}_{COMB}$ of 850 VOR is 1.05 x $10^{-5}s^{-1}$. The frequency distributions of time periods with 850 VOR at increments of 0.5 x $10^{-5}s^{-1}$ are also shown in Fig. 6.5b for the ND and PS1 data sets. Only 28% of the ND cases have 850 VOR greater than 1.0 x $10^{-5}s^{-1}$, compared with 78% of the PS1 cases. This suggests that many of the ND disturbances fail to undergo cyclogenesis due to a deficiency of low-level relative vorticity. The role of low–level vorticity in tropical cyclogenesis is discussed further in Chapter 8.

6.4 850 mb Convergence

Table 6.5 gives the 850 mb convergence means and standard deviations in the same format as Table 6.4. Note that the notation, –DIV, is used. This is because both ND and PS disturbances generally only persist with associated negative divergence, or convergence, in the low-levels. Therefore, to avoid confusion, all discussion and data refer to 850 mb convergence values which are denoted 850 –DIV. (Units are $10^{-5}s^{-1}$.) As with 850 VOR, a large difference in the mean 850 –DIV appears between the ND (0.20) and the PS1 (0.58) data sets. The standard deviations are quite high for all data sets.

The 850 –DIV analysis suggests that ND disturbances are differentiated from PS disturbances by a deficiency of low-level convergence. As discussed in sections 4.3 and 5.3, low-level mass convergence is associated with surges, which may or may not be well measured by the 2.5° BMRC conventional data analysis. In addition, 850 mb convergence occurs in and around individual tropical disturbances and also in association with the monsoon trough. The capability of the analysis to accurately assess the convergence fields might be questioned. Errors in measuring 850 –DIV may be more prevalent than with 850 VOR since the convergent wind components are typically smaller than the rotational wind.

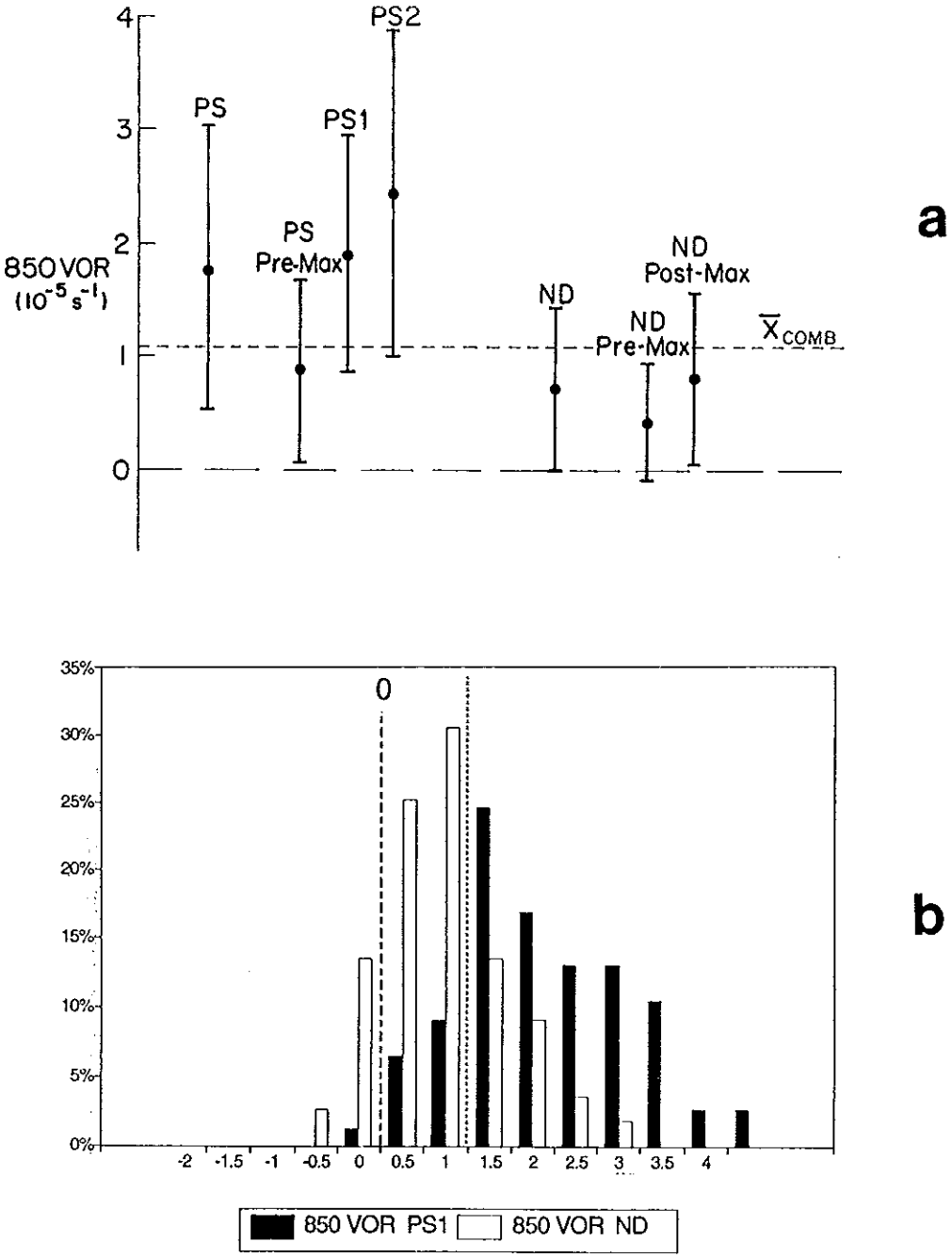

Figure 6.5: a) 850 VOR means (dots) with plus/minus one standard deviation depicted. b) Frequency distribution of 850 VOR for PS1 and ND stratifications. The vertical dotted line is the combined mean value.

Table 6.5: 850 –DIV mean ($\bar{X}$) and standard deviations (s). (Units are $10^{-5}s^{-1}$).

Data Set	$\bar{X}$	s	N
PS	0.59	0.62	167
ND	0.20	0.49	111
COMB	0.33		
PS Pre-Max	0.35	0.56	44
PS1	0.58	0.58	77
PS2	0.84	0.67	46
PS–Typical	0.61	0.56	81
PS–M–Stg	0.84	0.72	43
PS–Other	0.30	0.51	43
ND Pre-Max	0.13	0.34	31
ND Post-Max	0.23	0.54	80

Nevertheless, the 850 –DIV mean values (Table 6.5) compare well with previous radiosonde composite studies. 850 mb convergence in the composite data sets from Zehr (1976), McBride and Zehr (1981) and Lee (1989) are listed in Table 6.6 along with some of the 850 –DIV mean values from Table 6.5. The close agreement adds credence to the present analysis and suggests that 850 mb convergence greater than about 0.5 x $10^{-5}s^{-1}$ is distinctly favorable for tropical cyclogenesis.

6.4.1 Comparison of Individual Cases

An individual case comparison is shown in Fig. 6.6 where the 850 –DIV associated with the ND case (4NON13) is much less than with the PS disturbance (Clara). The 850 –DIV remains mostly below the $\bar{X}_{COMB}$ value during the entire lifetime of the ND case. In contrast, Fig. 6.7 is a time series plot of 850 –DIV for two individual cases, where the ND disturbance has relatively strong 850 mb convergence, comparable to that of the PS disturbance. Therefore, 850 –DIV by itself will not always differentiate between ND and PS disturbances. However, it appears to be an important factor in determining whether or not tropical cyclogenesis will occur for many individual cases. In fact, the large differences of mean 850 –DIV between ND and PS disturbances (Table 6.5) indicate that its influence is comparable to that of 850 VOR.

6.4.2 Summary

The quantitative results indicate that low-level mass convergence likely has important influences on tropical cyclogenesis. Figure 6.8 summarizes the 850 –DIV analysis, showing the means and standard deviations for various stratifications and the frequency distributions of 850 –DIV for the ND and PS1 data sets. The combined mean ($\bar{X}_{COMB}$) for 850 –DIV is 0.33 x $10^{-5}s^{-1}$. Sixty-five percent of the PS1 time periods have 850 –DIV exceeding 0.33 x $10^{-5}s^{-1}$, while only 40% of the ND data set exceed that value. The role of low-level convergence in tropical cyclogenesis is discussed further in Chapter 8.

Table 6.6: 850 mb convergence compared with previous radiosonde composites.

	Non–Developing		Pre–Tropical Storm	
Present Study	Data Set	850 –DIV ($10^{-5}s^{-1}$)	Data Set	850 –DIV ($10^{-5}s^{-1}$)
	ND	0.20	PS	0.59
			PS Pre-Max	0.35
			PS1	0.58
			PS2	0.84
Previous Studies (R = 0–4°)	Data Set	850 –DIV ($10^{-5}s^{-1}$)	Data Set	850 –DIV ($10^{-5}s^{-1}$)
	[1]Lee–NN2	0.45	Lee–1	0.50
	Lee–PN2	0.35	Lee–2	0.72
			Lee–3	0.81
	[2]McBride–N1	0.36	McBride–D2	0.59
			McBride–D3	0.90
	[3]Zehr–ND-0	0.35		

Note: Description of the various data sets are found in the following references:

[1]Lee (1986)
[2]McBride (1979)
[3]Zehr (1976)

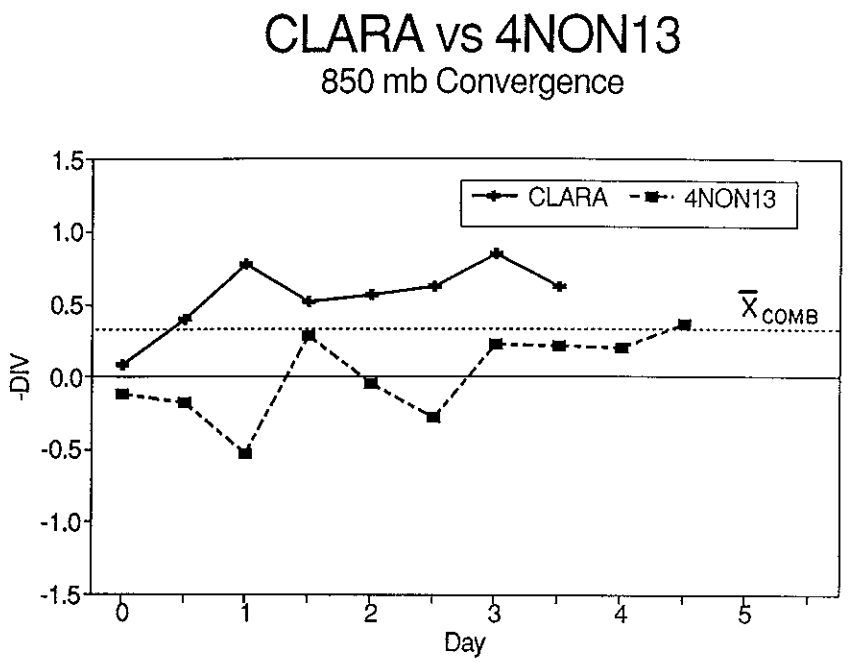

Figure 6.6: Time series of 850 -DIV ($10^{-5}s^{-1}$) for pre-tropical storm Clara and non-developing disturbance, 4NON13. The dotted line is the combined mean, $\bar{X}_{COMB}$.

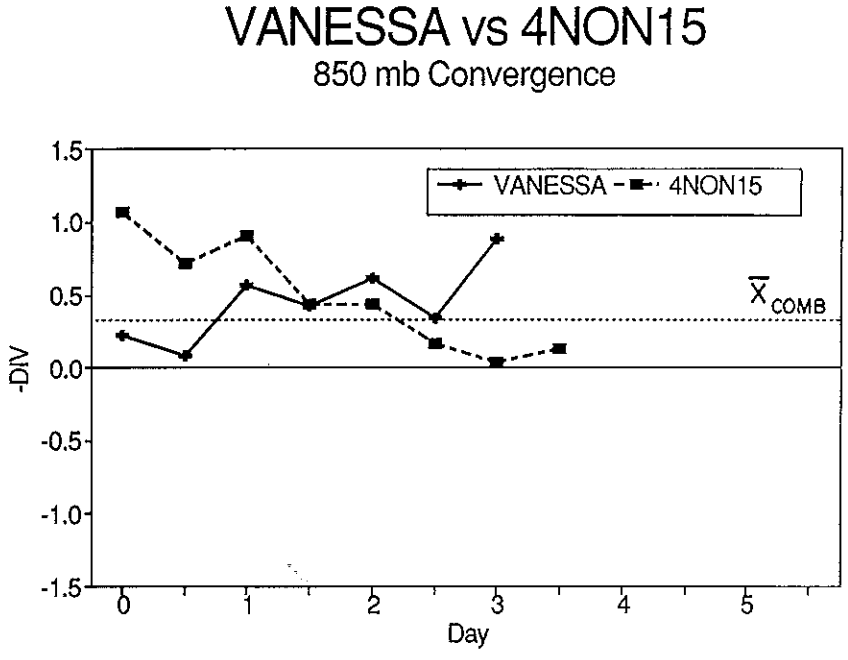

Figure 6.7: Time series of 850 -DIV ($10^{-5}s^{-1}$) for pre-tropical storm Vanessa and non-developing disturbance, 4NON15.

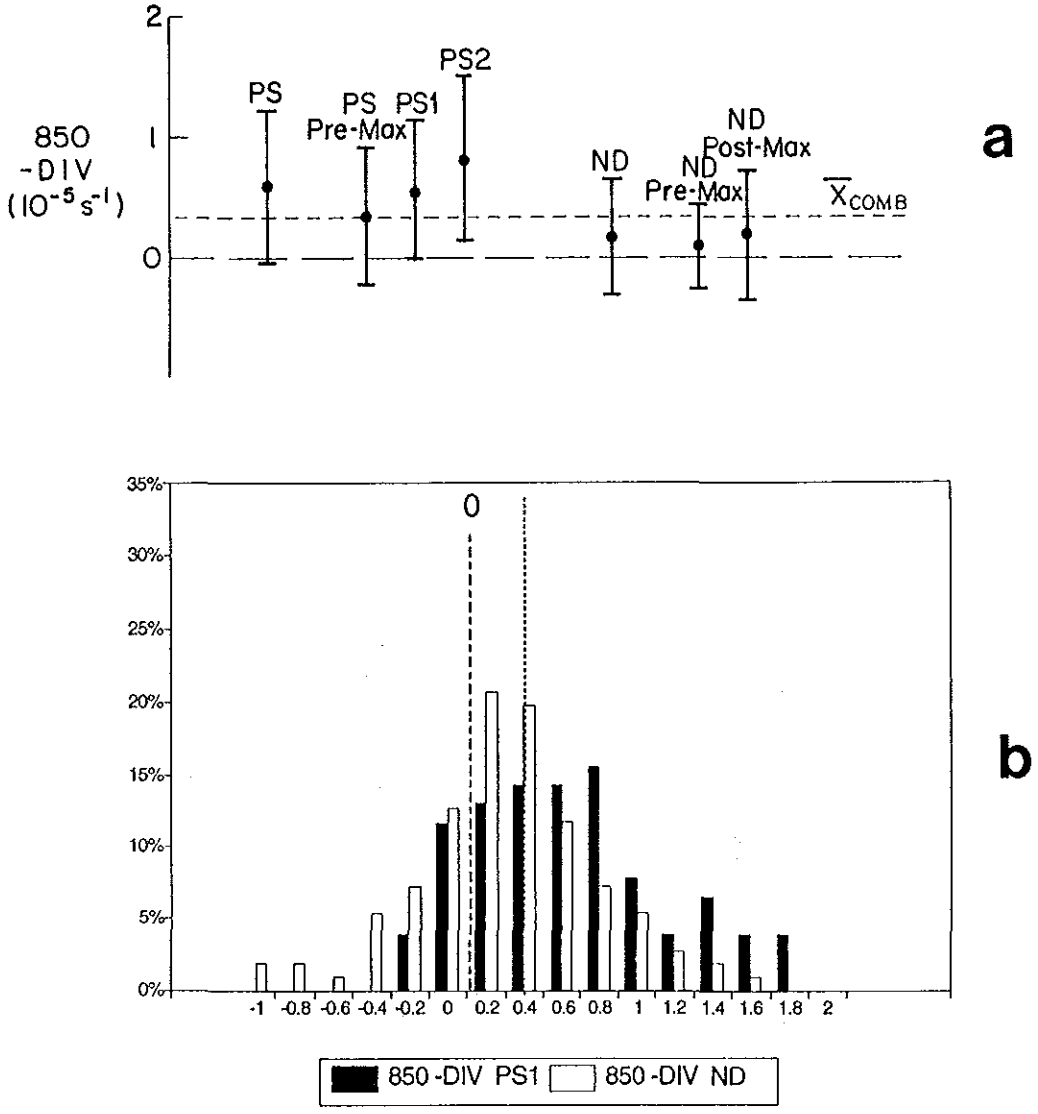

Figure 6.8: a) 850 –DIV means (dots) with plus/minus one standard deviation depicted. b) Frequency distribution of 850 –DIV for PS1 and ND stratifications. The vertical dotted line is the combined mean value.

6.5 200–850 mb Vertical Wind Shear

The vector difference of the 850 mb wind vector subtracted from the 200 mb wind vector gives an indication of the vertical wind shear in the mid-troposphere. The wind speed of that vector, denoted 200–850 SHEAR, has been interpolated from the 2.5° latitude grid point data to each Best Track position. The means and standard deviations of 200–850 SHEAR are listed for each data set in Table 6.7. Only very small differences appear among the data sets. The PS Stage 1 mean value is 10.1 ms^{-1}, compared with 10.2 ms^{-1} for the ND data set.

Table 6.7: 200–850 SHEAR mean ($\bar{X}$) and standard deviations (s). (Units are ms^{-1}).

Data Set	$\bar{X}$	s	N
PS	10.1	4.7	167
ND	10.2	5.1	111
COMB	10.3		
PS Pre-Max	10.6	3.8	44
PS1	10.1	5.3	77
PS2	9.7	4.5	46
PS–Typical	10.1	4.7	81
PS–M–Stg	11.9	5.0	43
PS–Other	8.3	3.6	43
ND Pre-Max	10.2	3.6	31
ND Post-Max	10.2	5.5	80

Since it is well known that tropical cyclogenesis will only occur with low vertical wind shear (Gray 1968, 1975) it may seem surprising that the ND and PS disturbances show such small differences in mean 200–850 SHEAR. This is simply due to the fact that ND disturbances typically also occur in low vertical shear environments. As discussed in Chapter 3, the ND disturbances which were chosen for the present study persisted for at least two days. Most ND disturbances which appear in satellite images as an identifiable cloud cluster do not persist for two days. If non-persistent cloud clusters were included in the ND data set, it is likely that the mean 200–850 SHEAR would be larger.

Another important consideration is that during much of the genesis period the deep convection is inactive. Perhaps the tropical disturbance is more susceptible to vertical wind shear effects on cyclogenesis during active convective periods. If that is true, one might expect larger vertical wind shear with the ND disturbances than with the PS disturbances, when only the active convective periods are considered. Table 6.8 gives the results of an evaluation of this type. The values of 200–850 SHEAR are averaged only at those times nearest a distinct convective maximum. The differences between those select ND and PS data sets are larger (11.9 ms^{-1} for ND vs. 9.9 ms^{-1} for PS1) than for the complete data sets. Sixty-nine percent of these limited ND cases have 250–850 SHEAR greater than 10 ms^{-1}, compared to only 35% for the PS1 cases. This suggests that the vertical shear may have a larger influence on genesis when only the active convective periods are considered.

Table 6.8: 200–850 SHEAR for analysis time nearest convective maximum.

	N	Average ms^{-1}	% Cases > 10.0 ms^{-1}
ND	26	11.9	69
PS1	19	9.9	35

6.5.1 Individual Case Analysis

Despite the small differences in mean 200-850 SHEAR, a few individual ND cases included periods of 1-2 days where 200-850 SHEAR was well above the combined mean value, ($\bar{X}_{COMB} = 10.3$ ms^{-1}). Figure 6.9 is a time series of 200-850 SHEAR values for a non-developing disturbance (4NON11) which are plotted along with the 850 VOR and 850 –DIV data. During the first two days, the vertical shear remains quite high while the low-level vorticity and convergence are unusually high for a non-developing disturbance. This indicates that for this two day period, since vorticity and convergence are favorable for tropical cyclogenesis, the vertical shear may be the primary influence which is inhibiting the cyclogenesis process.

6.5.2 Direction of Vertical Wind Shear

Are there any large differences between ND and PS disturbances with regard to the direction of the 200 to 850 mb shear vector? Figure 6.10 is a frequency distribution of the shear vector directions for all time periods in the ND and PS1 data sets, except for speeds less than 5 ms^{-1}. There is a slight tendency for ND disturbances to undergo easterly shear more often than PS1 disturbances, but the differences are rather small. Both data sets show relatively even distributions of shear direction.

6.5.3 Summary

The vertical wind shear may be an important influence on tropical cyclogenesis in some cases, but the shear vector magnitude by itself cannot reliably differentiate between the ND and PS disturbances. With regard to distinguishing PS disturbances from persistent non-developing disturbances, vertical wind shear is not as important as low-level convergence and relative vorticity.

Table 6.9 gives the percentage of time periods with 200-850 SHEAR values with respect to several reference values. A threshold value of 200–850 SHEAR above which tropical cyclogenesis does not occur, is very useful information. Considering the data in Table 6.9, that value appears to be about 12.5–15.0 ms^{-1}. The role of vertical wind shear in tropical cyclogenesis is discussed further in Chapter 8.

6.6 200 mb Divergence

Table 6.10 lists the means and standard deviations of 200 mb divergence (200 DIV) with the various data stratifications. The patterns of 200 DIV in the 2.5° latitude resolution objective analyses are typically well related to the distribution of 850 DIV. Upper-level divergence areas are generally located above low-level convergence areas and vice–versa, as shown in Fig. 6.11. Therefore, since mean 850 mb convergence is greater with PS compared with ND disturbances, one would expect the 200 DIV to have larger mean values with PS disturbances. This is in fact the case with mean 200 DIV of 0.98 for the PS disturbances compared with 0.61 for ND. The 200 DIV data could also be used to differentiate between ND and PS disturbances since it is correlated with 850 –DIV. However, since the standard deviations of the 200 DIV data are greater than the 850 –DIV, the 850

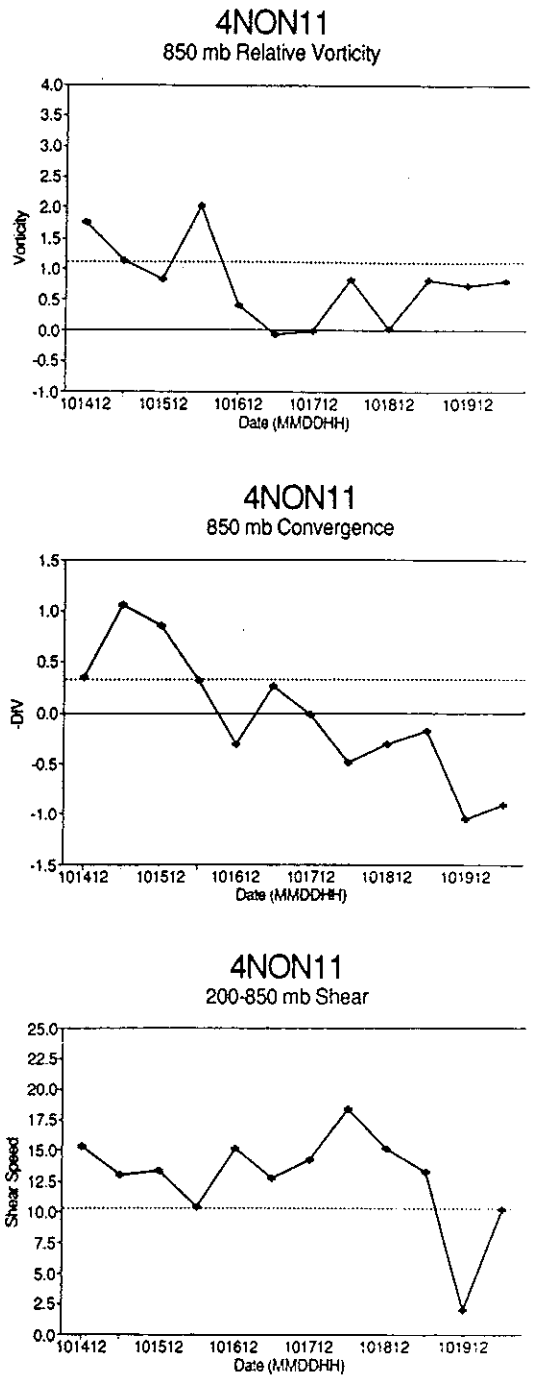

Figure 6.9: 200–850 SHEAR, 850 VOR, and 850 –DIV time series for non-developing disturbance, 4NON11. The dotted line is the combined mean value, $\bar{X}_{COMB}$.

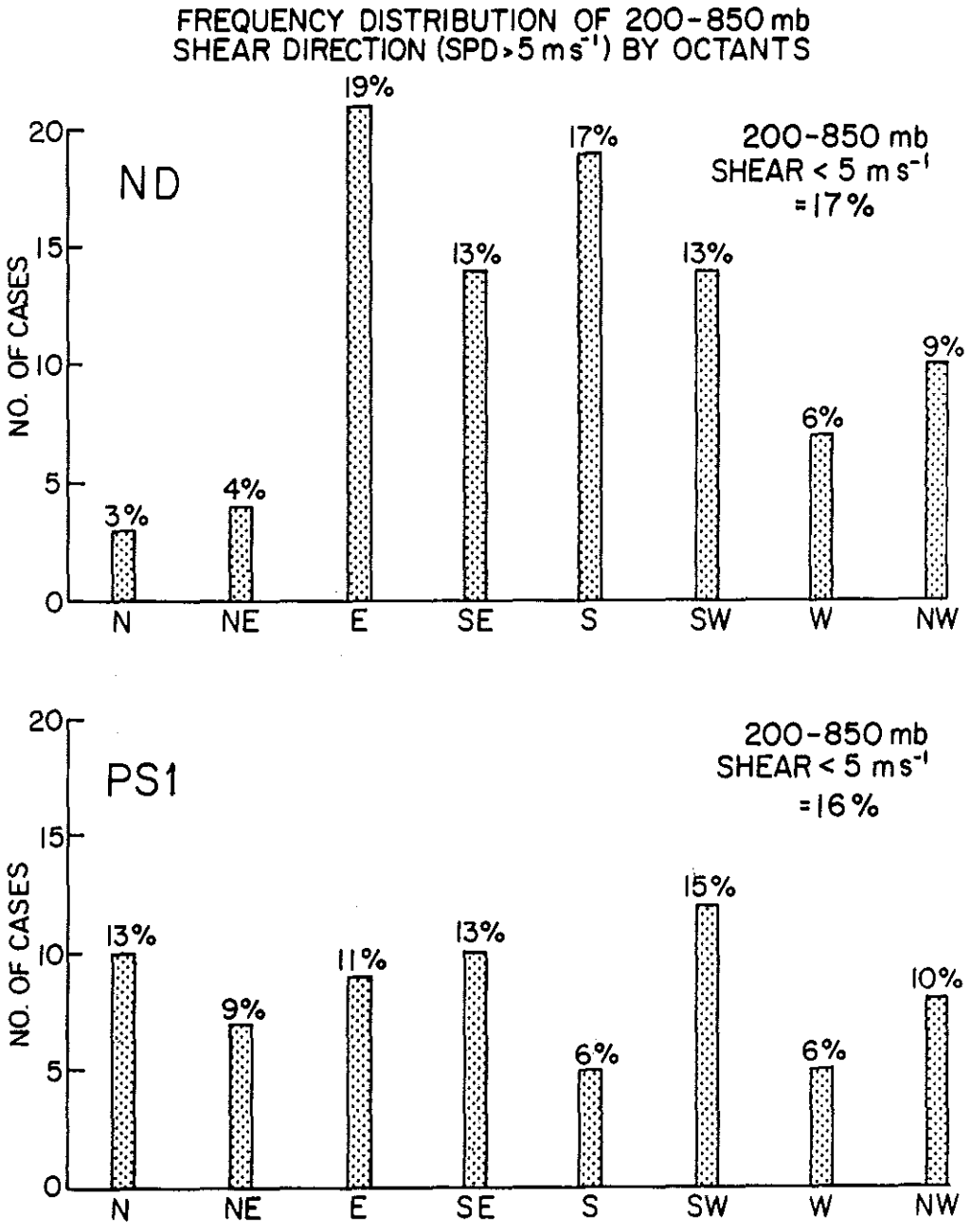

Figure 6.10: Frequency distribution of 200-850 mb vertical wind shear direction for ND and PS1 data sets.

Table 6.9: Percentage of 200–850 SHEAR values less than 10 ms^{-1}, 12.5ms^{-1}, and 15ms^{-1}.

Data Set	%
Less than 10 ms^{-1}	
ND	50
PS Pre–Max	36
PS1	54
PS2	52
Less than 12.5 ms^{-1}	
ND	68
PS Pre–Max	68
PS1	71
PS2	76
Less than 15.0 ms^{-1}	
ND	84
PS Pre–Max	89
PS1	86
PS2	87

mb data are likely preferable. The role of upper-level divergence in tropical cyclogenesis is discussed further in Chapter 8.

Table 6.10: 200 DIV mean ($\bar{X}$) and standard deviations (s) for each data stratification. (Units are $10^{-5}s^{-1}$).

Data Set	$\bar{X}$	s	N
PS	0.98	0.94	167
ND	0.61	0.85	111
COMB	0.71		
PS Pre-Max	0.63	0.97	44
PS1	1.00	0.88	77
PS2	1.28	0.88	46
PS–Typical	0.98	0.94	81
PS–M–Stg	1.38	0.67	43
PS–Other	0.58	0.99	43
ND Pre-Max	0.38	0.65	31
ND Post-Max	0.70	0.90	80

6.7 200 mb Relative Vorticity

Table 6.11 lists the means and standard deviations of the 200 mb relative vorticity (200 VOR) for the various data stratifications. The mean 200 VOR is negative with all data sets. No large systematic differences are seen among the data sets and the standard deviations are very large. There is likely no useful information to differentiate between ND and PS disturbances in the 200 VOR data, particularly with such a large standard deviation. This agrees with the qualitative assessment of upper-level synoptic scale patterns presented in section 6.1.2. The role of upper-level vorticity in tropical cyclogenesis is discussed further in Chapter 8.

6.8 Summary

The results of the quantitative analyses indicate that a combination of 850 VOR, 850 –DIV, and 200–850 SHEAR values are needed to differentiate between ND and PS individual cases. ND disturbances are characterized by any one or more of the following:

1. a deficiency of low-level vorticity (850 VOR),
2. a deficiency of low-level convergence (850 –DIV),
3. too large vertical wind shear speed (200-850 SHEAR).

On the other hand, although one or more of those three characteristics which are unfavorable for genesis may occur at times with PS disturbances, they are not are persistent. Furthermore, at some time during the genesis period, both 850 VOR and 850 –DIV are simultaneously above the combined ND and PS1 data set average, while the 200-850 SHEAR is below average. This seldom occurs with ND disturbances.

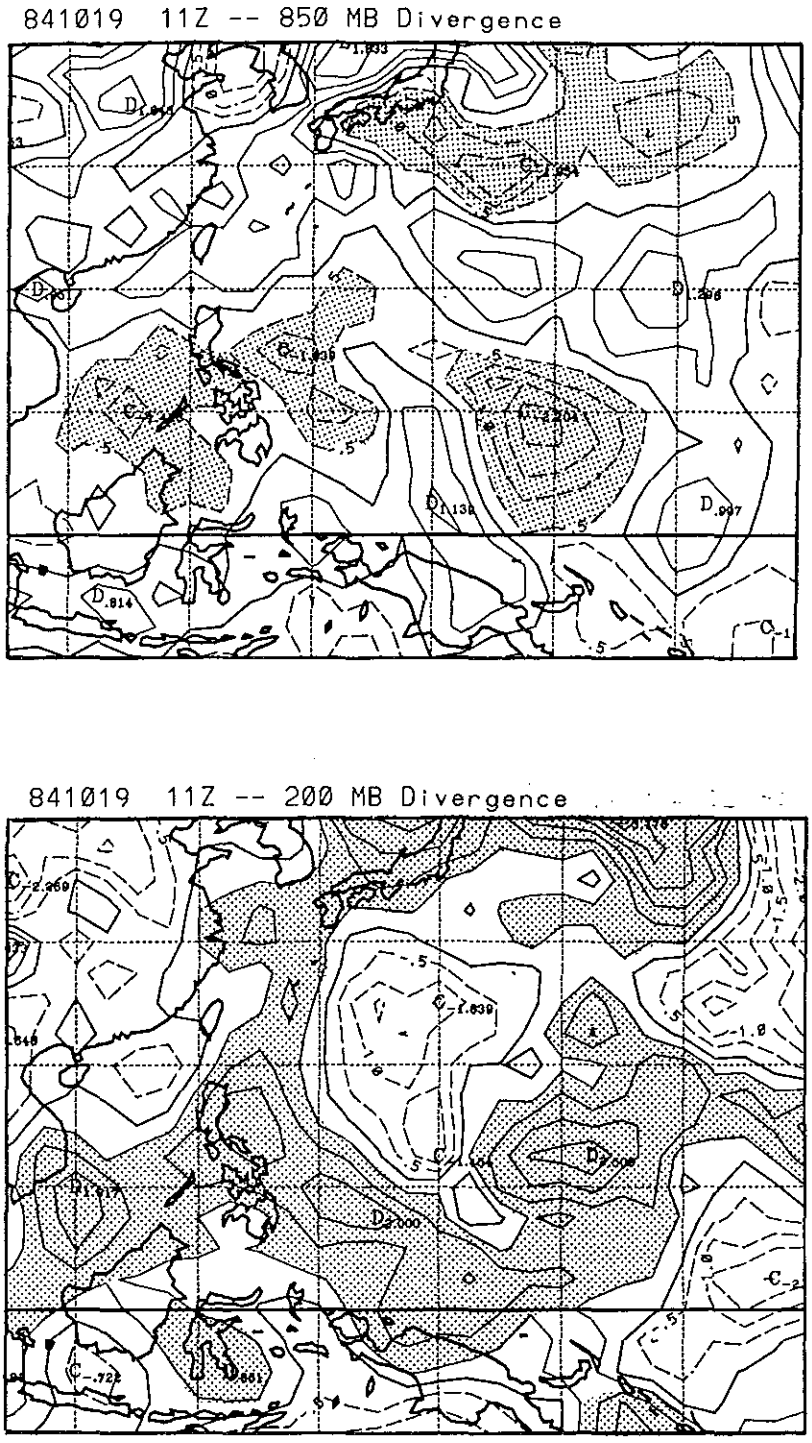

Figure 6.11: Objective analyses of a) 850 DIV and b) 200 DIV at 12 GMT 19 October, 1984. 850 mb convergence greater than $0.5x10^{-5}s^{-1}$ and 200 mb divergence greater than $0.5x10^{-5}s^{-1}$ are shaded.

Table 6.11: 200 VOR mean ($\bar{X}$) and standard deviations (s) for each data stratification. (Units are $10^{-5}s^{-1}$).

Data Set	$\bar{X}$	s	N
PS	-0.90	1.87	167
ND	-0.99	1.59	111
COMB	-0.98		
PS Pre-Max	-1.22	2.14	44
PS1	-0.73	1.83	77
PS2	-0.87	1.60	46
PS–Typical	-0.60	1.49	81
PS–M–Stg	-1.74	1.13	43
PS–Other	-0.61	2.69	43
ND Pre-Max	-0.08	1.30	31
ND Post-Max	-1.40	1.50	80

Figure 6.12 shows time series plots of 850 VOR, 850 –DIV, and 200–850 SHEAR for the disturbance that developed into Supertyphoon Vanessa. The 850 VOR remains well above the combined mean ($\bar{X}_{COMB}$ = 1.05 x $10^{-5}s^{-1}$). The 850 –DIV is above the combined mean during all but the very early periods. The vertical shear is relatively low. This combination of favorable conditions results in tropical cyclogenesis. In contrast, Fig. 6.13 is a plot of the same variables for a non-developing disturbance, 4NON5, with which all three variables are unfavorable for tropical cyclogenesis throughout most of the entire lifetime of the disturbance.

Whether or not a variable is considered favorable for genesis, depends on its predominant value with respect to the combined mean ($\bar{X}_{COMB}$, see section 6.2.2). This determination is indicated for each variable in all of the time series plots in Figs. 6.12–6.16, which also show the $\bar{X}_{COMB}$. 850 VOR values greater than the $\bar{X}_{COMB}$ = 1.05 x $10^{-5}s^{-1}$ are considered favorable. 850 –DIV greater than $\bar{X}_{COMB}$ = 0.33 x $10^{-5}s^{-1}$ is favorable. 200-850 SHEAR less than $\bar{X}_{COMB}$ = 10.3ms^{-1} is designated as a favorable variable.

Another example is shown in Fig. 6.14 where the ND disturbance, 4NON6, exhibits generally favorable small vertical wind shears, but the 850 VOR and 850 –DIV variables are quite small and unfavorable for genesis. Figure 6.15 is an example of the 4NON17 disturbance with which 850 VOR is mostly deficient, but 850–DIV and 200–850 SHEAR are frequently favorable for tropical cyclogenesis. The ND disturbance variables plotted in Fig. 6.16 (4NON13) depict a case where the 850 –DIV is largely deficient. These examples (Figs. 6.12–6.16) along with the one in Fig. 6.9 illustrate that any one, or any combination of three factors listed above may characterize a particular non-developing disturbance. Therefore, this combined three-way quantitative analysis, not only differentiates ND cases from PS cases, but also categorizes the ND cases into different types depending on which of the three variables are unfavorable for cyclogenesis. Table 6.12 gives the predominant unfavorable conditions associated with each of the 15 non-developing disturbances.

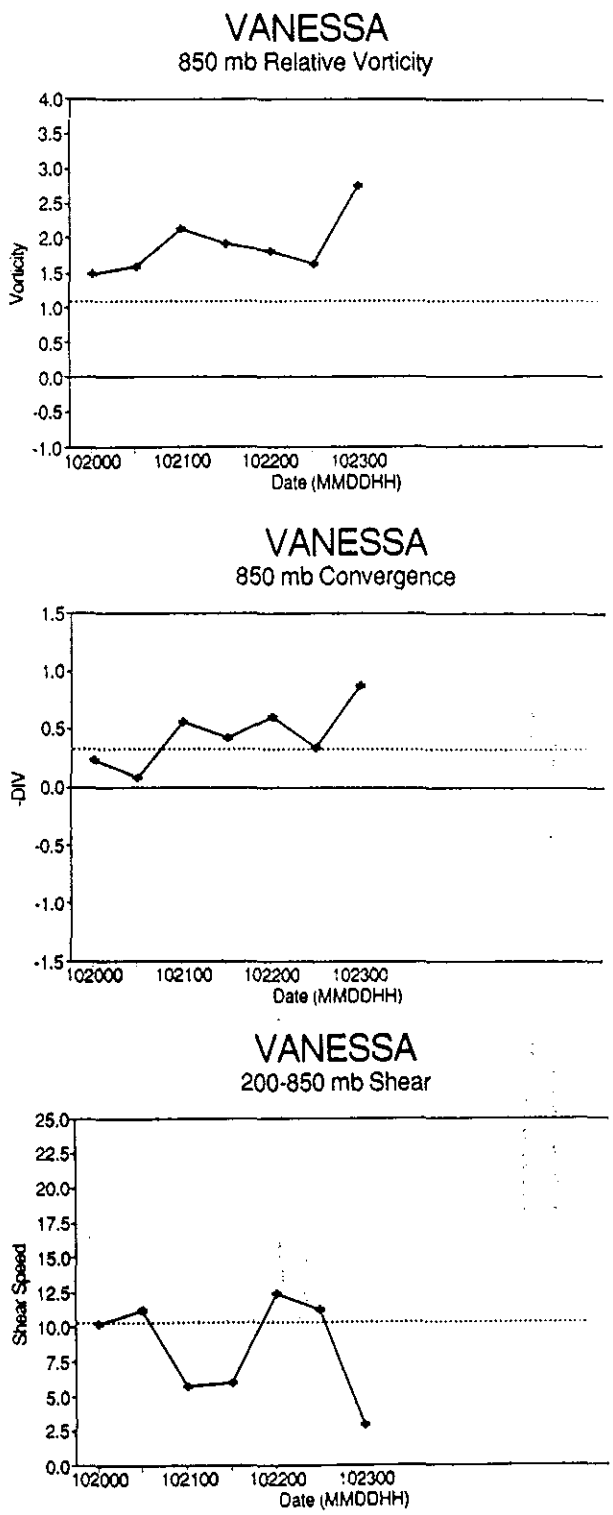

FAVORABLE

FAVORABLE

FAVORABLE

Figure 6.12: Time series of 850 VOR, 850 –DIV, and 200–850 SHEAR for pre-tropical storm Vanessa. The $\bar{X}_{COMB}$ values are indicated by the dotted lines.

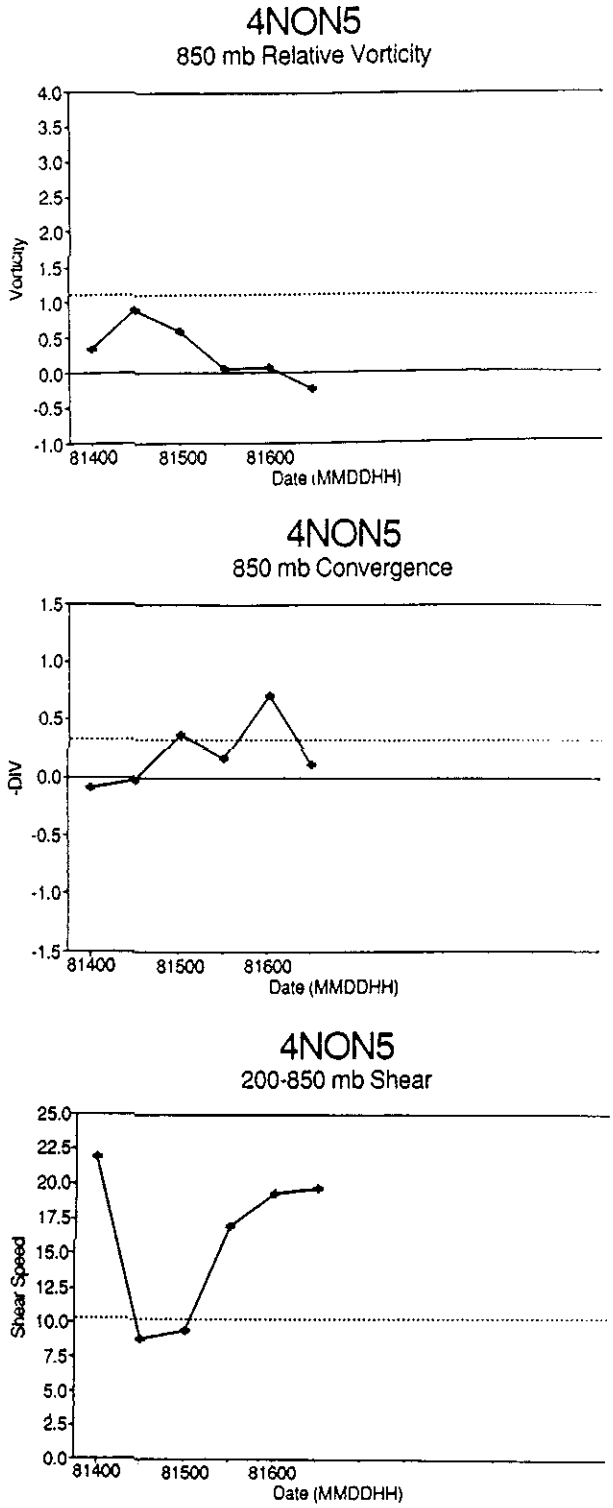

UNFAVORABLE

UNFAVORABLE

UNFAVORABLE

Figure 6.13: Time series of 850 VOR, 850 –DIV, and 200–850 SHEAR for 4NON5.

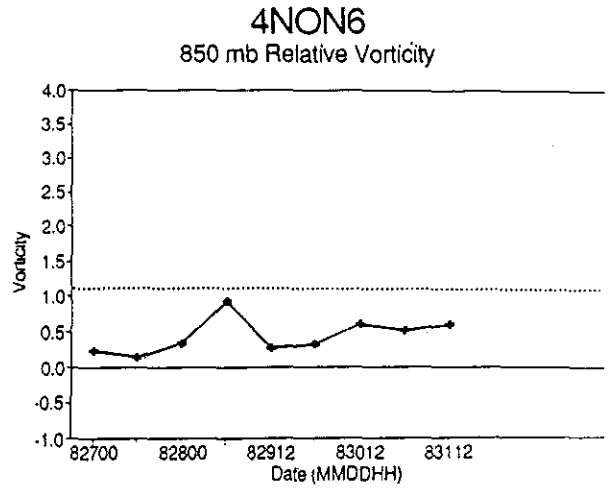

UNFAVORABLE

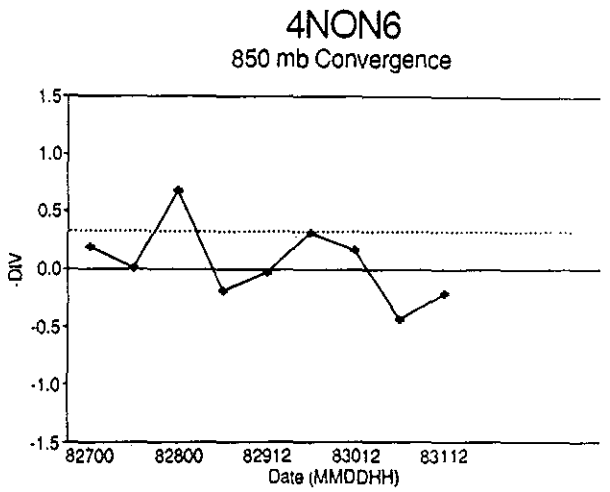

UNFAVORABLE

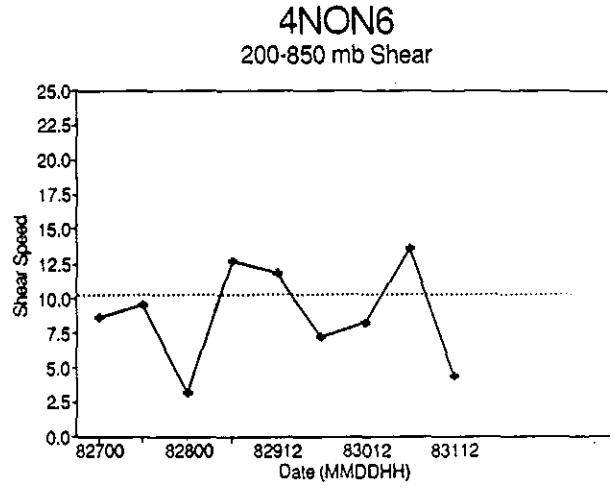

FAVORABLE

Figure 6.14: Time series of 850 VOR, 850 –DIV, and 200–850 SHEAR for 4NON6.

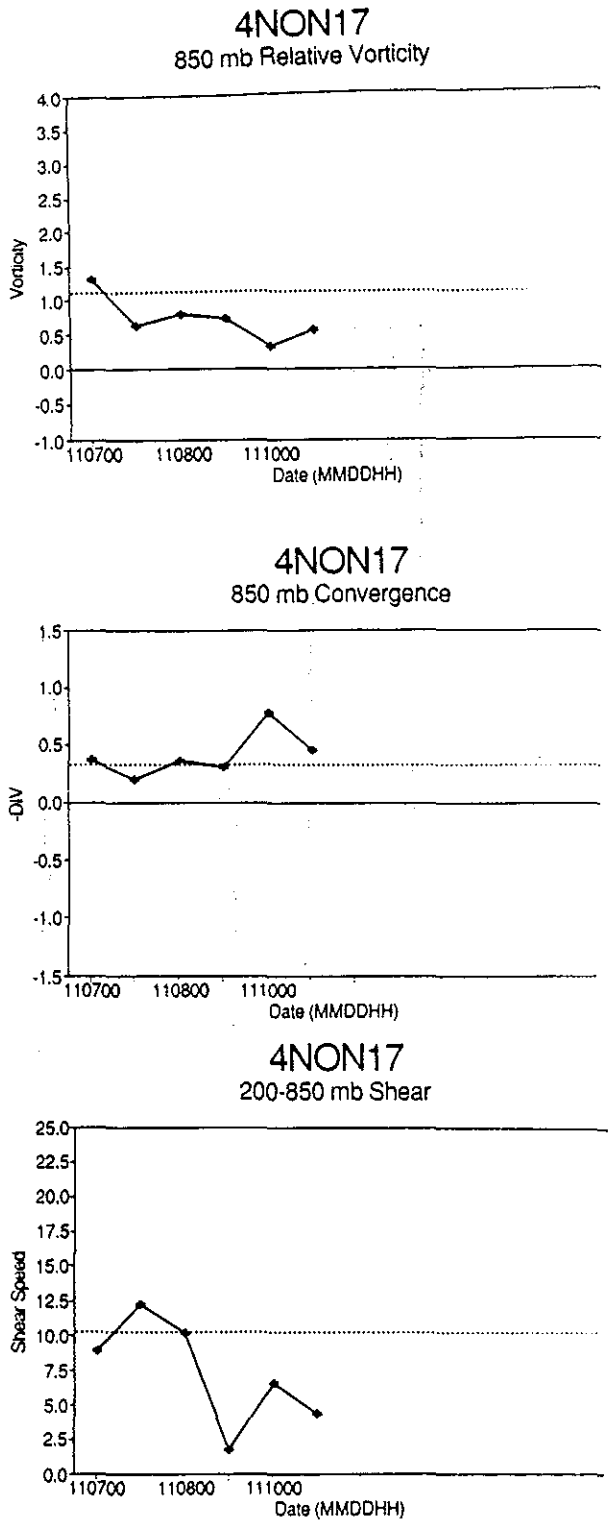

UNFAVORABLE

FAVORABLE

FAVORABLE

Figure 6.15: Time series of 850 VOR, 850 –DIV, and 200–850 SHEAR for 4NON17.

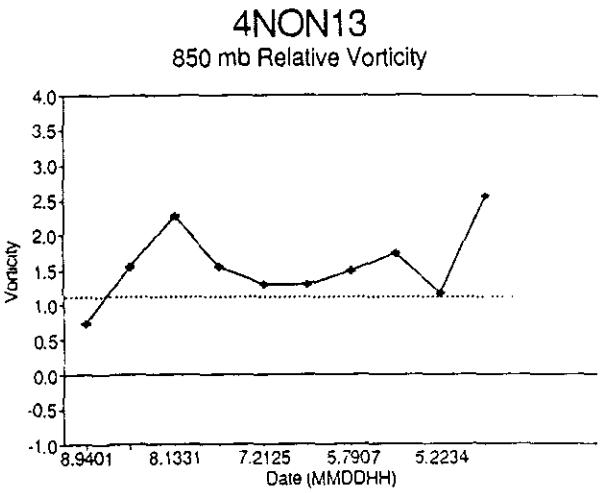

FAVORABLE

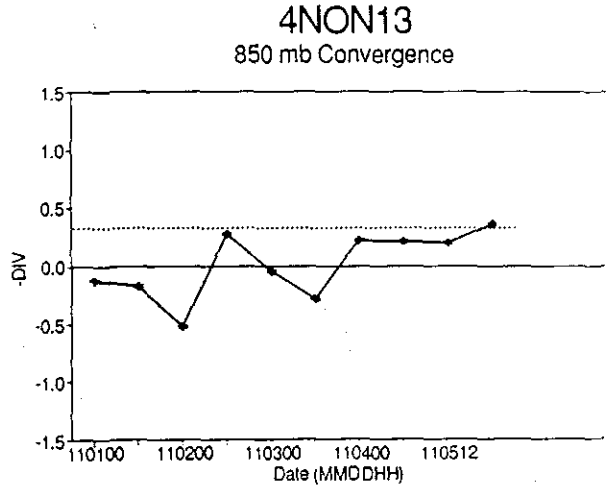

UNFAVORABLE

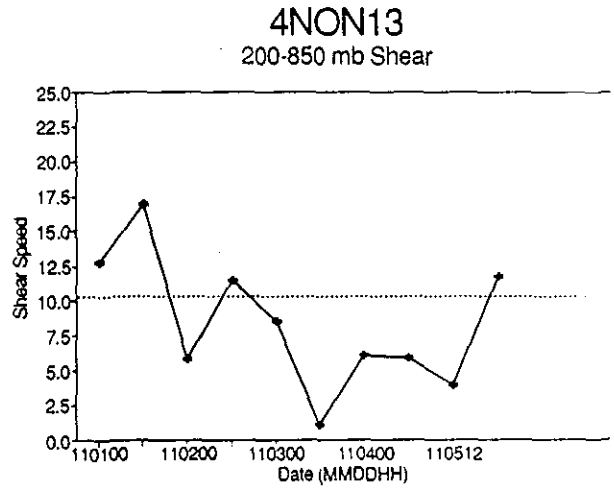

FAVORABLE

Figure 6.16: Time series of 850 VOR, 850 –DIV, and 200–850 SHEAR for 4NON13.

Table 6.12: Characteristics of individual non–developing disturbances.

Name	Predominant Unfavorable condition(s)
4NON1	850 VOR, 850 –DIV
4NON2	850 VOR
4NON3	850 –DIV
4NON4	850 VOR
4NON5	850 VOR, 200-850 SHEAR
4NON6	850 VOR, 850 –DIV
4NON7	850 VOR
4NON8	200–850 SHEAR, landfall
4NON9	850 –DIV
4NON11	200–850 SHEAR, 850 –DIV, 850 VOR
4NON13	850 –DIV
4NON14	850 VOR, landfall
4NON15	200 850 VOR, 850 –DIV
4NON16	200–850 SHEAR, 850 VOR
4NON17	850 VOR

6.9 Objective Techniques and Forecast Aids for Tropical Cyclogenesis

The 2.5° latitude objective analysis data appear suitable for the development of products to be used as aids to forecast genesis and non–genesis. Objective techniques to arrive at a yes–no decision on whether cyclogenesis will occur, or a genesis probability could be devised. Using quantitative IR data with respect to a particular tropical disturbance, more refined objective procedures could be proposed.

6.9.1 Combining Areas Defined by Threshold Values

A simple forecast aid uses the analyses of 850 VOR, 850 –DIV, and 200-850 SHEAR. Figure 6.17 shows these analyses for the entire western North Pacific region. Areas with 850 VOR larger than 1.0 x $10^{-5}s^{-1}$, 850 –DIV greater than 0.3 x $10^{-5}s^{-1}$, and 200–850 SHEAR less than 10 ms^{-1} are shaded. The shaded regions indicate where conditions are favorable for tropical cyclogenesis, but only with respect to one of the three variables. The threshold values correspond to the combined mean values, ($\bar{X}_{COMB}$, see section 6.2.2).

A two–way combination of the 850 VOR and 200–850 SHEAR analyses, and a three–way combination of the shaded regions in Fig. 6.17 are shown in Fig. 6.18. The analysis indicates that areas suitable for tropical cyclogenesis with regard to low–level vorticity and vertical shear are somewhat limited. Only very small areas are indicated as genesis regions when the three–way combination is used, which adds the 850 –DIV contribution. The areas with all three variables favorable for genesis are indicated in Fig. 6.18b.

Analyses of this type could be very useful as operational forecast aids. Tropical disturbances tracked in satellite imagery would likely undergo tropical cyclogenesis only in the indicated favorable genesis regions. The two–way combined analyses (Fig. 6.18a), with 850 VOR and 200–850 SHEAR are shown in Fig. 6.19 as daily 00 GMT maps for a six–day period. During the 15–20 October 1984 period, the Stage 1 convective maximum occurred for three pre–tropical storm disturbances (Thad, Warren and Vanessa) while a non–developing disturbance, 4NON11, persisted during much of the period. The locations of the disturbances are indicated on the pertinent daily analyses. The Stage 1 convective maximum of Thad occurs nearest to the analysis time of 00 GMT 18 October (Fig. 6.19d). The Stage 1 positions of Warren are shown in both Fig. 6.19e and 6.19f, while a pre-Stage

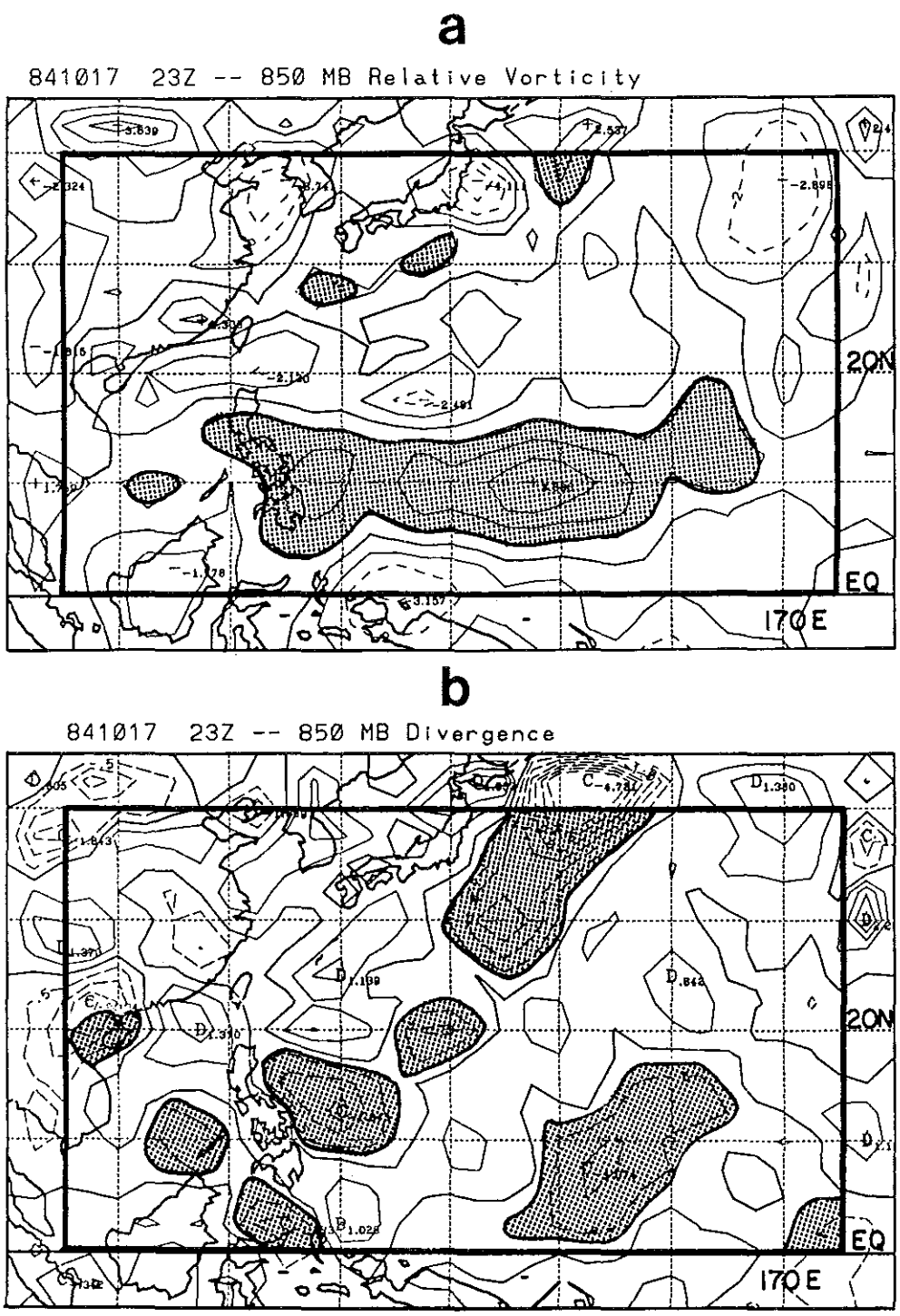

Figure 6.17: Contour analyses of the 2.5° latitude BMRC grid point data over the western North Pacific for 00 GMT 18 October 1984. a) 850 VOR, shaded if greater than $1.0x10^{-5}s^{-1}$, b) 850 –DIV, shaded if greater than $0.30x10^{-5}s^{-1}$, c) 200–850 SHEAR, shaded if less than $10ms^{-1}$.

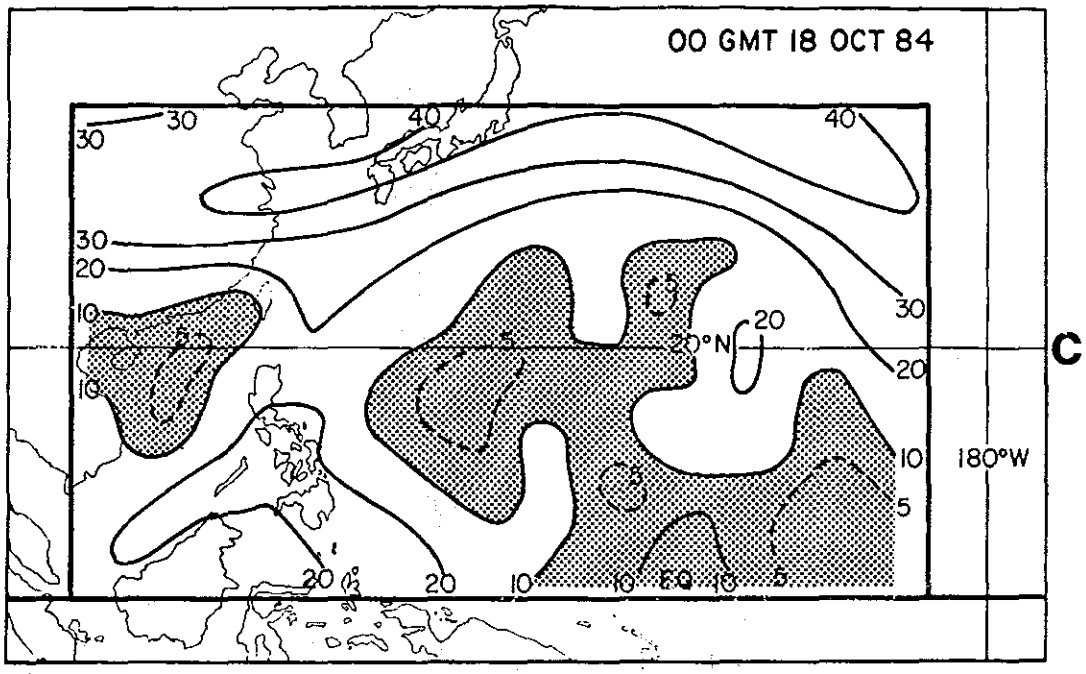

Figure 6.17: c: Continued.

1 Vanessa position is also indicated in Fig. 6.19f. This disturbance was very near the onset of the Stage 1 convective maximum at the analysis time (00 GMT 20 October). All three disturbances are located in a combined favorable region during their Stage 1 genesis period. The non-developing disturbance, 4NON11 remains outside the analyzed favorable genesis regions with respect to 850 VOR and 200–850 SHEAR, during the entire period.

6.9.2 Genesis Parameter, GP

An alternate approach is to combine the three quantities (850 VOR, 850 –DIV, and 200-850 SHEAR) into a single quantity. Contoured fields of a single genesis parameter can better pinpoint the most favorable genesis areas due to the combined influence of all three quantities.
The Genesis Parameter, GP, is defined as:

$$\text{GP} = (850\ \text{VOR}^*)(850\ -\text{DIV}^*)(\text{S}),$$

850 VOR* = 850 mb relative vorticity (850 VOR) if 850 VOR > 0
850 VOR* = 0, if 850 VOR < 0

850 –DIV* = 850 mb convergence (850 –DIV) if 850 –DIV > 0
850 –DIV* = 0, if 850 –DIV < 0 (i.e., divergence at 850 mb)

S = Shear Coefficient $= \frac{25.0 ms^{-1} - (200-850\,SHEAR)}{20.0 ms^{-1}}$
for 5.0 ms^{-1} < (200-850 SHEAR) < 25.0 ms^{-1}
if (200-850 SHEAR) < 5.0 ms^{-1}, S = 1.0
if (200-850 SHEAR) > 25.0 ms^{-1}, S = 0.0

GP is simply the product of the convergence and relative vorticity at 850 mb which is linearly weighted according to the 200-850 mb wind shear speeds between 5 and 25

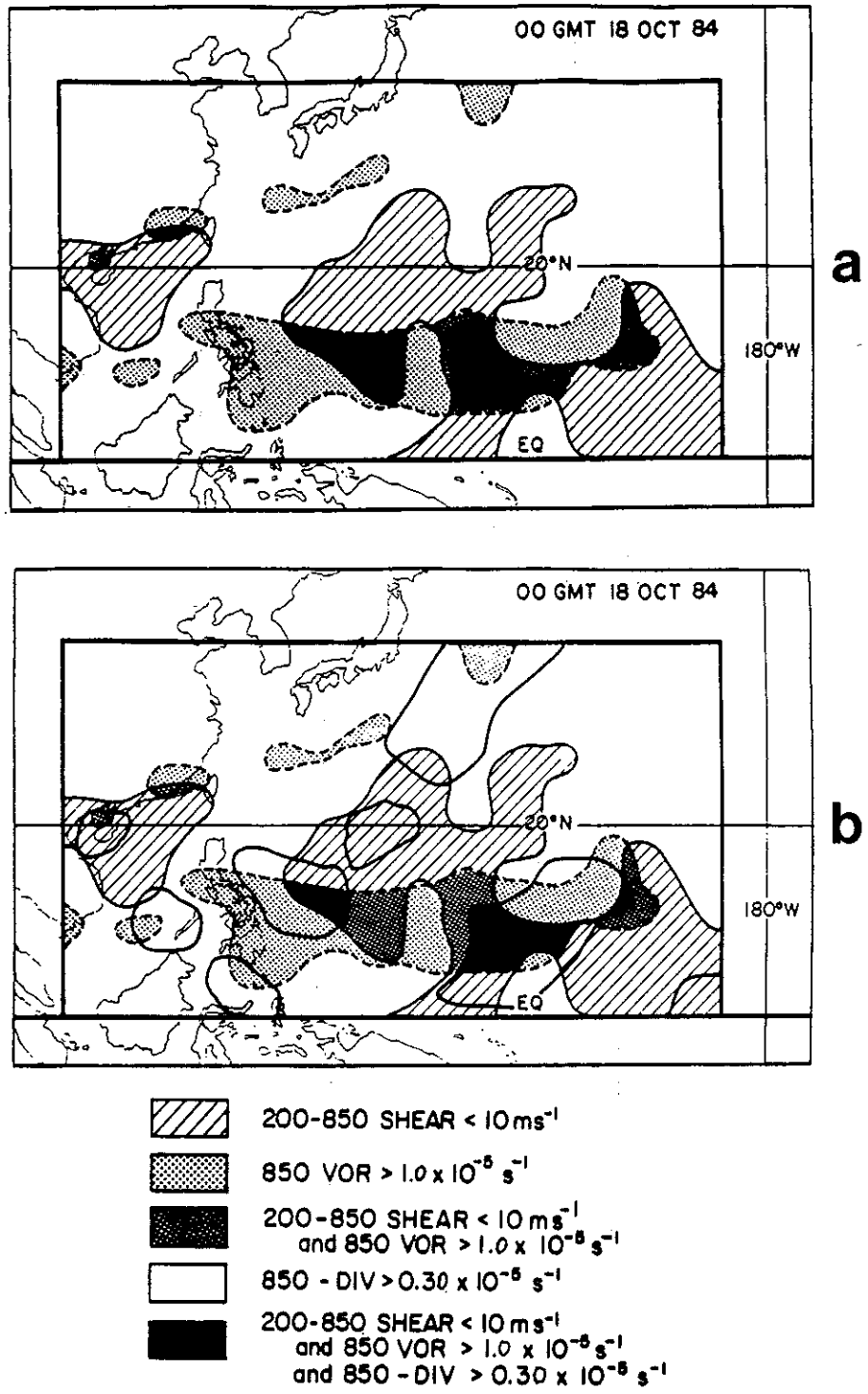

Figure 6.18: a) Two–way combination of shaded areas from Fig. 6.17a and 6.17c. b) Three–way combination of shaded areas from Fig. 6.17.

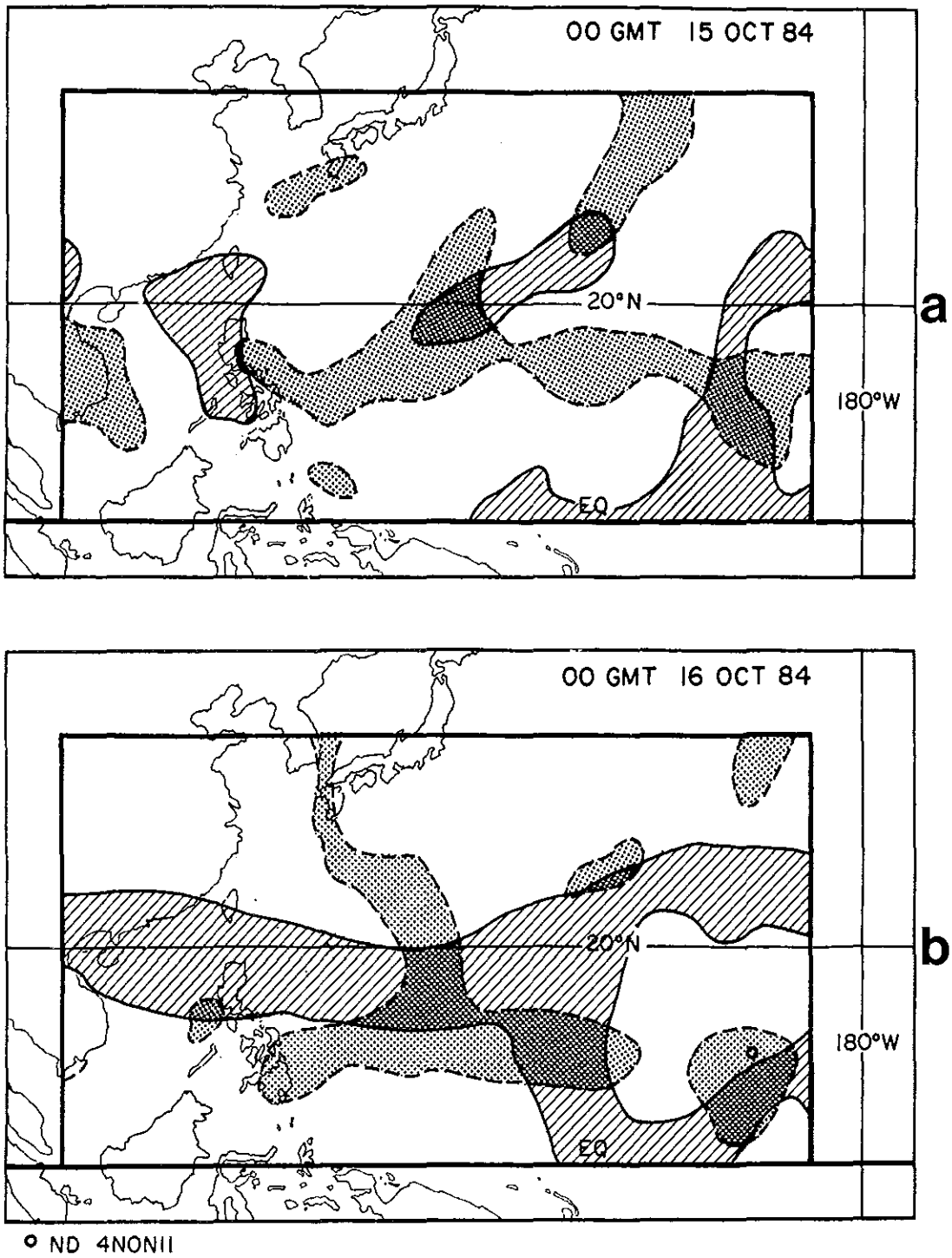

Figure 6.19: Daily 00 GMT combined analysis as in Fig. 6.18a for a 6–day period. a) 15 October 1984, b) 16 October 1984, c) 17 October 1984, d) 18 October 1984, e) 19 October 1984 and f) 20 October 1984.

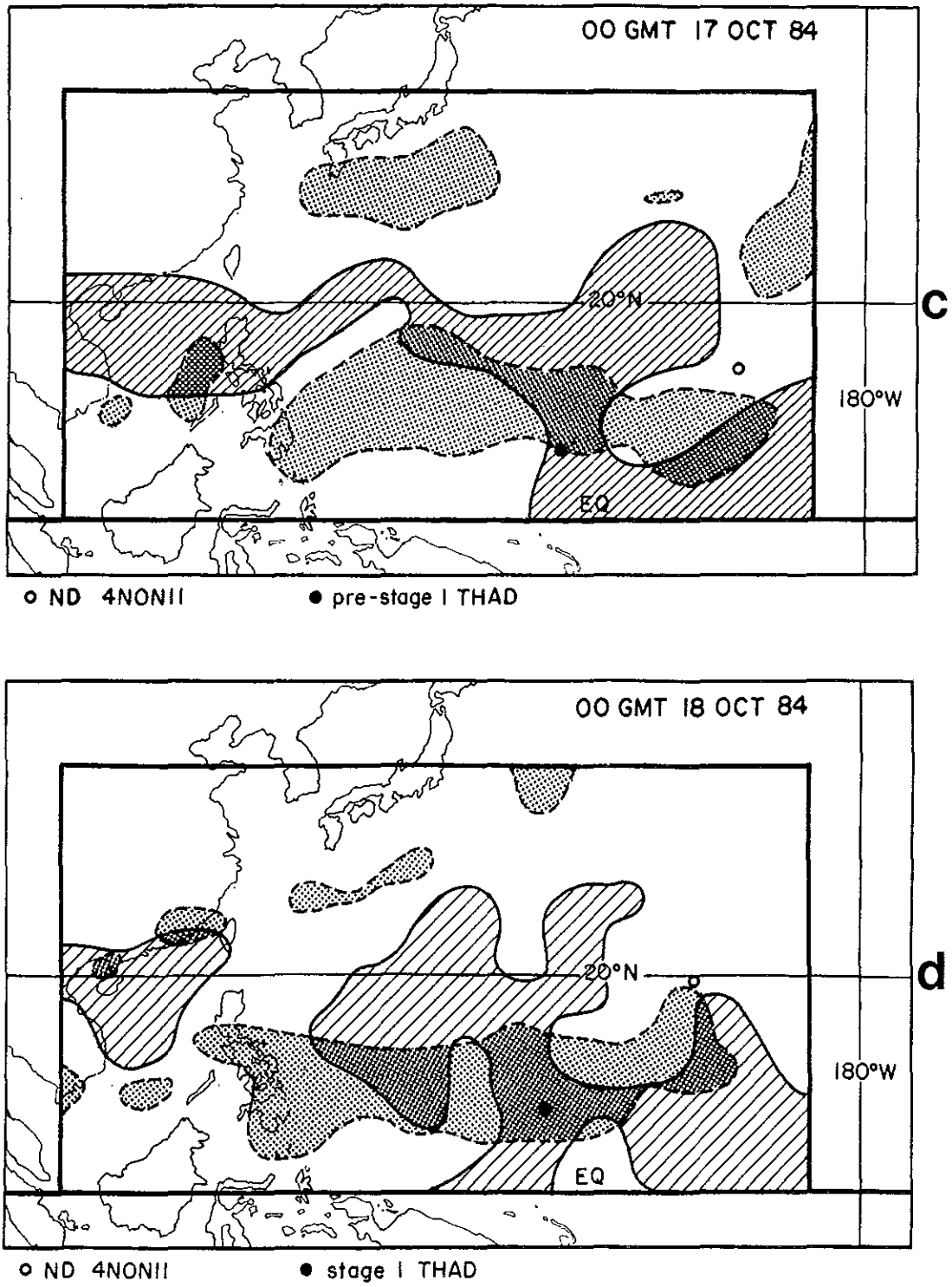

Figure 6.19: c) 17 October 1984, d) 18 October 1984.

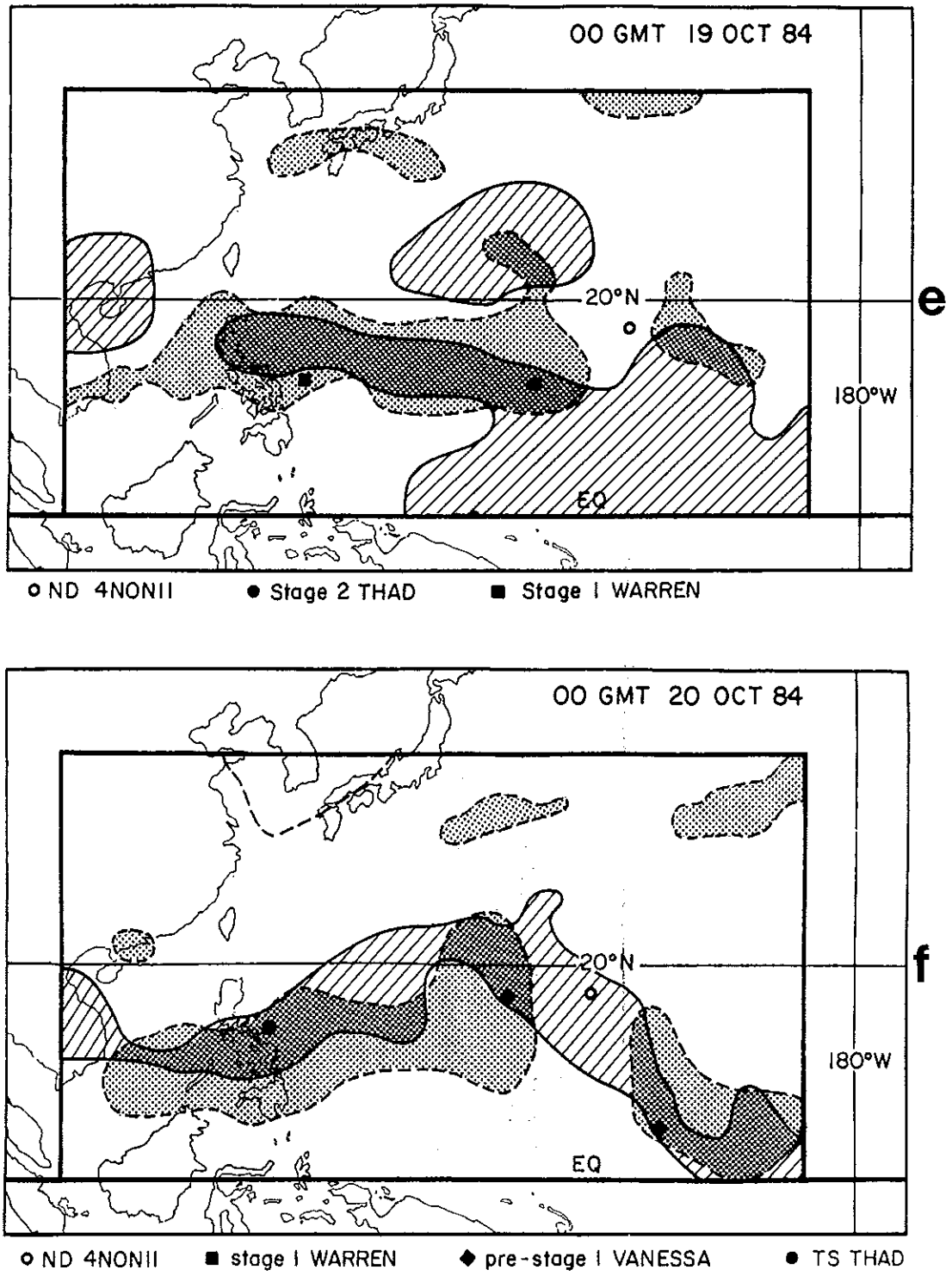

Figure 6.19: e) 19 October 1984 and f) 20 October 1984.

ms^{-1}. Wind shears greater than 25 ms^{-1} reduce GP to zero. GP is expressed in units of $10^{-12}s^{-2}$. The daily GP analyses and disturbance locations corresponding to the Fig. 6.19 analyses are shown in Fig. 6.20, with GP > 50 x $10^{-12}s^{-2}$, shaded.

The 00 GMT 18 October 1984 GP contour analysis, which is computed from the three analyses in Fig. 6.17, is shown in Fig. 6.20d. Comparison of the GP analysis with the corresponding three-way combination analysis is in Fig. 6.18b shows general agreement in the location of favorable genesis regions.

An additional GP analysis (Fig. 6.20g) at 00 GMT 21 October 1984 shows a GP maximum which coincides remarkably well with the Stage 1 location of pre-Tropical Storm Vanessa. This analysis also shows the GP field associated with a mature typhoon (labeled TY THAD in Fig. 6.20g), with V_{max} of 50 ms^{-1}.

The GP analyses (Fig. 6.20) illustrate that the pre-tropical storm disturbances are typically associated with GP > 50 x $10^{-12}s^{-2}$, while non-developing disturbances are typically located in areas with GP < 50 x $10^{-12}s^{-2}$. A more thorough evaluation of the capability of the objective analysis data in differentiating and PS disturbances follows in section 6.10.

6.10 Evaluation of the Objective Techniques

To illustrate the overall utility of this combined analysis approach, the 850 VOR, 850 –DIV, and 200-850 SHEAR quantities which have been interpolated to the Best Track center positions are used. In addition, the Genesis parameter (GP) is computed for each time period using those values. The two methods presented in section 6.9 are evaluated as objective techniques to differentiate PS and ND disturbances.

6.10.1 The Threshold Method

The three thresholds used in the combined area analyses shown in Figs. 6.17-6.19 are:

- A = 1.00 x $10^{-5}s^{-1}$, 850 VOR
- B = 0.30 x $10^{-5}s^{-1}$, 850 –DIV
- C = 10.0 ms^{-1}, 200–850 SHEAR

Table 6.13 lists the percentages of time periods for which any one of the following conditions are met:

850 VOR < A or 850 –DIV < B or 200–850 SHEAR > C .

Such conditions are unfavorable for tropical cyclogenesis and nearly all ND and pre-Stage 1 time periods have at least one variable which satisfies those conditions. This occurs with only 69% of the PS1 time periods and 65% of the PS2 data set. Although this is a smaller percentage than for the ND data set (97%), it appears too restrictive to correctly indicate which disturbances will become tropical cyclones.

However, when an alternate approach with those same thresholds is used, the ND and PS disturbances can be prescribed as developing or non-developing with a reasonably good degree of success. If all three of the following conditions are met for at least one time period up to 24 hr before first designation as a tropical storm, the case is defined as D, a developing tropical disturbance. Otherwise, it is defined as ND, a non-developing disturbance. Similarly, if all three of the following conditions are met for at least one time period at any time during the ND case lifetime, it is designated as D, and if not, it is designated ND. The conditions required are:

850 VOR > A and 850 –DIV > B and 200–850 SHEAR < C.

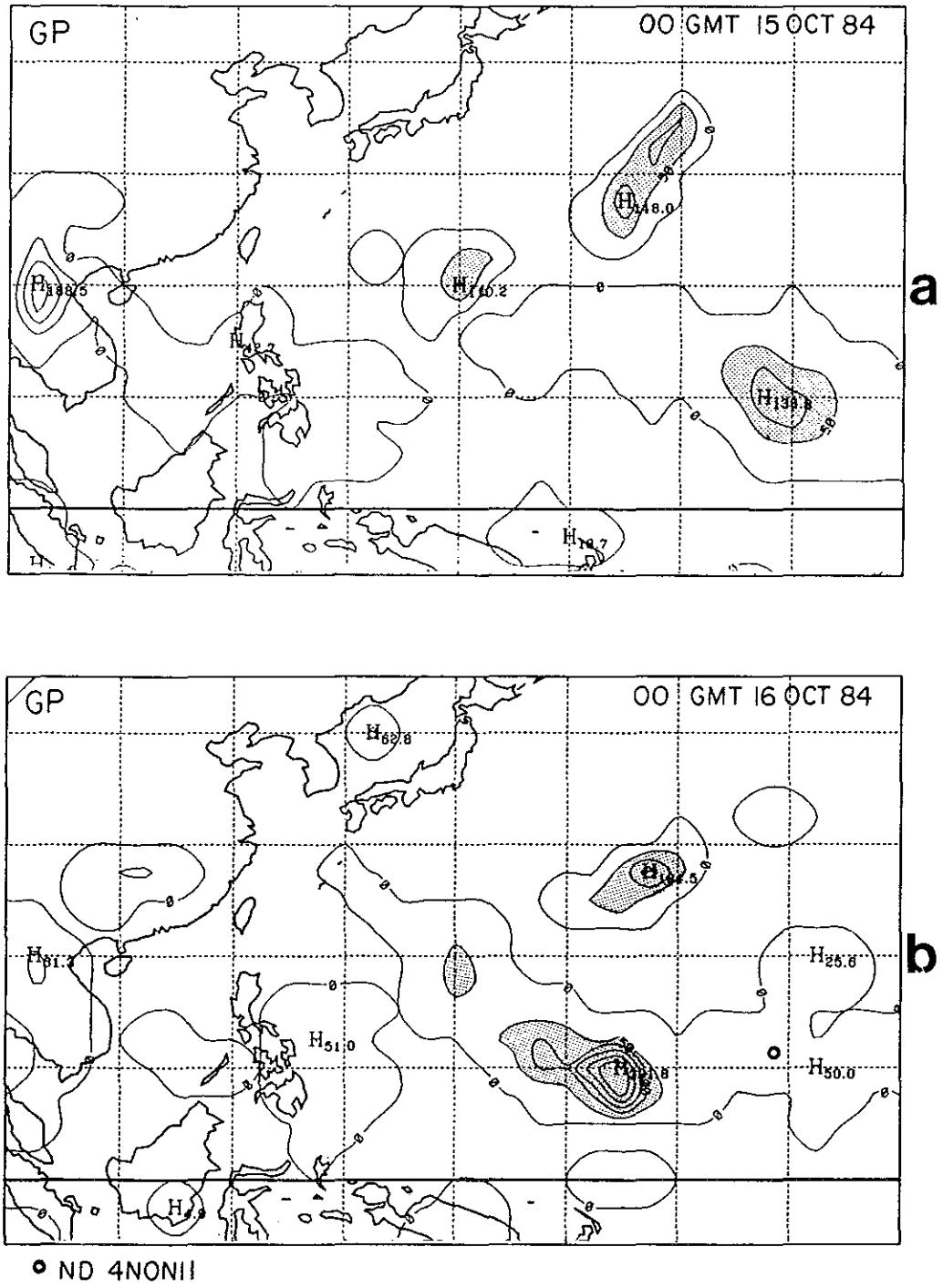

Figure 6.20: Daily series of 00 GMT contour maps of GP. Units are $10^{-12}s^{-2}$. Values greater than 50 are shaded. Locations of ND and PS disturbances are indicated. a) 15 October 1984; b) 16 October 1984.

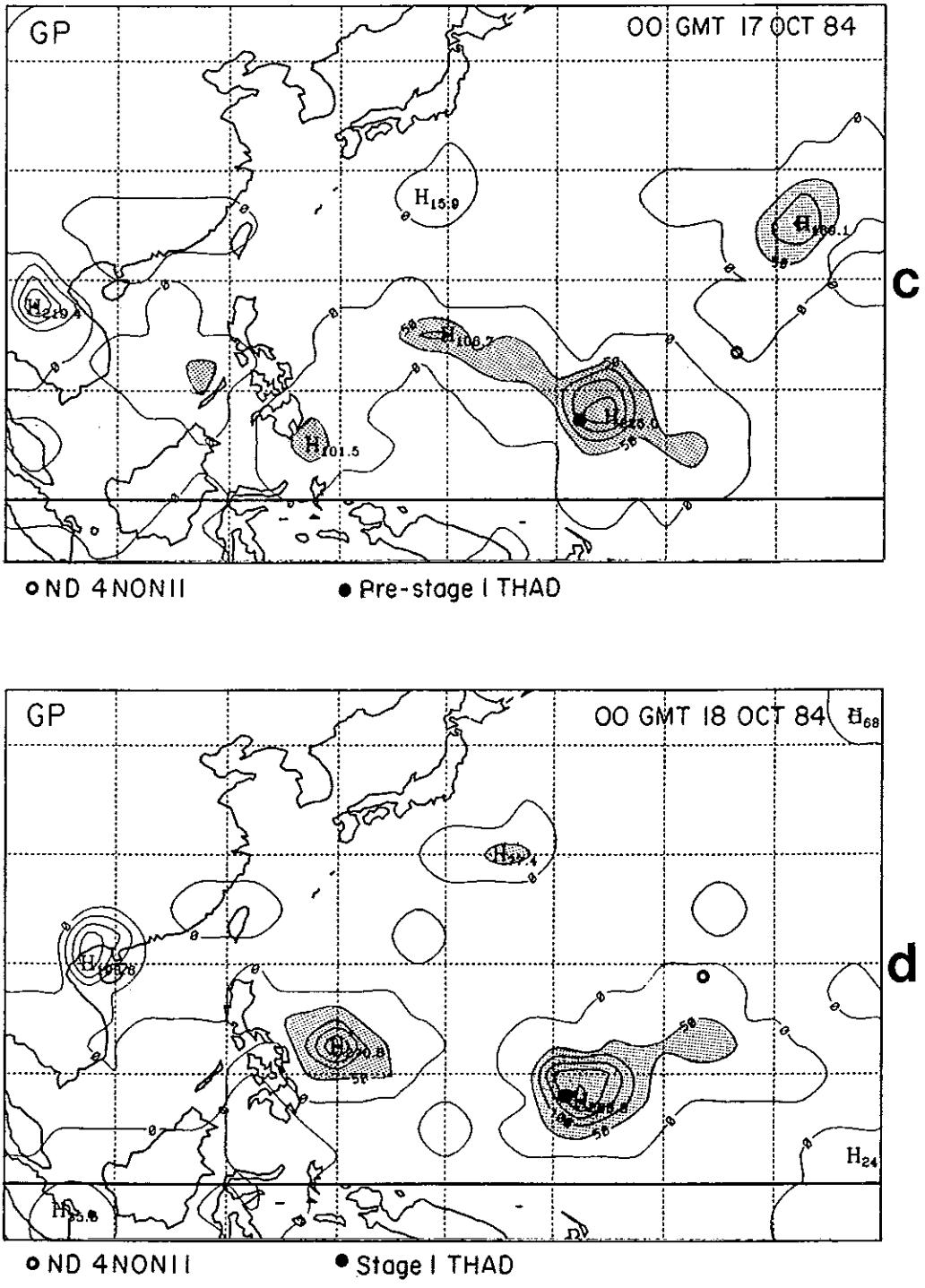

Figure 6.20: c) 17 October 1984; d) 18 October 1984.

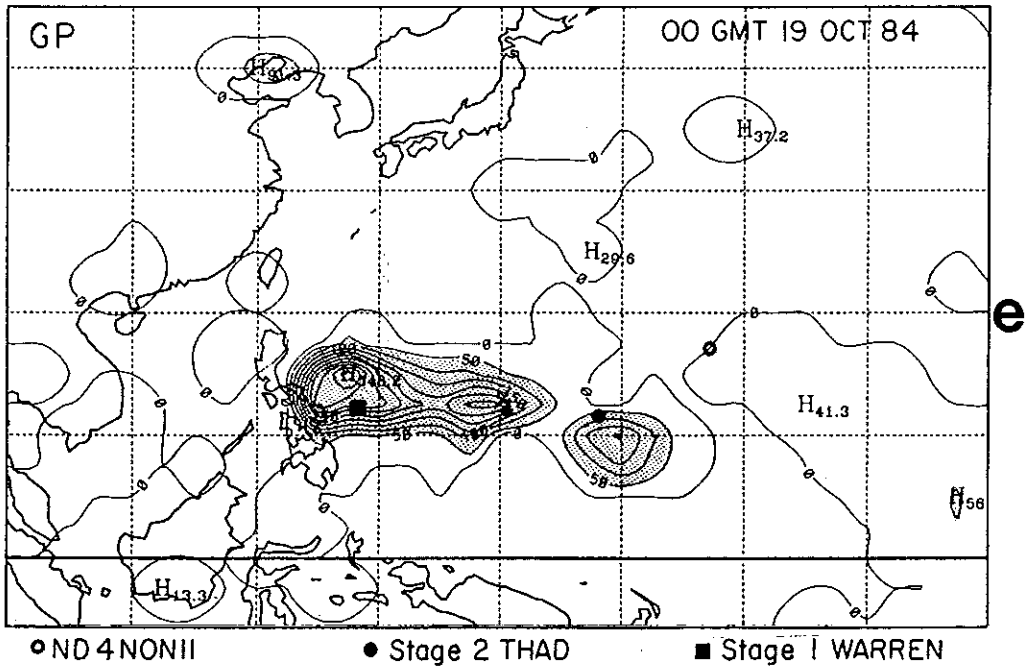

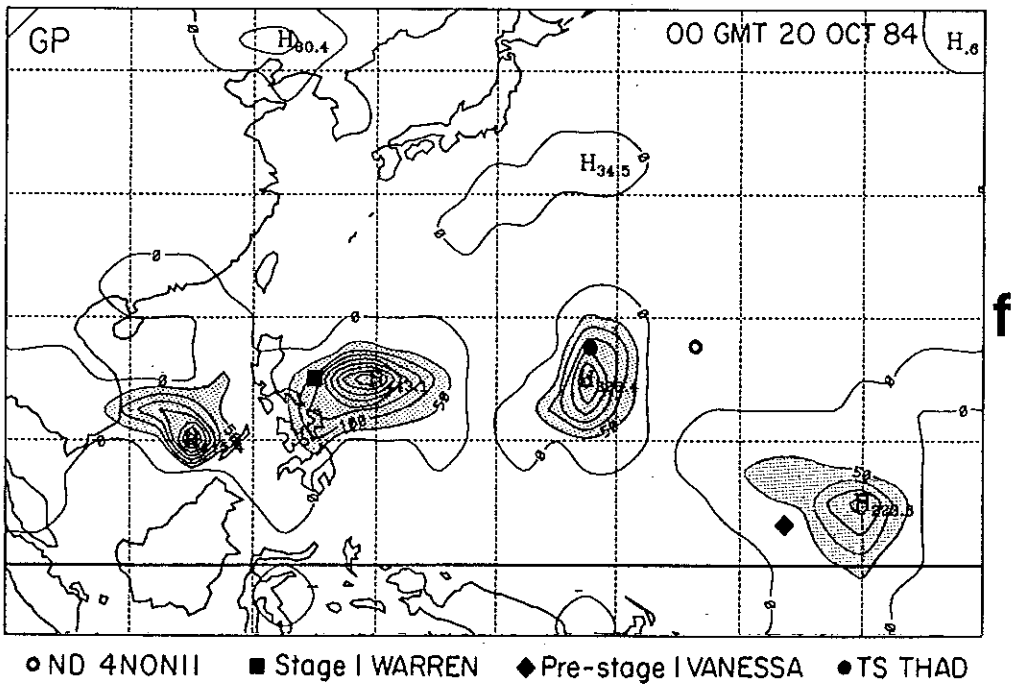

Figure 6.20: e) 19 October 1984; f) 20 October 1984.

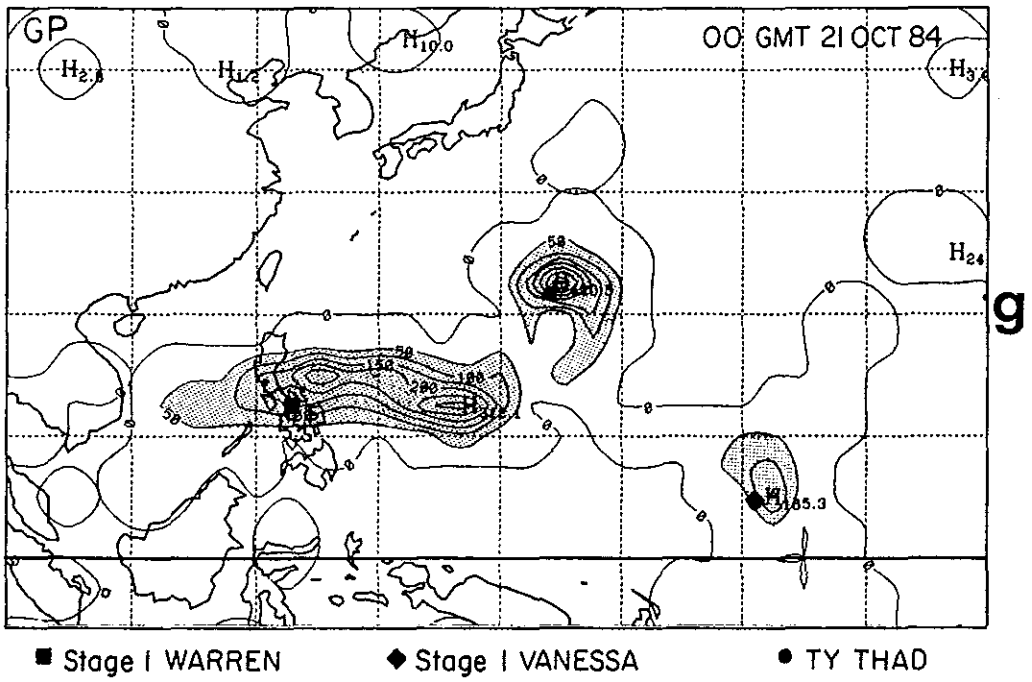

Figure 6.20: g) 21 October 1984.

Table 6.13: Percentage of time periods with at least one unfavorable genesis condition.

Data Set	%
ND	97
PS	75
PS Pre-Max	95
PS1	69
PS2	65
PS–Typical	58
PS–M–Stg	70
PS–Other	89

Table 6.14 lists the results of this analysis for all 15 ND disturbances and 23 PS disturbances. Sixty-five percent of the PS cases are correctly defined as D, using this method. For the ND cases, 80% are correctly defined as ND. Table 6.15 lists the percent of correctly defined cases when stratified according to 850 mb pattern. The data set classified as "Typical" provides the best results with 90%. Only 57% of the "Monsoon" type of 33% of the "Other" are correctly defined as D. The relatively poor results with the strong monsoon trough cases and the atypical cases classified as "Other" suggest that different thresholds are likely needed for those type cases.

Table 6.14: Objective classification of Developing (D) versus Non-Developing (ND) using the Threshold Method.

Name	(15 ND cases)	Name	(23 PS cases)
4NON1	ND	Wynne	D
4NON2	ND	Alex	D
4NON3	D	Betty	D
4NON4	ND	Cary	ND
4NON5	ND	Dinah	ND
4NON6	ND	Ed	ND
4NON7	ND	Freda	D
4NON8	ND	Holly	D
4NON9	ND	Ike	D
4NON11	ND	June	D
4NON13	ND	Kelly	ND
4NON14	ND	Maury	ND
4NON15	ND	Nina	ND
4NON16	D	Ogden	D
4NON17	D	Phyllis	D
		Roy	ND
		Thad	D
		Vanessa	D
		Warren	D
		Agnes	D
		Bill	D
		Clara	D
		Doyle	ND

6.10.2 Genesis Parameter (GP) Method

Using the 850 VOR, 850 -DIV, and 200-850 SHEAR quantities which have been interpolated to the Best Track positions, GP is computed for each disturbance. Table 6.16 lists the mean GP for various data stratifications. The mean GP for the PS1 data set is about six times larger than for the ND data set. The frequency distributions of GP (Fig. 6.21) show that GP is better at differentiating between ND and PS1 disturbances than either 850 VOR (Fig. 6.5b) or 850 -DIV (Fig. 6.6b).

Time series of GP for a non-developing disturbance (4NON3) and a pre-tropical storm disturbance (Vanessa) are plotted in Fig. 6.22. Even though the GP for one time period of 4NON3 is quite high (103), genesis does not take place. This is likely because GP is very low for all other time periods (Fig. 6.22a). In contrast, with the PS disturbances,

Table 6.15: Percentage of correct objective classifications using the Threshold Method.

Data Set	No. Correct/N	% Correct
ND	12/15	80
PS	15/23	65
PS–Typical	9/10	90
PS–M–Stg	4/7	57
PS–Other	2/6	33

Table 6.16: GP mean values ($10^{-12}s^{-2}$).

Data Set	GP	N
ND	14.6	111
PS	99.9	167
PS Pre-Max	29.0	44
PS1	89.3	77
PS2	185.3	46

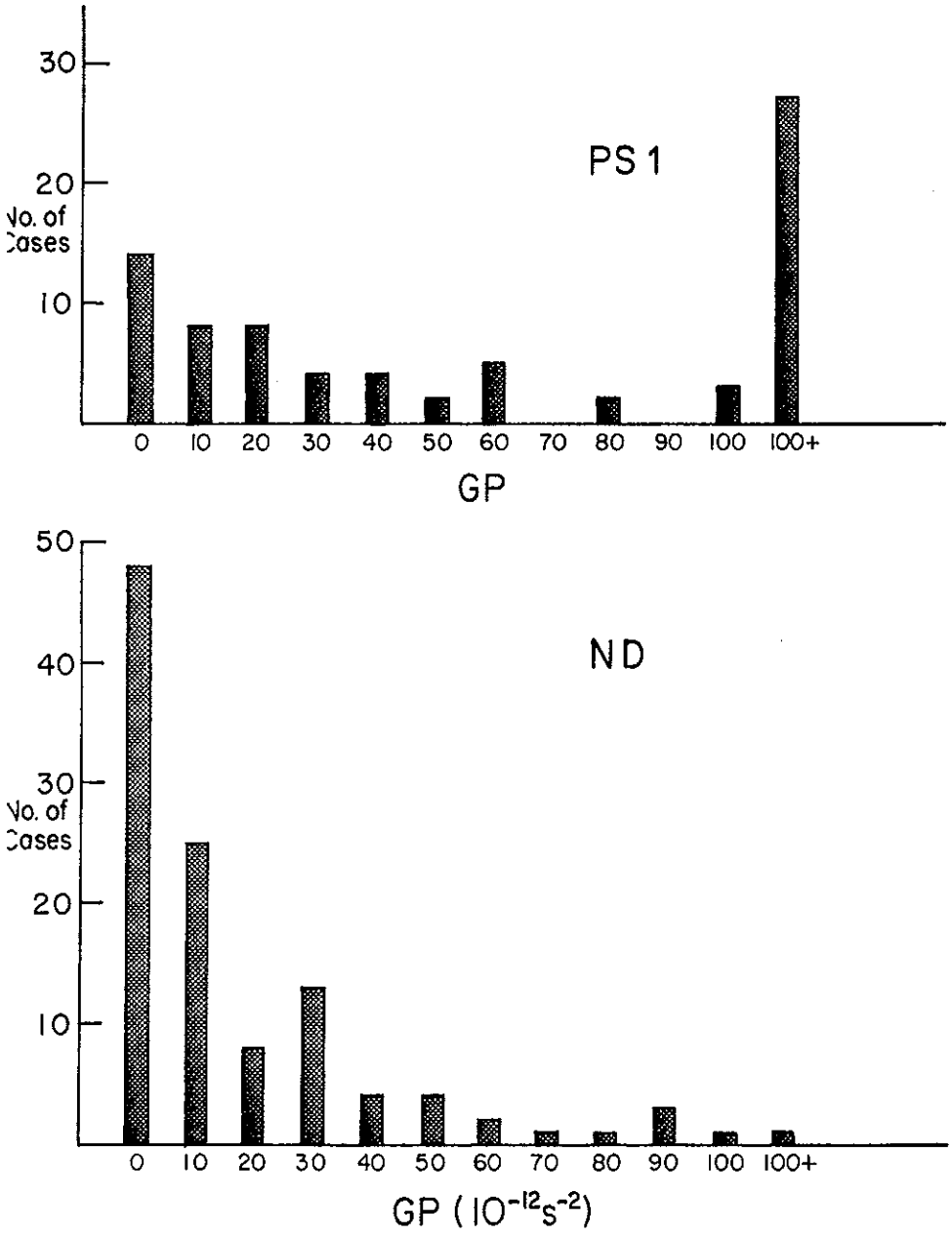

Figure 6.21: Frequency distribution of GP for the ND and PS1 data sets.

high GP values may persist, or a distinct GP maxima coinciding with Stage 1 and Stage 2 of genesis (Fig. 6.22b) may be present.

With those considerations in mind, a method is devised to evaluate the utility of GP quantities in differentiating PS from ND disturbances. If there are two or more time periods with GP $>$ 50, the disturbance is designated D (developing). Otherwise, the disturbance is designated ND (non-developing). The results of this analysis for each individual case are listed in Table 6.17, and the percentage of correct classifications are given in Table 6.18. Ninety-three percent of the ND cases and 78% of the PS disturbances are correctly classified. The PS-Typical stratification has 90% correct designations. Comparison of these results using the GP method shows improvement over the Threshold Method results (Table 6.15).

Table 6.17: Objective classification of Developing (D) versus Non–Developing (ND) using the GP Method.

Name	(15 ND cases)	Name	(23 PS cases)
4NON1	ND	Wynne	D
4NON2	ND	Alex	D
4NON3	ND	Betty	D
4NON4	ND	Cary	ND
4NON5	ND	Dinah	ND
4NON6	ND	Ed	D
4NON7	ND	Freda	D
4NON8	D	Holly	D
4NON9	ND	Ike	D
4NON11	ND	June	D
4NON13	ND	Kelly	D
4NON14	ND	Maury	ND
4NON15	ND	Nina	D
4NON16	ND	Ogden	D
4NON17	ND	Phyllis	D
		Roy	D
		Thad	D
		Vanessa	D
		Warren	D
		Agnes	D
		Bill	ND
		Clara	D
		Doyle	ND

6.10.3 Summary

Additional testing with larger and independent data samples are needed to refine the objective techniques and forecast aids. However, the results presented here show great promise that useful forecast techniques to indicate both tropical cyclogenesis and non–genesis can be developed.

The techniques are best suited for use along with satellite data for monitoring the location and evolution of deep convective cloud areas. A mesoscale convective system of sufficient size located in an area with high GP values, would be forecast to undergo

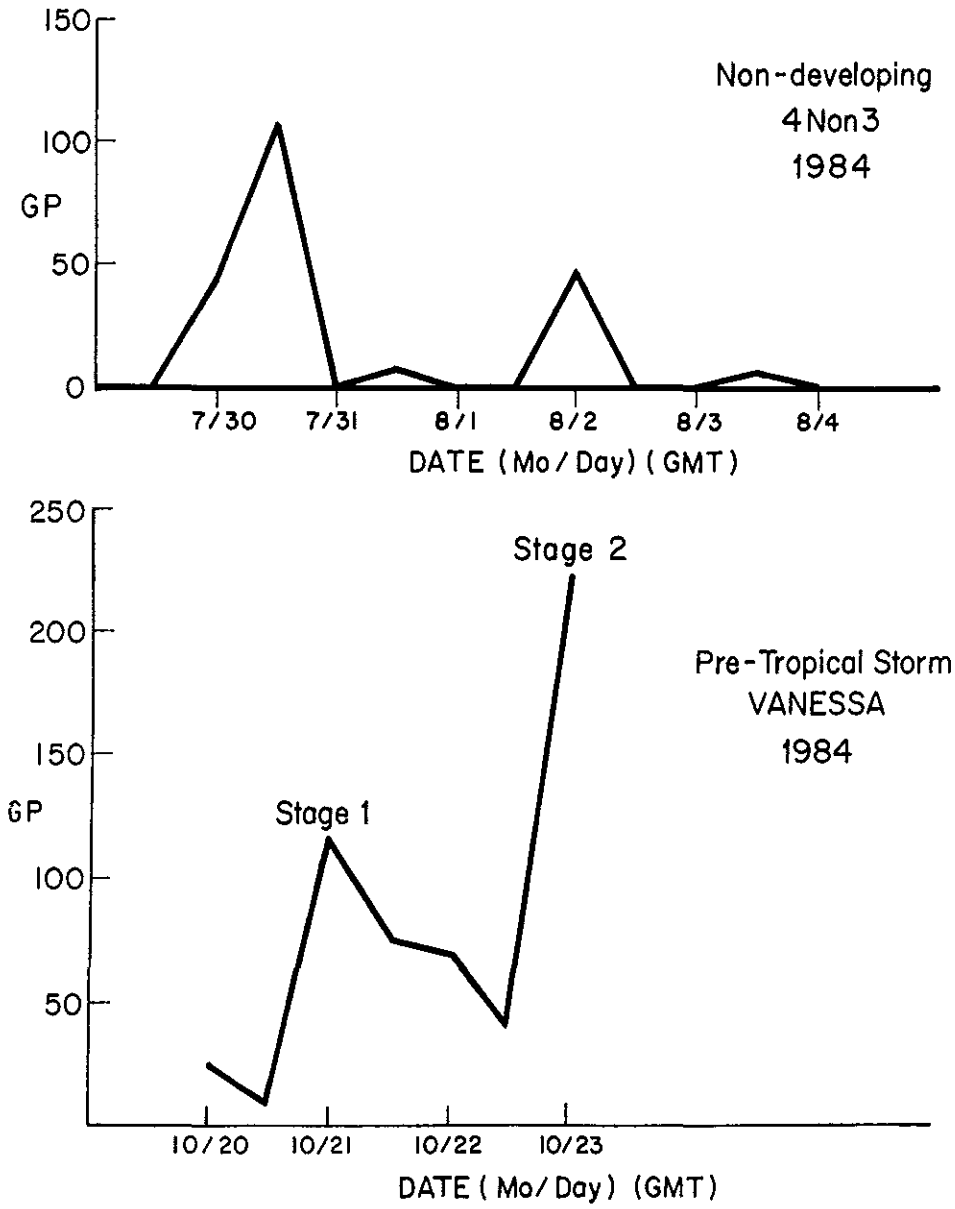

Figure 6.22: Time series of GP. Units are $10^{-12}s^{-2}$. a) Non-developing disturbance, 4NON3. b) Pre-tropical storm disturbances, Vanessa.

Table 6.18: Percentage of correct objective classifications using the GP Method.

Data Set	No. Correct/N	% Correct
ND	14/15	93
PS	18/23	78
PS–Typical	9/10	90
PS–M–Stg	6/7	86
PS–Other	3/6	50

cyclogenesis. More refined techniques employing quantitative satellite information require additional research. Prognostic numerical model data could also be used for longer range prediction.

Chapter 7

DETAILED CASE STUDIES

A thorough and careful analysis of all available data covering a period of several days, is needed to adequately understand the formation of an individual tropical cyclone. Detailed case studies have been completed for the entire genesis period with several select cases. Portions of various other genesis cases have also been studied using combined data sources. The purpose of this chapter is to use excerpts from the individual case studies to illustrate specific aspects important to understanding tropical cyclogenesis.

7.1 Low-level Wind Pattern Changes During Tropical Cyclogenesis

Some of the investigative aircraft reconnaissance flights fail to adequately represent the winds surrounding the disturbance center. Also, very few of the flights investigate tropical disturbances before the Stage 1 convective maximum occurs. Mesoscale and even cloud scale effects may make some winds unrepresentative. As shown in Chapter 5, the synoptic-scale patterns in which genesis occurs are quite variable. Due to these problems, there is no one set of aircraft flights for any single genesis case which adequately represents the important changes in the low-level winds commonly observed during cyclogenesis.

However, after analyzing observations from many aircraft flights with respect to both pre-tropical storm and non-developing disturbances, three flights have been chosen as a good depiction of the most commonly observed changes that occur during cyclogenesis. Each of the three flights include 15-minute wind observations at the 457 m (1500 ft) flight level.

7.1.1 Pre-Stage 1

The aircraft observations plotted in Fig. 7.1 are from the investigative flight into the tropical disturbance which eventually developed into Typhoon Warren. This is before the Stage 1 initial mesoscale vortex formation takes place. The cyclonic circulation center is poorly defined and the wind speeds near the center are generally 7.5 ms^{-1} or less. The higher winds of up to 12.5 ms^{-1} are located at about 2° latitude or more distance from the center. Thus the pre-Stage 1 disturbance is characterized by a broad cyclonic circulation about a poorly defined center. This wind pattern is also typical of many of the non-developing disturbances.

This disturbance is embedded within a distinct monsoon trough and is moving to the west at about 4 ms^{-1}. Figure 7.1b is a plot of the winds in the motion relative coordinate system. The vector of disturbance center's movement is subtracted from each wind observation, and they are plotted relative to the location of that center. Note that when the winds are converted to the motion relative coordinate system, the tangential winds are stronger to south of the disturbance center. The MSLP is 1005 mb, which is about 2-3 mb lower than the typical MSLP for pre–Stage 1 disturbances.

7.1.2 Stage 1

Figure 7.2 shows the typical appearance of wind observations surrounding the initial mesoscale vortex which first appears following the Stage 1 convective maximum. The wind speeds near the center are still quite weak (7.5 ms^{-1} or less) but the circulation

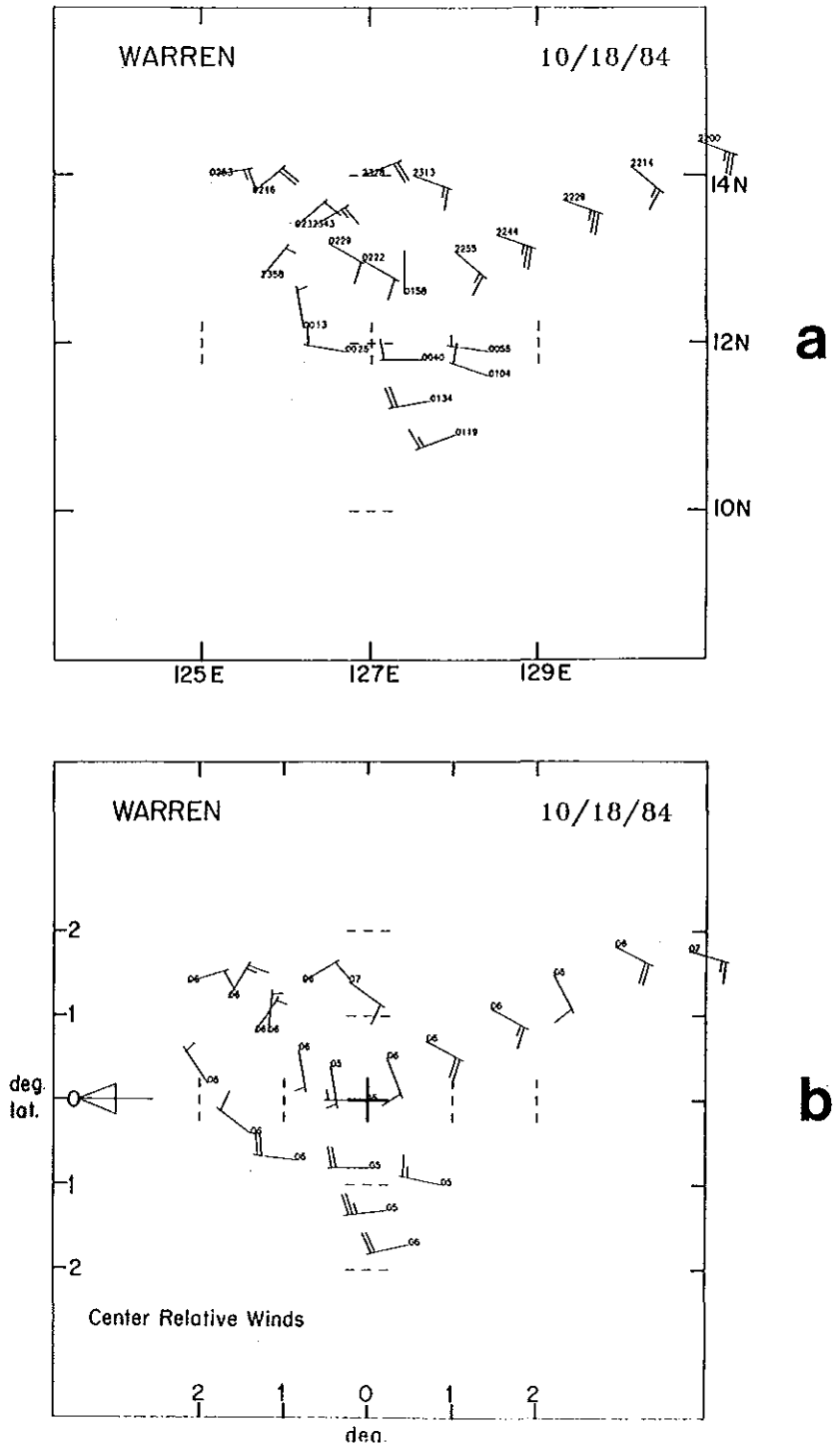

Figure 7.1: Wind observations at 457 m (1500 ft) from aircraft reconnaissance flight into a Pre–Stage 1 disturbance which became Typhoon Warren. a) Observations are labeled with the time (GMT). b) Observations are labeled with sea-level pressure (mb–1000), and are in the motion relative coordinate system. The arrow indicates the direction of the disturbance center.

center is well defined. A very tight cyclonic circulation with light winds characterizes the disturbance following the Stage 1 convective maximum. The highest wind speeds may still be located well away from the circulation center.

The observations in Fig. 7.2 are with the disturbance that became Tropical Storm Carmen. The flight observations at 00–03 GMT 11 August 1983, are almost two days following the Stage 1 convective maximum. First designation as a tropical storm was not until almost three days later, at 21 GMT 13 August 1983. The disturbance is moving to the north–northwest at about 2 ms^{-1}. With this slow movement, the motion relative winds show only small differences from the actual observed winds.

7.1.3 Stage 2

During Stage 2, the disturbance is typically designated a tropical depression. The aircraft observations in Fig. 7.3 depict the typical Stage 2 winds. This tropical depression was first designated Tropical Storm Wynne about 12 hr following this aircraft flight. The circulation center is well-defined and the highest wind speeds (about 17.5 ms^{-1}) are located near the circulation center. Movement is to the northwest at about 4ms^{-1}. The MSLP is 1001 mb and is beginning a significant decrease. The following aircraft flight, about 24 hr later recorded a MSLP of 998 mb.

7.2 Visible Satellite Images of Low-level Circulation Centers

7.2.1 Doyle

The tropical disturbance which became Typhoon Doyle formed in the vicinity of 4°N 157°E around 09 GMT 30 November 1984. This was the beginning of the disturbance as a persistent cloud cluster. The cloud cluster formed in a cyclonically sheared easterly 850-mb flow pattern. Figure 7.4 is the IR image at 18 GMT 1 December 1984. The disturbance can be classified as a non-developing disturbance at this time showing no signs of tropical cyclogenesis. Two days later, the associated deep convection increased to a very large extent as shown in the 21 GMT 2 December 1984 IR image (Fig. 7.5). This is the Stage 1 convective maximum. A very distinct circular mesoscale cold IR area is located near the disturbance center. The area colder than –65°C with this feature is about 3° latitude diameter. For about 24 hr following this convective maximum, the associated deep convection decreased greatly. It was during this time that a distinct smaller scale circulation center was first seen in the satellite images. The visible satellite image in Fig. 7.6 shows the distinct cyclonic circulation center. With animated satellite images the circulation center can be accurately located. The first investigative aircraft reconnaissance flight for this case confirmed the existence of the low-level circulation center. Those observations are shown in Fig. 7.7. Stage 1 of tropical cyclogenesis, characterized by a convective maximum and the initiation of a mesoscale low-level vortex, is clearly depicted with this case in Figs. 7.4–7.7.

A high resolution visible DMSP satellite image in Fig. 7.8 shows the distinct circulation center and deep convection beginning to appear near the center marking the onset of Stage 2. The date and time of the image is 0045 GMT 4 December, which is about 36 hr following the Stage 1 convective maximum, and 22 hr after the visible image in Fig. 7.6. Stage 2 is characterized by the resurgence of deep convection near the circulation center. This process continued, and Doyle was first designated a tropical storm at 18 GMT 4 December 1984.

7.2.2 Additional Examples of Stage 1 Genesis in Satellite Images

The pre-Tropical Storm Doyle disturbance is an example of a Stage 1 convective maximum genesis which is very large. The resultant initial mesoscale circulation center is easy to recognize in the satellite images. Many cases are not nearly so clear cut. Frequent

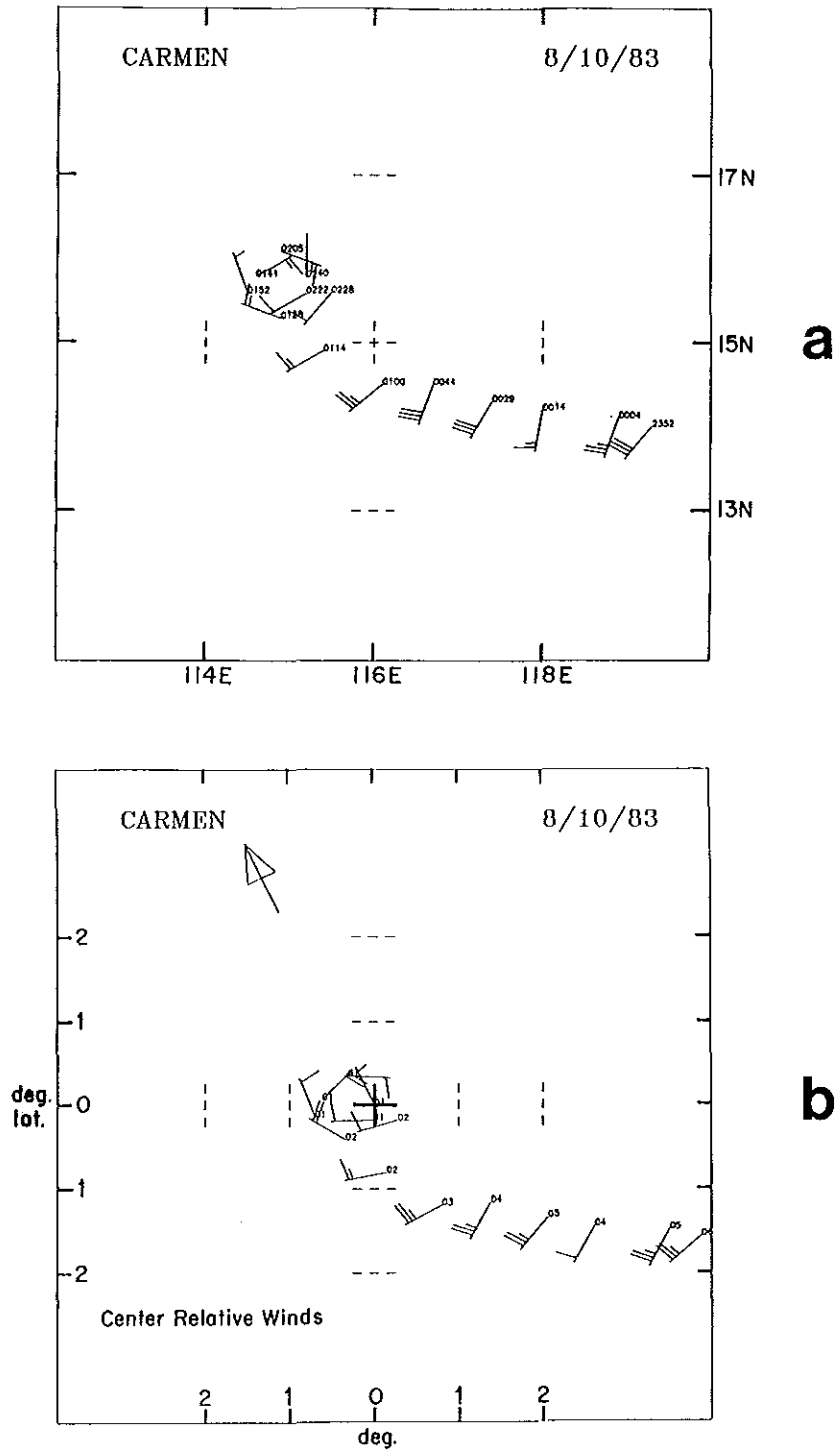

Figure 7.2: Aircraft wind observations at 457 m with a Stage 1 disturbance which became Tropical Storm Carmen. a) Observations are labeled with the time (GMT). b) Observations are labeled with sea level pressure (mb-1000), and are in the motion relative coordinate system.

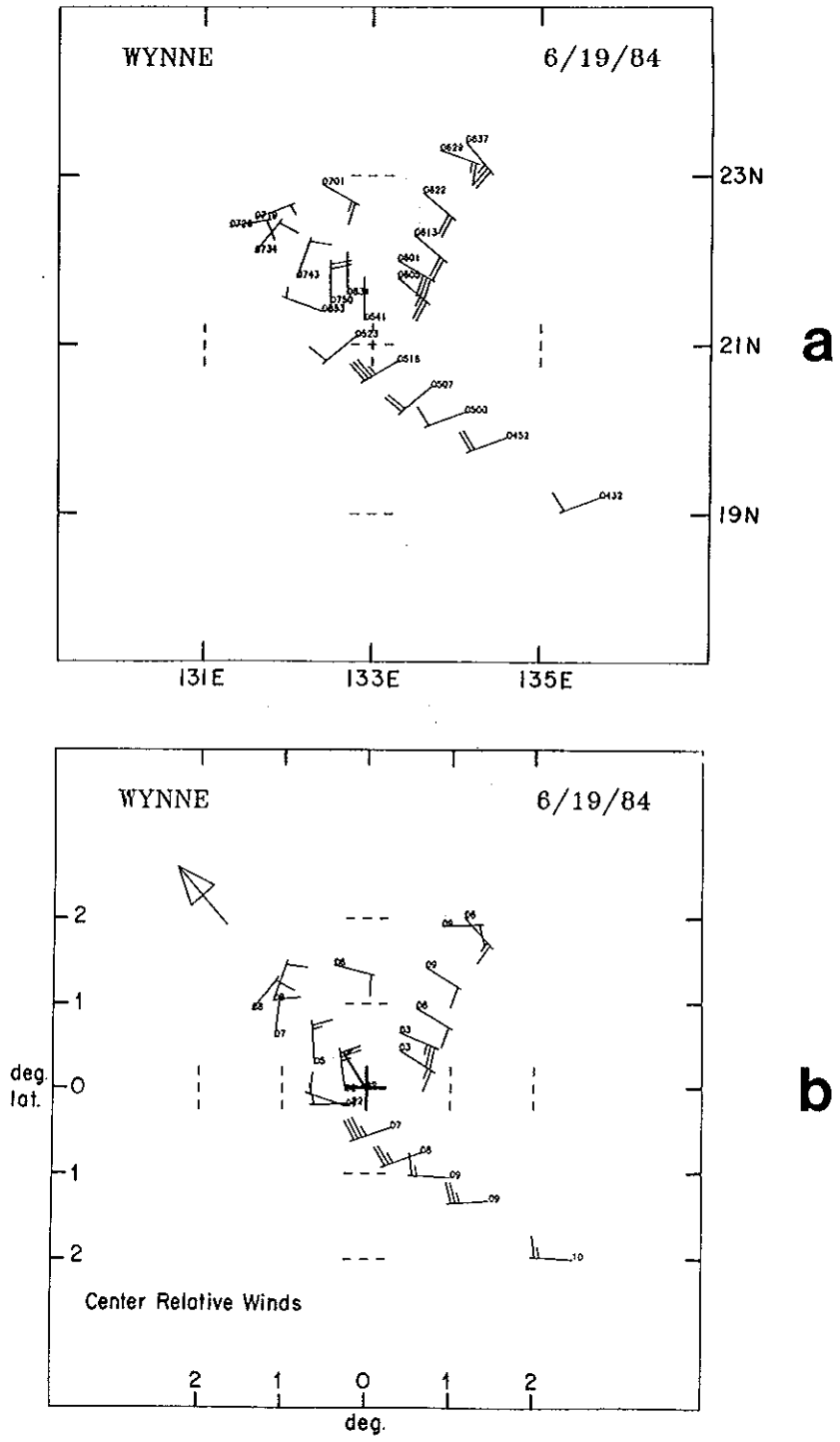

Figure 7.3: Aircraft wind observations at 457 m with a Stage 2 tropical depression which became Tropical Storm Wynne. a) Observations are labeled with the time (GMT). b) Observations are labeled with the sea-level pressure (mb–1000), and are in the motion relative coordinate system.

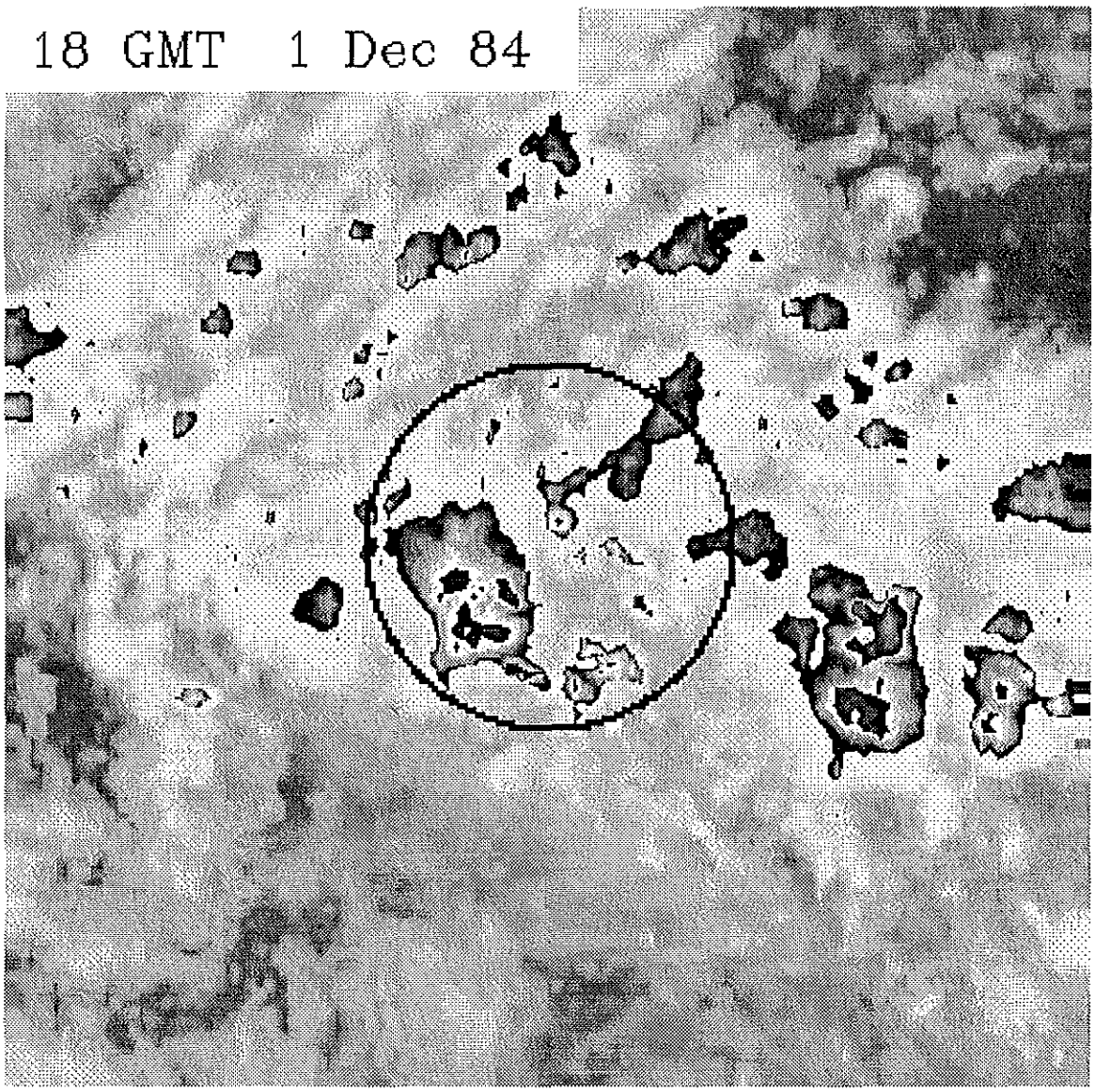

Figure 7.4: Enhanced IR image, 18 GMT 1 Dec 1984. Pre-Stage 1 tropical disturbance which developed into Typhoon Doyle. The circle is 2 degrees latitude radius centered on the Best Track location (5.4°N, 152°E). The IR enhancement is shown in Fig. 2.1c.

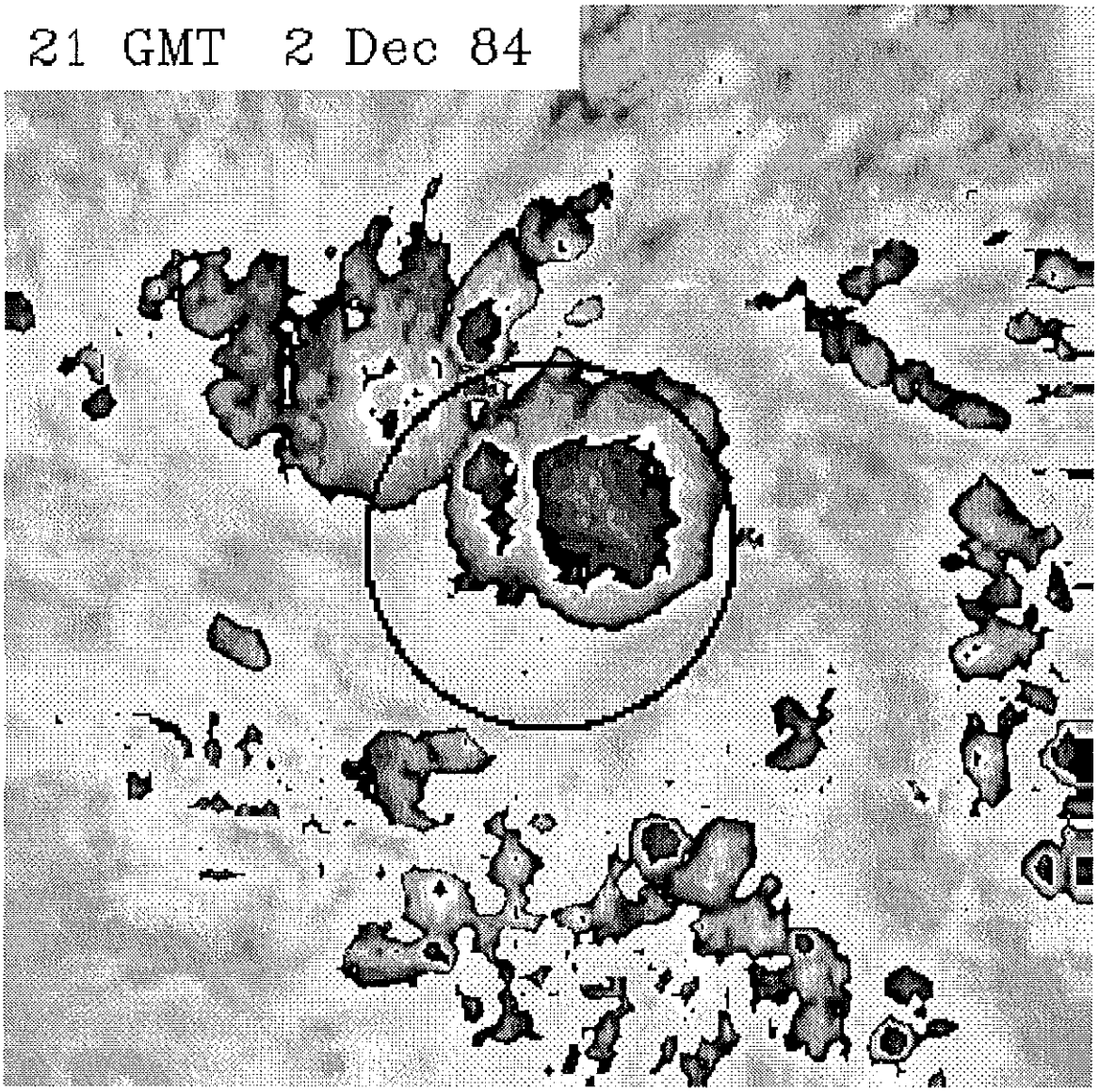

Figure 7.5: Enhanced IR image, 21 GMT 2 Dec 1984. Pre-tropical storm Doyle during Stage 1 convective maximum. The circle is 2 degrees latitude radius centered on the Best Track location (6.8°N, 146.1°E). The IR enhancement is shown in Fig. 2.1c.

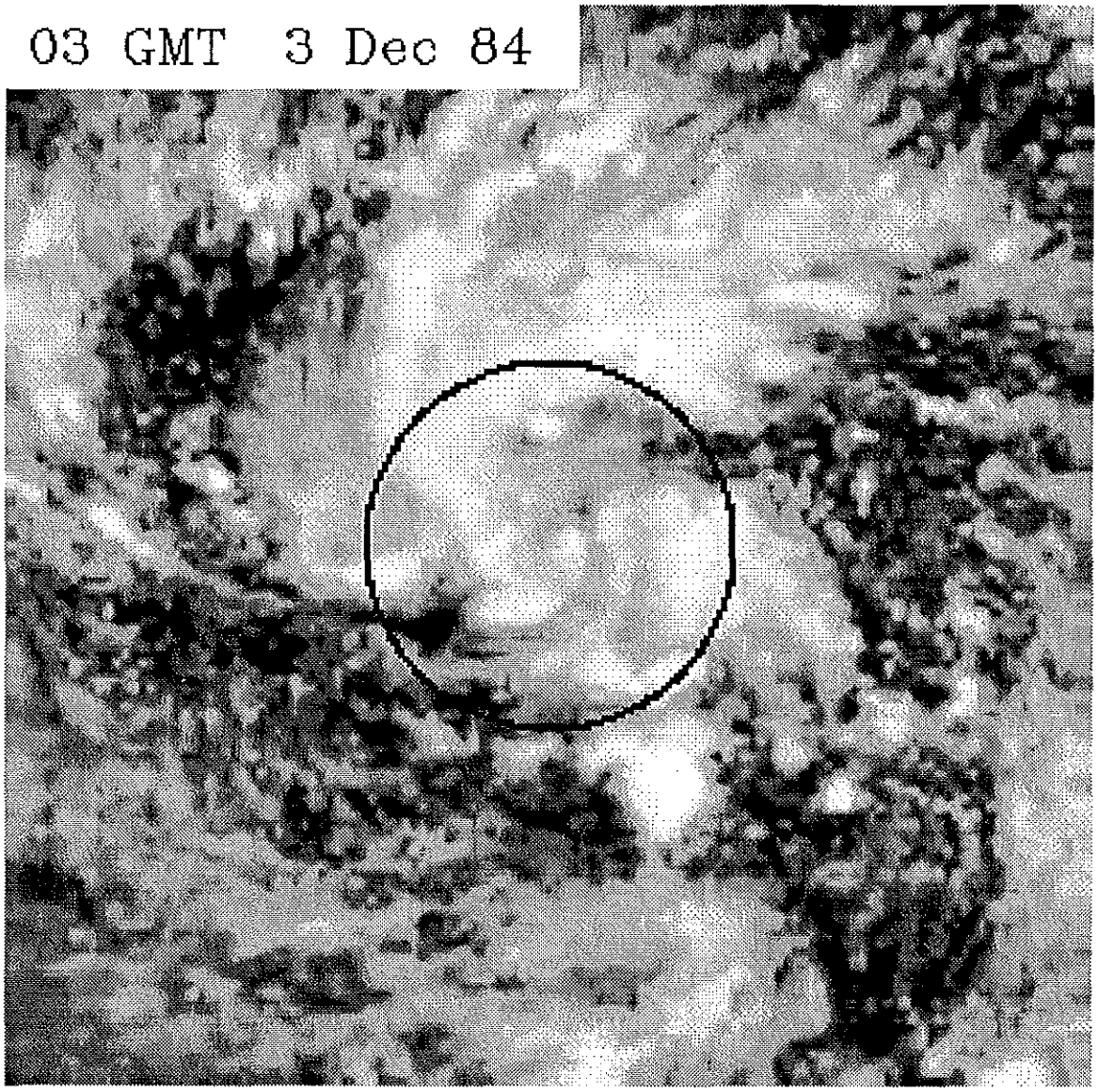

Figure 7.6: Visible satellite image, 03 GMT 3 Dec 1984, showing mesoscale vortex circulation which later developed into Typhoon Doyle. The circle is 2 degrees latitude radius centered on the Best Track location (7.0°N, 144.8°E).

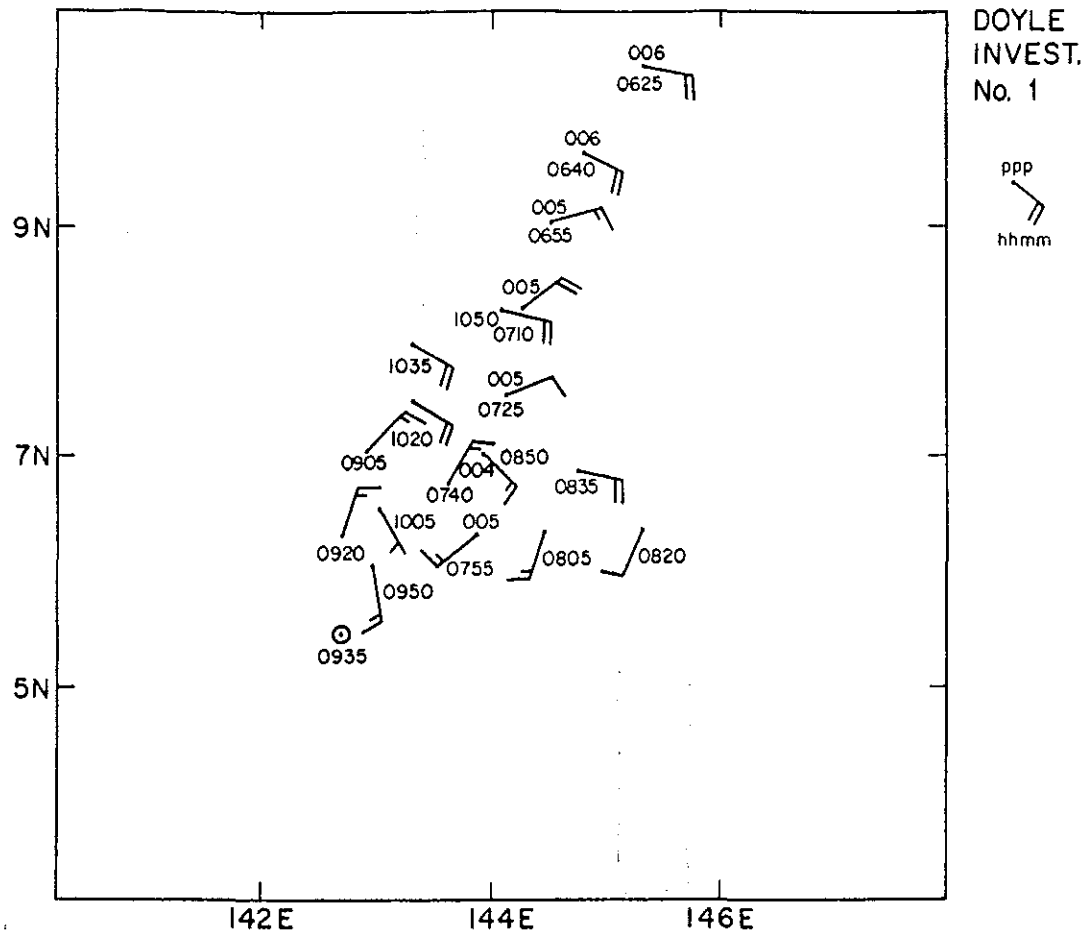

Figure 7.7: Aircraft observations of wind and sea-level pressure (SLP) for 457 m (1500 ft) level investigative flight showing the low-level circulation center of pre-tropical storm Doyle on 3 Dec 1984. The SLP for each observation is in mb-1000. The GMT time (hhmm) is plotted with each observation.

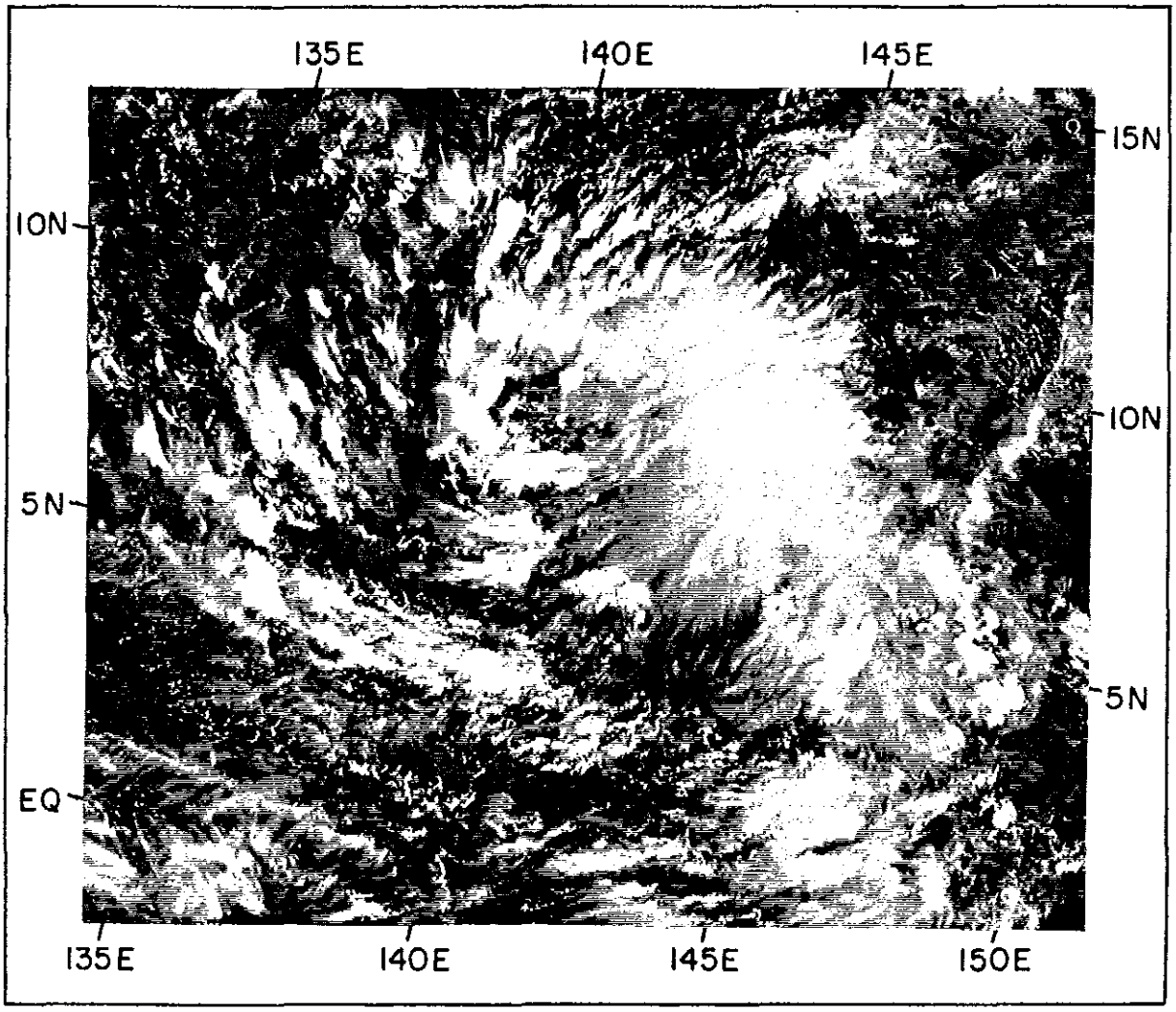

Figure 7.8: Visible DMSP satellite image at 0045 GMT 4 Dec 1984, showing pre-tropical storm Doyle at the onset of Stage 2.

interval and high spatial resolution visible satellite images are the best tools for locating low-level circulation centers (LLCCs), particularly when animated images are used. Even though the higher resolution satellite images are generally unavailable for the present study, several examples showing this important feature have been found.

Three additional examples of LLCCs observed following a Stage 1 convective maximum as depicted by the low resolution (10 km) GMS visible images, are illustrated in Fig. 7.9. The enhanced IR images of the preceding Stage 1 convective maxima are also shown. Three general characteristics of the LLCCs are identified with regard to their appearance in the visible images.

1. They form initially in the area of extensive very cold IR cloud top temperatures.
2. They may persist for long periods (i.e. several days) in the absence of deep convective clouds.
3. They may often exist but cannot be clearly observed due to obscuration by thick cirrus cloud shields.
4. The best method to identify them is by using animated frequent interval (ie. 30 min or 1 hr) satellite images.
5. The mesoscale vortex often extends upward through the mid-troposphere and thus can be observed by the appearance and motion of higher level clouds.

The extensive cold IR cloud shield is the cloud top of the active precipitating mesoscale stratiform region typically found in tropical cloud clusters. Any large cold IR area in the climatological genesis areas should be a suspect area for the formation of a mesoscale vortex. The LLCC identified in satellite imagery is the cloud signature associated with the mesoscale vortex, and is best observed after the mesoscale convective system dissipates.

Since the vortex often persists even with no deep convection near the center and may be obscured by nearby ongoing deep convection and cirrus clouds, will often make it very difficult to track. Some tropical cyclones are analyzed to form quickly and suddenly appear as a tropical depression or tropical storm. It is likely that many of those are simply the Stage 2 tropical cyclogenesis with a mesoscale vortex which has gone undetected in the analysis.

As discussed in Chapter 3, some tropical cyclones form without a well-defined early convective maximum. In those cases, the initial mesoscale vortex formation is not followed by the typical 24 hr or more of reduced convection, but by even greater convective activity. Therefore, the LLCC may not be observed, and satellite cloud characteristics typical of Stage 2 (e.g. deep cyclonically curved cloud bands) may then appear, indicating the existence of the LLCC.

7.3 Westerly Surge Initiating a Convective Maximum

The pre-tropical storm disturbance which became Typhoon Forrest was associated with a westerly surge, both during Stage 1 and Stage 2. As shown in Table 5.1 the surge with Stage 1 was identified in all three data sources and assigned a direction of west-southwest. The Stage 2 surge was detected by aircraft and assigned a due west direction.

7.3.1 Forrest, Stage 1

The aircraft observations of the surge which initiated the Stage 1 convective maximum are plotted in Fig. 5.8. Figure 7.10 depicts qualitative streamline-isotach analyses at 6 hr intervals which show the surge interacting with the pre-existing tropical disturbance. The analyses are based on all three data sources. The disturbance center and its track are plotted in the analyses. The enhanced IR images corresponding to the 6-hourly analyses are shown in Fig. 7.11.

The main effect of the surge is to enhance the low-level convergence of the pre-existing disturbance and not to directly spin up its cyclonic circulation. This results in the Stage 1 convective maximum. It first appears as a very large area of convection in Fig. 7.11c and becomes even larger 6 hr later (Fig. 7.11d), as the surge interacts with the disturbance. In Fig. 7.11e, the convection has diminished and a circulation center becomes much more

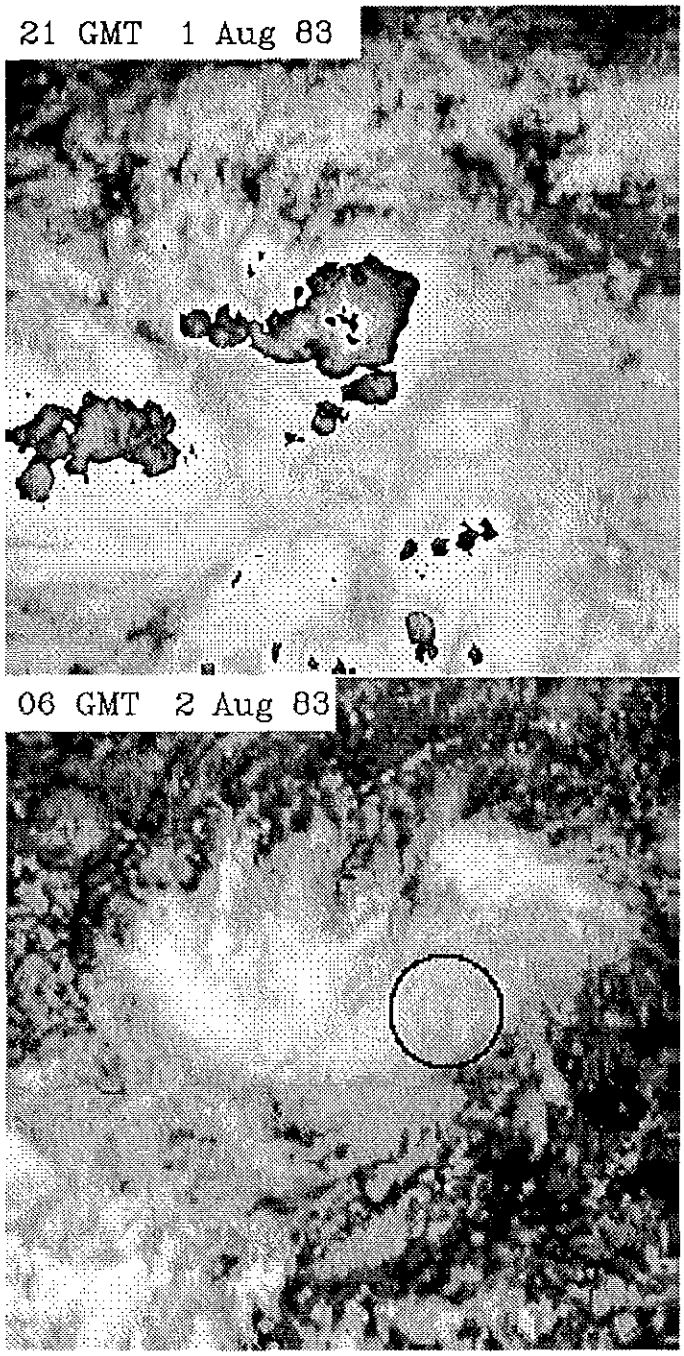

Figure 7.9: Examples of distinct mesoscale circulation centers (LLCCs) in the visible images, and the enhanced IR images of the associated Stage 1 convective maxima. a) Abby, 21 GMT 1 August 1983, enhanced IR. b) Abby, 06 GMT 2 August 1983, visible. c) Forrest, 21 GMT 18 September 1983, enhanced IR. d) Forrest, 03 GMT 19 September 1983, visible. e) Phyllis, 21 GMT 8 October 1984, enhanced IR. f) Phyllis, 00 GMT 10 October 1984, visible.

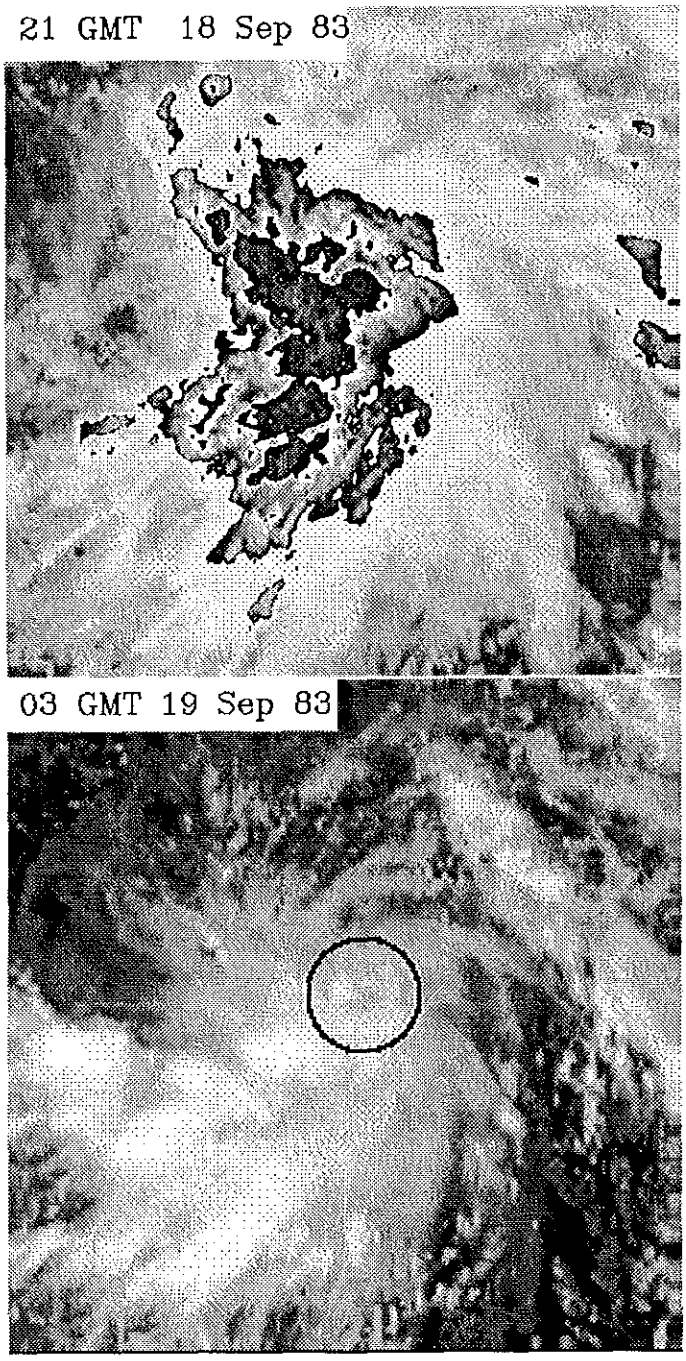

Figure 7.9: c-d: Continued.

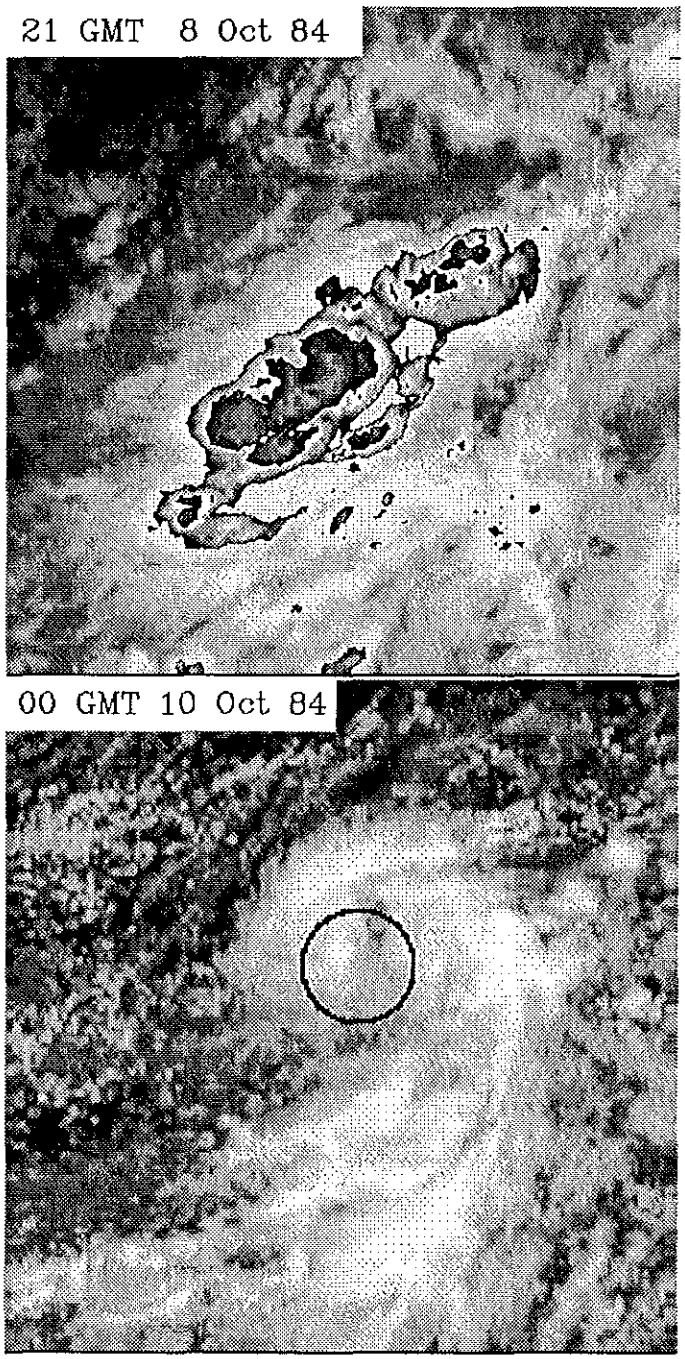

Figure 7.9: e-f: Continued.

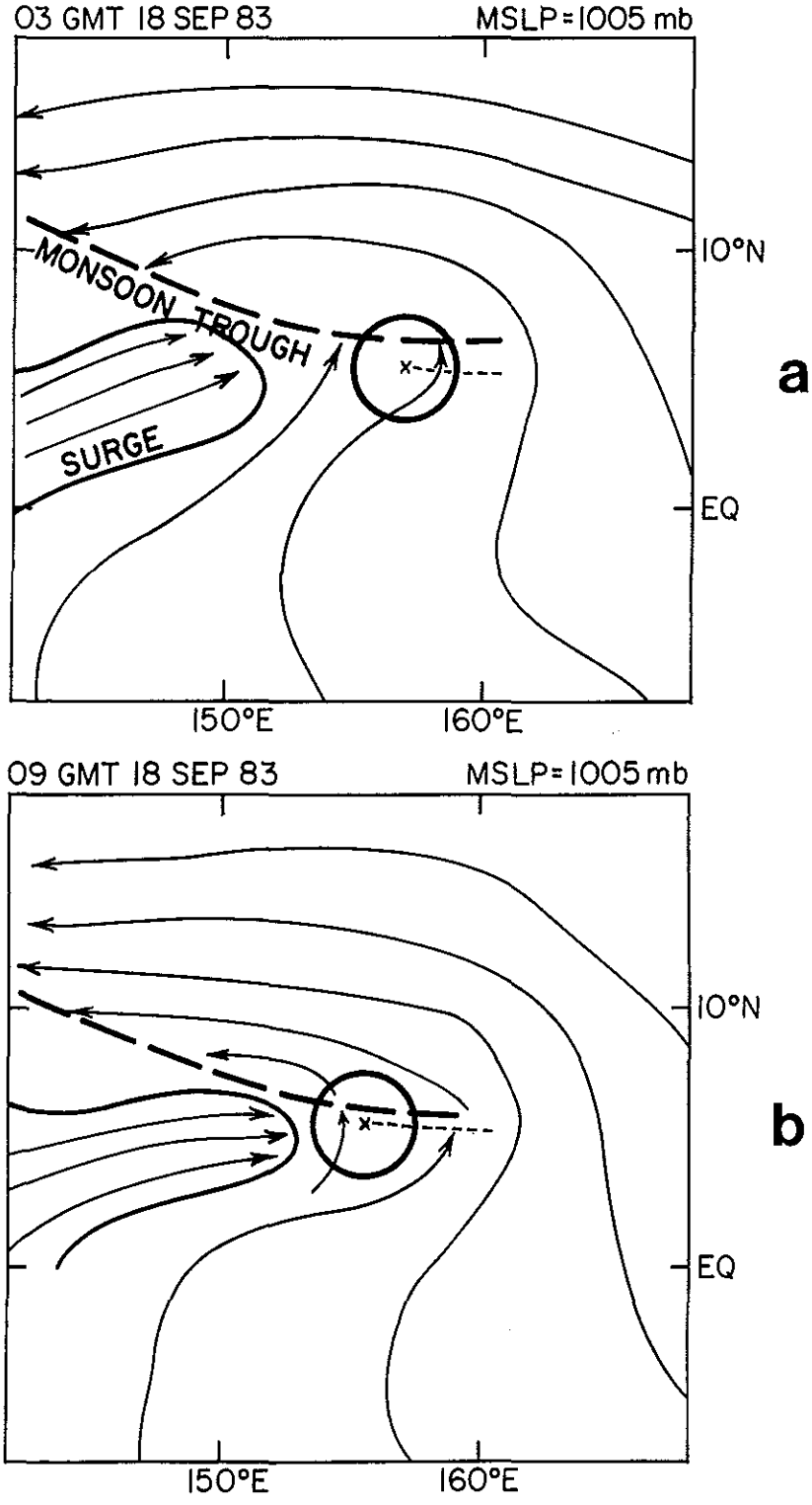

Figure 7.10: Six hourly sequence of 850 mb streamline analyses during Stage 1 of tropical cyclogenesis of Forrest, showing time evolution of the surge, the monsoon trough, the broadscale cyclonic circulation center location of the pre-Stage 1 disturbance (denoted by the 4° latitude diameter circle with an X at the center). The mesoscale vortex location is denoted by a ⊕. MSLP and Date/Time are indicated on each analysis.

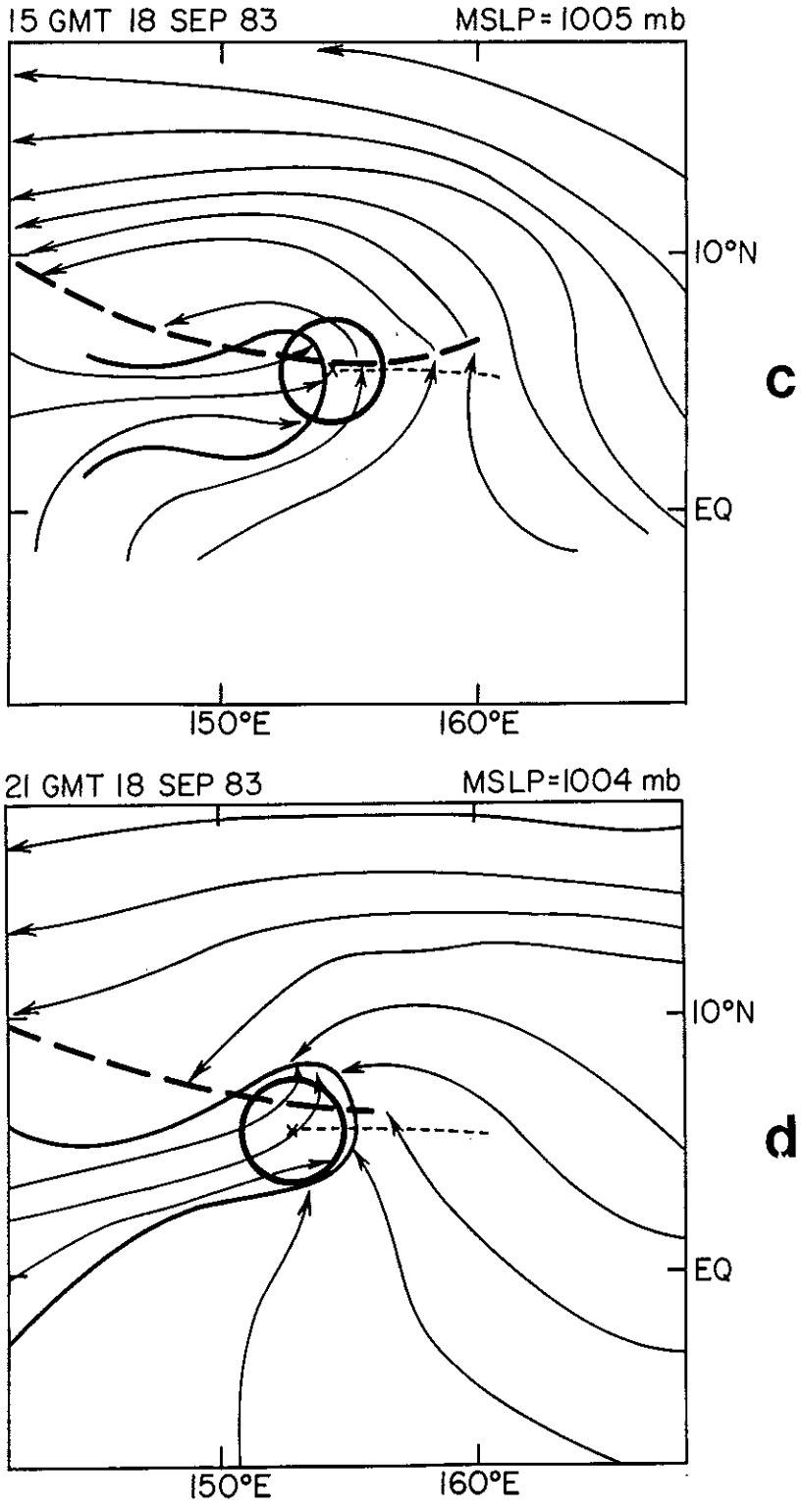

Figure 7.10: Continued.

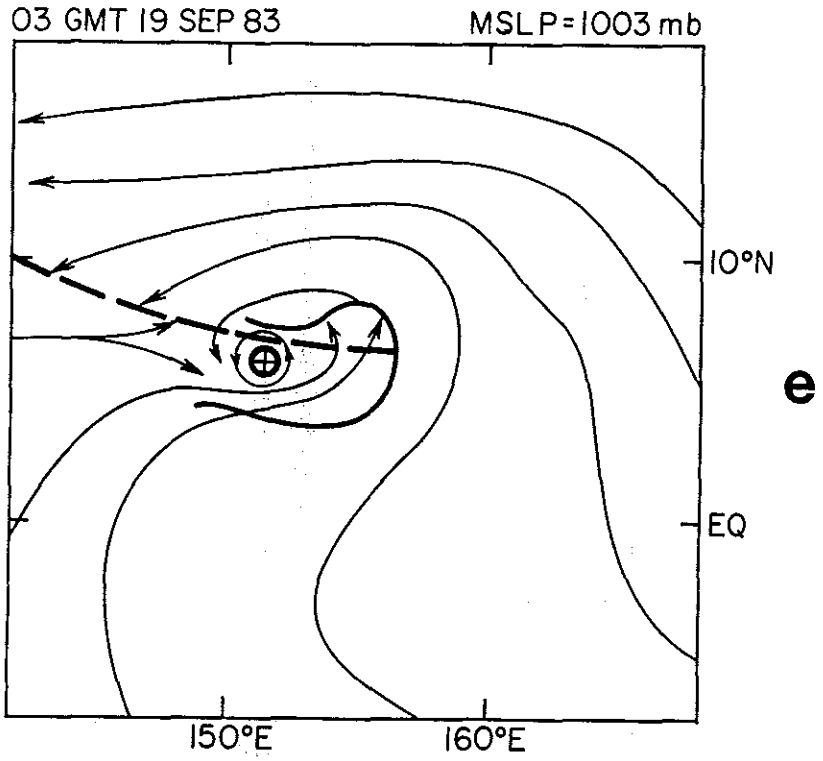

Figure 7.10: Continued.

evident. This is due to the initial mesoscale vortex which is depicted in the analysis in Fig. 7.10e.

Note that in addition to the disturbance convection there is also some deep convection associated with the surge (Fig. 7.11a). Therefore, the convective maximum appears to be the result of merging convective systems. Merging cloud clusters or merging mesoscale convective systems should be viewed as preferred regions for Stage 1 of tropical cyclogenesis. The analyses also include the MSLP at 6 hr intervals (Fig. 7.10). A MSLP decrease of only 2 mb is associated with Stage 1 of pre-Tropical Storm Forrest.

7.3.2 Forrest, Stage 2

Two days later on 20 September, the disturbance is embedded in a strong monsoon trough, but little or no decrease in MSLP has been observed. The aircraft reconnaissance center fix at about 00 GMT on the 20th found a MSLP of 1004 mb which is the same MSLP measured by the first reconnaissance flight on 18 September. However, in the next 24 hr, the MSLP dropped to 993 mb with an aircraft observation at about 00 GMT on the 21st. This initial significant drop of MSLP was accompanied by another surge from the west and enhanced deep convection as depicted in Figs. 7.12 and 7.13. Once again as with Stage 1, the effect of the surge is to greatly enhance the deep convection with the pre-tropical storm disturbance. New deep convection is located at the center of the disturbance circulation. The mesoscale vortex already exists having been initiated by the Stage 1 convective maximum. The important change which occurs with this Stage 2 surge is that the central pressure within mesoscale vortex begins falling, and very quickly results in a tropical cyclone of tropical storm intensity. Figure 7.12 includes the MSLP from three aircraft missions interpolated to the 6 hr analysis times. The disturbance is first designated a tropical storm at 18 GMT on 20 September, marking the end of the genesis period.

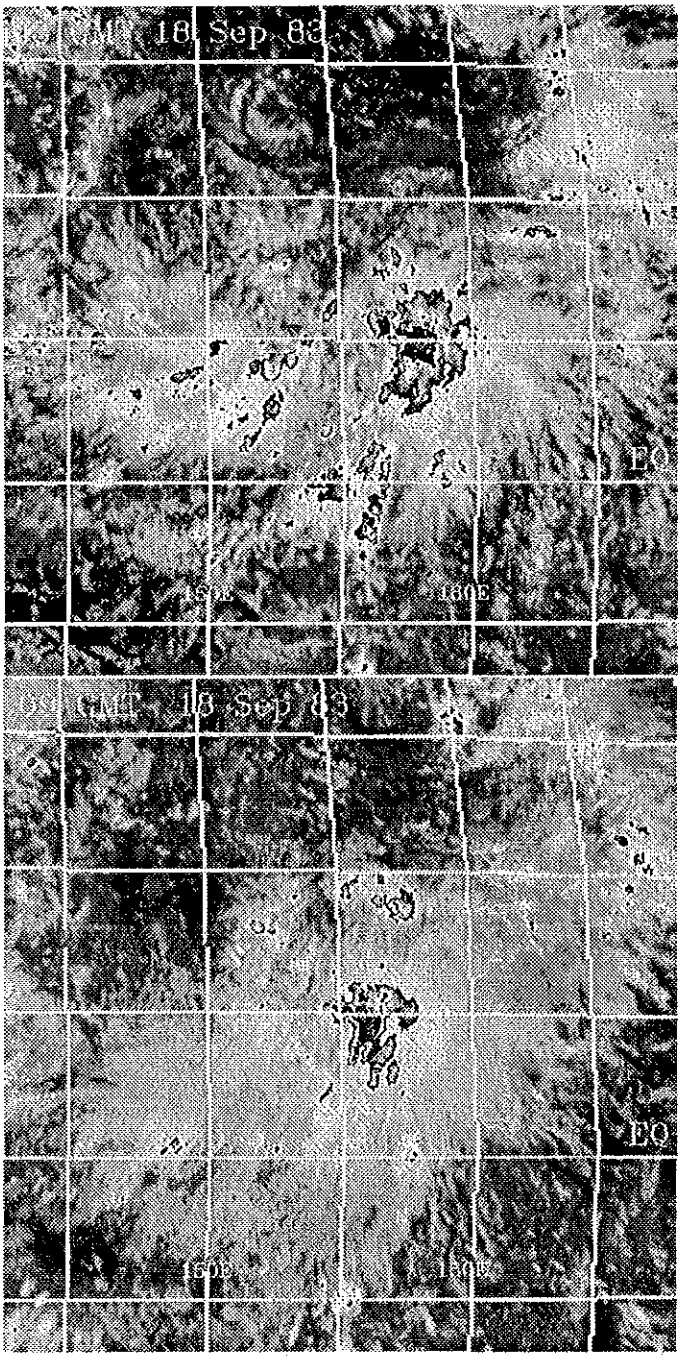

Figure 7.11: Six hourly sequence of enhanced IR images corresponding to Fig. 7.10.

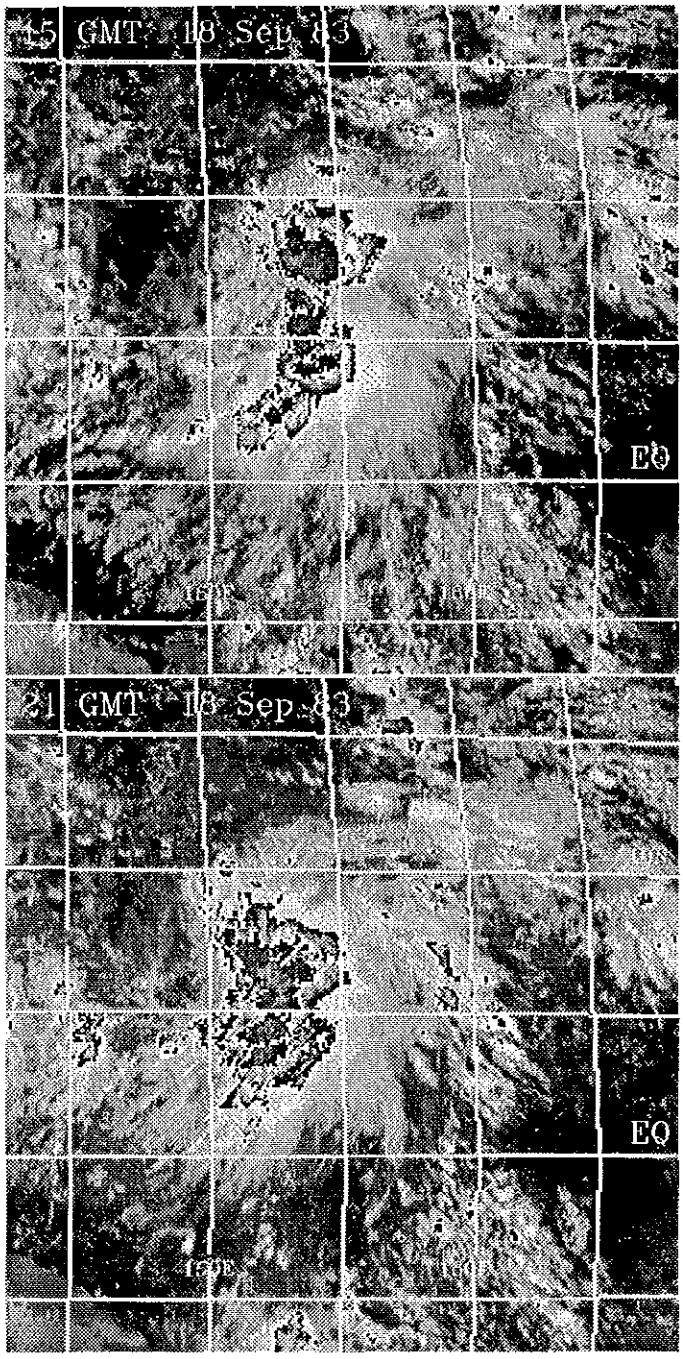

c

d

Figure 7.11: Continued.

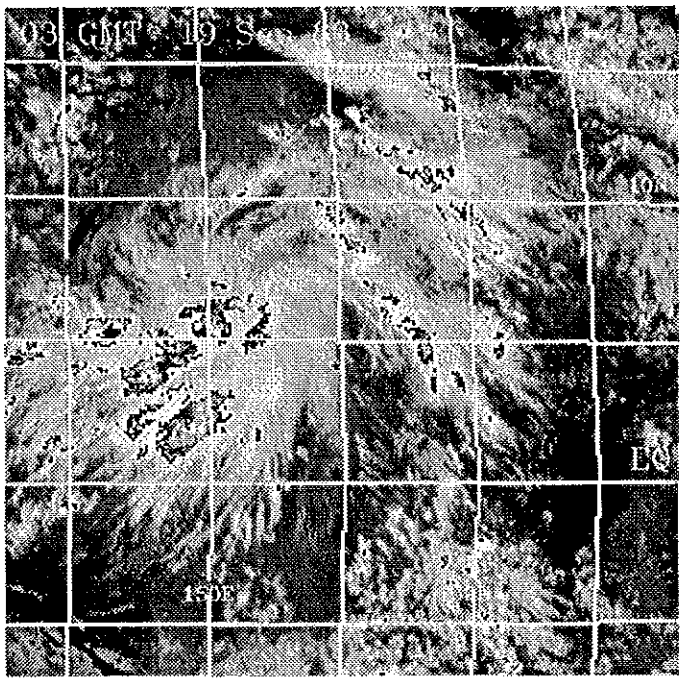

e

Figure 7.11: Continued.

7.3.3 Quantitative Combined Satellite-Aircraft Analysis

The aircraft reconnaissance data available during the genesis period of Typhoon Forrest was quite good. There were five flights in less than three days which included both Stage 1 and Stage 2. Observations about the circulation center were fairly well-distributed. This allowed the averages of the tangential wind and radial wind observations to be representative of the overall disturbance. The tangential winds are averaged as relative vorticity components ($2V_T/r$) for the 0-2° latitude radius circle. These quantities and the MSLP data are plotted in Fig. 7.14 with the R = 0–2, $T_B < -75$°C IR cloud areas. This quantitative assessment captures the same features described earlier. The maximum radial inflow is associated with each of the two surges, and also with a distinct convective maximum. Low-level relative vorticity increases are observed in response to both convective maxima. The MSLP decreases during Stage 2, but very little decrease occurs with Stage 1.

7.3.4 Summary

Tropical cyclogenesis occurs under a wide variety of synoptic-scale patterns as illustrated in Chapter 5. Therefore, detailed observational analyses will vary greatly among individual cases with regard to some aspects or features. The appearance of individual cyclogenesis cases in satellite images shows large variations. The observational data presented in this chapter are used to emphasize important features common to the majority of genesis cases. In addition, the data are presented in the framework of the conceptual model described in Chapter 4. Hopefully, this approach enhances the understanding of the cyclogenesis process.

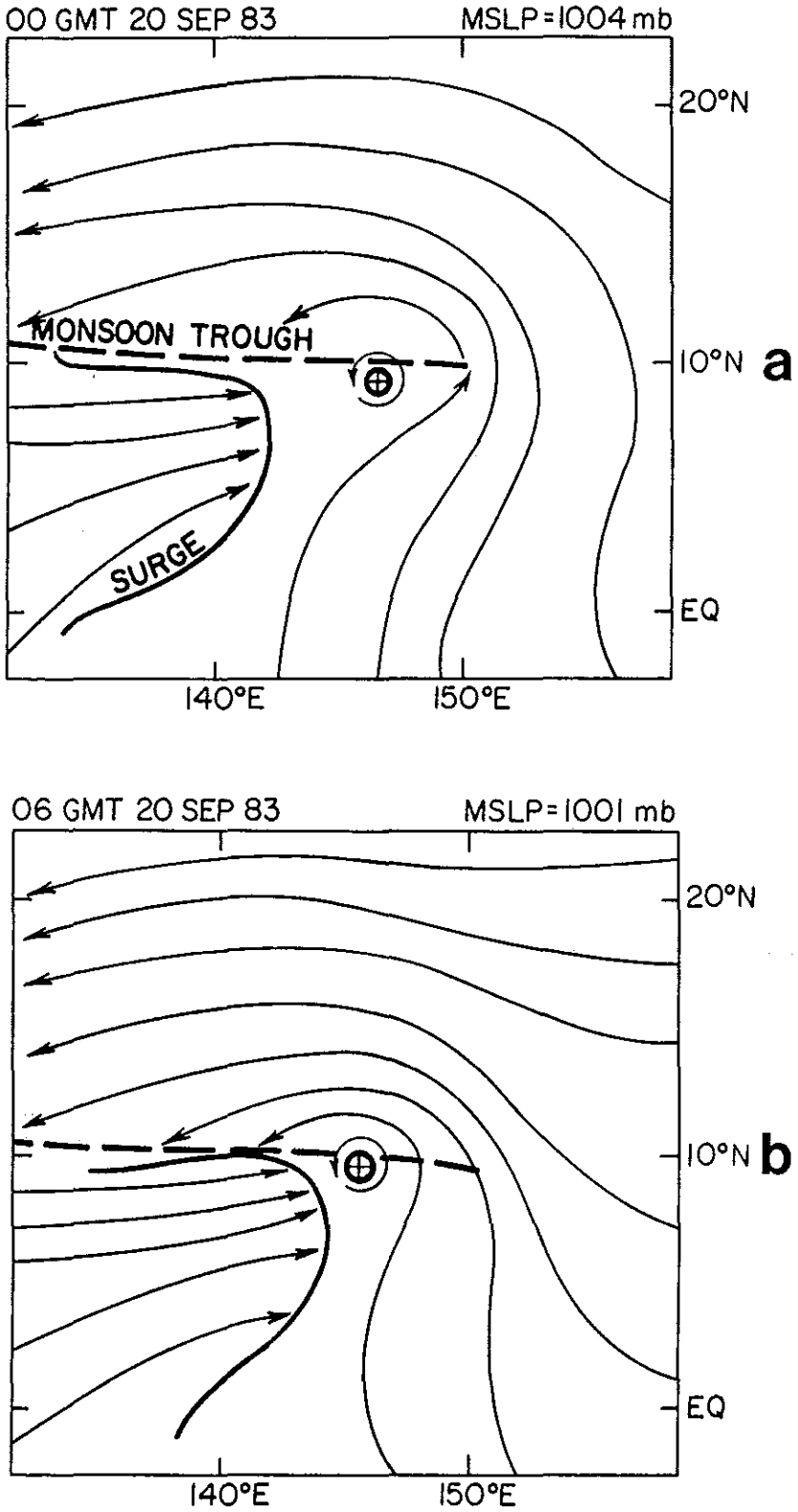

Figure 7.12: Same analysis as in Fig. 7.10, except time and area depicts Stage 2 of Forrest.

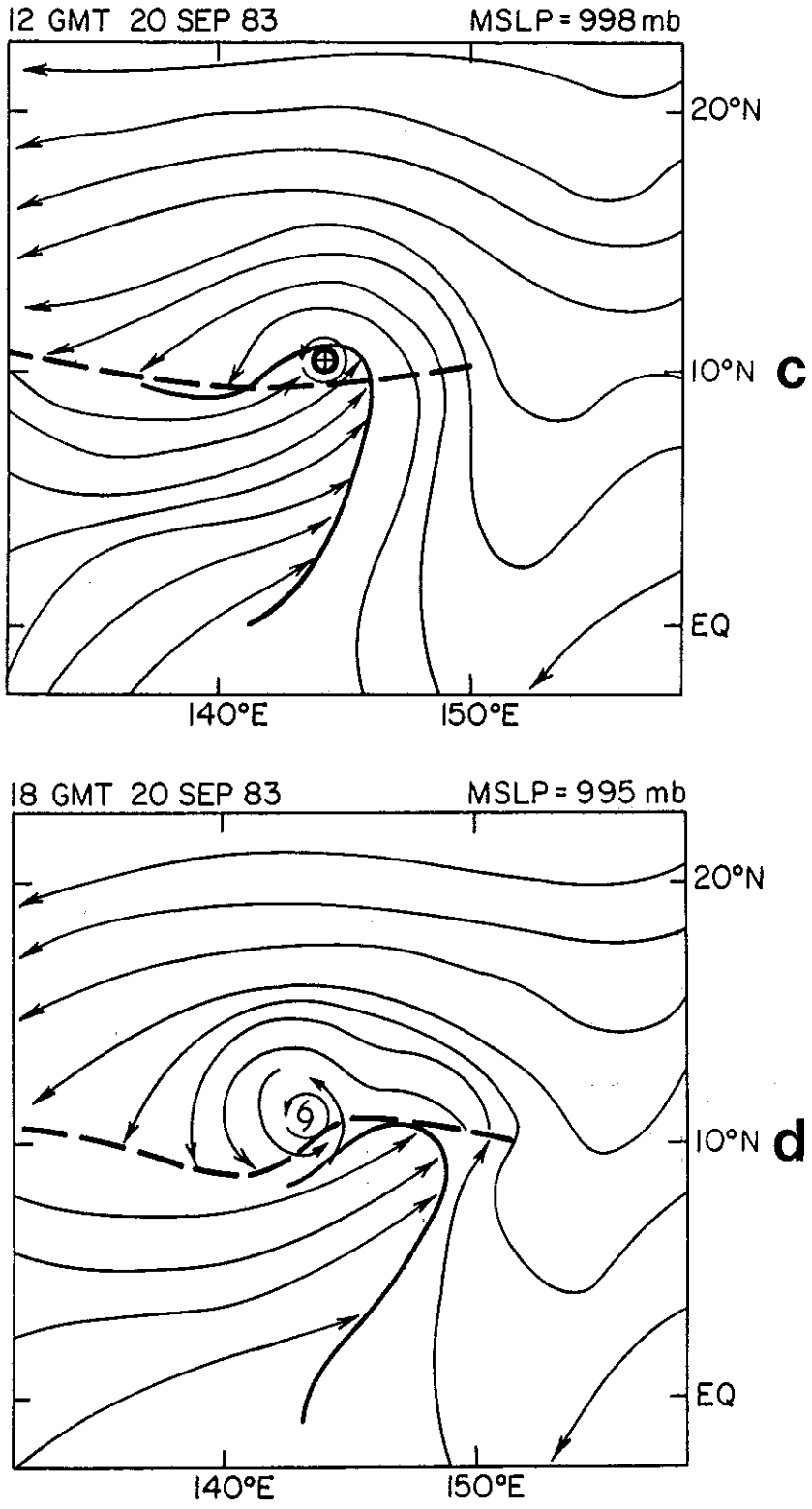

Figure 7.12: Continued.

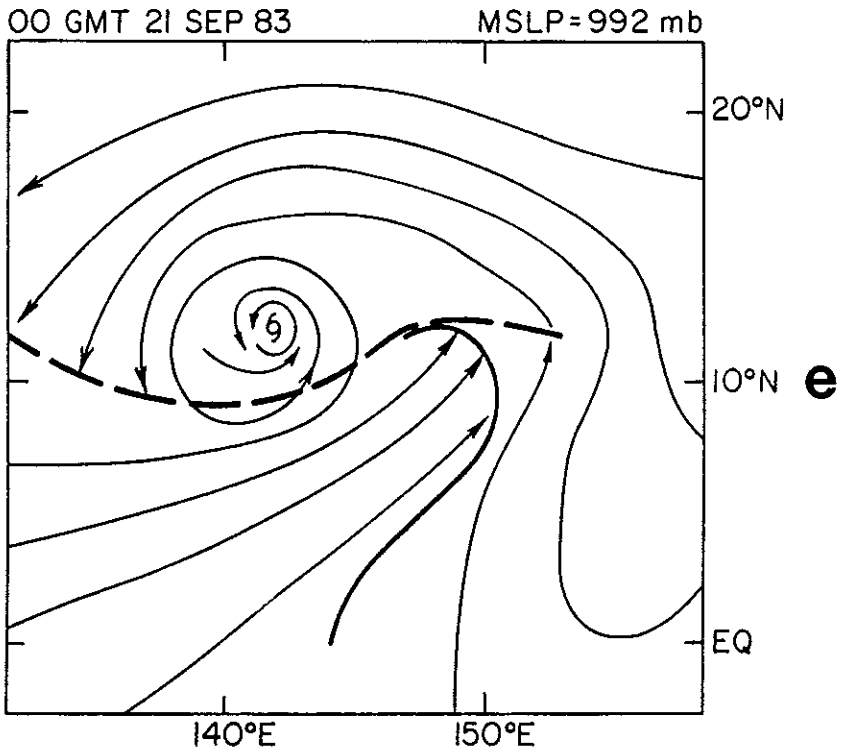

Figure 7.12: Continued.

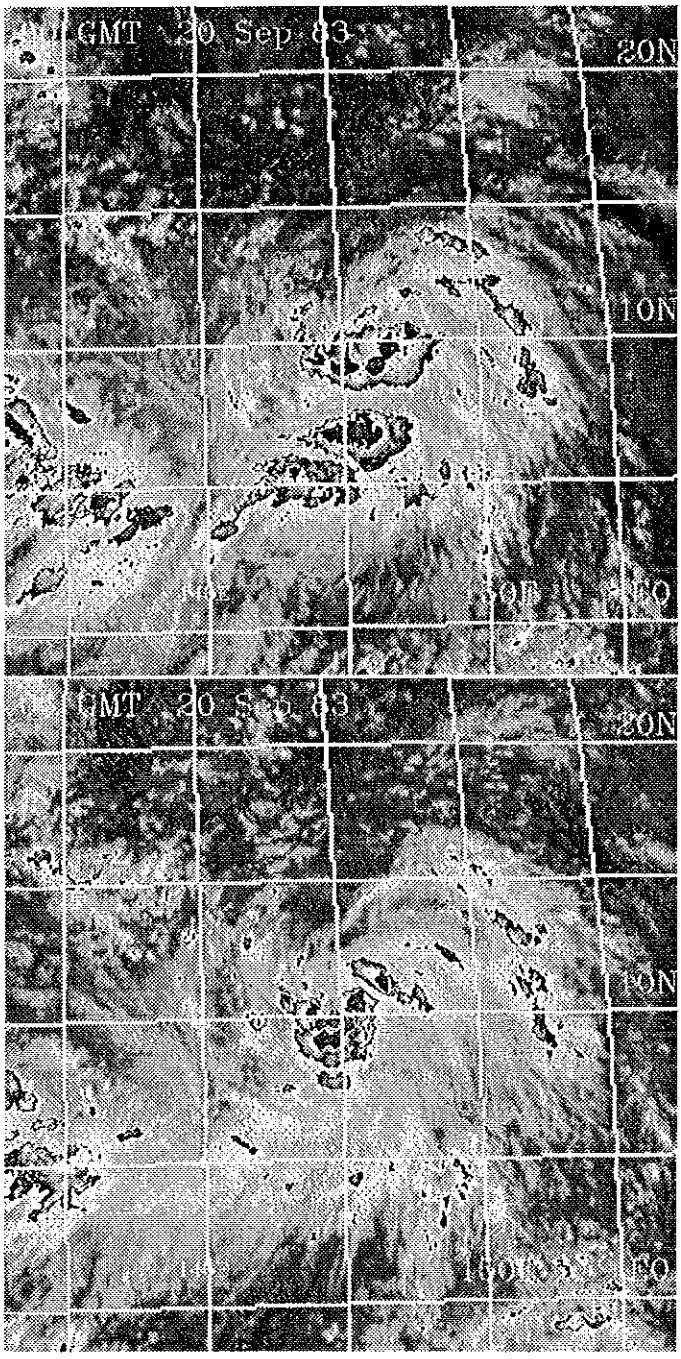

Figure 7.13: Six-hourly sequence of enhanced IR images corresponding to Fig. 7.12.

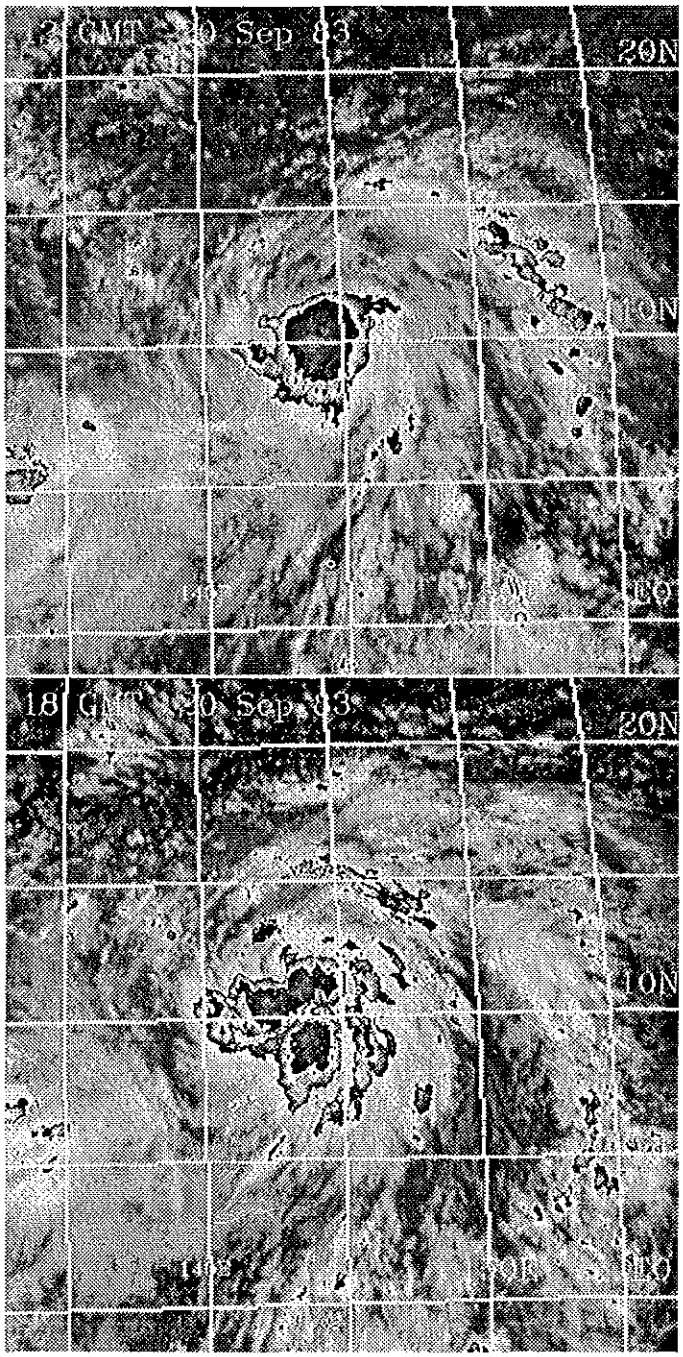

c

d

Figure 7.13: Continued.

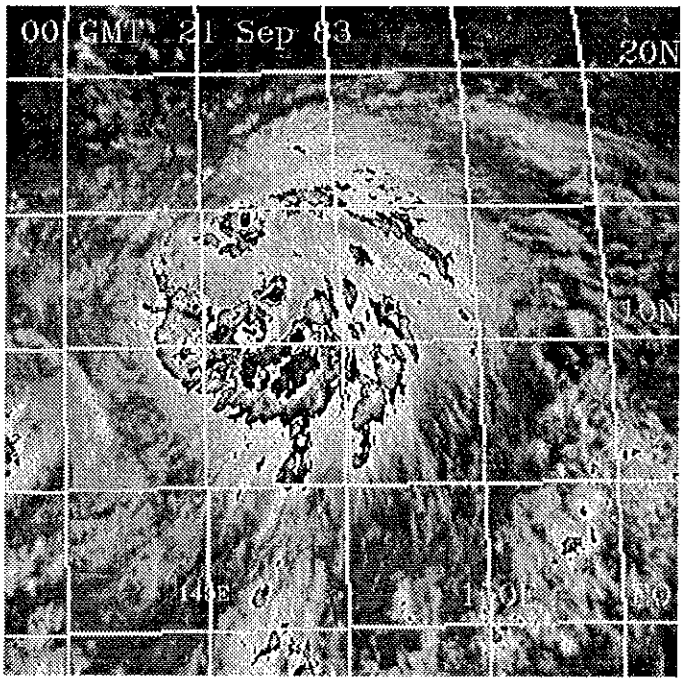

Figure 7.13: Continued.

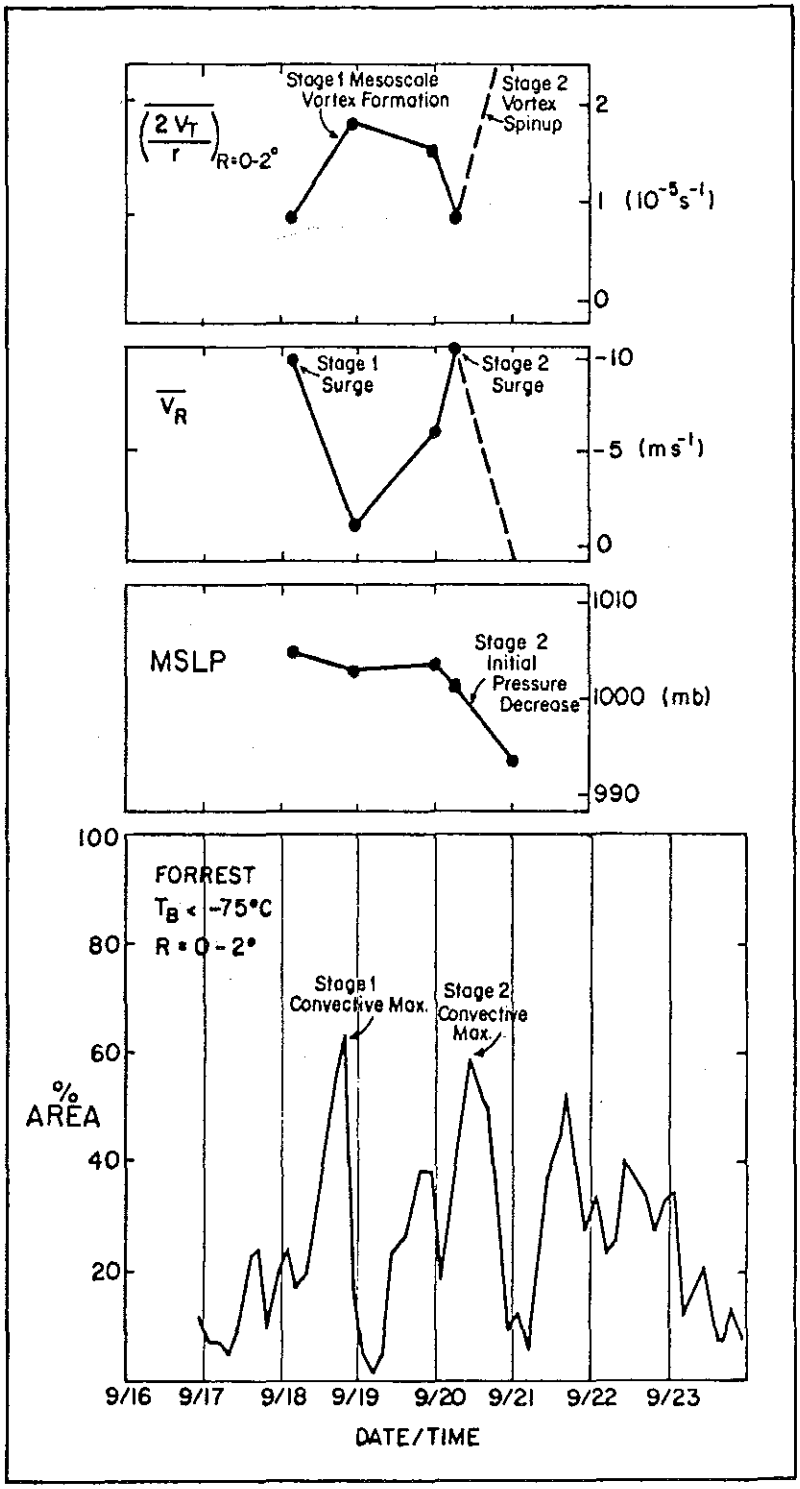

Figure 7.14: Quantitative satellite and aircraft derived parameters plotted on the same time scale during the cyclogenesis of Typhoon Forrest. Relative vorticity, mean radial wind, and MSLP are computed from each aircraft flight. R = 0-2, $T_B < -75°C$ areas are plotted from the IR satellite analysis. The dashed lines indicate that the quantities for the final aircraft flight were inferred, and not well measured, since all the observations were on one side of the center. The MSLP, however, is a valid observation.

Chapter 8

DISCUSSION

The purpose of this chapter is to assimilate the findings of the present study along with previous observational studies to describe a detailed conceptual model of tropical cyclogenesis. In addition, the observational evidence of various aspects of tropical cyclogenesis are discussed in a theoretical framework.

8.1 Detailed Conceptual Model

Minimum sea-level pressure (MSLP) and maximum sustained surface wind speed (V_{max}) are widely used to express tropical cyclone intensity. Those quantities and local relative vorticity maximum (VOR_{max}) are used here as the attributes to best describe both the non-developing and pre-tropical storm disturbance. VOR_{max} is a measure of the mesoscale vortex cyclonic circulation if one is present. Since the best direct measurements of this feature are from the aircraft observtions, the VOR_{max} quantities are applicable to the fight level of 1500 ft (457 m). However, this vortex likely extends vertically from the surface to the middle troposphere.

The conceptual model of MSLP and V_{max} changes during the genesis period (Fig. 4.3) are shown in Fig. 8.1 along with the VOR_{max} changes. Figure 8.2 depicts the conceptual model for the typical persistent non-developing disturbance. Time series of those three quantities (MSLP, V_{max}, VOR_{max}) differentiate the typical western North Pacific pre-tropical storm disturbance (Fig. 8.1) from the persistent non-developing disturbance (Fig. 8.2). Of course, the most important differences are shown by the quantities at the right hand side of Fig. 8.1. These are the attributes of a tropical cyclone when it is first designated a tropical storm. They are the end result of tropical cyclogenesis. V_{max} increases to 17.5 ms^{-1}. MSLP drops to 997 mb. Since environmental sea-level pressure (SLP_{outer}) may vary, this quantity should be expressed as ($\triangle P = SLP_{outer} - MSLP$). SLP_{outer} averages 1010 mb in the western North Pacific (Zehr, 1976). Therefore, $\triangle P$ increases to 13 mb for a minimal tropical storm. VOR_{max} increases from values of less than 5 x $10^{-5}s^{-1}$ to nearly 30 x $10^{-5}s^{-1}$. A mean tangential wind, $\bar{V}_T$, of 10 ms^{-1} at a radius, r, of 75 km are representative values for a minimal tropical storm (Middlebrooke, 1988), and have an associated relative vorticity of 27 x $10^{-5}s^{-1}$.

$$Vor_{max} = 2\bar{V}_T/r \approx 27\ x\ 10^{-5}s^{-1}$$

The non-developing disturbance, on the other hand, never attains this combination of the three quantities at any time during its lifetime (Fig. 8.2). Typical values of V_{max} are 7.5–12.5 ms^{-1}. MSLP ranges from about 1005 to 1009 mb ($\triangle P = 1-5\ mb$). VOR_{max} remains below 10 x $10^{-5}s^{-1}$ ($\bar{V}_T$ of 5 ms^{-1} at r = 100 km). Best estimates of average VOR_{max} for non-developing disturbances are about 2-3 x $10^{-5}s^{-1}$ (Middlebrooke, 1988).

The most significant change with Stage 1 is the increase of VOR_{max} while with Stage 2 it is the decrease of MSLP. However, some non-developing disturbances may attain VOR_{max} values of about 10 x $10^{-5}s^{-1}$, which are typical of Stage 1 pre-tropical storm disturbances. As discussed in Chapter 6, some non-developing disturbances may have undergone Stage 1 of genesis, and have an associated weak mesoscale vortex. However, such disturbances do not become tropical storms because Stage 2 of tropical cyclogenesis does not occur. This may sometimes happen because the disturbance makes landfall. In

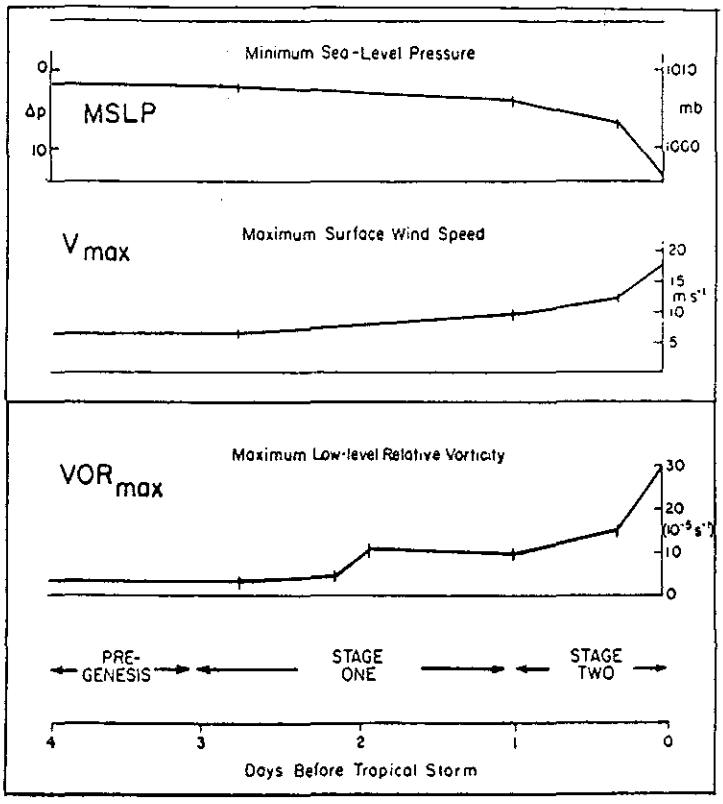

Figure 8.1: Conceptual model showing three attributes of a pre-tropical storm disturbance during cyclogenesis.

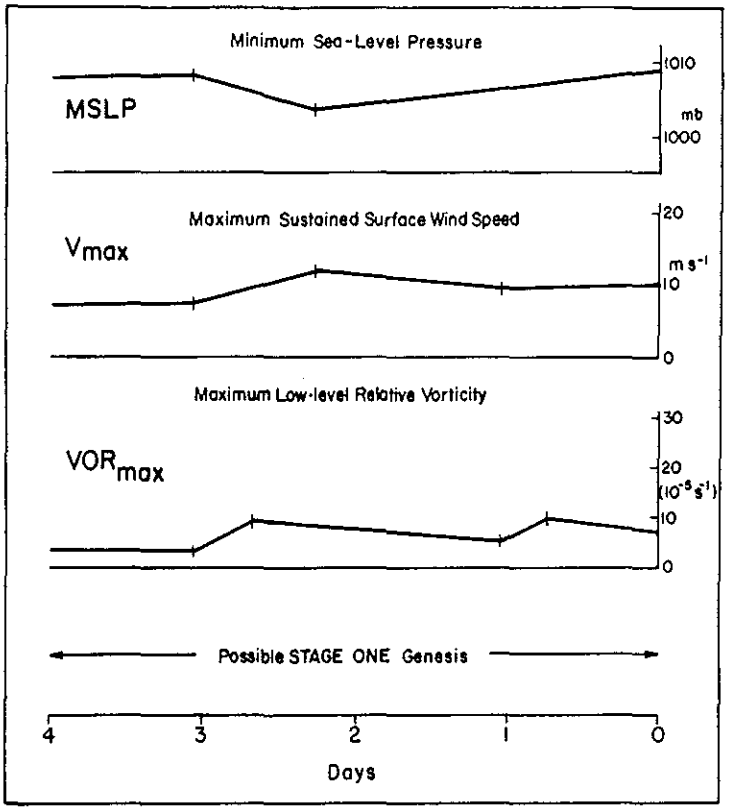

Figure 8.2: Conceptual model showing three attributes of a non-developing tropical disturbance.

addition, three other mechanisms are identified in Chapter 6 which may prevent a disturbance from undergoing Stage 2 of cyclogenesis. They are insufficient low-level vorticity, insufficient low-level convergence, and too much vertical wind shear.

Figure 8.3 is an expanded illustration of the tropical cyclogenesis conceptual model introduced in Chapter 4. In addition to deep convective clouds (CB), MSLP, and V_{max}, several other quantities have been added. They are VOR_{max} (from Fig. 8.1), mean low-level relative vorticity (VOR_{mean}), and mean low-level convergence ($-DIV_{mean}$). VOR_{mean} and $-DIV_{mean}$ represent average quantities over a 2° latitude radius area.

While VOR_{max} shows a substantial increase during Stage 1, the VOR_{mean} increase is much smaller. This is because the VOR_{max} increase is primarily due to a concentration of the cyclonic circulation rather than an increase in wind speed. The difference of VOR_{mean} between the pre-genesis and Stage 1 periods are due primarily to the synoptic-scale characteristic differences between non-developing and pre-tropical disturbances, as discussed in Chapter 6. The large VOR_{max} increase during Stage 1 is due to the formation of the initial mesoscale vortex which has only a small effect on VOR_{mean}.

VOR_{mean} shows a larger increase during Stage 2 from values of about 1-2 x $10^{-5}s^{-1}$ to 9 x $10^{-5}s^{-1}$. This is due primarily to an increase of the outer cyclonic circulation just prior to becoming a named storm. The inner mesoscale circulation also spins up during this period contributing to the increase of VOR_{mean}.

The mean low-level convergence ($-DIV_{mean}$) shows two sharp increases which coincide with the "surges" indicated in the plot of deep convective clouds. This occurs both during Stage 1 and again during Stage 2, typically about two days later. The enhanced low-level convergence is forced by environmental influences external to the disturbance itself. Such influences appear as maxima of inward radial wind, analyzed relative to the center of the disturbance and its motion (Lunney, 1988). They are referred to as surges and act to enhance the $-DIV_{mean}$. The temporarily enhanced low-level convergence is the

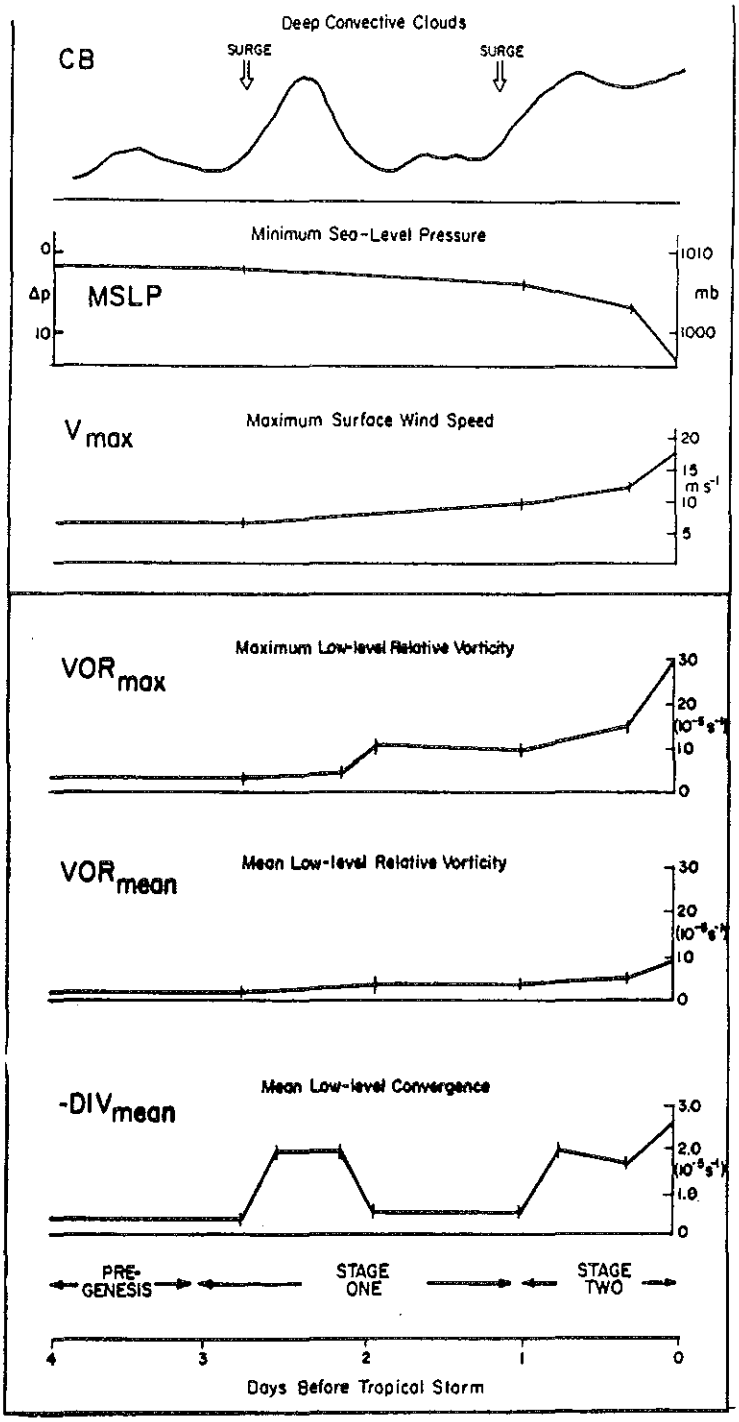

Figure 8.3: Depiction of changes of the important quantities of a pre-tropical storm disturbance according to detailed conceptual model of tropical cyclogenesis. CB represents a quantitative time-averaged satellite measurement of cold IR cloud area. VOR_{mean} and $-\mathrm{DIV}_{mean}$ are averages over a R = 0–2° latitude area.

forcing responsible for the convective maxima. The deep convection is essential in order for cyclogenesis to occur, however, it may only be required at key periods on time scales of less than 24 hr, to allow the important structural changes to take place. Substantial portions of the genesis period may be inactive with regard to deep convection located near the circulation center. The mean low-level convergence averaged over a 3-4 day period may be sufficient to maintain a persistent tropical disturbance, but it is likely inadequate in forcing deep convection of the magnitude needed for tropical cyclogenesis. Therefore, external forcing in the form of low-level wind surges is required both at Stage 1 for initial vortex formation and at Stage 2 for initial vortex deepening.

8.1.1 Summary

A conceptual model of the observable quantitative structural changes which take place during tropical cyclogenesis are presented in Fig. 8.3. This view of cyclogenesis has several unique features which distinguish it from previous explanations of genesis.

1. Rather than a gradual transition from a pre-existing disturbance to a tropical cyclone, cyclogenesis is described by two distinct phases or events (Stage 1 and Stage 2). Both are observed in association with enhanced intensity and areal coverage of deep convective clouds. They occur on a time scale of 6-24 hr and may be separated by variable time periods of up to several days, often characterized by inactive convective periods. An important structural change is noted with each of the two stages. During Stage 1, a mesoscale vortex is initiated, which is embedded within the pre-existing disturbance circulation. During Stage 2, the central pressure of that vortex decreases, and the tangential wind increases in response, resulting in a minimal tropical storm. This process is illustrated qualitatively in Fig. 8.4.

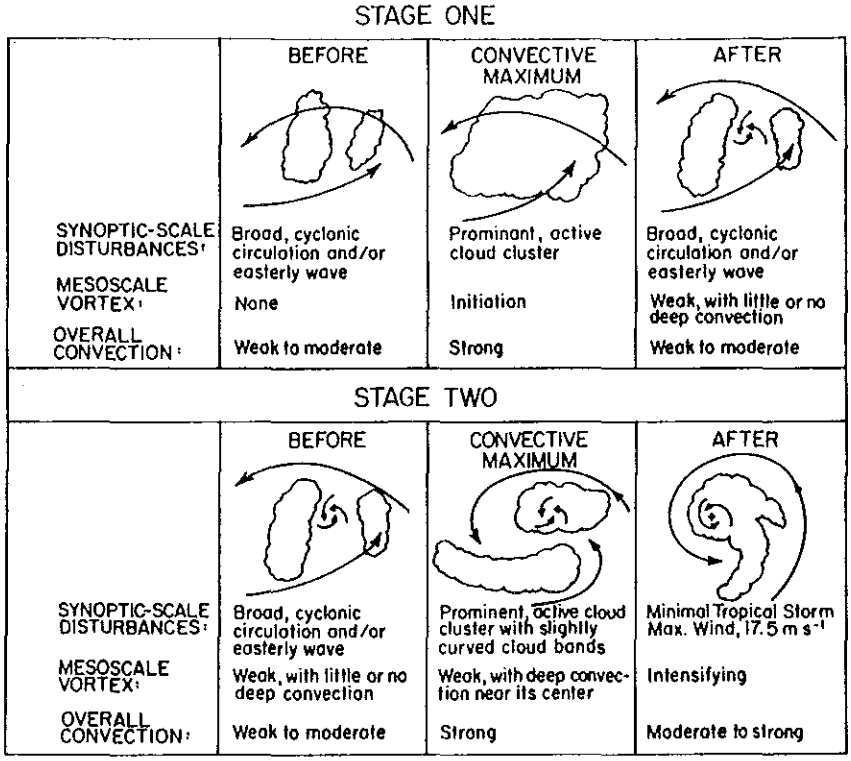

Figure 8.4: Conceptual model of tropical cyclogenesis with illustrations and descriptions of characteristics which are observable using satellite images.

2. The enhanced convection at both stages is forced by external low-level wind influences, referred to as surges.

3. In addition to having deep convection, three necessary conditions must be present in order for cyclogenesis to occur. 1) Vertical wind shear near the circulation center must be small. 2) Low-level vorticity associated with the pre-tropical storm disturbance must be sufficiently high. 3) Low-level convergence must be sufficient not only to maintain the disturbance, but also to provide the additional forcing required for the enhanced convection (No. 2 above). If any one of the three conditions are unfavorable, cyclogenesis will not proceed. The resultant weather system may persist as a non-developing tropical disturbance. If Stage 1 of tropical cyclogenesis has occurred and deep convective clouds are located near the circulation center, it may be designated a tropical depression. However, it does not become a named storm, unless Stage 2 of tropical cyclogenesis occurs.

The physical mechanisms which can theoretically induce tropical cyclogenesis as described by this conceptual model are discussed in the following sections. Two features require an physical explanation: the initial mesoscale vortex formation and the initial significant central pressure (MSLP) decrease.

8.2 Initial Mesoscale Vortex Formation

Mesoscale convective complexes (MCCs), which occur over the central U.S. Plains states during summer (Maddox, 1980), frequently produce mesoscale vortices which sometimes persist for several days (Johnston, 1981; Menard and Fritsch, 1989; Bartels and Maddox, 1991). These mesoscale convectively generated vortices (MCVs) appear qualitatively to be very similar to those observed with pre-tropical storm disturbances (Fig. 7.9). They are inertially stable, warm core vortices, which have their strongest cyclonic circulation at mid-levels (450–700 mb), but extend downward to near the surface (Menard and Fritsch, 1989).

They are initiated in the stratiform rain region of MCCs. This stratiform rain region is a feature of mesoscale convective systems which is also observed with tropical cloud clusters and tropical disturbances. The initiation of the MCV is accompanied by a distinct increase of the local relative vorticity maximum. The main vorticity source for this increase is the convergence of the ambient absolute vorticity (Chen, 1990). The same mechanism is hypothesized to induce the initial mesoscale vortex formation during tropical cyclogenesis (Frank, 1987).

In order for a mesoscale vortex to be initiated, large values of convergence and upward vertical motion must take place over a mesoscale area. These conditions are characteristic of the 6-12 hr active convective phase of a pre-tropical storm disturbance. The deep convection produces a 2-4° latitude diameter stratiform rain region which is supported by a mesoscale updraft and strong deep convergence layer. However, the conditions do not persist and are not representative of the overall disturbance vertical motion over a period of several days. This important point has also been demonstrated by Lee's (1989b) detailed angular momentum budget study using radiosonde composites of pre-tropical storm disturbances. Lee concludes that the mean transverse circulation is too small to produce the observed increase in tangential wind. This requires a large residual source of positive tangential momentum to balance the momentum budget. This large inward eddy vorticity flux is likely due to the early convective maximum (Stage 1) which accompanies initial mesoscale vortex formation. The associated convergence and vertical motion occur on small time and space scales, and thus contribute little to the mean transverse circulation.

Mesoscale vortex initiation requires an active convective phase, which is essential for cyclogenesis to proceed. This active convective phase is not something resulting from internal disturbance dynamics or instability, but rather a response to external forcing. A wide variety of low-level flow patterns and interactions between the disturbance and its environment may provide this forcing. It can often be recognized as a wind surge interacting with the disturbance which provides the enhanced low-level convergence to trigger the active convective phase.

8.2.1 Summary

The tropical cyclogenesis process begins with a very active mesoscale convective system embedded within a tropical disturbance. The associated convergence of ambient absolute vorticity is large enough to produce the local vorticity maximum at the center of an initial mesoscale vortex. This weak vortex persists when the active mesoscale convective phase dissipates. It is embedded within the larger cyclonic circulation of the tropical disturbance. Under favorable conditions, it may later become a tropical cyclone during a second phase of tropical cyclogenesis.

8.3 Initial MSLP Decrease

The second feature of tropical cyclogenesis which requires a theoretical explanation is the initial decrease of central pressure (MSLP). This pressure change is illustrated in Figs. 8.1 and 8.3 and occurs during Stage 2 of tropical cyclogenesis. Since it is very difficult to specify when cyclogenesis processes end and intensification processes begin, the exact magnitude of the MSLP decrease required for genesis, is uncertain. However, it is apparent that the MSLP decrease with Stage 1 is only about 1-3 mb, and another 8-10 mb of MSLP decrease is observed prior to initial tropical storm stage. It may be argued that intensification processes begin before initial tropical storm stage and are responsible for some of this pressure change. Nevertheless, some portion of this pressure decrease cannot be explained by intensification processes and thus is an important feature of cyclogenesis. The initial significant MSLP decrease is likely 3-8 mb occurring during a 6-24 hr period of Stage 2. What is the physical mechanism responsible for this small but critical pressure change?

Schubert *et al.* (1980) have shown that typically in the tropics the mass (pressure) field adjusts to the changes in the wind field. Only under specific conditions will deep convective clouds produce changes in the mass field (heating) which will persist and not be dissipated by gravity waves. A mature tropical cyclone is an example of one such condition. The very low central pressure in the eye is the hydrostatic effect of the deep warm column above. The warming in the eye is due to forced subsidence responding to the upward motion in the eye wall. The diabatic heat source is the latent heating of condensation within the clouds. This heating, in turn, cannot persist without surface flux of the latent energy of evaporation from the warm ocean surface.

Although the circulation and pressure gradients are much weaker during tropical cyclogenesis, the diabatic heat sources available to produce pressure changes are similar. An important consideration with regard to convective heating is inertial stability (Schubert and Hack, 1982). Inertial stability quantifies the atmospshere's resistance to horizontal accelerations. Through mass balance requirements, it is also related to vertical motions.

$$I = \left(f + \frac{\partial rv}{r\partial r}\right)\left(f + \frac{2v}{r}\right)$$

where

I = inertial stability
v = tangential wind component
r = radial distance
f = Coriolis parameter.

The distribution of inertial stability is comparable to the distribution of absolute vorticity. The heating efficiency is defined by Schubert and Hack (1982) as the ratio of local warming to the diabatic heating rate. Typically, in tropical disturbances the heating efficiency is quite low. The heating efficiency is shown to be largely determined by the distribution of inertial stability.

Therefore, the important dynamical consideration for Stage 2 of tropical cyclogenesis is to have a mesoscale convective system located coincident with a local vorticity maximum. Environmental forcing in the form of enhanced low-level convergence is necessary to induce another active convective phase similar to the Stage 1 convective maximum. However,

this time it must occur in the same location as the pre-existing mesoscale vortex. The local maximum of absolute vorticity (inertial stability) provided by the mesoscale vortex allows local warming to be realized. This results in the initial 3–8 mb MSLP decrease, characteristic of Stage 2 of cyclogenesis.

It is important to note that this vertical motion must occur coincident with the mesoscale vortex location. A mesoscale convective system might form in response to a surge, but the local vorticity maximum may not be located within the active mesoscale updraft region. When this happens, little or no MSLP decrease occurs and Stage 2 of tropical cyclogenesis fails. If the mesoscale vortex persists, the initial MSLP decrease may occur later with another active convective phase.

8.3.1 Summary

In order for the tropical cyclogenesis process to be completed, the pre-existing mesoscale vortex must become embedded within an active mesoscale convective system. This happens when environmental low-level forcing (a surge) enhances the low-level convergence in the immediate area of the mesoscale vortex. A mesoscale convective system forms and envelopes the pre–existing vortex. The high local vorticity with the mesoscale vortex allows the transverse circulation of the mesoscale convective system to produce the initial MSLP decrease. This marks the end of the tropical cyclogenesis process.

8.4 Role of Sea Surface Temperature, Thermodynamics, and Deep Convective Clouds

Sea-surface temperature (SST) has a very strong influence on whether or not tropical cyclones will form. This fact has been recognized and well understood for many years. July through September and October through December average SST maps are shown in Fig. 8.5. The tropical Pacific near Hawaii and eastward, and the tropical Atlantic along the African coast have SST's which are climatologically less than 26°C. These areas are generally free from tropical cyclone formation. Since anomalies from the climatological mean do occur and genesis takes place in some areas which are near the mean 26°C isotherm, SST distribution can be an important forecast tool on a day-to-day basis.

It is important to note in Fig. 8.5 that the western North Pacific region which includes all 50 of the cyclogenesis events of the present study lies entirely within the area that has climatological mean SST warmer than 26°C. In fact, within the study area during the 6-month tropical cyclone season, SST < 26°C is almost never observed. For this reason, SST influences cannot be considered as a factor to differentiate between western North Pacific non-developing and pre-tropical storm disturbances, and thus are not included in the present study.

Similar reasoning is applicable to the influences of thermodynamic vertical profiles on cyclogenesis. Previous studies have shown no systematic differences between the environmental vertical profiles of pressure, temperature and dew point between non-developing and pre-tropical storm disturbances (McBride, 1979; McBride and Zehr, 1981; Lee, 1986, Lee, 1989a). The importance of thermodynamic vertical profiles in understanding tropical cyclogenesis is simply in the atmosphere's ability to support deep convection, which is a necessary condition as detailed in the previous section.

The role of deep convection in tropical cyclogenesis has received much attention over the years. The CISK (Conditional Instability of the Second Kind) mechanism (Charney and Eliassen, 1964) has been the focus of many theoretical and numerical modeling studies (Ooyama, 1969, 1982). CISK refers to the growth of weak cyclonic disturbances resulting from low-level frictional convergence (Ekman pumping) which supplies ample water vapor necessary for the disturbance to sustain deep convective clouds. The feedback effects of those clouds induce vortex growth and intensification which further enhance convergence. This frictional convergence predominates the mass inflow of mature tropical cyclones and undoubtedly plays an important role in the maintenance and intensification of the tropical

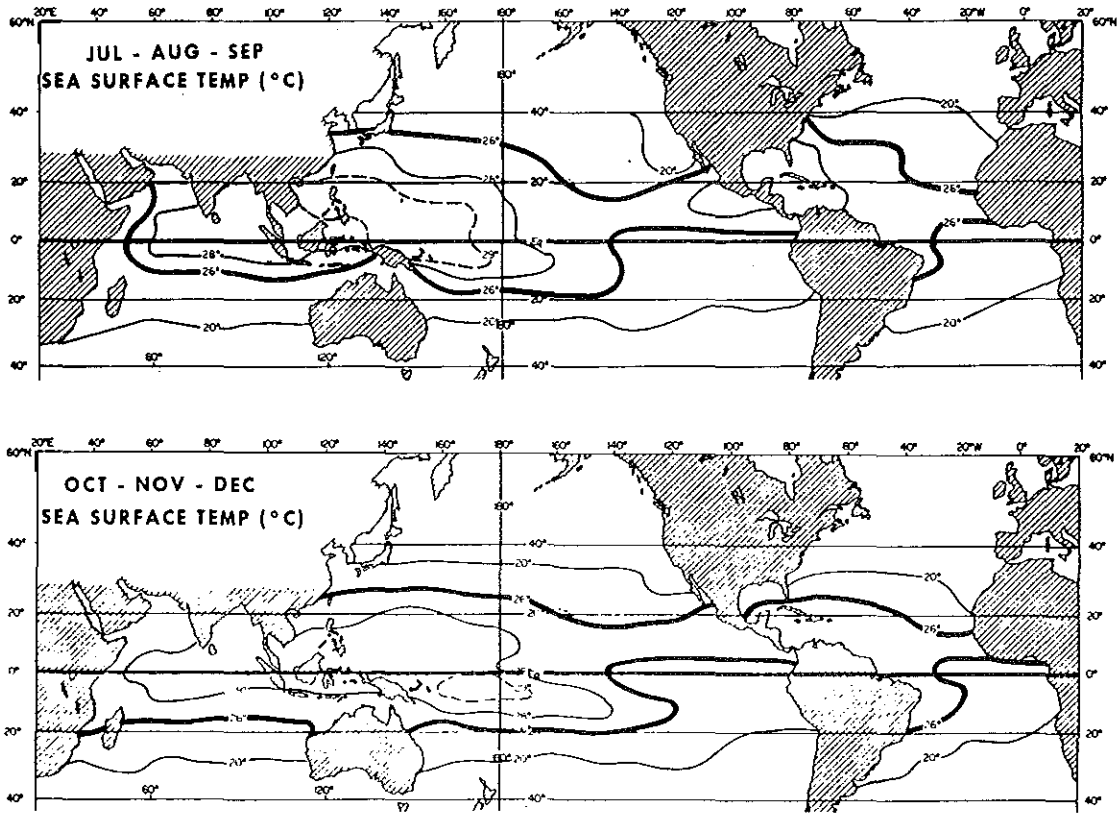

Figure 8.5: Global tropical analysis of SST (°C) from Gray (1975). a) Average for July through September. b) Average for October through December.

cyclone circulation. However, it has been shown that during the tropical cyclogenesis, most of the inflow occurs above the layer of frictional convergence (Gray, 1979; McBride, 1979; Chang, 1979; Lee, 1989a). The mean vertical velocities of pre–tropical storm disturbances do not appear to be strongly dependent on the relative vorticity in the boundary layer as prescribed by the CISK theory.

The role of deep convection in the new conceptual model of cyclogenesis presented in the previous section is quite different than the CISK approach. It is the large convergence and upward vertical motion associated with deep convection on mesoscale time and space scales which concentrate the distribution of vorticity within a pre-existing disturbance. This process acts initially to produce a mesoscale vortex during Stage 1, and later to spin up that vortex sufficiently during Stage 2 to produce a minimal tropical storm. In addition, the deep convection is not forced by the internal dynamics of the pre-existing disturbance, but by external environmental forcing. This external forcing has the effect of increasing the low-level convergence which in turn enhances the deep convection. This influence on cyclogenesis is discussed in the next section.

8.5 Role of Low–Level Convergence and Surges

Synoptic-scale low-level convergence in the tropics is typically very small. The importance of this convergence lies in its ability to initiate deep convective clouds. Cumulonimbus clouds are often observed over warm tropical oceans and they are readily initiated by small localized low-level convergence. However, cumulonimbus clouds within persistent active convective areas such as those characteristic of tropical disturbances are maintained by synoptic-scale low-level convergence. The pre-tropical storm disturbance is further characterized by even stronger low-level convergence. This is partly due to the influence of surges as they interact with the disturbance. The surge interactions likely also occur at times with non-developing disturbances. However, they occur less often, and are distinctly weaker overall, when compared with pre-tropical storm disturbances.

The role of low-level convergence in the conceptual model of tropical cyclogenesis has already been discussed in Sections 8.2 and 8.3. Its importance lies in determining when and where deep convection will occur. Momentum and pressure distributions over a wide range of space and time scales produce very complex and changeable patterns of divergence and vertical motion, particularly in active convective areas. With conventional wind observations which include satellite cloud drift winds, synoptic-scale convergence is difficult to measure accurately and the smaller scales may be impossible to measure. The distribution and intensity of the deep convective clouds from the satellite images provide an independent qualitative assessment of low-level convergence.

Although unanswered questions remain about the role of low-level convergence, the observational evidence of the present study and conclusions from previous studies indicate that low-level convergence is an important forcing mechanism for tropical cyclogenesis. On the other hand, the non–developing disturbances' failure to undergo cyclogenesis may likely often be attributed to insufficient low-level convergence.

8.6 Role of Synoptic–Scale Low–Level Vorticity

Its role as the vorticity source for the VOR_{max} increases shown in Fig. 8.1 has already been discussed in sections 8.2 and 8.3. It is well known that the area near the equator is free of tropical cyclone formation. This is undoubtedly due to the low absolute vorticity ($\zeta + f$) environment, since f = 0 at the equator. The typical range of low-level synoptic-scale relative vorticity in the primary genesis region is about –2.5 to 2.5 x $10^{-5}s^{-1}$. The Coriolis parameter, f, ranges from 1.27 x $10^{-5}s^{-1}$ at 5°N to 4.97 x $10^{-5}s^{-1}$ at 20°N. Therefore, typical absolute vorticity values range from about –1.0 to 7.5 x $10^{-5}s^{-1}$. This quantity is the source of the local vorticity increases observed with mesoscale vortex formations and its initial spin-up. There is likely a threshold value for absolute vorticity which is necessary for cyclogenesis to proceed. This threshold is difficult to quantify, and it may

be different for Stage 1 and Stage 2 of genesis. The results from Chapter 6 indicate that a large percentage of non-developing cases have 850 mb relative vorticity of less than 1.0 x $10^{-5}s^{-1}$, while most of the pre-tropical storm disturbances have values greater than 1.0 x $10^{-5}s^{-1}$. Using this value and assuming an average f of 2.5 x $10^{-5}s^{-1}$, one obtains a threshold of 3.5 x $10^{-5}s^{-1}$ for absolute vorticity, as rough estimate of a minimum value associated with tropical cyclogenesis.

Another aspect of the role of low-level vorticity is the maintenance of the disturbance outer cyclonic circulation. This is important not only as a vorticity source for the mesoscale vortex, but also provides the favorable environment for deep convection. The synoptic-scale low-level vorticity of the disturbance is due to this outer circulation. It must be maintained against dissipative forces.

Weak disturbances with small (< 1.0 x $10^{-5}s^{-1}$) associated low-level relative vorticity are less likely to undergo cyclogenesis than the stronger ones. In addition, disturbances which are moving into an environment with negative low-level relative vorticity are less likely to undergo cyclogenesis than those moving into a positive relative vorticity area. For example, a disturbance propagating through the anticyclonic curved flow associated with the subtropical ridge, still has associated positive relative vorticity but is moving through a hostile environment with regard to vorticity. On the other hand, a disturbance embedded within the monsoon trough is in a more favorable environment and the dissipative forces on its outer circulation are greatly reduced.

Several unanswered questions concerning the role of vorticity have yet to be addressed. For example, what portions of the large vorticity differences between ND and PS disturbances are due to:

1. the strength of the cyclonic outer circulation of the disturbance itself?
2. the environmental vorticity of the surrounding region in which the disturbance is located?
3. the spin-up of the disturbance circulation from the enhanced convergence due to interactions with surges?

It is very difficult to separate the roles of each of these mechanisms. It is likely that all of them are important to some extent.

Another question involves the role of mid-level vorticity (400–700 mb). Are the vorticity differences observed in the low levels (700–950 mb) also observed similarly in the mid-levels? Or, are there sometimes significant differences between the two layers?

Despite the unanswered questions, the low-level relative vorticity is clearly of critical importance to tropical cyclogenesis. Tropical cyclogenesis will not proceed with disturbances that are deficient in low-level synoptic-scale vorticity.

8.7 Role of Vertical Wind Shear

The unfavorable influence of large vertical wind shear on tropical cyclogenesis is rather straightforward. Even a minimal tropical storm has a nearly vertical deep tropospheric structure which depends on the hydrostatic influence of the upper warm core to maintain the lower level circulation. A decoupling of this structure by environmental vertical wind shear influences will undoubtedly prevent tropical cyclogenesis.

With the present study, only very small differences are noted in the mean vector wind shear speed between the ND and PS data sets. This indicates that persistent non-developing tropical disturbances during the western North Pacific tropical cyclone season are typically found in low wind shear environments. Perhaps in other ocean basins, non-developing disturbances may persist with relatively high vertical wind shear but it happens infrequently in the western North Pacific. Nevertheless, despite the small differences in the mean shear values, several individual non-developing disturbances (Fig. 6.5) did have relatively high vertical wind shear at least for short periods. Since the low-level

convergence and vorticity values were also quite high during those periods, the vertical shear appears have inhibited genesis for a few time periods with a few non-developing cases.

It can be concluded that small vertical wind shear of the order of about 12.5 ms^{-1} or less in the 200–850 mb layer is a necessary condition for cyclogenesis. However, it may not be as important as low-level vorticity or convergence in differentiating between individual cases of genesis versus non-genesis. This is because tropical disturbances seldom persist for more than two days in a high vertical shear environment.

An unanswered question involves specification of the layer of vertical wind shear which is most directly influential on genesis. The 200–850 mb layer is chosen for the present study primarily because the additional satellite wind observations are typically assigned to those pressure levels. Perhaps the objective analysis scheme and observed winds are such that the exact levels chosen to measure vertical wind shear are not particularly important. On the other hand, is it possible that the cyclogenesis process is effected more by the environmental vertical shear vector computed from other layers (e.g., 300–850 mb, 500–900 mb, 300–700 mb)? This question remains unresolved and requires extensive additional research with high quality data sets.

Vertical wind shear information is unquestionably useful for eliminating large areas from consideration as cyclogenesis areas (see Chapter 6). However, in the western North Pacific, the average persistent, non-developing disturbance is characterized by vertical shear speeds which are about the same as the pre-tropical storm disturbances. Therefore, vertical shear is not as important a factor as low-level convergence and vorticity in differentiating between non-developing and pre-tropical storm disturbances.

8.8 Upper-level Flow Patterns

Recent studies conclude that tropical cyclogenesis may partly be forced by upper-level environmental influences (Challa and Pfeffer, 1990; Molinari and Vollaro, 1989; and Davidson, *et al.*, 1990). The eddy flux convergences of angular momentum, which include both divergence and vorticity influences at upper levels, are considered by those studies to be important genesis mechanisms. As previously discussed with regard to the influence of the TUTT and the importance of the CISK mechanism, upper-level forcing may be important in tropical cyclone intensification. However, there is not sufficient observational evidence with the present study to include upper-level influences as primary forcing mechanisms on tropical cyclogenesis.

Upper-level divergence appears to occur mostly in response to low-level convergence and to active convective areas, rather than vice-versa. The synoptic analysis of 200 mb flow characteristics in Chapter 5, the detailed case studies, and the 200 mb divergence analyses in Chapter 6, all suggest that the divergence plays a passive role in cyclogenesis. The important differences in low-level convergence between non-developing and pre-tropical storm disturbances are also reflected in the upper-level divergence (section 6.6). However, the percentage differences are smaller and the standard deviations are larger.

Upper-level relative vorticity tends to be negative for both non-developing and pre-typhoon disturbances. Previous radiosonde composites (McBride and Zehr, 1981; Lee, 1989) all show greater negative tangential wind at upper levels with pre-tropical storm disturbances compared with non-developing disturbances. However, those differences are primarily at outer radii and show up better in the later stages.

The upper level relative vorticity associated with both non-developing and pre-tropical storm disturbances is highly variable on a case-by-case basis. Based on the results of section 6.7 and the TUTT analysis of the present study, upper-level vorticity differences do not appear to play an important role in cyclogenesis.

In summary, the results of the present study support the conclusion that upper-level wind patterns do not take an active role as a forcing function on cyclogenesis. They may have a negative effect if they contribute to high vertical wind shear. They are also related to the important lower tropospheric factors since they may be linked through vertical

motion and deep transverse circulations. Also, it should be emphasized that upper level influences may be important in the process of intensification.

Chapter 9

CONCLUDING REMARKS

One of the goals of this study is to assimilate all available observational data for a large number of individual cases, to arrive at the best possible description of the tropical cyclogenesis process. That description is given here.

Tropical cyclogenesis occurs when low-level convergence larger than that necessary to maintain a persistent tropical disturbance acts to enhance deep convection. If the associated synoptic-scale vorticity is large enough and the vertical wind shear is small enough, Stage 1 of tropical cyclogenesis will occur. The initial formation of a mesoscale vortex occurs with Stage 1. During Stage 2, typically 2-3 days later, the pre-tropical storm disturbance once again experiences low-level forcing such that enhanced deep convection is located coincident with the local low-level vorticity maximum. With sufficiently favorable low-level vorticity and wind shear influences, the minimum sea-level pressure decreases to a level at which the surface winds will begin to respond to the pressure gradient. Soon after this happens, a minimal tropical storm ($V_{max} > 17.5$ ms^{-1}) exists and tropical cyclogenesis is complete. At both stages, the low-level forcing is external to the disturbance itself, often appearing as an interaction with an environmental wind surge.

Some additional noteworthy findings are:

1. Tropical cyclogenesis occurs in two distinct stages. It is not a gradual process, but rather more of an impulsive process. In the first stage, the low-level local vorticity maximum increases, while in the second stage the minimum sea-level pressure decreases. Those are the most significant changes which occur with sufficient magnitudes for a tropical cyclone to form and attain minimal tropical storm intensity. They occur on mesoscale time and space scales. However, they are embedded within an outer cyclonic circulation, which has synoptic-scale attributes.

2. The satellite imagery is essential to quantitatively and qualitatively assessing and evaluating the ongoing cyclogenesis process. A distinct early convective maximum can usually be identified with Stage 1 of genesis. A mesoscale vortex circulation which becomes enveloped within an active mesoscale convective system characterizes Stage 2 of genesis. These features can usually be observed in satellite images.

3. Tropical cyclogenesis occurs with a wide variety of synoptic-scale patterns. A complete two-year synoptic climatology in the western North Pacific provides the basis to identify certain patterns as typical or as rare events. Most of the cases are associated with monsoon trough.

4. A quantitative objective approach using 2.5° resolution objective analyses of conventional data can be used to differentiate individual pre-tropical storm disturbances from non-developing disturbances with a reasonable degree of success. The non-developing disturbances can be further characterized by one or more of three physical mechanisms which act to prevent tropical cyclogenesis. They are insufficient low-level vorticity, insufficient low-level convergence, and too much vertical wind shear.

ACKNOWLEDGEMENTS

The author wishes to thank Dr. William M. Gray for his support and encouragement in pursuing research on this topic over many years. The author's M.S. research in 1974–1976 was conducted under Dr. Gray's direction on the same research topic. NOAA/NESDIS Satellite Applications Laboratory and the Regional and Mesoscale Meteorology Branch directed by Mr. Donald Miller and Dr. James Purdom, respectively are acknowledged for their support. This research project could not have been completed without the financial support and data sources of Dr. Gray's project and NOAA/NESDIS.

Excellent computer programming expertise was contributed primarily by Debra Lubich, CIRA; and Bill Thorson, CSU. Additional computer programming and data processing was provided by Todd Massey, Sheila Long, Amie Hedstrom, Bob Gray, and Dale Reinke.

The experience and competence of Barbara Brumit in manuscript preparation is greatly appreciated. Assistance in preparation of manuscript was provided by Laneigh Walters and Debbie Eckdahl.

The high quality of figures is mostly attributed to the excellent work of Judy Sorbie-Dunn, who drafted most of the figures, which also included "touch up" work on some of the computer plots.

The Cooperative Institute for Research in the Atmosphere (CIRA), directed by Dr. Thomas VonderHaar, is acknowledged for the excellent computer facilities and software available for satellite image processing and display. Nan McClurg, Shazi Naqvi, Garrett Campbell, among many others, provided assistance in satellite analysis.

The satellite data were made available by NOAA/NESDIS Satellite Data Services Division and the International Satellite Cloud Climatology Project (ISCCP).

The 1984 objective analysis data was obtained from Australia Bureau of Meteorology Research Centre (BMRC). This data set and the aircraft data was contributed by Dr. William M. Gray's project.

The persons who aided this research through scientific discussions are far too numerous to mention. Some of the more valuable discussions took place with Vern Dvorak, Vince Oliver, Lt. Col. Chip Guard, Bill Frank, John McBride, Bob Merrill, Greg Holland, Cheng-Shang Lee, Mike Fritsch, Shuyi Chen, Pat Lunney, Mike Middlebrooke, Roger Edson, Greg Tripoli, and Ray McAnely. The most valuable source for scientific discussion, of course, was Bill Gray.

The author's Ph.D. committee members are thanked for their manuscript review and helpful comments: Dr. William M. Gray, Dr. Stephen Cox, Dr. Peter Sinclair, and Dr. John Stednick. Additional reviews were provided by Dr. James Purdom and Dr. William Frank (Penn State).

NOAA Grant NA85RAH05045 provided additional financial support for this research.

REFERENCES

Alaka, M. A., 1962: On the occurrence of dynamic instability in incipient and developing hurricanes. *Mon. Wea. Rev.*, 90, 49–58.

Allison, L. J. and G. Warnecke, 1966: Synoptic interpretation of TIROS III radiation data recorded on 16 July, 1961. *Bull. Amer. Meteor. Soc.*, 47, 374–383.

Anthes, R. A., 1982: Tropical cyclones: Their evolution, structure and effects. *Meteor. Monogr.*, 41, 208 pp.

Anthes, R. A., S. L. Rosenthal and J. W. Trout, 1971a: Preliminary results from an asymmetric model of the tropical cyclone. *Mon. Wea. Rev.*, 99, 744–758.

Anthes, R. A., J. W. Trout and S. L. Rosenthal, 1971b: Comparison of tropical cyclone simulation with and without the assumption of circular symmetry. *Mon. Wea. Rev.*, 99, 759–766.

Arnold, C. P., 1977: Tropical cyclone cloud and intensity relationships. Dept. of Atmos. Sci. Paper No. 277, Colo. State Univ., Ft. Collins, CO, 154 pp.

Atkinson, G. D., 1971: Forecaster's guide to tropical meteorology. Technical Report 240. United States Air Force, Air Weather Service, 350 pp.

Atkinson, G. D. and C. R. Holliday, 1977: Tropical cyclone minimum sea level pressure maximum sustained wind relationship for the western North Pacific. *Mon. Wea. Rev.*, 105, 421–427.

Bandeen, W. R., V. Kunde, W. Nordberg and H. P. Thompson, 1964: TIROS III meteorological satellite radiation observations of a tropical hurricane. *Tellus*, 16, 481—502.

Bartels, D. L., and R. A. Maddox, 1991: Midlevel cyclonic vortices generated by mesoscale convective systems. *Mon. Wea. Rev.*, 119, 104–118.

Case, R. A., 1986: Atlantic hurricane season of 1985. *Mon. Wea. Rev.*, 114, 1390–1399.

Case, R. A. and Gerrish, 1984: Atlantic hurricane season of 1983. *Mon. Wea. Rev.*, 112, 1083–1092.

Chang, S. W.-J., 1979: The response of an axisymmetric model tropical cyclone to local variations of sea-surface temperature. *Mon. Wea. Rev.*, 107, 662–666.

Challa, M. and R. L. Pfeffer, 1984: The effect of cumulus momentum mixing on the development of a symmetric model hurricane. *J. Atmos. Sci.*, 41, 1313–1319.

Charney, J. G. and A. Eliassen, 1964: On the growth of the hurricane depression. *J. Atmos. Sci.*, 31, 1241–1255.

Challa, M. and R. L. Pfeffer, 1990: Formation of Atlantic hurricanes from cloud clusters and depressions. *J. Atmos. Sci.*, 47, 909–927.

Chen, S., 1990: A numerical study of the genesis of extratropical convective mesovortices. Ph.D. Thesis. Pennsylvania State University, Dept. of Meteorology.

Colon, J. A. and W. R. Nightingale, 1963: Development of tropical cyclones in relation to circulation patterns at the 200 mb level. *Mon. Wea. Rev.*, 91, 329–336.

Cotton, W. R., M.-S. Lin, R. L. McAnelly and C. J. Tremback, 1989: A composite model of mesoscale convective complexes. *Mon. Wea. Rev.*, 117, 765–783.

Davidson, N. E., G. J. Holland, J. L. McBride, and T. D. Keenan, 1990: On the formation of AMEX tropical cyclones Irma and Jason. *Mon. Wea. Rev.*, 118, 1981–2000.

Davidson, N. E. and A. Kumar, 1990: Numerical simulation of the development of AMEX tropical cyclone Irma. *Mon. Wea. Rev.*, 118, 2001–2019.

Davidson, N. E. and B. J. McAvaney, 1981: The ANMRC tropical analysis scheme. *Aust. Met.*, 29, 155–168.

Deppermann, C. E., 1947: Notes on the origin and structure of Phillipine typhoons. *Bull. Amer. Meteor. Soc.*, 28, 399–404.

Dunn, G. E., 1940: Cyclogenesis in the tropical Atlantic. *Bull. Amer. Meteor. Soc.*, 21, 215–229.

Dunn, G. E., 1951: Tropical cyclones. *Compendium of Meteorology.*, Amer. Meteor. Soc., Boston, MA, 889–901.

Dvorak, V. F., 1975: Tropical cyclone intensity analysis and forecasting from satellite imagery. *Mon. Wea. Rev.*, 103, 420–430.

Dvorak, V. F., 1984: Tropical cyclone intensity analysis using satellite data. NOAA Technical Report NESDIS 11, U. S. Dept. of Commerce, Washington, D. C., 47 pp.

Emanuel, K. A., 1989: The finite-amplitude nature of tropical cyclogenesis. *J. Atmos. Sci.*, 46, 3431–3456.

Erickson, S. L., 1977: Comparison of developing and non-developing tropical disturbances. Dept. of Atmos. Sci. Paper No. 274, Colo. State Univ., Ft. Collins, CO, 81 pp.

Europeon Centre for Medium Range Weather Forecasts (ECMWF), 1983-1984: Daily Global Analyses, Reading, Berkshire RG29AX, England.

Fett, R. W., 1968: Typhoon formation within the zone of the intertropical convergence. *Mon. Wea. Rev.*, 96, 106–117.

Fett, R. W., 1966: Upper-level structure of the formative tropical cyclone. *Mon. Wea. Rev.*, 94, 9–15.

Fingerhut, W. A., 1980: On the role of cumulus rearrangement of horizontal momentum during tropical cyclone development. 13th Technical Conference on Hurricanes and Tropical Meteorology, Dec. 1-5, Miami Beach, FL.

Fingerhut, W. A., 1978: A numerical model of a diurnally varying tropical cloud cluster disturbance. *Mon. Wea. Rev.*, 106, 2, 255–264.

Foster, I. J. and T. J. Lyons, 1988: The development of tropical cyclones in the north-west of Australia. *Quart. J. Roy. Meteor. Soc.*, 114, 1187–1199.

Frank, N. L., 1963: Synoptic case study of tropical cyclogenesis utilizing TIROS data. *Mon. Wea. Rev.*, 91, 355–366.

Frank, W. M., 1977a: The structure and energetics of the tropical cyclone, Part I: Storm structure. *Mon. Wea. Rev.*, 105, 9, 1119–1135.

Frank, W. M., 1977b: The structure and energetics of the tropical cyclone, Part II: Dynamics and energetics. *Mon. Wea. Rev.*, 105, 9, 1136–1150.

Frank, W. M., 1983: The cumulus parameterization problem. *Mon. Wea. Rev.*, 111, 1859–1871.

Frank, W. M., 1987: Chapter 3: Tropical cyclone formation. *A global view of tropical cyclones.* R. Elsberry, ed., Office of Naval Research, Monterey, CA, 53–90.

Frank W. M. and C. C. Cohen, 1987: Simulation of tropical convective systems. Part I: A cumulus parameterization. *J. Atmos. Soc.*, 44, 3787–3799.

Fritz, S., 1962: Satellite pictures and the origin of Hurricane Anna. *Mon. Wea. Rev.*, 90, 507–513.

Gray, W. M., 1968: Global view of the origin of tropical disturbances and storms. *Mon. Wea. Rev.*, 96, 669–700.

Gray, W. M., 1975: Tropical cyclone genesis. Dept. of Atmos. Sci. Paper No. 234, Colo. State Univ., Ft. Collins, CO, 121 pp.

Gray, W. M., 1979: Hurricanes: their formation, structure and likely role in the tropical circulation. Supplement to Meteorology Over the Tropical Oceans. Published by RMS, James Glaisher House, Grenville Place, Bracknell, Berkshire, RG 12 1BX, D. B. Shaw, ed., 155–218.

Gray, W. M., 1981: Recent advances in tropical Cyclone research from rawinsonde composite analysis, World Meteorological Organization, Geneva, Switzerland, 407 pp.

Gray, W. M., 1988: Environmental influences on tropical cyclones. *Aust. Met. Mag.*, 36, 127–139.

Gray, W. M., 1989: Tropical cyclone formation. Invited paper presented at the International Workshop on Tropical Cyclones, Manila, Philippines, Proceedings of 2nd WMO Sponsored Workshop on Tropical Cyclones, Issued by WMO, Nov. 25-Dec. 7, pp. 95-121.

Henderson, R. S., 1978: USAF Aerial Weather Reconnaissance using the Lockhead WC-130 aircraft. *Bull. Amer. Meteor. Soc.*, 59, 1136–1143.

Heta, Y., 1990: An analysis of tropical wind fields in relation to typhoon formation over the Western Pacific. *J. Meteor. Soc. of Japan*, 68, 65–76.

Holland, G. J., 1984: On the climatology and structure of tropical cyclones in the Australian/Southwest Pacific region. *Aust. Met. Mag.*, 32, 1–32.

Holland, G. J., 1986: Tropical cyclone intensity and structure change. Chapter 8, Topic 4 of Proceedings of the WMO International Workshop on Tropical Cyclones (IWTC), Bangkok, Thailand, 25-November-5 December, 1985, 52–61.

Holland, G. J. and R. T. Merrill, 1984: On the dynamics of tropical cyclone structural changes. *Quart. J. Roy. Meteor. Soc.*, 110, 723–745.

Houze, R. A., Jr., 1982: Cloud clusters and large scale vertical motions in the tropics. *J. Meteor. Soc. of Japan*, 60, 396–410.

Hubert, L. F., 1955: A case study of hurricane formation. *J. Meteor.*, 12, 486–492.

Huschke, R. E., (Ed.), 1959: Glossory of meteorology. *Amer. Meteor. Soc.*, 45 Beacon St., Boston, MA, 02108, 638 pp.

Japan Meteorological Agency (JMA), Monthly Report of Meteorological Satellite Center, 1983-1984: Meteorological Satellite Center, Tokyo, Japan. [ISSN 0387-4028]

Johnston, E. C., 1981: Mesoscale vorticity centers induced by mesoscale convective complexes. M.S. Thesis, Dept. of Meteor., University of Wisconsin, Madison, WI, 54 pp.

Johnson, R. H., S. Chen, and J. J. Toth, 1989: Circulations associated with a mature-to-decaying midlatitude convective system. *Mon. Wea. Rev.*, 117, 942–959.

Johnson, R. H. and D. L. Bartels, 1991: Circulations associated with a mature-to-decaying mesoscale convective system. Part II: Upper-level featurse. (Submitted to *Mon. Wea. Rev.*.

Joint Typhoon Warning Center (JTWC), 1984: *Annual tropical cyclone report.* US Naval Oceanography Command Center, COMNAVMARIANAS Box 17, FPO, San Francisco, 96630, 219 pp.

Krishnamurti, T. N., D. Oosterhaf and N. Dignon, 1989: Hurricane prediction with a high resolution global model. *Mon. Wea. Rev.*, 117, 631–669.

Kuo, H. L., 1965: On formation and intensification of tropical cyclones through latent heat release by cumulus convection. *J. Atmos. Sci.*, 22, 40–63.

Kurihara, Y., 1975: Budget analysis of a tropical cyclone simulated in an axisymmetric numerical model. *J. Atmos. Sci.*, 32, 25–29.

Kurihara, Y. and M. Kawase, 1985: On the transformation of a tropical easterly wave into a tropical depression: A simple numerical study. *J. Atmos. Sci.*, 42, 68–77.

Kurihara, Y. and R. E. Tuleya, 1974: Structure of a tropical cyclone developed in a three-dimensional numerical simulation model. *J. Atmos. Sci.*, 31, 893–919.

Kurihara, Y. and R. E. Tuleya, 1981: A numerical simulation study on the genesis of a tropical storm. *Mon. Wea. Rev.*, 109, 1629–1653.

Leary, C. A. and E. N. Rappoport, 1987: The life cycle and internal structure of a mesoscale convective complex. *Mon. Wea. Rev.*, 115, 1503–1527.

Lee, C.-S., 1986: An observational study of tropical cloud cluster evolution and cyclogenesis in the western North Pacific. Dept. of Atmos. Sci. Paper No. 403, Colo. State Univ., Ft. Collins, CO, 250 pp.

Lee, C.-S., 1989a: Observational analysis of tropical cyclogenesis in the western North Pacific: I: Structural evolution of cloud clusters. *J. Atmos. Sci.*, 46, 16, 2580–2598.

Lee, C.-S., 1989b: Observational analysis of tropical cyclogenesis in the western North Pacific: II: Budget analysis. *J. Atmos. Sci.*, 46, 16, 2599–2616.

Lopez, R., 1968: Investigation of the importance of cumulus convection and ventilation in early tropical storm development. Dept. of Atmos. Sci. Paper No. 124, Colo. State Univ., Ft. Collins, CO, 88 pp.

Love, G. B., 1982: The role of large-scale flow fields in tropical cyclone genesis. Paper presented at the 14th Technical Conference on Hurricanes and Tropical Meteorology, AMS, 7-11 June, San Diego, CA.

Love, G., 1985: Cross-equatorial influence of winter hemisphere subtropical cold surges. *Mon. Wea. Rev.*, 113, 1487–1498.

Lubich, P. A. and R. M. Zehr, 1989: Quantitative satellite analyses of four tropical cyclones during AMEX/EMEX. Preprints, 4th Conf. of Satellite Meteorology and Oceanography, San Diego, Amer. Meteor. Soc.

Lunney, P. A., 1988: Environmental and convective influence on tropical cyclone development vs. non–development. Dept. of Atmos. Sci. Paper No. 436, Colo. State Univ., Ft. Collins, CO, 105 pp.

Maddox, R. A., 1980: Mesoscale convective complexes. *Bull. Amer. Meteor. Soc.*, 61, 1374–1387.

McBride, J. L., 1979: Observational Analysis of tropical cyclone formation. Dept. of Atmos. Sci. Paper No. 308, Colo. State Univ., Ft. Collins, CO, 230 pp.

McBride, J. L., 1981a: Observational analysis of tropical cyclone formation. Part I: Basic description of data sets. *J. Atmos. Sci.*, 38, 1117–1131.

McBride, J. L., 1981b: Observational analysis of tropical cyclone formation. Part III: Budget analysis. *J. Atmos. Sci.*, 38, 1152–1166.

McBride, J. L. and H. E. Willoughby, 1986: Comment - An interpretation of Kurihara and Kawase's two-dimensional tropical cyclone development model. *J. Atmos. Sci.*, 43, 3279–3283.

McBride, J. L. and T. D. Keenan, 1982: Climatology of tropical cyclone genesis in the Australian region. *J. Climate*, 2, 13–33.

McBride, J. L. and R. Zehr, 1981: Observational analysis of tropical cyclone formation. Part II: Comparison of non-developing versus developing systems. *J. Atmos. Sci.*, 38, 1132–1151.

Menard, R. D. and J. M. Fritsch, 1989: A mesoscale convective complex-generated inertially stable warm core vortex. *Mon. Wea. Rev.*, 117, 1237–1261.

Middlebrooke, M. G., 1988: Investigation of tropical cyclone genesis and development using low-level aircraft flight data. Dept. of Atmos. Sci. Paper No. 429. Colo. State Univ., Ft. Collins, CO, 94 pp.

Molinari, J. and D. Vollaro, 1989: External influences on hurricane intensity. Part I: Outflow layer eddy angular momentum fluxes. *J. Atmos. Sci.*, 46, 1093–1105.

Molinari, J. and S. Skubis, 1985: Evolution of the surface wind field in an intensifying tropical cyclone. *Mon. Wea. Rev.*, 42, 2856–2864.

Mundell, D. B., 1990: Prediction of tropical cyclone rapid intensification events. Dept. of Atmos. M.S. Thesis, Colo. State Univ., Ft. Collins, CO, 186 pp.

Oliver, V. J. and R. K. Anderson, 1969: Circulation in the tropics as revealed by satellite data. *Bull. Amer. Meteor. Soc.*, 50, 702–707.

Ooyama, K. V., 1969: Numerical simulation of the life cycle of tropical cyclones. *J. Atmos. Sci.*, 26, 3–40.

Ooyama, K. V., 1982: Conceptual evaluation of the theory and modeling of the tropical cyclone. *J. Meteor. Soc. of Japan*, 60, 369–380.

Palmen, E., 1948: On the formation and structure of tropical hurricanes. *Geophysics*, 3, 26–38.

Palmen, E. and H. Riehl, 1957: Budget of angular momentum and energy in tropical cyclones. *J. Meteor.*, 14, 150–159.

Ramage, C. S., 1974: Monsoonal influences on the annual variation of tropical cyclone development over the Indian and Pacific Oceans. *Mon. Wea. Rev.*, 102, 745–753.

Riehl, H., 1948: On the formation of typhoons. *J. Meteor.*, 5, 247–264.

Riehl, H., 1954: Tropical meteorology. McGray-Hill Book Company, New York, N.Y., 392 pp.

Riehl, H. and J. S. Malkus, 1961: Some aspects of Hurricane Daisy, 1958. *Tellus*, 13, 181–213.

Rosenthal, S. L., 1970: A circularly symmetric primitive equation model of tropical cyclone development containing an explicit water vapor cycle. *Mon. Wea. Rev.*, 98, 643–663.

Rosenthal, S. L., 1978: Numerical simulation of tropical cyclone development with latent heat release by the resolvable scales I: Model description and preliminary results. *J. Atmos. Sci.*, 35, 258–271.

Rossby, C.-G., 1938: On the mutual adjustment of pressure and velocity distributions in certain simple current systems, II. *J. Marina Res.*, 1, 239–256.

Rossow, W. B., L. C. Garder, P. Lu and A. Walker, 1988: International satellite cloud climatology project (ISCCP) documentation of cloud data. *WMO/TD-No. 266*, World Meteorological Organization, Geneva, Switzerland.

Rotunno, R. and K. A. Emanuel, 1987: An air-sea interaction theory for tropical cyclones. *J. Atmos. Sci.*, 44, 542–560.

Ruprecht, E. and W. M. Gray, 1976: Analysis of satellite-observed tropical cloud clusters, I: Wind and dynamic fields. *Tellus*, 28, 391–413.

Rutledge, S. A., R. A. Houze, M. I. Biggerstaff, and T. Matejka, 1988: The Oklahoma-Kansas mesoscale convective system of 10-11 June 1985. Precipitation structure and single-Doppler radar analysis.

Sadler, J. C., 1976a: A role of the tropical upper tropospheric trough in early season typhoon development. *Mon. Wea. Rev.*, 104, 1266–1278.

Sadler, J. C., 1976b: Tropical cyclone initiation by the tropical upper tropospheric trough. Navy Environmental Prediction and Research Facility Technical Paper No. 2-76, 103 pp. [NTLS No. ADA 025456]

Sadler, J. C., 1978: Mid-season typhoon development and intensity changes and the tropical upper tropospheric trough. *Mon. Wea. Rev.*, 106, 1137–1152.

Sawyer, J. S., 1947: Notes on the theory of tropical cyclones. *Quart. J. Roy. Meteor. Soc.*, 73, 101–126.

Schiffer, R. A. and W. B. Rossow, 1983: The international satellite cloud climatology project (ISCCP): The first project of the World Climate Research Program. *Bulletin*, Amer. Meteor. Soc., 64, 779–784.

Schubert, W. H., J. J. Hack, P. L. Silva and S. R. Fulton, 1980: Geostrophic adjustment in an axisymmetric vortex. *J. Atmos. Sci.*, 37, 1464–1484.

Schubert, W. H. and J. J. Hack, 1982: Inertial stability and tropical cyclone development. *J. Atmos. Sci.*, 39, 1687–1697.

Shapiro, L. J., 1977: Tropical storm formation from easterly waves: A criterion for development. *J. Atmos. Sci.*, 34, 1007–1021.

Shoemaker, D. N., 1989: Relationships between tropical cyclone deep convection and the radial extent of damaging winds. Dept. of Atmos. Sci. Paper No. 457, Colo. State Univ., Ft. Collins, CO, 109 pp.

Silva Dias, P. L., W. H. Schubert and M. DeMaria, 1983: Large-scale response of the tropical atmosphere to transient convection. *J. Atmos. Sci.*, 40, 2689–2707.

Smull, B. F. and R. A. Houze, Jr., 1987: Dual-Doppler radar analysis of a mid-latitude squall line with a trailing region of stratiform rain. *J. Atmos. Sci.*, 44, 2128–2148.

Sundquist, H., 1970: Numerical simulation of the development of tropical cyclones with a ten-layer model, Part I. *Tellus*, 22, 359–390.

Tripoli, G. J. and W. R. Cotton, 1989: Numerical study of an orogenic mesoscale convective system. Part I: Simulated genesis and comparison with observations. *Mon. Wea. Rev.*, 117, 273–304.

Tuleya, R. E., 1991: Sensitivity studies of tropical storm genesis using a numerical model. *Mon. Wea. Rev.*, 119, 721–733.

Tuleya, R. E. and Y. Kurihara, 1981: A numerical study on the effects of environmental flow on tropical storm genesis. *Mon. Wea. Rev.*, 109, 2487–2506.

Velasco, I. and J. M. Fritsch, 1987: Mesoscale convective complexes in the Americas. *J. Geophys. Res.*, 92, 9591–9613.

Weatherford, C. L., 1985: Typhoon structural variability. Dept. of Atmos. Sci. Paper No. 391, Colo. State Univ., Ft. Collins, CO, 77 pp.

Weatherford, C., and W. M. Gray, 1988: Typhoon structure as revealed by aircraft reconnaissance: Part I: Data analysis and climatology. *Mon. Wea. Rev.*, Vol. 116, 5, 1032-1043.

Weatherford, C., and W. M. Gray, 1988: Typhoon structure as revealed by aircraft reconnaissance: Part II: Structural variability. *Mon. Wea. Rev.*, Vol. 116, 5, 1044-1056.

Williams, K. and W. M. Gray, 1973: Statistical analysis of satellite observed cloud clusters in the western Pacific. *Tellus*, 21, 313-336.

Yamasaki, M., 1968: Numerical simulation of tropical cyclone development with the use of primitive equations. *J. Meteor. Soc. of Japan*, 46, 178–201.

Yanai, M., 1961a: A detailed analysis of typhoon formation. *J. Meteor. Soc. of Japan*, 39, 4, 187–214.

Yanai, M., 1961b: Dynamical aspects of typhoon formation. *J. Meteor. Soc. of Japan*, 39, 282–309.

Yanai, M., 1968: Evolution of a tropical disturbance in the Carribean Sea region. *J. Meteor. Soc. of Japan*, 46, 86–108.

Zehr. R. M., 1976: Tropical disturbance intensification. Dept. of Atmos. Sci. Paper No. 259, Colo. State Univ., Ft. Collins, CO, 91 pp.

Zehr, R. M., 1987: The diurnal variation of deep convective clouds and cirrus with tropical cyclones. Preprints, 17th Conf. on Hurricanes and Tropical Meteorology, Miami, Amer. Meteor. Soc., 276–279.

Zehr, R. M., 1988: Satellite diagnosis of tropical cyclones. Preprints, 3rd Conf. on Satellite Meteorology and Oceanography, Anaheim, Amer. Meteor. Soc., 241–246.

Zehr, R. M., 1989: Tropical cyclone genesis in the northwest Pacific. Preprints, 18th Conf. on Hurricanes and Tropical Meteorology, San Diego, Amer. Meteor. Soc., 143–144.

Zhang, D. L. and J. M. Fritsch, 1988: A numerical investigation of a convectively generated, inertially stable, extra tropical warm-core mesovortex overland. *Mon. Wea. Rev.*, 116, 2660–2687.

Appendix A

BEST TRACK PLOTS OF THE NON-DEVELOPING DISTURBANCES

Dates and times of each disturbance found in Appendix B.

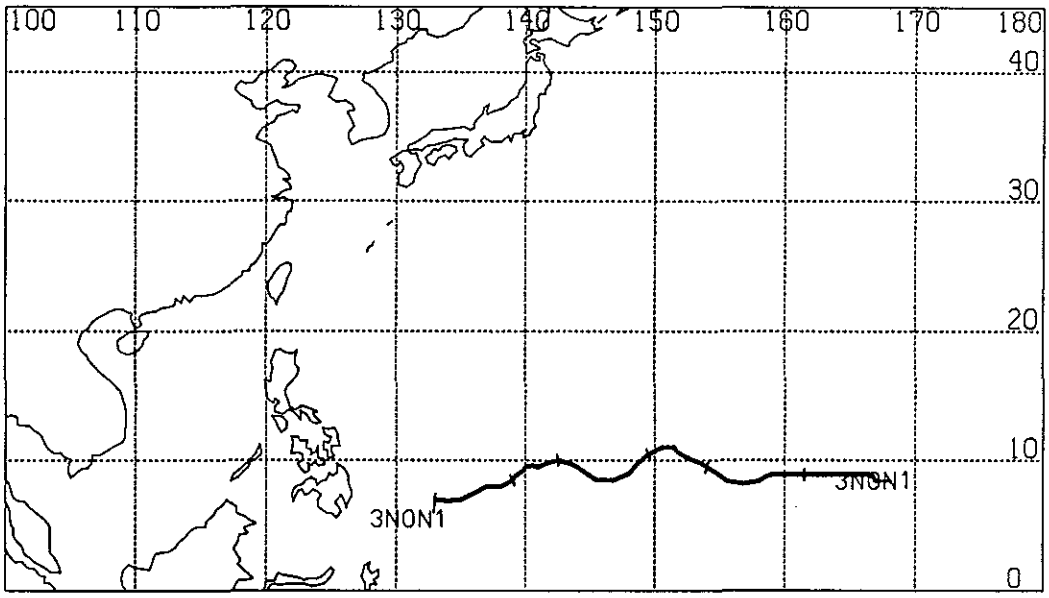

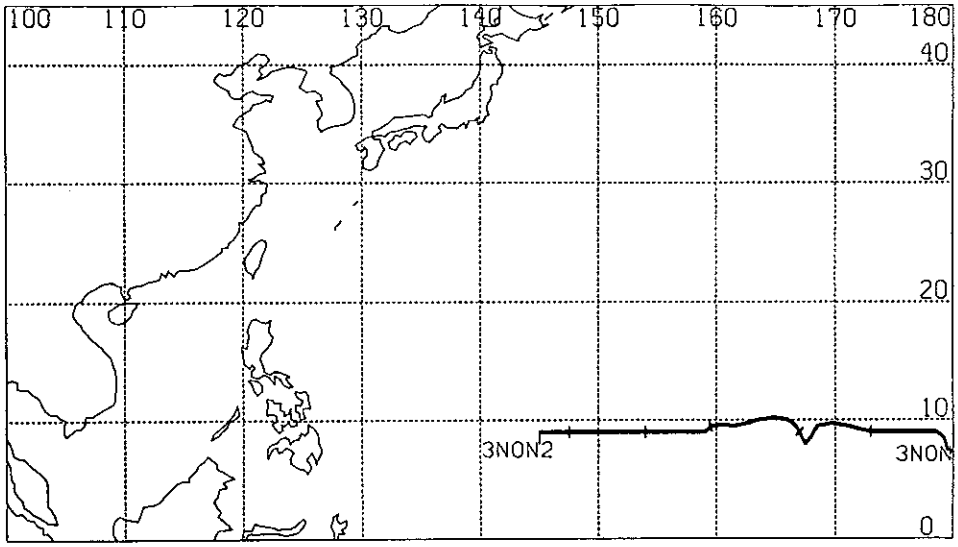
100
110
120
130
140
150
160
170
180
40
30
20
10
0
3NON2
3NON

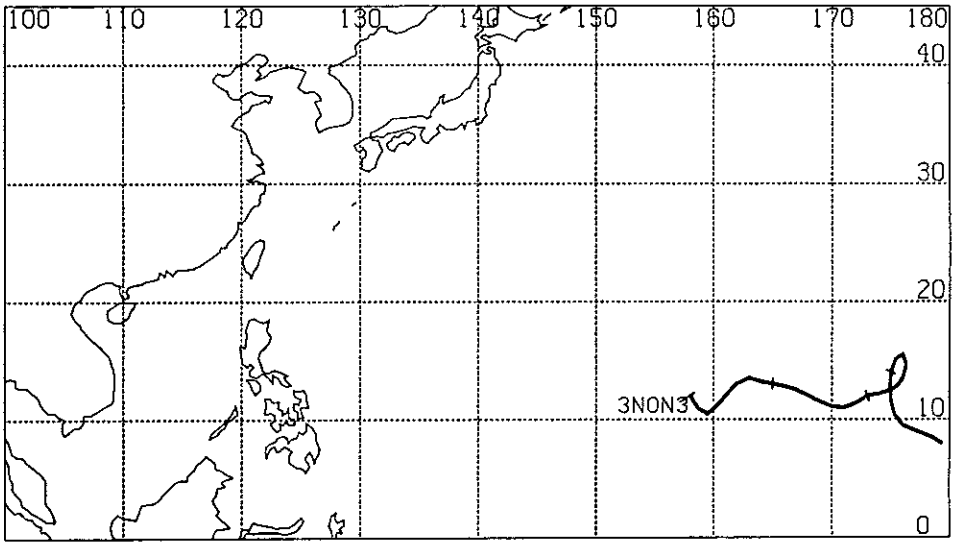
100
110
120
130
140
150
160
170
180
40
30
20
10
0
3NON3

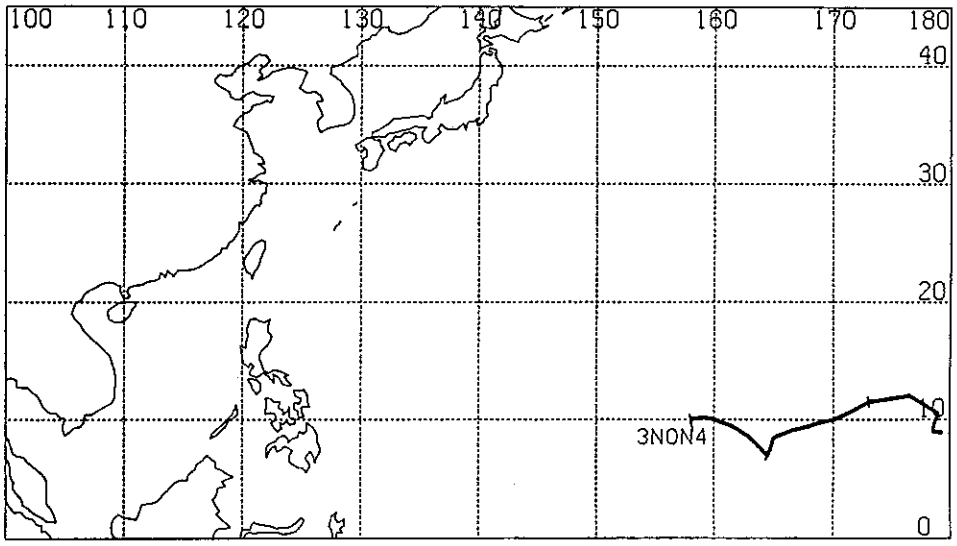
100
110
120
130
140
150
160
170
180
40
30
20
10
0
3NON4

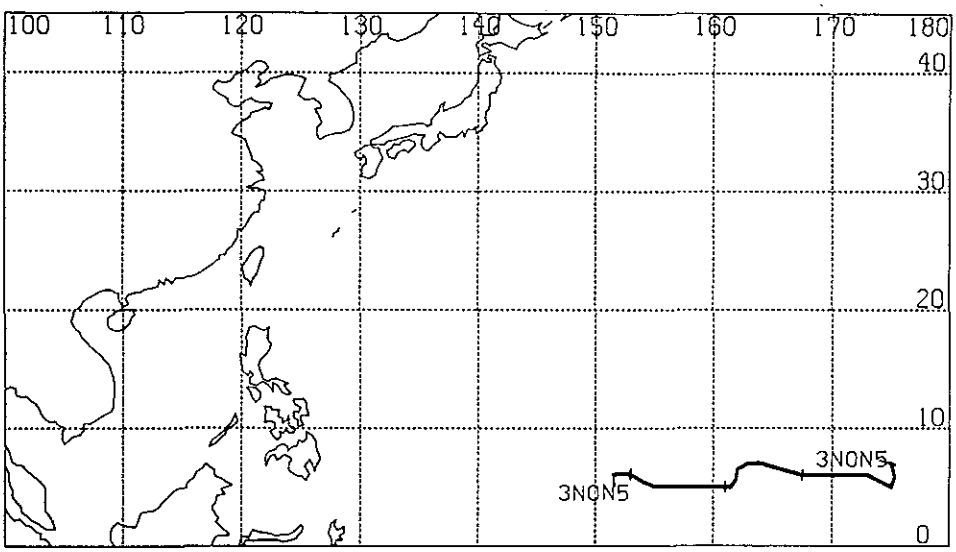
100
110
120
130
140
150
160
170
180
40
30
20
10
0
3N0N5
3N0N5

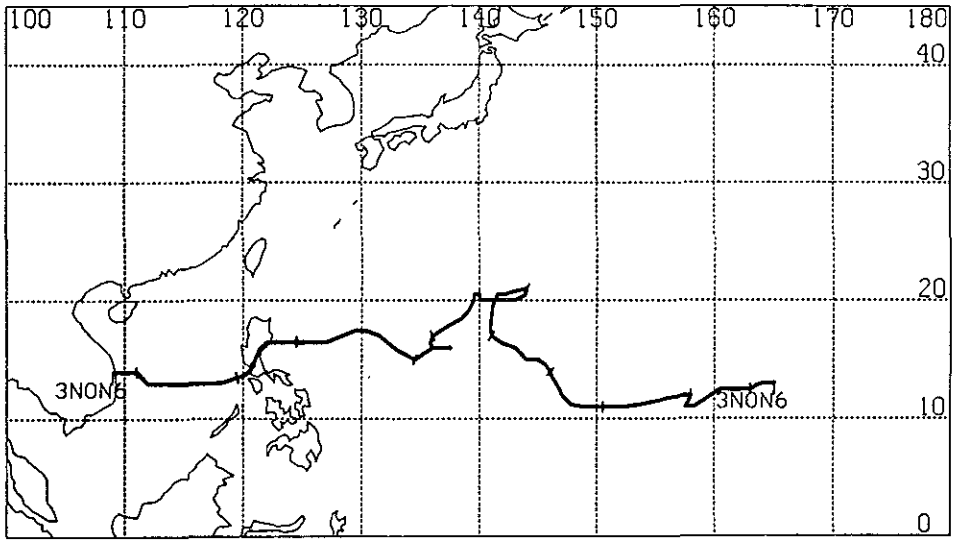
100
110
120
130
140
150
160
170
180
40
30
20
10
0
3N0N6
3N0N6

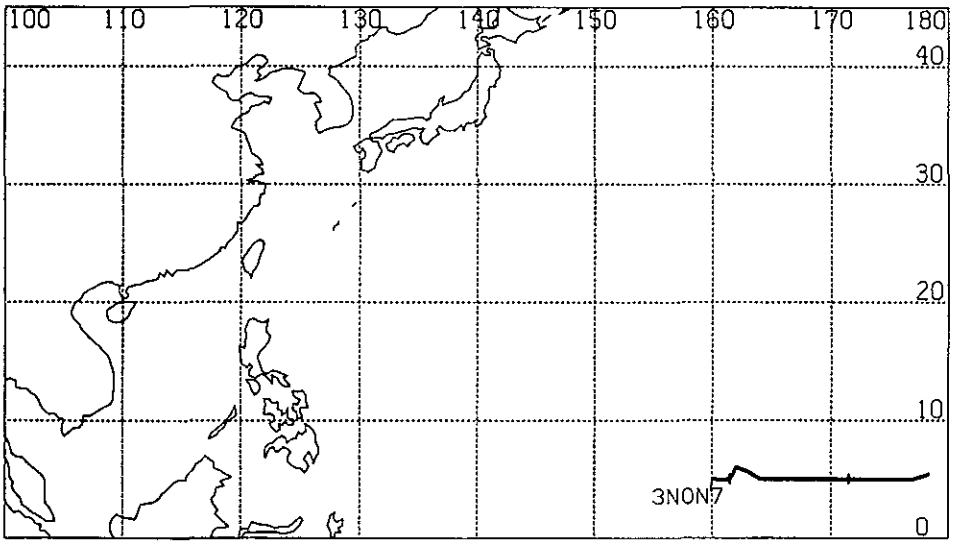
100
110
120
130
140
150
160
170
180
40
30
20
10
0
3N0N7

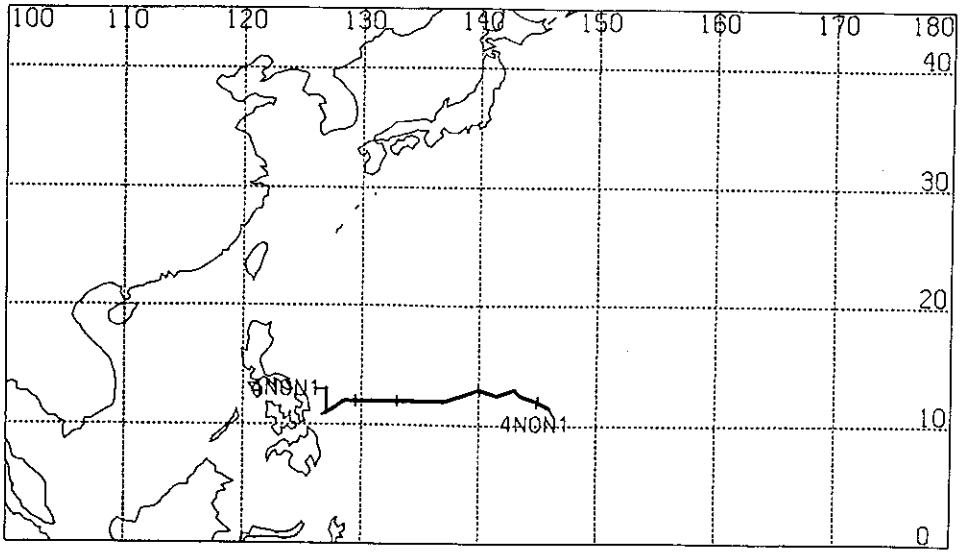
100
110
120
130
140
150
160
170
180
40
30
20
10
0
4NON1
4NON1

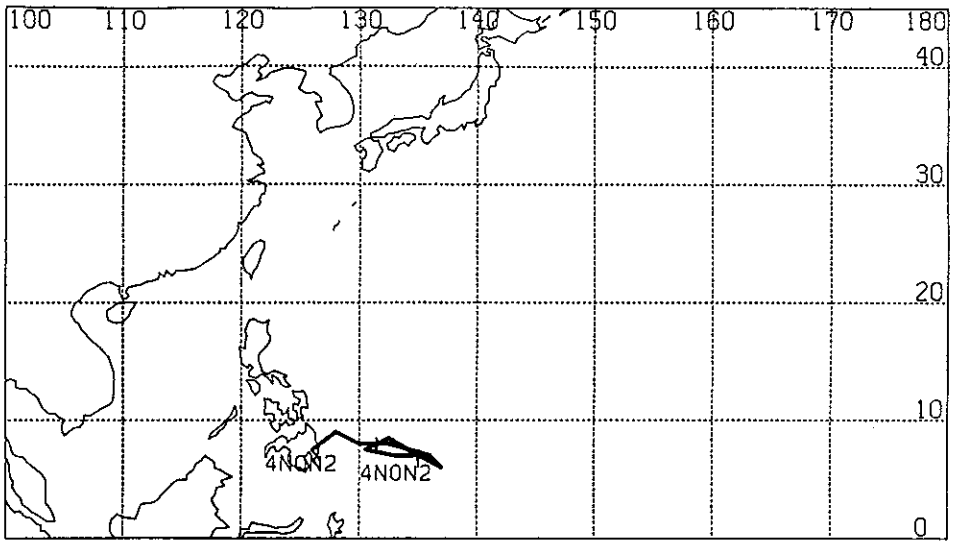
100
110
120
130
140
150
160
170
180
40
30
20
10
0
4NON2
4NON2

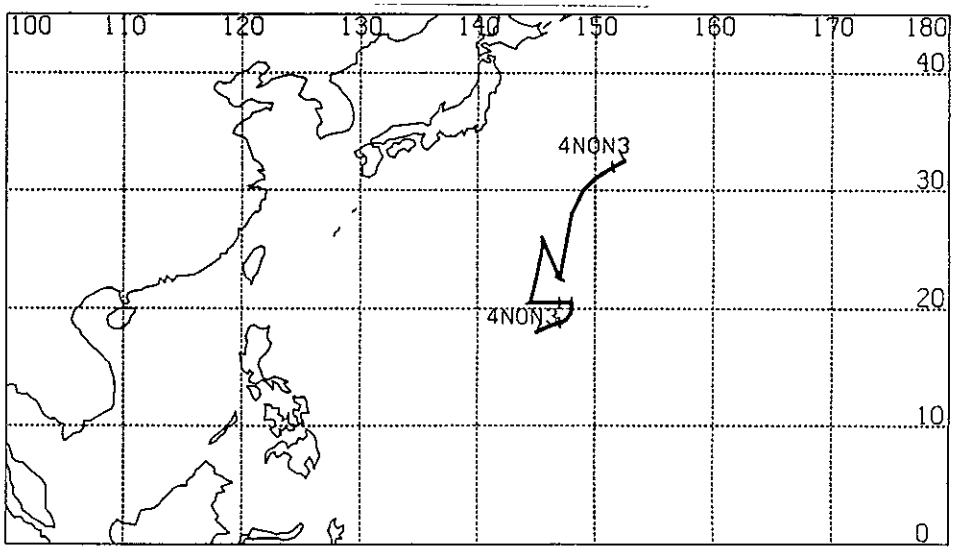
100
110
120
130
140
150
160
170
180
40
30
20
10
0
4NON3
4NON3

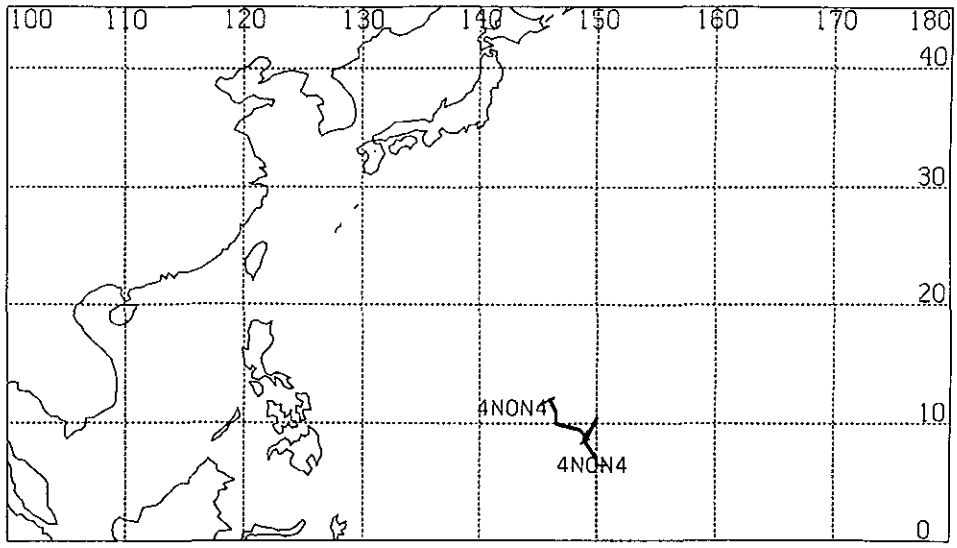
100
110
120
130
140
150
160
170
180
40
30
20
10
0
4NON4
4NON4

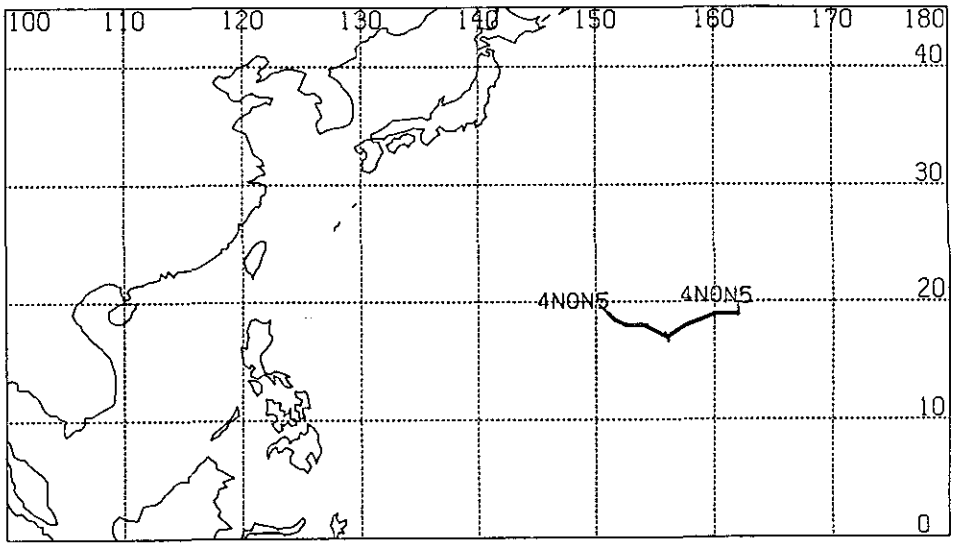
100
110
120
130
140
150
160
170
180
40
30
20
10
0
4NON5
4NON5

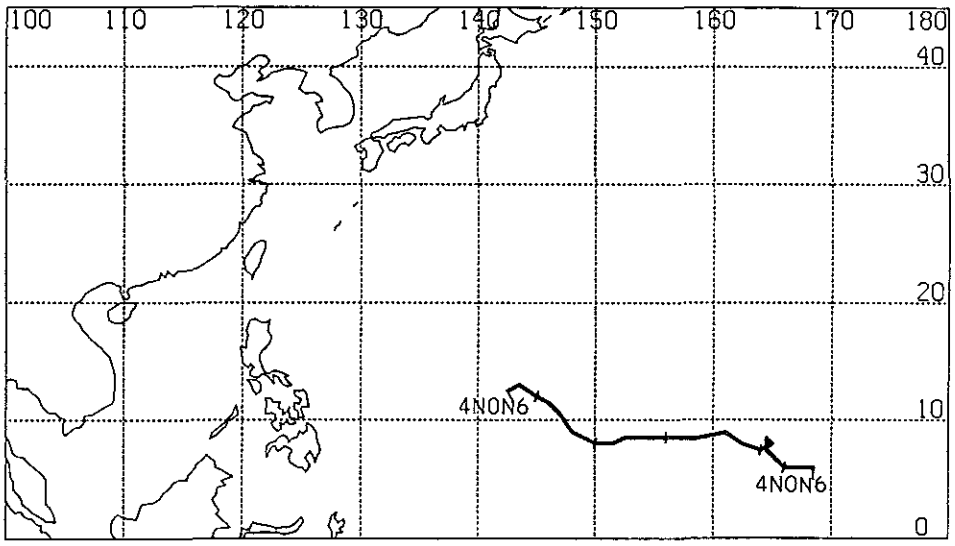
100
110
120
130
140
150
160
170
180
40
30
20
10
0
4NON6
4NON6

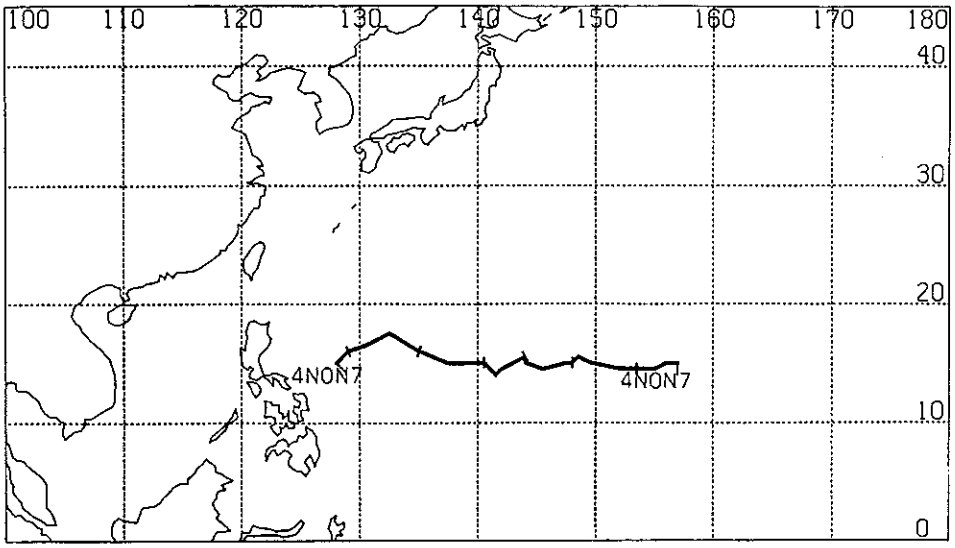
100
110
120
130
140
150
160
170
180
40
30
20
10
0
4NON7
4NON7

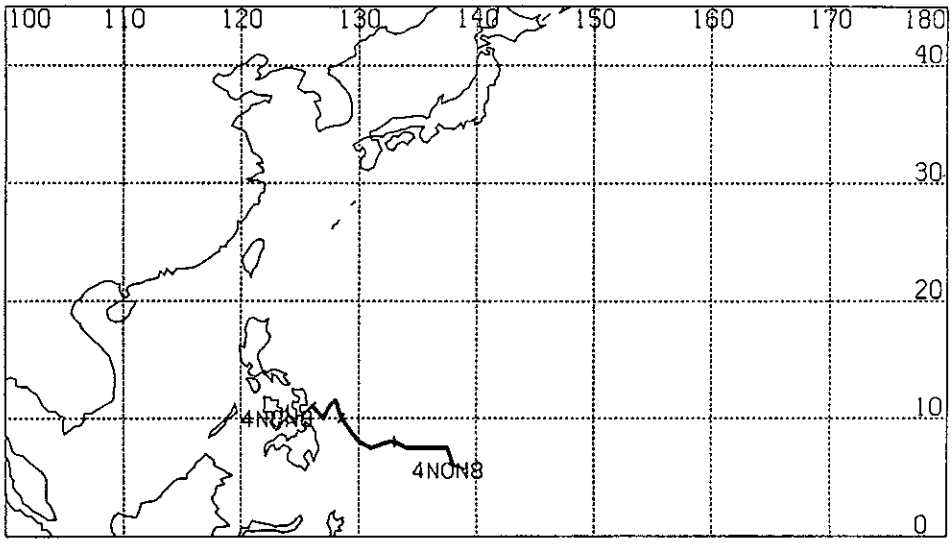
100
110
120
130
140
150
160
170
180
40
30
20
10
0
4NON8
4NON8

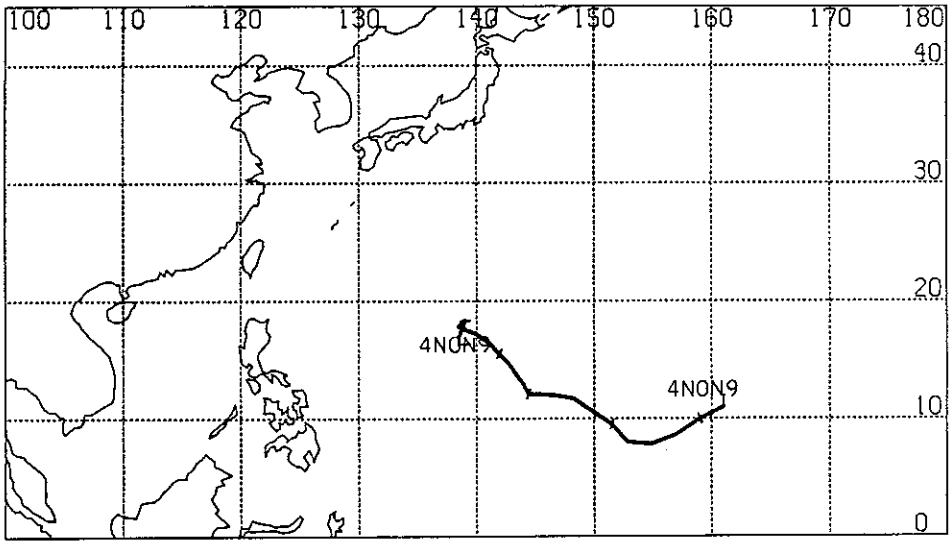
100
110
120
130
140
150
160
170
180
40
30
20
10
0
4NON9
4NON9

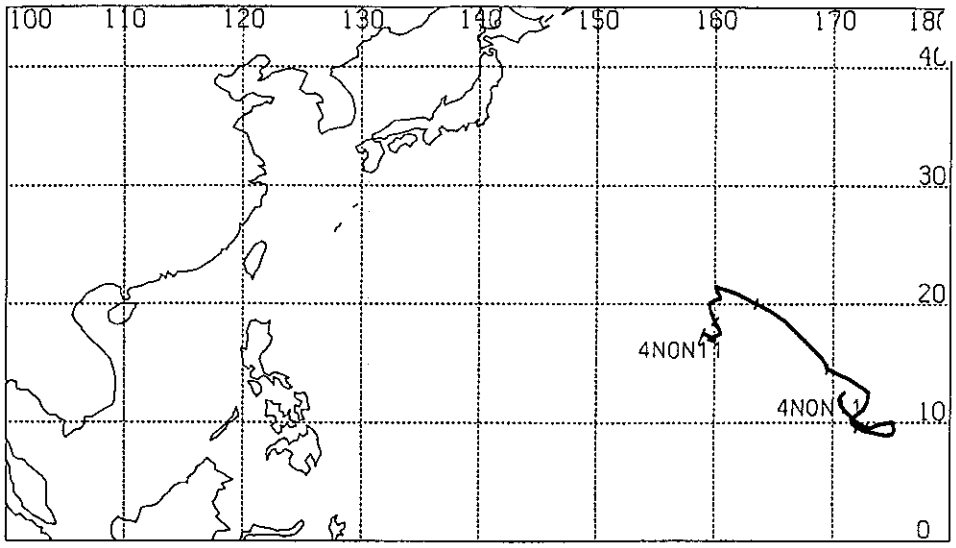
100
110
120
130
140
150
160
170
180
40
30
20
10
0
4NON11
4NON11

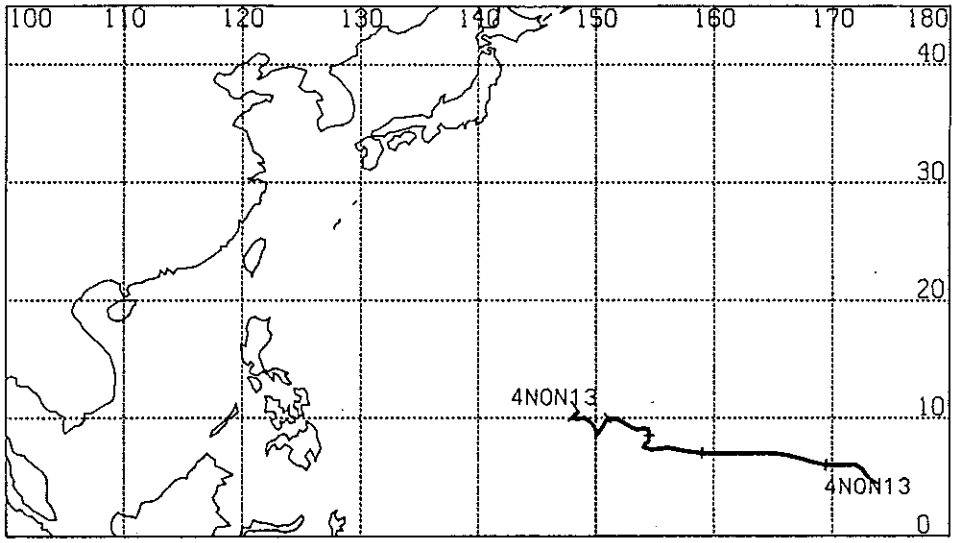
100
110
120
130
140
150
160
170
180
40
30
20
10
0
4NON13
4NON13

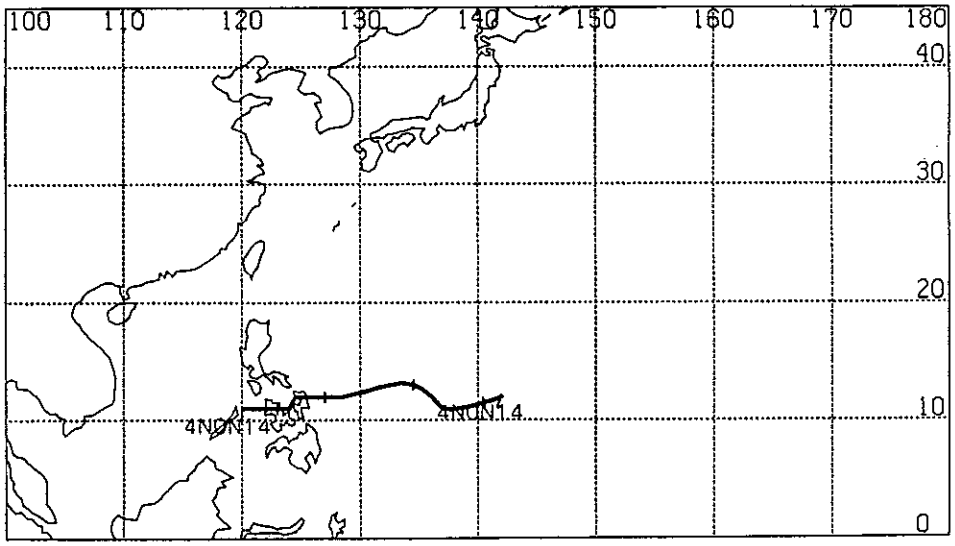
100
110
120
130
140
150
160
170
180
40
30
20
10
0
4NON14
4NON14

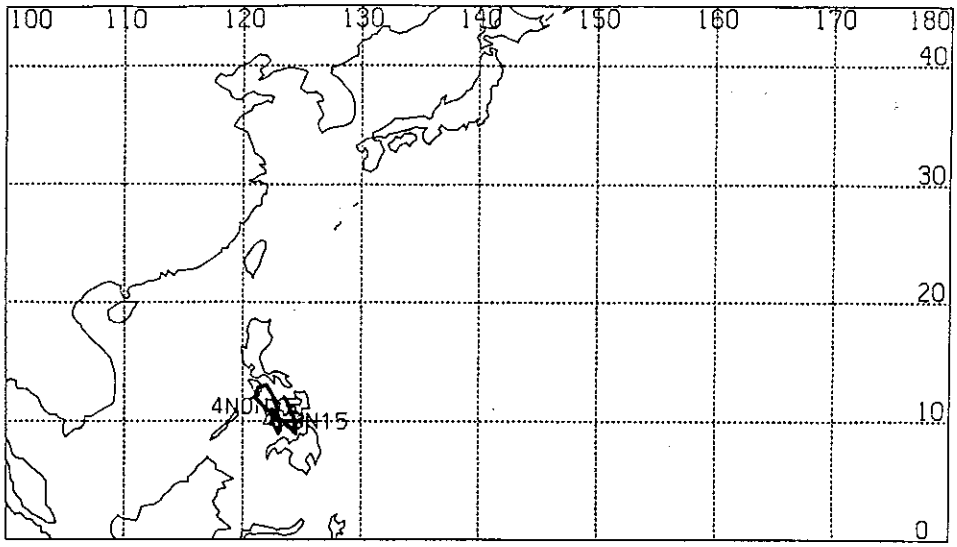
100
110
120
130
140
150
160
170
180
40
30
20
10
0
4NON15

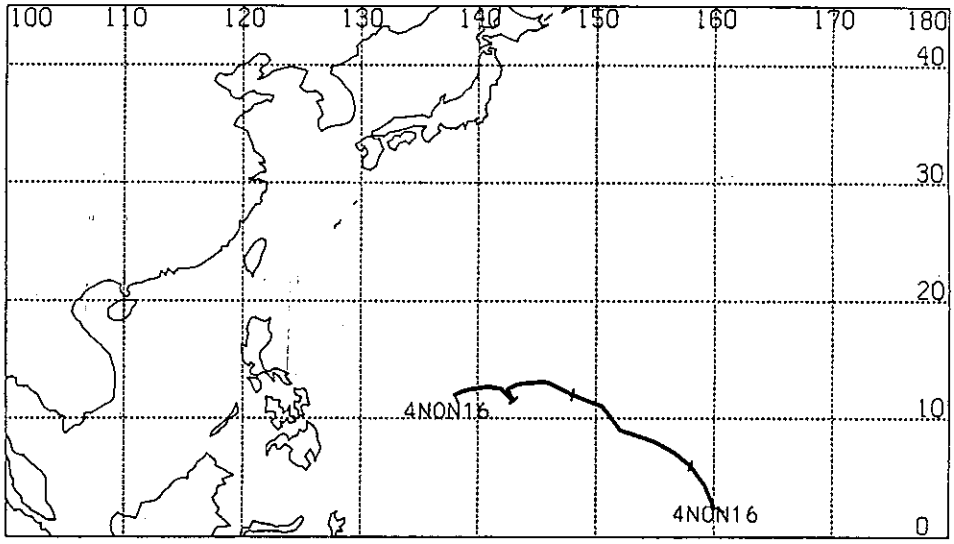
100
110
120
130
140
150
160
170
180
40
30
20
10
0
4NON16
4NON16

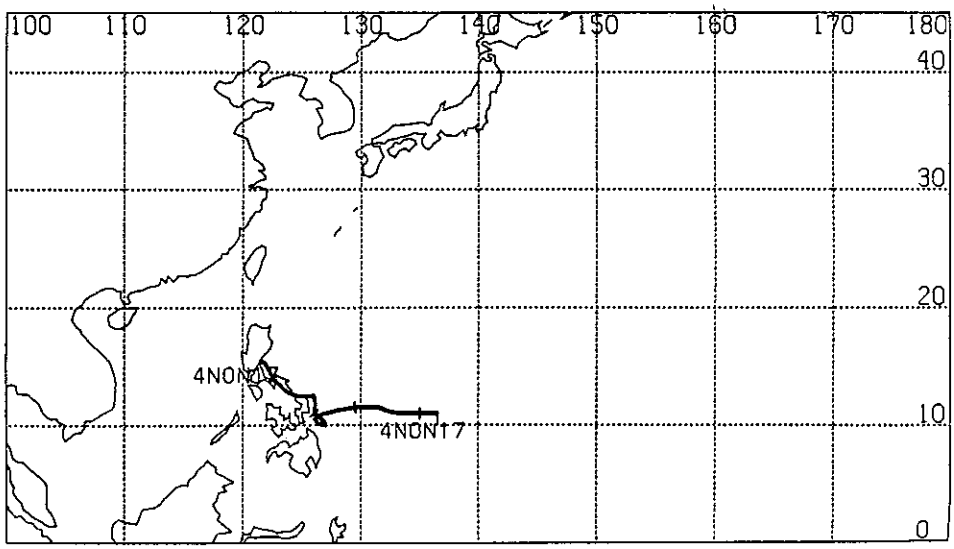
100
110
120
130
140
150
160
170
180
40
30
20
10
0
4NON17
4NON17

Appendix B

CENTER LOCATIONS OF THE NON-DEVELOPING DISTURBANCES USED IN THE CHAPTER 6 ANALYSIS AT 12-HOUR INTERVALS

Name		YYMMDD	HH	lat N	lon E
4NON11	11	841014	12	12.0	170.5
4NON11	11	841015	0	9.5	173.0
4NON11	11	841015	12	9.0	175.0
4NON11	11	841016	0	9.6	172.0
4NON11	11	841016	12	11.0	172.5
4NON11	11	841017	0	14.5	169.5
4NON11	11	841017	12	17.5	167.0
4NON11	11	841018	0	20.0	163.5
4NON11	11	841018	12	20.5	160.5
4NON11	11	841019	0	18.5	160.0
4NON11	11	841019	12	17.0	159.5
4NON11	11	841020	0	17.5	159.0
4NON13	13	841101	0	5.0	173.0
4NON13	13	841101	12	6.0	171.5
4NON13	13	841102	0	6.0	169.5
4NON13	13	841102	12	7.0	165.0
4NON13	13	841103	0	7.0	159.0
4NON13	13	841103	12	7.5	154.0
4NON13	13	841104	0	8.5	154.5
4NON13	13	841104	12	9.0	153.5
4NON13	13	841105	0	10.0	151.0
4NON13	13	841105	12	9.0	150.0
4NON13	13	841106	0	10.0	148.0
4NON14	14	841123	0	11.5	140.5
4NON14	14	841123	12	11.0	137.0
4NON14	14	841124	0	13.0	134.5
4NON14	14	841124	12	12.5	130.5
4NON14	14	841125	0	12.0	127.0
4NON14	14	841125	12	12.0	124.5
4NON14	14	841126	0	11.0	123.0
4NON14	14	841126	12	11.0	120.0

Name		YYMMDD	HH	lat N	lon E
4NON15	15	841214	12	10.0	125.0
4NON15	15	841215	0	10.0	125.0
4NON15	15	841215	12	10.0	123.0
4NON15	15	841216	0	10.0	122.5
4NON15	15	841216	12	10.5	123.0
4NON15	15	841217	0	12.0	121.0
4NON15	15	841217	12	9.5	124.0
4NON15	15	841218	0	11.0	124.0
4NON16	16	841229	0	6.0	158.0
4NON16	16	841229	12	9.0	152.0
4NON16	16	841230	0	12.0	148.0
4NON16	16	841230	12	13.0	144.5
4NON16	16	841231	0	11.5	143.0
4NON16	16	841231	12	12.5	139.5
4NON17	17	841107	0	11.0	135.0
4NON17	17	841107	12	11.5	131.5
4NON17	17	841108	0	11.5	129.5
4NON17	17	841108	12	10.5	126.0
4NON17	17	841109	0	11.0	126.0
4NON17	17	841109	12	12.5	124.5
4NON17	17	841110	0	14.0	122.5
4NON17	17	841110	12	15.5	121.5
4NON1	1	840720	0	12.0	145.0
4NON1	1	840720	12	13.0	143.0
4NON1	1	840721	0	13.0	140.0
4NON1	1	840721	12	12.0	137.0
4NON1	1	840722	0	12.0	133.0
4NON1	1	840722	12	12.0	131.0
4NON1	1	840723	0	12.0	129.5
4NON1	1	840723	12	12.0	128.5
4NON1	1	840724	0	11.0	127.0
4NON2	2	840726	0	7.0	135.0
4NON2	2	840726	12	7.5	130.5
4NON2	2	840727	0	7.0	135.0
4NON2	2	840727	12	7.0	136.0
4NON2	2	840728	0	8.0	131.5
4NON2	2	840728	12	9.0	128.0
4NON3	3	840729	12	18.3	145.6
4NON3	3	840730	0	18.8	147.0
4NON3	3	840730	12	19.7	148.0
4NON3	3	840731	0	20.5	148.0
4NON3	3	840731	12	20.5	147.6
4NON3	3	840801	0	20.5	147.0

Name		YYMMDD	HH	lat N	lon E
4NON3	3	840801	12	20.5	146.2
4NON3	3	840802	0	20.5	144.5
4NON3	3	840802	12	25.0	145.5
4NON3	3	840803	0	22.5	147.0
4NON3	3	840803	12	30.0	149.0
4NON3	3	840804	0	32.0	151.5
4NON4	4	840803	12	6.5	150.0
4NON4	4	840804	0	8.5	149.0
4NON4	4	840804	12	10.5	150.0
4NON4	4	840805	0	9.0	149.0
4NON4	4	840805	12	10.0	146.5
4NON4	4	840806	0	12.0	146.0
4NON5	5	840814	0	19.0	151.0
4NON5	5	840814	12	18.0	152.5
4NON5	5	840815	0	18.0	154.0
4NON5	5	840815	12	18.0	154.0
4NON5	5	840816	0	17.0	156.0
4NON5	5	840816	12	19.0	160.0
4NON6	6	840827	0	6.0	166.0
4NON6	6	840827	12	8.5	164.5
4NON6	6	840828	0	7.5	164.0
4NON6	6	840828	12	9.0	161.0
4NON6	6	840829	0	8.5	156.0
4NON6	6	840829	12	8.5	152.5
4NON6	6	840830	0	8.0	150.0
4NON6	6	840830	12	10.5	147.0
4NON6	6	840831	0	12.0	145.0
4NON6	6	840831	12	12.5	142.5
4NON7	7	840906	12	15.0	156.0
4NON7	7	840907	0	14.5	153.5
4NON7	7	840907	12	15.0	149.5
4NON7	7	840908	0	15.0	148.0
4NON7	7	840908	12	14.5	145.5
4NON7	7	840909	0	15.5	144.0
4NON7	7	840909	12	14.5	142.0
4NON7	7	840910	0	15.0	140.5
4NON7	7	840910	12	15.0	138.5
4NON7	7	840911	0	16.0	135.0
4NON7	7	840911	12	17.0	131.5
4NON7	7	840912	0	16.0	129.0
4NON8	8	840917	0	6.0	138.0
4NON8	8	840917	12	7.5	136.0
4NON8	8	840918	0	8.0	133.0
4NON8	8	840918	12	7.5	131.0

Name		YYMMDD	HH	lat N	lon E
4NON8	8	840919	0	10.0	128.5
4NON8	8	840919	12	11.0	127.5
4NON8	8	840920	0	11.0	126.0
4NON9	9	840919	0	10.0	159.0
4NON9	9	840919	12	7.8	154.8
4NON9	9	840920	0	9.5	151.5
4NON9	9	840920	12	11.7	148.2
4NON9	9	840921	0	12.1	144.4
4NON9	9	840921	12	13.8	143.3
4NON9	9	840922	0	15.5	141.9
4NON9	9	840922	12	17.2	139.9
4NON9	9	840923	0	18.3	139.0
4NON9	9	840923	12	16.3	138.5

Appendix C

CENTER LOCATIONS OF THE PRE-TROPICAL STORM DISTURBANCES USED IN THE CHAPTER 6 ANALYSIS AT 12-HOUR INTERVALS

Name		YYMMDD	HH	lat N	lon E
VERNON	1	840606	0	11.8	118.2
VERNON	1	840606	12	11.8	117.2
VERNON	1	840607	0	11.8	116.2
VERNON	1	840607	12	11.8	115.1
VERNON	1	840608	0	12.1	114.0
VERNON	1	840608	12	12.6	113.3
VERNON	1	840609	0	13.4	112.7
VERNON	1	840609	12	14.9	111.9
WYNNE	2	840617	12	20.0	140.0
WYNNE	2	840618	0	20.2	138.0
WYNNE	2	840618	12	20.3	135.8
WYNNE	2	840619	0	20.8	133.4
WYNNE	2	840619	12	21.3	132.2
WYNNE	2	840620	0	22.0	131.0
BETTY	4	840702	0	6.0	139.0
BETTY	4	840702	12	6.9	136.0
BETTY	4	840703	0	8.5	133.7
BETTY	4	840703	12	11.2	130.4
BETTY	4	840704	0	14.8	128.3
BETTY	4	840704	12	14.8	126.5
BETTY	4	840705	0	14.5	125.0
BETTY	4	840705	12	14.8	122.8
BETTY	4	840706	0	15.5	120.9
BETTY	4	840706	12	16.3	119.4
BETTY	4	840707	0	17.2	117.9
BETTY	4	840707	12	18.1	116.6

Name		YYMMDD	HH	lat N	lon E
GERALD	10	840813	12	16.1	114.8
GERALD	10	840814	0	16.8	116.0
GERALD	10	840814	12	17.5	117.1
GERALD	10	840815	0	18.2	118.3
GERALD	10	840815	12	19.2	119.1
GERALD	10	840816	0	20.0	118.3
JUNE	14	840824	12	16.8	139.8
JUNE	14	840825	0	17.0	138.0
JUNE	14	840825	12	17.2	136.3
JUNE	14	840826	0	17.5	134.0
JUNE	14	840826	12	17.5	131.8
JUNE	14	840827	0	17.4	130.5
JUNE	14	840827	12	17.5	128.0
NINA	18	840925	0	15.1	138.0
NINA	18	840925	12	16.5	139.0
NINA	18	840926	0	17.9	140.0
NINA	18	840926	12	19.3	141.0
NINA	18	840927	0	20.8	141.5
NINA	18	840927	12	22.3	141.3
NINA	18	840928	0	22.8	140.9
ROY	21	841008	0	6.0	133.0
ROY	21	841008	12	7.0	135.0
ROY	21	841009	0	8.0	136.7
ROY	21	841009	12	8.9	139.0
ROY	21	841010	0	9.8	141.0
ROY	21	841010	12	11.0	142.4
ROY	21	841011	0	12.7	143.2
ROY	21	841011	12	14.2	143.2
SUSAN	22	841009	12	11.0	114.0
SUSAN	22	841010	0	11.0	114.0
SUSAN	22	841010	12	10.7	114.6
SUSAN	22	841011	0	11.4	116.5
SUSAN	22	841011	12	11.4	114.6
SUSAN	22	841012	0	12.1	111.6
CARY	5	840705	0	16.4	154.0
CARY	5	840705	12	16.7	152.0
CARY	5	840706	0	16.9	150.3
CARY	5	840706	12	17.3	148.6
CARY	5	840707	0	18.0	146.9
CARY	5	840707	12	19.0	146.4
IKE	13	840825	0	6.0	146.6
IKE	13	840825	12	7.0	146.4
IKE	13	840826	0	8.2	146.0
IKE	13	840826	12	9.4	145.8
IKE	13	840827	0	10.8	144.9

Name		YYMMDD	HH	lat N	lon E
OGDEN	19	841004	12	10.5	151.3
OGDEN	19	841005	0	12.4	151.7
OGDEN	19	841005	12	14.1	152.2
OGDEN	19	841006	0	15.3	152.5
OGDEN	19	841006	12	16.8	152.6
OGDEN	19	841007	0	18.1	152.3
OGDEN	19	841007	12	20.4	152.2
PHYLLIS	20	841008	0	14.2	147.0
PHYLLIS	20	841008	12	15.6	148.5
PHYLLIS	20	841009	0	17.1	150.1
PHYLLIS	20	841009	12	18.4	151.3
PHYLLIS	20	841010	0	19.1	151.9
PHYLLIS	20	841010	12	19.4	152.2
PHYLLIS	20	841011	0	19.7	152.4
VANESSA	25	841020	0	3.6	163.5
VANESSA	25	841020	12	4.4	162.5
VANESSA	25	841021	0	5.2	161.7
VANESSA	25	841021	12	6.2	160.8
VANESSA	25	841022	0	7.5	159.2
VANESSA	25	841022	12	8.6	156.4
VANESSA	25	841023	0	9.4	153.4
ALEX	3	840628	12	16.2	129.1
ALEX	3	840629	0	16.1	128.3
ALEX	3	840629	12	16.1	127.5
ALEX	3	840630	0	16.0	126.6
ALEX	3	840630	12	16.0	125.5
ALEX	3	840701	0	16.0	124.4
ALEX	3	840701	12	16.3	124.0
BILL	28	841102	12	19.90	177.5
BILL	28	841103	0	22.00	176.5
BILL	28	841103	12	22.20	174.4
BILL	28	841104	0	21.40	171.2
BILL	28	841104	12	21.00	168.0
BILL	28	841105	0	20.90	164.3
BILL	28	841105	12	20.00	161.9
BILL	28	841106	0	18.50	159.5
BILL	28	841106	12	17.50	157.8
BILL	28	841107	0	16.20	156.1
BILL	28	841107	12	15.10	154.6
BILL	28	841108	0	14.30	153.9
BILL	28	841108	12	14.10	153.5

Name		YYMMDD	HH	lat N	lon E
CLARA	29	841111	12	6.10	167.0
CLARA	29	841112	0	4.90	162.5
CLARA	29	841112	12	4.60	159.9
CLARA	29	841113	0	4.40	157.3
CLARA	29	841113	12	4.80	155.8
CLARA	29	841114	0	5.50	154.4
CLARA	29	841114	12	6.30	153.2
CLARA	29	841115	0	7.20	151.7
DOYLE	30	841130	12	4.20	156.7
DOYLE	30	841201	0	4.80	155.0
DOYLE	30	841201	12	5.30	153.1
DOYLE	30	841202	0	5.80	151.2
DOYLE	30	841202	12	6.30	149.0
DOYLE	30	841203	0	6.90	145.4
DOYLE	30	841203	12	7.20	142.9
DOYLE	30	841204	0	7.50	141.0
DOYLE	30	841204	12	8.00	139.2
AGNES	27	841028	0	1.40	148.4
AGNES	27	841028	12	1.66	147.9
AGNES	27	841029	0	1.80	147.6
AGNES	27	841029	12	2.00	147.2
AGNES	27	841030	0	2.30	146.8
AGNES	27	841030	12	3.00	146.1
AGNES	27	841031	0	3.60	145.6
AGNES	27	841031	12	4.40	144.9
AGNES	27	841101	0	5.40	143.8
THAD	24	841017	12	6.80	151.9
THAD	24	841018	0	7.70	150.6
THAD	24	841018	12	9.70	149.6
THAD	24	841019	0	11.90	148.5
THAD	24	841019	12	14.30	147.4
THAD	24	841020	0	16.70	146.1
THAD	24	841020	12	19.00	145.0
THAD	24	841021	0	21.60	143.9
THAD	24	841021	12	23.70	143.7
THAD	24	841022	0	26.10	145.2
THAD	24	841022	12	28.60	149.0
THAD	24	841023	0	31.70	153.2
THAD	24	841023	12	34.60	158.5
THAD	24	841024	0	35.50	165.6

Name		YYMMDD	HH	lat N	lon E
WARREN	26	841018	0	12.50	129.5
WARREN	26	841018	12	12.50	128.5
WARREN	26	841019	0	12.50	127.6
WARREN	26	841019	12	12.50	126.6
WARREN	26	841020	0	12.50	125.4
WARREN	26	841020	12	12.20	124.2
WARREN	26	841021	0	12.00	123.1
WARREN	26	841021	12	11.60	121.6
WARREN	26	841022	0	11.00	120.0
WARREN	26	841022	12	10.60	118.1
WARREN	26	841023	0	11.10	116.0
WARREN	26	841023	12	12.00	116.3
DINAH	6	840719	0	21.8	162.8
DINAH	6	840719	12	23.0	163.3
DINAH	6	840720	0	23.5	164.0
DINAH	6	840720	12	22.7	163.8
DINAH	6	840721	0	21.4	163.1
DINAH	6	840721	12	21.2	162.2
DINAH	6	840722	0	21.0	161.3
DINAH	6	840722	12	20.9	160.4
DINAH	6	840723	0	20.4	159.1
DINAH	6	840723	12	21.0	158.2
DINAH	6	840724	0	21.6	157.3
DINAH	6	840724	12	21.3	155.4
ED	7	840722	0	28.5	126.8
ED	7	840722	12	28.8	128.2
ED	7	840723	0	27.7	130.0
ED	7	840723	12	27.5	131.7
ED	7	840724	0	27.5	133.0
ED	7	840724	12	27.9	134.0
ED	7	840725	0	28.2	135.0
ED	7	840725	12	27.0	135.6
FREDA	8	840802	0	20.5	147.0
FREDA	8	840802	12	19.5	145.0
FREDA	8	840803	0	19.0	142.3
FREDA	8	840803	12	19.5	139.6
FREDA	8	840804	0	18.5	137.0
FREDA	8	840804	12	17.0	134.5
FREDA	8	840805	0	16.5	131.5
FREDA	8	840805	12	17.6	127.5

Name		YYMMDD	HH	lat N	lon E
HOLLY	11	840812	0	15.0	139.0
HOLLY	11	840812	12	16.0	139.0
HOLLY	11	840813	0	17.0	139.0
HOLLY	11	840813	12	18.0	138.6
HOLLY	11	840814	0	19.2	137.8
HOLLY	11	840814	12	19.7	136.7
HOLLY	11	840815	0	20.1	135.4
HOLLY	11	840815	12	21.1	134.1
KELLY	15	840910	0	19.0	178.0
KELLY	15	840910	12	19.3	177.7
KELLY	15	840911	0	19.6	177.3
KELLY	15	840911	12	20.0	176.5
KELLY	15	840912	0	20.7	175.2
KELLY	15	840912	12	20.9	173.5
KELLY	15	840913	0	20.8	171.8
KELLY	15	840913	12	20.8	171.0
MAURY	17	840925	0	18.5	148.2
MAURY	17	840925	12	19.7	147.7
MAURY	17	840926	0	20.9	147.0
MAURY	17	840926	12	21.6	147.0
MAURY	17	840927	0	23.6	149.2
MAURY	17	840927	12	24.4	151.1